ORNL/TM-6478

Structural Model Testing for Prestressed Concrete Pressure Vessels: A Study of Grouted vs Nongrouted Posttensioned Prestressing Tendon Systems

D. J. Naus

OAK RIDGE NATIONAL LABORATORY
OPERATED BY UNION CARBIDE CORPORATION · FOR THE DEPARTMENT OF ENERGY

ORNL/TM-6478
Dist. Category UC-77

Contract No. W-7405-eng-26

Engineering Technology Division

HTGR BASE TECHNOLOGY PROGRAM

Prestressed Concrete Nuclear Pressure Vessel Development (189a 01331)

Concrete Structures Testing — Milestone 7b

STRUCTURAL MODEL TESTING FOR PRESTRESSED CONCRETE PRESSURE VESSELS: A STUDY OF GROUTED VS NONGROUTED POSTTENSIONED PRESTRESSING TENDON SYSTEMS

D. J. Naus

Date Published: April 1979

Prepared by the
OAK RIDGE NATIONAL LABORATORY
Oak Ridge, Tennessee 37830
operated by
UNION CARBIDE CORPORATION
for the
DEPARTMENT OF ENERGY

DISCLAIMER

CONTENTS

	Page
ACKNOWLEDGMENTS	v
ABSTRACT	1
1. INTRODUCTION	1
1.1 General	1
1.2 Study Origination, Objectives, and Scope	2
2. GROUTED-NONGROUTED TENDON POSTTENSIONED PRESTRESSING SYSTEMS FOR PCPVs	4
2.1 General	4
2.2 Protection of Prestressing Tendons from Corrosion	4
2.3 Arguments against and for the Use of Grouted Tendons in PCPVs	7
3. EVALUATION OF GROUTED TENDON POSTTENSIONED PRESTRESSING SYSTEMS FOR APPLICATION TO PCPVs	9
3.1 Grouted-Nongrouted Tendon Behavior	10
3.2 Evaluation of Selected Material Systems	18
3.3 Bench-Scale Corrosion Studies	33
3.4 Applicability of Acoustic Emission to Concrete Material Systems	41
3.5 Groutability of Large Posttensioned Prestressing Tendon Systems	50
4. SUMMARY AND CONCLUSIONS	159
REFERENCES	161
APPENDIX A	165
APPENDIX B	187

ACKNOWLEDGMENTS

The planning and execution of this investigation required the assistance and cooperation of numerous people in the Solid Mechanics Section of the Engineering Technology Division and in the Y-12 Plant. The author is indebted to those people for their cooperation and concern for the success of the investigation. A note of appreciation is due J. P. Callahan, T. M. Cate, C. B. Oland, and J. E. Smith for contributions during the investigation. A special note of appreciation is due C. C. Hurtt who made substantial contributions and was instrumental in coordinating many facets of the investigation.

STRUCTURAL MODEL TESTING FOR PRESTRESSED CONCRETE PRESSURE VESSELS: A STUDY OF GROUTED VS NONGROUTED POSTTENSIONED PRESTRESSING TENDON SYSTEMS

D. J. Naus

ABSTRACT

Nongrouted tendons are predominantly used in this country as the prestressing system for prestressed concrete pressure vessels (PCPVs) because they are more easily surveyed to detect reductions in prestressing level and distress such as results from corrosion. Grouted tendon systems, however, offer advantages which may make them cost-effective for PCPV applications. Literature was reviewed to (1) provide insight on the behavior of grouted tendon systems, (2) establish performance histories for structures utilizing grouted tendons, (3) examine corrosion protection procedures for prestressing tendons, (4) identify arguments for and against using grouted tendons, and (5) aid in the development of the experimental investigation. The experimental investigation was divided into four phases: (1) grouted-nongrouted tendon behavior, (2) evaluation of selected "new" material systems, (3) bench-scale corrosion studies, and (4) preliminary evaluation of acoustic emission techniques for monitoring grouted tendons in PCPVs. The groutability of large tendon systems was also investigated. Results indicate that grouted tendon flexure specimens exhibit improved performance relative to nongrouted members; the polymer-silica and fibrous concrete material systems exhibit potential for applications to PCPVs; the corrosion-inhibiting ability of grout in the environments investigated is equivalent to that of organic-petrolatum-based commercial corrosion inhibitors; acoustic emission is capable of monitoring plain concrete and simple concrete structures; and techniques are available for grouting large prestressing tendon systems such as would be used in a PCPV.

1. INTRODUCTION

1.1 General

Requirements for increased generating capacity of nuclear reactors in conjunction with increased operating pressure have pushed the limits of steel primary containment vessel design where postweld heat treatment is not permitted. This has led to the development of designs utilizing

concrete for fabrication of the primary containment structure. Because the structures must remain crack free and behave elastically at working stress levels, large quantities of reinforcement must be incorporated. This has necessitated the use of large-capacity posttensioned tendons, which may be either grouted or nongrouted.

Prestressed concrete pressure vessels (PCPVs) for high-temperature gas-cooled reactors are massive concrete structures. They are constructed of relatively high-strength concrete, which is reinforced by both conventional steel and a steel posttensioning system consisting of vertical tendons and circumferential wire-strand windings. The PCPV is anchored to the support structure and foundation mat by reinforcing bars, vertical tendons, or a combination of the two. Although only one PCPV has been built in the United States, European experience has demonstrated that these structures are safe and economical.

Presently in this country, nongrouted tendons are predominantly used as the prestressing system for PCPVs because they are easier to survey; however, grouted tendon prestressing systems offer advantages that make them potentially cost-effective for application to PCPVs. Prior to acceptance of grouted tendon systems for PCPVs, it must be demonstrated that (1) the grout provides an effective corrosion-inhibiting medium under conditions more severe than would be encountered in-service, (2) prestressing losses may be corrected for during posttensioning, and (3) a technique can be either developed for monitoring grouted tendon systems or the monitoring requirement modified as a result of proven performance. Also, because performance requirements for PCPVs dictate that extremely large prestressing systems must be utilized to reduce steel congestion as much as possible, these systems must be demonstrated to be effectively grouted.

1.2 Study Origination, Objectives, and Scope

This study resulted from the Prestressed Concrete Pressure Vessel Base Technology Program Review Meeting held at Oak Ridge National Laboratory (ORNL) on January 22, 1975, and a letter from Mr. F. S. Ople, General Atomic Company, dated March 11, 1975, to Mr. J. P. Callahan, ORNL,

expressing an interest in a test program to investigate the merits of grouted tendons for application to PCPVs.

The primary objective of this study was to provide background information on grouted and nongrouted tendons for PCPV applications. Secondary objectives included evaluations of (1) the relative performance of grouted and nongrouted tendons, (2) potential new materials for PCPV applications, (3) the effectiveness of grouting as a means of protecting prestressing tendons from corrosion environments, and (4) acoustic emission as a potential technique for monitoring structural integrity of PCPVs.

Relevant literature has been reviewed to establish current prestressing practices and to aid in the development of the experimental program. The experimental investigation was divided into four phases: (1) grouted-nongrouted tendon behavior; (2) evaluation of selected material systems; (3) bench-scale corrosion studies; and (4) preliminary evaluation of acoustic emission as a potential technique for monitoring the structural integrity of prestressed concrete structures. An overview was also conducted on the groutability of large tendon systems.

2. GROUTED-NONGROUTED TENDON POSTTENSIONED PRESTRESSING SYSTEMS FOR PCPVs

2.1 General

A posttensioned prestressing system consists of a prestressing tendon in combination with methods of stressing and anchoring the tendon to hardened concrete. Three general categories of prestressing systems exist, depending on the type of tendon utilized: wire, strand, and bar. Wound or circumferential prestressing could be a fourth category, but this system generally utilizes either a wire or strand system. The system is anchored by wedges, button-heading, or nuts. Table 1 (from Ref. 1) presents a listing of large (load capacities >6200 kN) tendon systems. Also included in the table are vendors and properties of the systems. A brief description of these systems may be obtained from Ref. 2.

Current practice in the construction of PCPVs in the United States is to use posttensioned steel tendons that are nongrouted.* The philosophy behind this approach is that, because the tendons are ungrouted, they may be readily surveyed, retensioned to eliminate losses resulting from creep and shrinkage of the concrete and relaxation of the steel, and replaced, if necessary. Licensing requires that a reactor containment be designed to permit (1) periodic inspection of all important areas and (2) an appropriate surveillance program.[3] As noted in Ref. 4, prestressing losses are predictable from laboratory studies conducted using representative environments and material systems; thus, material degradation resulting from corrosion remains the primary threat to effective performance of the prestressing system.

2.2 Protection of Prestressing Tendons from Corrosion

Corrosion protection of ungrouted tendons in PCPVs during their anticipated 30- to 40-year service life is generally provided by encapsulating the tendons in organic-petrolatum-based greases and waxes containing

---

*As of late 1975, all concrete reactor vessels and containments designed and built in the United States used nongrouted tendons except for H. B. Robinson Unit 2 (bar tendons), Three Mile Island Unit 2 (strand tendons), and Forked River (strand tendons).[2]

Table 1. Properties of large tendon systems[a]

Type	Vendor	System		Maximum load capacity (MN)	Elongation at ultimate load (%)
		Number of elements	Element diameter (mm)		
Button-head wire	Prescon	186	6.35	9.75	4.0
		163	7.01	10.38	4.0
	Inland Ryerson	170	6.35	8.90	3.5
	WCS	170	6.35	8.90	4.4
Seven-wire strand	Freyssinet Monogroup	19 Dyform	17.80	7.03	3.3
		37 Dyform	17.80	13.69	3.2
	Stressteel S/H	54	12.7	9.92	2.3
	VSL	55	12.7	10.10	4.0+
	WCS	48	12.7	8.82	[b]
Bars	Stressteel	6	34.9	6.35	4.0+
Wound	BBR		9.5 (strand)	[c]	[b]
	Preload BBR Crum		5.1 (wire)	[c]	Should be 3+

[a] Extracted from Ref. 1.

[b] Not available.

[c] No limit.

inhibitors. As required in Ref. 3, in-service inspections (visual, prestress monitoring, and material tests) should be performed one, three, and five years after the initial containment structural integrity test and every five years thereafter. During the operating life of the vessel, this may amount to as many as ten inspections. These inspections are performed under a surveillance contract and the costs could be substantial.[5]

Alternate measures have been attempted to prevent or significantly reduce tendon corrosion. Included in these attempts has been organic and inorganic coatings, cathodic protection, galvanized steel, stainless steel, and fiberglass tendons. However, these measures have been only moderately successful. During placement, organic and inorganic protective coatings may be removed from the tendons through friction with the conduit. Cathodic protection is impracticable economically because of the extensive amount ($\sim 9 \times 10^5$ kg prestressing is in the primary containment of Fort St. Vrain)[1] and types of steel. Galvanized reinforcement has up to 35% increased costs relative to conventional prestressing because of the additional cost of the process and increased steel contents required to compensate for the strength reduction that occurs with galvanizing. In addition, possible reduction in bond strength to concrete, the tendency for increased slip at friction type anchorages, and the possible corrosion of galvanized steel under certain conditions[6] also make the use of galvanized steel unattractive. Material costs of stainless steel tendons may be an order of magnitude greater than conventional prestressing. Fiberglass tendons have reduced moduli and strength, have not been proved alkaline resistant for extended periods of exposure, and have presented anchorage problems. An alternate approach for corrosion protection of tendons contained in PCPVs is to grout them.

Since 1930, approximately 18 million posttensioned prestressing tendons have been grouted.[7] An indication of the effectiveness of grout as a corrosion-inhibiting medium is contained in Ref. 4, which presents results of an extensive survey of structures containing prestressing tendons that have been in service for extended periods of time while being subjected to a variety of environments ranging from sewage tanks

to freeze-thaw. One of the most meaningful of the field tests noted in the survey was conducted by the U.S. Army Corps of Engineers at their Treat Island, Maine, exposure station. Nineteen posttensioned grouted beams were subjected to freezing and thawing and wetting and drying in a saline water environment. Examination of five of the beams after 1737 freezing and thawing cycles over 12 winters reveals that only 22 of 157 wires examined failed to meet ASTM requirements for total elongation under load and elongation at 1% of load. It was concluded from the investigation that filling a conduit containing tendons with a grout mixture provides protection from the severe environment of freezing and thawing in a saline environment. The survey also noted that there had been no known catastrophic failures in members posttensioned with stress-relieved wire or strand or with high-strength bars. Where the few known incidents of corrosion did occur, they were generally minor and the result of poor workmanship or improper material selection and thus could have been prevented. The survey concluded that, where proper construction procedures were followed, correct material formulations utilized, and proper detailing observed, a tendon system in which the tendon was encased in a portland cement grout and contained in a steel duct provided a corrosion-inhibiting alkaline environment with positive exclusion of corrosion agents.

2.3 Arguments against and for the Use of Grouted Tendons in PCPVs

As noted previously, present practice in the United States for fabrication of PCPVs is to use posttensioned prestressing tendons that are nongrouted. This decision has been based largely on one or more of the following arguments in favor of unbonded tendons:

1. Tendon loads may be periodically monitored with retensioning, as required.
2. Tendons may be removed, inspected for corrosion, and replaced, if necessary.
3. Poor grouting practices can lead to an acceleration of the corrosion process.

4. Tendon stresses are distributed along the full length of the tendon, which can lead to more ductile behavior than with bonded systems.
5. Corrosion-inhibiting compound reduces friction losses because it acts as a lubricant.

Proponents of bonded tendon systems feel that grouted tendons provide superior performance at reduced cost.* Arguments cited for using grouted tendon systems are as follows:

1. Performance is superior for flexure members with ultimate load increases of up to 50% and cracking load increases of up to 10 to 15% relative to unbonded tendon companion specimens.[8]
2. Effective grouting has been shown to provide an easy technique for corrosion protection with possible avoidance of periodic monitoring and maintenance of the corrosion-inhibiting medium.
3. Crack control is improved. More cracks form, but average crack widths are smaller so that strains transferred to the liner at crack locations are significantly reduced.
4. Dynamic effects are eliminated or significantly reduced if a tendon were to fail, with prestressing force lost only in the vicinity of the failure; that is, if an anchorage or tendon fails, effects are localized and overall strength insignificantly affected.
5. Grouting provides conservatism in seating and overall anchorage, particularly under fluctuating load conditions such as occur with an earthquake; that is, reduction in anchorage efficiency may result without a reduction in ultimate load.

---

*Initial costs of grouted and nongrouted tendons are approximately equal, but surveillance costs may be reduced.

3. EVALUATION OF GROUTED TENDON POSTTENSIONED PRESTRESSING SYSTEMS FOR APLICATION TO PCPVs

Despite a history of proven performance that actually predates that of nongrouted tendons, grouted tendon systems are still not generally utilized in PCPVs. This results from the requirement that there should be available a means of evaluating the functional capability of the structure during its lifetime.[2] This requirement resulted in a need to develop reliable quality assurance procedures for both tendon installation and structural in-service inspection programs. This has been easier to accomplish with nongrouted tendons because lift-off tests may be performed to evaluate the level of prestressing, tendons may be retensioned to eliminate losses resulting from steel relaxation and concrete creep, tendons may be removed for corrosion inspections, and the tendons may be replaced if required. If an effective means of monitoring grouted prestressing tendons can be developed or if it can be demonstrated that the in-service inspection requirement can be reduced, the advantages of grouted tendons to potentially reduce costs may be realized in PCPVs.*

Prior to accepting or recommending a priori the use of grouted tendon systems in PCPVs, a modest test program should be conducted to evaluate grouted tendon behavior, especially in an aggressive environment. Also, because the corrosion-inhibiting effect of grout is dependent on the grout being in intimate contact with the tendon over its entire length, the groutability of the large tendon systems (such as presented in Table 1) needs to be demonstrated.

The experimental investigation has been divided into four phases: (1) grouted-nongrouted tendon behavior, (2) evaluation of selected material systems, (3) bench-scale corrosion studies, and (4) tendon monitoring techniques. The groutability of large tendon systems (such as presented in Table 1) was also investigated through a review of literature.

---

*An inspection program for tendon installation would still be required for grouted tendons, but it would be related to certifying that quality assurance guidelines developed to ensure effective grouting were followed.

3.1 Grouted-Nongrouted Tendon Behavior

The relative structural performance under static, dynamic, and cyclic loading conditions of grouted and nongrouted posttensioned structures was evaluated by testing in flexure simple beam members* either 0.15 m wide by 0.30 m deep by 3.1 m long or 0.30 m wide by 0.30 m deep by 3.1 m long, such as shown in Figs. 1(a) and (b), respectively. The 0.15-m-wide beams were cast in the steel mold shown in Fig. 2(a) and the 0.30-m-wide beams were cast in the plywood mold shown in Fig. 2(b). Analysis results for these beam geometries are contained in Appendix A.

Prior to specimen fabrication, shear reinforcement (see Appendix A for location) and the tendon(s) (also the conduit for the grouted beams) were positioned in the mold and sufficient tension was applied to the prestressing strand (Table 2 presents prestressing strand properties) to ensure that alignment was maintained during beam casting. Concrete was then mixed in the Omni-Mixer shown in Fig. 3 using the concrete mix design presented in Table 3. The mix procedure included prewetting the mixer; draining excess water from the mixer; adding and blending the gravel, sand, and cement; adding the mix water; mixing for 1 min; letting the mixture set for 3 min; and remixing for 30 sec. After mixing, the slump, unit weight, and air contents were obtained for the plastic concrete according to ASTM Portland Cement Standards C143-74, C138-75, and C231-75, respectively. The beams† were then cast in two lifts, with compaction by internal vibration after each lift. The exposed surface was then leveled and finished. Flexure and compression control specimens were then cast according to ASTM C192-76. The beam and flexure specimens were covered with wet, absorbent paper and plastic and the compression cylinders capped with a portland cement paste 3 to 4 hr after casting, according to ASTM C617-76. Specimens were removed from their molds 48 to 72 hr

*A beam structural element was selected as the model to investigate performance of grouted and nongrouted tendons to simplify testing and analysis requirements. These models are considered an idealized representation of the barrel portion of a PCPV which (in some designs) is posttensioned longitudinally and loaded laterally.

†The 0.30-m-wide beams required two mixes because the capacity of the mixer was insufficient to fill the mold from one mix. Control specimens were obtained from each mix to ensure that concrete properties for the two mixes were reasonably close.

Table 2. Mechanical properties of prestressing strand

Ultimate load, kN	186.8
Load at 1% extension, kN	176.6
Yield strength at 0.2% offset, kN	182.6
Proportional limit at 0.02% offset, kN	166.6
Ultimate elongation in 0.61 m, %	6.25
Area, mm^2	98.4
Modulus of elasticity, GPa	194.5

Table 3. Concrete mix design

Material	Size range	Mix proportion (wt %)
Type II cement		16.37
Sand	<No. 4	33.35
Gravel	No. 4 to 20 mm	43.12
Water		6.96

after casting and were stored in the laboratory environment. Table 4 presents plastic concrete properties for each of the concrete mixes.

After curing for a minimum of three months, the beams were post-tensioned to the desired level of either 50, 60, or 70% of the prestressing strand ultimate strength. Figure 4 presents the setup for posttensioning of the beams. Because the beams were relatively short (3.1 m), anchorage seating prestressing losses were significant; thus the wedge-seating feature of the ram in Fig. 4 could not be used. The procedure utilized for posttensioning the beams included tensioning the strand to the approximate prestressing level desired; seating the wedge anchor by releasing the ram pressure; retensioning the strand to a level slightly greater than desired and placing split washer shims between the anchorage

Table 4. Grouted and nongrouted tendon beam mix properties[a] and test results for structural behavior test series

Beam designation	Concrete properties					Grout compressive strength (MPa)	Tendon posttensioning level[b] (% f'_s)	Beam test results		
	Plastic			Hardened						
	Air content (vol %)	Slump (mm)	Unit weight (kg/m^3)	Ultimate strength (MPa)	Elastic modulus (GPa)			Maximum load (kN)	Maximum centerline deflection (mm)	Type of failure
Grouted tendon beams										
G1	2.30	64	2425	36.7	35.2	35.3	50	107.3	25	Shear
G2	2.20	70	2425	35.6	31.9	35.3	69	110.6	15	Steel strand
G3	2.40	48	2438	38.1	33.9	35.3	59	108.4	19	Concrete crushing
G4	2.20	83	2435	38.9	32.0	35.3	65	108.4	19	Concrete crushing
G5	2.30	70	2428	39.8	37.5	35.3	59	105.9	25	Concrete crushing
G6	2.00	89	2428	37.4	30.6	35.3	59	103.4	23	Concrete crushing
G7	2.40	64	2428	38.2	34.0	21.7	59	[f]	[f]	Steel strand
G8	2.00	95	2428	39.9	37.0	35.3	54	109.4	37	Concrete crushing
G10	2.40	76	2409	38.5	35.4	32.8	62	113.0	34	Concrete crushing
G15	2.75	44	2422	37.9	33.0	24.1	58	105.6	23	Concrete crushing
G24	2.60	25	2435	43.6	36.7	24.1	58	102.3	18	Concrete crushing
G25	1.60	38	2460	45.5	35.8	24.1	60	101.2	28	Concrete crushing
G26	2.50	25	2444	42.6	36.1	24.1	62	103.4	37	Concrete crushing
LGC	2.70	67	2412	41.2	35.2	29.0	60	244.7	6	No failure[c]
LGF	2.25	51	2457	45.0	36.9	29.0	59	233.4	11	No failure[c]
Nongrouted tendon beams										
NG9	2.40	38	2435	37.7	32.5		50	84.5	23	Concrete crushing
NG10	2.30	38	2416	38.2	35.5		62	82.8	27	[f]
NG11	2.55	38	2438	39.0	34.1		62	104.5	32	Concrete crushing
NG12	2.25	32	2435	39.7	33.9		61	96.7	46	Concrete crushing
NG13	2.30	32	2428	38.9	36.4		59	99.0	31	Concrete crushing
NG14	2.55	32	2435	38.3	35.8		49	89.4	30	Concrete crushing
NG15	2.55	64	2393	31.0	28.8		61	97.0	32	Concrete crushing
NG16	2.65	38	2419	34.3	30.7		66	95.2	24	Concrete crushing
NGC	2.37	41	2425	40.6	31.6		61	244.7	17	No failure[c]
NGF	2.65	35	2432	47.2	36.3		61	204.6	28	Concrete crushing

[a] The concrete batch weights for cement, sand (SSD), gravel (SSD), and water were 79.4, 162.7, 209.1, and 33.8 kg, respectively.

[b] f'_s = ultimate tensile strength of the tendon.

[c] Deflection exceeds range of displacement gage.

[d] Not applicable; fatigue test.

[e] Exceeds testing machine capacity.

[f] Dropped while placing in test fixture.

and the reaction plate, which had been cast into the beam; releasing the ram pressure; and retensioning the strand and noting the ram pressure* at which the shim washers first became loose. If posttensioning values were not correct,† the procedure was repeated with shims added or subtracted to obtain correct values. Table 4 presents posttensioning levels for each of the beams tested in this test series.

Beams to be grouted were generally grouted two to three days after tensioning. If more than one week lapsed between tensioning and grouting, beam tension was rechecked and adjusted just prior to grouting. The grouting procedure included (1) adding a commercially available grout to a 0.06-m^3-capacity concrete mixer, (2) adding 10 kg of water per 25 kg of grout, (3) mixing for 2 min, (4) checking fluid consistency by conducting a flow cone test in accordance with Corps of Engineers Handbook Specification CRD-C79 (if a flow cone reading in excess of 40 sec was obtained, water was added, the mixture remixed, and flow cone test repeated), (5) transferring the grout to the grout pump shown in Fig. 5 with intermediate sieving through a No. 4 screen to remove lumps, (6) attaching the hose of the grout pump to the beam grout tube and fixture at the low end of the beam, as shown in Fig. 6 (one end of the beam was elevated approximately 100 mm to help ensure complete grouting by forcing the grout to flow "uphill"), (7) opening the 10-mm gate valve attached to the end of the beam where the grout was applied, and (8) pumping grout into the beam conduit until it flowed freely and uniformly from the grout tube at the elevated end of the beam. Pumping was then stopped, the grout tube sealed at the elevated end, and the grout pump restarted with grout pumped until the line pressure reached ∿400 kPa, at which time pumping was again stopped and the gate valve at the lower end of the beam closed. Control specimens obtained for each grout mix included six 50.8-mm compression cubes and one 76-mm-diam by 250-mm-long cylinder cast in

---

*Ram pressure gage has been calibrated so that ram pressure may be converted to applied load.

†Fifteen of the beams also contained load cells so that the accuracy of the tensioning technique could be checked. Differences in load readings were generally <5%.

a plexiglass mold. This mold allowed verification that excessive bleeding (segregation) of the mix did not occur. Grout properties are presented in Table 4.

Variables investigated during this test series were prestressing level, loading rate, and fatigue load ranges. Table 5 presents a summary of the variables for the grouted and nongrouted tendon beams and the pertinent test specimen related to each test parameter. Also investigated in this series was a comparison of grouted and nongrouted tendon performance in 0.30-m-wide beams [Fig. 1(b)] in which a simulated tendon failure was induced in the center tendon strand.

Table 5. Grouted and nongrouted tendon test variables

Variable	Test parameter	Relevant test specimen	
		Grouted	Nongrouted
Prestressing level	0.5 f'_s[a]	G1	NG14
	0.6 f'_s	G3,[b] G4, G15, G24, G25, G26	NG15, NG10[b]
	0.7 f'_s	G2	NG16
Load rate	74 N/sec	G4	NG15
	0.74 kN/sec	G10	
	7.4 kN/sec	G5	NG11
	74 kN/sec	G8	NG12
Fatigue	0.10 to 0.50 P_u[c]	G6	NG9
	0.10 to 0.70 P_u	G7	NG13

[a] f'_s = ultimate tensile strength of the tendon.
[b] Preloaded.
[c] P_u = static failure load.

Static flexure tests were used to compare the performance of beams posttensioned nominally to either 50, 60, or 70% of strand ultimate strength with the tendons then either grouted or ungrouted. The test fixture used is shown in Fig. 7, and the testing procedure consisted of (1) calibrating and zeroing load and displacement transducers, (2) applying load with a 245-kN capacity closed-loop test system at a rate

of 74 N/sec until first cracking occurred, (3) holding the load constant while the extent of crack propagation was marked, and (4) continuing loading in 4.45-kN increments until failure occurred, with crack extent marked at each load increment. Centerline deflection was monitored throughout testing with a direct current differential transformer (DCDT), which had been calibrated using steel spacers that have precisely known thicknesses.* Grouted tendon load-centerline deflection curves for prestressing posttensioned to strand ultimate strength levels of 50% are presented in Fig. 8 (G1);† those to 60% in Figs. 9 (G3), 10 (G4), 11 (G15), 12 (G24), 13 (G25), and 14 (G26); and those to 70% in Fig. 15 (G2). Corresponding nongrouted tendon load-centerline deflection curves for prestressing posttensioned to strand ultimate strength levels of 50% are presented in Fig. 16 (NG14); those to 60% in Figs. 17 (NG15) and 18 (NG10);‡ and those to 70% in Fig. 19 (NG16). Photographs of each of the beams (except beam NG10) after testing have been overlaid on the appropriate load-centerline deflection curves so that crack patterns and extent of cracking as a function of load (kips) may be identified. Maximum load level, centerline deflection, and type of beam failure for each of these beams is presented in Table 4. Figure 20 presents a summary of the effects of prestressing level on the load-centerline deflection behavior of grouted and nongrouted tendon beams. Results from this test series indicate that (1) grouted tendon beams develop more cracks, but the cracks are of smaller width, which results in smaller localized strains and less chance of penetration by corrosive environments; (2) for the range of prestressing levels investigated, as the level of prestressing increased, the load at which first cracking occurred and the ultimate load values increased; and (3) ultimate loads for grouted tendon beams were larger than for nongrouted beams at the same level of prestressing.

---

*Initially, a few beams were tested in which a dial gage was used to monitor deflections, but near-failure deflections increased so rapidly that readings could not be obtained and thus part of the load-deflection curve was lost.

†Designations in parentheses identify the pertinent beam.

‡Beam cracked prior to loading.

Dynamic flexure tests were conducted using the same test setup as for the static flexure tests. Nominal prestressing levels of 60% ultimate strand strength were used for both the grouted and nongrouted tendon beams. The test procedure was the same as for the static tests, except loading rates of 0.074, 0.74, 7.4, and 74 kN/sec were used and cracks were only marked for the slowest loading rate. Grouted tendon load-centerline deflection curves for beams loaded at rates of 0.074, 0.74, 7.4, and 74 kN/sec are presented in Figs. 10 (G4), 21 (G10), 22 (G5), and 23 (G8), respectively. Nongrouted load-centerline deflection curves for beams loaded at rates of 0.074, 7.4, and 74 kN/sec are presented in Figs. 17 (NG15), 24 (NG11), and 25 (NG12), respectively. Photographs of each of the beams after testing have been overlaid on the appropriate load-centerline deflection curves. Table 4 presents maximum load level, centerline deflection at maximum load, and type of beam failure for each of these beams. Figure 26 presents a summary of the effects of loading rate on the load-centerline deflection behavior of the grouted and nongrouted tendon beams. Results indicate no significant difference (<8%) in ultimate load capacities for either grouted or nongrouted tendon beams for the range of loading rates investigated. The load capacities of the beams were anticipated to increase as the loading rate increased,[9,10] but this trend was not apparent because the stiffness and capacity of the testing machine were apparently not sufficient to apply a truly dynamic loading effect, and results were thus within the static domain. However, there was a trend for the beam centerline deflections at ultimate load to increase as the loading rate increased for both types of beams.

Flexure fatigue loading of grouted and nongrouted tendon beams post-tensioned to 60% steel ultimate strength (except for NG9, which was tensioned to 50% ultimate) were also tested using the static flexure test setup. The beams were loaded sinusoidally at a rate of 1 Hz either between 10 and 50% or 10 and 70% of the ultimate load capacity of the appropriate companion static flexure specimen. Each cyclic test was terminated when the beam failed or 10^6 load cycles had been applied. Fatiguing both the grouted (G6) and nongrouted (NG9) tendon beams

between 10 and 50% of their static flexure capacity did not produce failures within 10^6 cycles; thus the tests were terminated and the beams statically loaded (74 N/sec) to failure. Failures occurred at loads corresponding to 95% of the corresponding static flexure values for both the grouted and nongrouted tendon control beams. Figures 27 and 28 present load-centerline deflection curves obtained when these beams were reloaded. The grouted tendon beam (G7) fatigued between 10 and 70% of its static flexure value failed at 625,400 cycles by fracture of the prestressing strand. Failure of the corresponding nongrouted tendon beam (NG13) did not occur within 10^6 load cycles, so the test was terminated and the beam statically loaded to failure, which occurred at 102% of the static flexure value. Figure 29 presents the load-centerline deflection curve for the nongrouted tendon beam on reloading. Results indicate that, for the beams that did not fail, there was only a 5% decrease in load capacity after 10^6 cycles of loading and deflections at maximum load and extent of crack propagation tended to stabilize in the first 100,000 to 200,000 load cycles. In contrast, for the beam that failed in fatigue, the deflection at maximum load and extent of crack propagation continuously increased until failure.

Beam structural members 0.30 m wide by 0.30 m deep by 3.1 m long were utilized to indicate the effect on flexural performance of an element in which a tendon failure had occurred. Beam width was selected so that three prestressing tendons could be contained within a beam and thus the simulated failure could be placed in the center strand to maintain prestressing symmetry. Two grouted (LGC, LGF)* and two nongrouted (LNGC, LNGF)† beams were cast using the same mix design and mix procedures as for the 0.15-m-wide beams. Mix properties are presented in Table 4. The first beam of each set (LGC, LNGC) was used as a control, and the second (LGF, LNGF) had a simulated tendon failure induced. Nominal prestressing levels for all beams were 60% of strand ultimate strength.

---

*LGC = large grouted tendon control beam. LGF = large grouted tendon beam with simulated tendon failure.

†LNGC = large nongrouted tendon control beam. LNGF = large nongrouted tendon beam with simulated tendon failure.

Simulated tendon failures were induced (1) in the nongrouted tendon beam by overtensioning the center strand sufficiently so that a shim restraining the wedge anchorage could be removed and the load released, and (2) in the grouted tendon beam by using a grinder to slowly cut the central tendon, which was exposed by a slot (Fig. 30) that had been precast into the beam at a distance 406 mm from one end (failure located in the shear region of the beam). Beams were tested by loading to failure at a rate of 74 N/sec using the static flexure test fixture. Extent of crack propagation was noted as a function of load for each beam. Load-centerline deflection curves for the control specimens and the specimens with a simulated tendon failure are presented in Figs. 31 (LGC) and 32 (LGF) for the grouted tendon beams and in Figs. 33 (LNGC) and 34 (LNGF) for the nongrouted tendon beams, respectively. Each of these curves also has a photographic overlay showing the beams after testing. Figure 35 presents a summary of results for the simulated tendon failure test series. As noted in Appendix A, analysis results predicted failure very close to the 245-kN capacity of the testing machine; thus, both grouted beams and the nongrouted control beam could not be loaded to failure because their ultimate load capacity exceeded the testing machine capacity. The nongrouted beam with the simulated tendon failure was loaded to failure. Some results that can still be derived are (1) a tendon failure occurring in a nongrouted tendon beam is more critical than a tendon failure in a corresponding grouted tendon beam and (2) for the beam geometry of the investigation, both the grouted and nongrouted beams with simulated tendon failure exhibited reduced cracking loads and increased deflections for the same load levels after cracking. Also, after first cracking, deflections of nongrouted beams were greater than those of companion grouted beams at the same load level.

3.2 Evaluation of Selected Material Systems

An overview has been conducted of three material systems relatively new to PCPV applications: shrinkage-compensating (expansive) cement, polymer-silica cement, and fibrous concrete. Shrinkage-compensating cement was investigated as a potential grout material so that its

expansion could be utilized to eliminate or reduce shrinkage and its associated problems such as cracking or incomplete filling of the tendon conduits. Polymer-silica cements (inorganic corrosion-resistant materials recently formulated at the Southwest Research Institute) were investigated as both potential grout materials and materials for elevated temperature environments where their desirable properties of rapid strength development, nonshrinking, good bond to minerals, and high-temperature capability (>980°C) could be utilized. Steel-fiber-reinforced concrete was investigated as a potential structural material because of its increased flexure strength, ductility (energy absorption), and resistance to penetration relative to conventional concretes. A summary of the test variables, parameters, and relevant test specimens utilized in the study of these material systems is presented in Table 6.

3.2.1 Potential grout materials for PCPVs

Both shrinkage-compensating and polymer-silica cements were investigated as potential grout materials. Three test series were conducted as part of their evaluation: grouted tendon beam tests, prestressing bond transfer length tests, and prestressing strand pull-out tests. Companion specimens fabricated using a conventional grout were tested and used as control results for each test series.

Grouted tendon beam tests. The first test series to evaluate these grout materials involved the fabrication, testing, and analysis of beam structural members having the geometry presented in Fig. 1(a). The 0.15-m-wide by 0.30-m-deep by 3.1-m-long specimens were fabricated and post-tensioned using the same materials and procedures as for previous test series. The only difference was the grout material, which was either shrinkage-compensating cement or polymer-silica cement. Posttensioning levels of interest were 50, 60, and 70% of prestressing strand ultimate strength. Posttensioning levels, grout properties, and plastic and hardened concrete properties for each of the beams in this test series are presented in Table 7.

Specimen testing procedures were identical to those for the static flexure tests. Load-centerline deflection curves for the beams post-tensioned nominally to 50, 60, and 70% strand ultimate strength and

Table 6. Test variables for study of new materials

Variable	Test parameter	Relevant test specimens: Grouted beam	Nongrouted beam	Bond pull-out (specimens)	5.1-cm cubes (specimens)
Posttensioning level (grout material)	0.5 f_s^* PS	G19, [c] G21, [c] G27			
	0.5 f_s^* SC	G16			
	0.5 f_s^* CG	G1			
	0.5 f_s^* CNG		NG14		
	0.6 f_s^* PS	G11, [b] G14, G22, [c] G28 [d]			
	0.6 f_s^* SC	G18			
	0.6 f_s^* CG	G4, G15, G24–G26			
	0.6 f_s^* CNG		NG15		
	0.7 f_s^* PS	G12, [b] G23, [c] G29 [d]			
	0.7 f_s^* SC	G13			
	0.7 f_s^* CG	G2			
	0.7 f_s^* CNG		NG16		
Bond development length failed anchorage	PS	G20			
	SC	G17			
	CG	G9			
Tendon bond strength	0.5 f_s^* PS			3	
	0.5 f_s^* SC			3	
	0.5 f_s^* GC			3	
	0.6 f_s^* PS			3	
	0.6 f_s^* SC			3	
	0.6 f_s^* CG			3	
	0.7 f_s^* PS			3	
	0.7 f_s^* SC			3	
	0.7 f_s^* CG			3	
Temperature	Room temp.				2 (mixes 1 and 2)
	260°C				5 (mix 2)
	540°C				5 (mix 1)
	816°C				5 (mix 2)
	1093°C				5 (mix 1)
Structural material	0.5 f_s^* FC	FC9	FC5		
	0.5 f_s^* CG	G1			
	0.5 f_s^* CNG		NG14		
	0.6 f_s^* FC	FC3, FC10	FC1, FC6, GC8		
	0.6 f_s^* CG	G4			
	0.6 f_s^* CNG		NG15		
	0.7 f_s^* FC	FC4, FC11	FC2, FC7		
	0.7 f_s^* CG	G2			
	0.7 f_s^* CNG		NG16		

[a] PS = polymer-silica cements; SC = shrinkage-compensating cement; CG = control, grouted; CNG = control, nongrouted; FC = fibrous concrete; f_s^* = ultimate tensile strength of tendon.

[b] Polymer-silica material A: material not up to specifications.

[c] Polymer-silica material B: material used in laboratory but too viscous for field grouting using required water content.

[d] Polymer-silica material C: material formulated for field grouting.

Table 7. Grouted and nongrouted tendon beam mix properties[a] and test results for new materials test series

Beam designation	Concrete properties					Grout compressive strength (MPa)	Tendon posttensioning level[b] (% f'_s)	Beam test results		
	Plastic			Hardened						
	Air content (vol %)	Slump (mm)	Unit weight (kg/m^3)	Ultimate strength (MPa)	Elastic modulus (GPa)			Maximum load (kN)	Maximum centerline deflection (mm)	Type of failure
Grouted tendon beams										
G9	2.00	76	2444	40.3	36.5	35.3	63	55.6	>51[c]	Steel strand pullout
G11	2.75	76	2403	36.8	32.0	16.5	61	102.9	27	Concrete crushing
G12	2.70	51	2406	31.3	31.6	16.5	69	105.9	30	Concrete crushing
G13	2.90	44	2416	34.5	32.2	51.0	69	118.4	24	Concrete crushing
G14	2.90	32	2412	35.0	32.9	16.5	60	100.1	26	Concrete crushing
G16	2.50	38	2438	37.1	29.6	51.0	49	111.8	31	Shear
G17	2.65	25	2435	39.8	35.7	51.0	58	63.4	>20[c]	Steel strand pullout
G18	2.35	32	2419	38.0	33.9	51.0	58	118.4	32	Concrete crushing
G19	1.85	89	2428	37.8	35.0	13.4	50	96.7	36	Concrete crushing
G20	1.75	127	2435	39.3	38.2	27.0	62	100.6	27	Concrete crushing[d]
G21	2.70	38	2422	45.4	35.7	19.7	53	101.2	24	Concrete crushing[d]
G22	2.25	64	2454	45.6	36.0	19.7	61	104.0	38	Concrete crushing
G23	1.90	57	2448	42.7	34.1	19.7	70	94.5	18	Concrete crushing
G27	2.40	25	2448	36.1	33.8	26.2	52	106.8	32	Concrete crushing
G28	2.45	32	2435	39.6	31.4	26.2	62	100.6	23	Concrete crushing
G29	2.70	19	2441	41.6	31.1	26.2	69	105.6	32	Concrete crushing
FC3	3.60	57	2153	17.9	12.3	32.8	59	97.9	>20[c]	Concrete crushing
FC4	4.10	13	2191	20.2	13.5	32.8	69	106.2	>19[c]	Concrete crushing
FC9	2.50	51	2387	38.4	28.7	29.0	51	103.4	>51[c]	Steel strand fracture
FC10	3.00	51	2390	33.5	26.2	29.0	60	107.3	>51[c]	Steel strand fracture
FC11	3.05	48	2390	47.0	32.3	29.0	73	105.1	38	Steel strand fracture
Nongrouted tendon beams										
FC1	3.40	38	2163	16.2	10.5		61	82.3	>50[c]	Concrete crushing
FC2	3.50	29	2179	21.9	15.3		69	102.8	>23[c]	Concrete crushing
FC5	2.65	108	2319	31.2	22.8		50	92.3	>51[c]	Concrete crushing
FC6	2.30	89	2371	30.9	21.9		61	92.3	>51[c]	Concrete crushing
FC7	2.70	89	2348	29.1	24.3		71	81.2	14	Concrete crushing
FC8	1.95	64	2422	37.7	30.6		59	96.7	>51[c]	Concrete crushing

[a] The plain concrete and fibrous concrete batch weights for cement, sand (SSD), gravel (SSD), and water were 79.4, 162.7, 209.1, and 33.8 kg, and 83.9, 251.7, 83.9, and 50.3 kg, respectively. The fibrous concrete beams also contained 1.5% by volume of 2.54-cm-long steel fibers.

[b] f'_s = ultimate tensile strength of the tendon.

[c] Deflection exceeds range of displacement gage.

[d] Tendon not straight in beam.

grouted with shrinkage-compensating cement are presented in Figs. 36 (G16), 37 (G18), and 38 (G13), respectively. Figures 39 (G27), 40 (G28), and 41 (G29) present load-centerline deflection values for beams grouted with polymer-silica cement and posttensioned nominally to values of 50, 60, and 70% strand ultimate strength, respectively. Figures 42–48 (included for academic interest only) also present load-centerline deflection information for beams grouted with polymer-silica cement; however, these beams were grouted while the polymer-silica material formulations for grouting were still being developed by the supplier. With the exception of beam G23, which on inspection was not completely grouted, the ultimate loads obtained by these beams were still within 10% of the values obtained by the control beams. Pertinent beams and specific problems for the beams of Figs. 42–48 may be derived from the figures and Table 6. Each figure also contains a photograph of the beam after testing.

Figures 49, 50, and 51 summarize results for nominal prestressing levels of 50, 60, and 70%, respectively. Results for conventionally grouted and nongrouted tendon beams have also been included for comparison. All grouted tendon beams exhibited improved performance relative to the nongrouted tendon beams. Ultimate load capacities for shrinkage-compensating cement grouted beams posttensioned to 50, 60, and 70% strand ultimate strength exhibited improvements of 4, 9, and 7%, respectively, relative to the conventionally grouted control specimens. Corresponding percentage changes obtained for the polymer-silica cement grouted beams were 0, −7, and −5%, respectively. Results indicate that the grout materials did not significantly influence (<10% change) beam flexure be-behavior as long as the grout completely encased the prestressing strand within the conduit. This concurs with the results presented in Ref. 11, in which the influence of grout properties on grouted posttensioned concrete beams was investigated.

Prestressing bond transfer length tests. Results of the preceding section indicate that the properties of the grout do not significantly influence the results obtained for grouted tendon concrete beams loaded in flexure. Although unlikely, a situation could occur where an anchorage could fail and the transfer of prestressing force to the concrete would have to be via bond. An indication of the relative efficiency of

the grout materials in transferring force to the concrete can be obtained from a prestress bond transfer test.

Prestressing bond transfer (transmission) length may be defined as the length of tendon from a free end required to attain maximum stress. It is a function of the prestress level and properties of the prestressing steel and grout. The influence of the grout material on this length may be evaluated by using prestressing steel from the same batch and the same level of prestressing so that the grout material is the only variable. The relative efficiency of the grout material is inversely proportional to the transfer length obtained from the tests.

The test procedure utilized for determining relative prestress transfer lengths for shrinkage-compensating cement, polymer-silica cement, and commercial grouts included (1) fabricating a 0.15-m-wide by 0.30-m-deep by 3.1-m-long beam structural element for each of the grout materials using the standard mix design and casting procedures; (2) permitting the beams to cure in excess of four months; (3) posttensioning the beam tendons to 60% strand ultimate strength using the same technique described previously, except that the two steel brackets shown in Fig. 4 were interchanged and the anchorage was attached after the bracket (shown adjacent to the tensioning ram in the figure);* (4) grouting the beams with either shrinkage-compensating cement, polymer-silica cement, or commercial grout, following previously described procedures; (5) permitting the grout to cure a minimum of two months; (6) epoxying mechanical gage points (such as shown in Fig. 30) on the bottom surface of the beam at 51-mm intervals along the prestressing tendon for a total distance of 1.57 m; (7) taking initial mechanical gage readings for each adjacent set of gage points; (8) slowly cutting the tendon between the anchorage and end of the beam; and (9) determining from the mechanical gage readings the length of beam required for the difference in strain readings before and after cutting the strand to less than 40 μm/m.† For comparison

---

*This permitted approximately 300 mm of the prestressing strand to be exposed for cutting.

†This value was arbitrarily selected. One division of mechanical gage was equivalent to 20 μm/m. The value was selected so there would be a minimum change of one dial division with an uncertainty of one division.

of the grout materials, the prestressing transfer length was defined as the distance (from the end of the beam where the prestressing was cut) required for the difference between initial and final mechanical gage readings to be less than 40 μm/m. Figure 52 presents results used to determine prestressing transfer lengths for the three grout materials. Lengths obtained were 0.41, 0.30, and 0.77 m for the shrinkage-compensating cement, polymer-silica cement, and commercial grouts, respectively. The shrinkage-compensating cement and polymer-silica cements required only 53 and 39% of the length required for a commercial grout to develop complete prestressing force transfer, thus indicating superior bond.

After conduction of the prestressing bond transfer length tests, each of the beams was statically loaded to failure in the test fixture shown in Fig. 7. Testing procedures were identical to those used for the static flexure test specimens. Load-centerline deflection curves for the shrinkage-compensating cement, polymer-silica cement, and commercially grouted beams with one anchorage removed are shown in Figs. 53 (G17), 54 (G20), and 55 (G9), respectively. These figures also show photographs of the particular beams after testing. A summary of the results, including those for a grouted tendon beam in which a simulated anchorage failure has not been induced, are presented in Fig. 56. As anticipated, the beams having one anchorage removed and grouted with shrinkage-compensating cement and conventional grout failed by tendon pull-out* at 58 and 51% of the ultimate load of a grouted tendon beam

*Development length (ℓ_d) is the sum of (1) the distance over which the strand must be bonded to the concrete to develop the effective prestress and (2) the additional length over which the strand must be bonded to develop the ultimate stress in the prestress. Reference 12 presents the following expression for estimating the development length for a strand with diameter, d_b (in.), ultimate stress in prestress, f_{su} (ksi), and effective prestress, f_{se} (ksi), $\ell_d = d_b\,[f_{su} - (2/3\ f_{se})]$. Using an ultimate strand stress of 1.86 GPa, an effective prestress of 1.12 GPa, and a strand diameter of 12.7 mm yields a development length of 2.06 m, which is greater than one-half the beam length. It was therefore anticipated that the strand would pull out for the shrinkage-compensating cement and conventionally grouted beams; however, the equation is obviously conservative for the polymer-silica grouted beam because of the improved bond characteristics of the material relative to conventional cement-based grouts.

having nonfailed anchorages. However, the polymer-silica grouted beam with one anchorage removed was able to attain 93% of the ultimate load of the control beam and failed by concrete compression rather than tendon pull-out. Results thus indicate improved bond characteristics of the polymer-silica cement materials.

Prestressing strand pull-out tests. Another test that may be utilized to compare materials bond strength is a pull-out test. Procedures for conducting this test are described in ASTM C234-71, *Standard Test Method for Comparing Concrete on the Basis of Bond Developed with Reinforcing Steel*. However, because prestressing steel is the material of interest and not reinforcing bars, the procedures required some modification, as noted in the following.

Test specimens were fabricated in two stages. The first stage consisted of casting annular concrete specimens in molds, such as those shown in Fig. 57. The exteriors of the molds were formed by 152-mm-OD by 737-mm-long cast iron pipes, which remained around the specimens during testing to prevent concrete splitting. Centrally located within each pipe and running the complete length of each mold was a 32-mm-diam bright metal conduit that was cast into each specimen and served as a passageway for the prestressing strand and grout. The molds were filled through the slot running the length of the mold, with concrete formulated from the mix presented in Table 3. Compaction of the specimens was by external vibration, and the specimens were permitted to cure in the laboratory environment until the second fabrication stage.

The second fabrication stage for the bond pull-out test specimens incorporated the prestressing strand. The procedure at this stage included (1) positioning three of the previously fabricated annular concrete specimens in the reaction test fixture shown in Fig. 58; (2) inserting a prestressing strand through the three test specimens; (3) placing a calibrated load cell and anchorage on the prestressing at the opposite end of the beam from the tensioning ram; (4) positioning the specimens so that the prestressing strand was centrally located in the conduit; (5) attaching fixtures for grouting; (6) tensioning the prestressing to the desired load level as verified by the load cell;

and (7) grouting the specimens using procedures described previously. Approximately seven days after grouting, the strand tension was relieved and the strand was cut between specimens by grinding to form three test specimens such as shown in Fig. 59. A total of nine sets of three specimens each were fabricated using this procedure. Variables investigated were level of prestressing (50, 60, and 70% strand ultimate strength) and type of grout material (shrinkage-compensating cement, polymer-silica cement, and a commercial grout).

Specimens were prepared for testing according to the following procedure: (1) wrapping prestressing strand adjacent to the concrete cylinder with two layers of fiberglass-reinforced tape so the set screws in the yoke of the slip measuring device could be attached to the prestressing strand without marring it and creating stress concentrations; (2) placing a 12.7-mm-thick by 152-mm-square steel bearing plate adjacent to the concrete; (3) attaching the yoke device for measuring slip of the prestressing strand; (4) measuring the distance between the point where the yoke attached to the prestressing strand and the face of the concrete; (5) placing the spherical seating reaction platens on the specimen; (6) placing the specimen in the 445-kN-capacity hydraulic testing machine; (7) attaching a wedge anchorage to the strand at the loading end both to hold the specimen in position prior to testing and to act as the testing machine grip during testing; and (8) attaching the dial gage fixture to the specimen. A specimen positioned in the testing machine just prior to testing is shown in Fig. 60.

Specimens were tested using a bond test apparatus which conformed to ASTM C234-71. The testing procedure followed for evaluating relative bond strengths of the grout materials to prestressing strand included (1) zeroing the load reading of the testing machine; (2) applying a preload of 445 N to straighten the prestressing strand and ensure that the spherical platens were in contact with the lower head of the testing machine; (3) zeroing dial gages on opposite sides of the specimen; and (4) loading the specimen at a rate less than 22.2 kN/min with dial readings obtained at each 2.22-kN load increment until either the strand

started pulling out of the specimen or the yoke moved into contact with the platen.*

Prestressing strand slip at the loaded end of the bar as a function of applied load was evaluated by determining the difference between the average dial reading and strand elongation as follows:

$$S_P = \overline{DD} - (P\ell/AE) \ ,$$

where

S_P = slip of prestressing strand at load P,
$\overline{DD}$ = average of two dial displacement readings,
P = applied load,
ℓ = length of strand between concrete face and point of attachment of yoke (30.7 mm),
A = area of prestressing strand (98.4 mm^2),
E = modulus of elasticity of prestressing strand (194.5 GPa).

Displacements of the steel-encased annular concrete section between the concrete bearing surface and the point where the yoke was attached were neglected in the calculations.

Load-slip curves for specimens grouted with shrinkage-compensating cement, polymer-silica cement, and a conventional grout are presented in Figs. 61, 62, and 63, respectively. Curves are presented for nominal prestressing levels during fabrication of 50, 60, and 70% prestressing strand ultimate strength. Each curve is an average of three test specimens. A summary of the bond pull-out test results, which can be used to compare performance of the grout material at the same nominal prestressing level, is presented in Figs. 64, 65, and 66 for the prestressing levels of 50, 60, and 70% strand ultimate strength, respectively.

---

*During tensioning, the prestressing strand twisted, which rotated the yoke of the slip-measuring device. To obtain the maximum number of readings prior to the yoke either "bottoming out" or hitting the side of of the reaction platen, the yoke was initially positioned as far to one side of the slot as it could be without making contact.

Results indicate that:

1. The bond developed by the polymer-silica cement was superior to those developed by the shrinkage-compensating and commercial grouts for all three prestressing levels of interest.
2. There was no significant difference in test results between the shrinkage-compensating cement and a conventional grout at prestressing levels of 50 and 70%; however, the shrinkage-compensating cement showed improved performance at the 60% level.
3. Both the conventional grout and the shrinkage-compensating cement grout test results indicated a trend toward a reduction in bond strength with an increase in prestressing level; however, the polymer-silica cement specimens exhibited an improvement in performance with an increase in prestressing level.*

3.2.2 Fibrous concrete for PCPV structural application

Fiber-reinforced concrete consists of hydraulic cements containing fine aggregate (or fine and coarse aggregates) and discontinuous, discrete fibers, which are blended into the concrete during the mix cycle. Incorporation of these fibers (steel, glass, and nylon have been used most commonly) into a concrete matrix has been shown to produce the following results[13,14] relative to plain concrete: (1) 2.5 times increase in first crack flexural strength; (2) dynamic strength increases of up to an order of magnitude; (3) shear strength improvement of 1.75 times; (4) fatigue endurance limit 2.25 times higher; (5) 3.25 times the impact resistance; and (6) 3 times the heat-spalling resistance. Fibrous concrete thus exhibits several advantages that make it a candidate structural material for PCPV applications.

Although fibrous concrete had potential cost- and performance-effective application in a PCPV to reduce reinforcing steel congestion

*A possible explanation for this last result is that, as the strand was released after specimen fabrication, the strand had a tendency to rotate and decrease the adhesion between the strand and grout so the primary bond mechanism remaining was friction. Apparently, the adhesion of the polymer-silica cement to the strand was sufficiently strong that, when the strand was released, the bond was not significantly decreased and the bond mechanism was a function of both friction and adhesion.

such as in areas of penetrations and although it possessed superior impact and penetration resistance so that it may have had application as a barrier to missiles generated by such things as equipment, tornadoes, or aircraft, these applications were not investigated in this study. Because this study was related to grouted and nongrouted tendon prestressing systems, fibrous concrete was investigated as a potential structural material for fabrication of flexure structural elements.

Fibrous concrete structural members 0.15 m wide by 0.30 m deep by 3.1 m long were fabricated using the mix design presented in Table 8.* The mix procedure was the same as described previously, except, during blending of the dry ingredients, the steel fibers were slowly added to minimize "balling" of the fibers. Specimens were fabricated using the same procedures as described previously, except the shear reinforcement present in previous beams was eliminated because it has been shown by Batson[15] that steel fibers will act as shear reinforcement in beams. After curing, the beams were posttensioned to the desired level of either 50, 60, or 70% of prestressing strand ultimate strength. Beams to be grouted were then grouted using a conventional grout and previously described procedures. Plastic and hardened concrete properties,

*A 9.5-mm maximum-aggregate-size river gravel and a much larger sand content were used in the fibrous concrete mixes because the effectiveness of the fibers was reduced as the maximum aggregate size and content increased.

Table 8. Fibrous concrete mix design

Material	Size range	Mix proportion (wt %)
Type II cement		17.00
River sand	>No. 4	51.01
River gravel	No. 4 to 9.5 mm	17.00
Water		10.20
Steel fibers	25.4 0.25 0.56 mm	4.79[a]

[a]Fiber volume content was 1.5%.

grout properties, and steel posttensioning levels for the fibrous-concrete (FC) beams are presented in Table 7 under information corresponding to beams designated FC.

Load-centerline deflection curves for fibrous concrete beams with grouted tendons that have been posttensioned to 50, 60, and 70% strand ultimate strength are shown in Figs. 67 (FC9), 68 (FC10), and 69 (FC11), respectively. Corresponding curves for nongrouted tendons posttensioned to these levels are shown in Figs. 70 (FC5), 71 (FC8), and 72 (FC7), respectively. Figures 73 (FC3) and 74 (FC4) shows results for the first series of grouted tendon fibrous concrete beams, which were fabricated with an unsatisfactory aggregate.* Corresponding results for nongrouted tendon fibrous concrete beams fabricated using the same unsatisfactory aggregate source are shown in Figs. 75 (FC1), 76 (FC2), and 77 (FC6).

A summary of test results obtained for the fibrous concrete beams for posttensioning levels of 50, 60, and 70% prestressing strand ultimate strength is presented in Figs. 78, 79, and 80, respectively. Also included in each of these figures are results of a grouted and nongrouted conventional concrete beam posttensioned to the appropriate prestressing level. Results indicated little difference between load-centerline deflection curves for the fibrous and conventional concrete beams when comparing corresponding grouted and nongrouted tendon beams at the same prestressing level. The primary difference was that both the grouted and nongrouted fibrous concrete beams were much more ductile than their conventional concrete counterparts, indicating that they had increased toughness. Also, the beam first crack load apparently was generally greater for the fibrous concrete beams.

3.2.3 Polymer-silica cement for elevated-temperature applications

Polymer-silica cements are chemically setting inorganic polymers that have a high bonding strength to minerals. Additional advantages

*The aggregate supplied by a local vendor was to have been suitable for use in concrete. Based on strength results presented in Table 7, the aggregate obviously had not been washed and contained a deleterious substance. The coarse aggregate was washed prior to its use for fabrication of beams FC9, FC10, FC11, FC5, FC7, and FC8.

that make the material potentially suitable for PCPV applications other than grouting of tendons are nonshrinking, complete cure within 24 hr, resistance to most hot or cold chemicals (exceptions are ammonium hydroxide, barium hydroxide, barium sulfide, calcium hydroxide, hydrofluoric acid, magnesium hydroxide, and sodium carbonate), low porosity, ability to withstand thermal shock, and suitability for elevated-temperature applications up to 980°C.

A special formulation of the polymer-silica cement purported to have application in thermal environments up to 1093°C was obtained from the manufacturer for evaluation. Two mixes of twelve 51-mm cubes were fabricated from the materials supplied. After curing several weeks in the laboratory environment, five cubes from mix 1 were placed in one oven, where the temperature was to be maintained at 260°C, and an additional set of five cube specimens was placed in a second oven, where the temperature was to be held at 816°C. Similarly, five-cube sets of mix 2 were placed in ovens to be maintained at 540 and 1093°C. The remaining two cubes of each set served as control specimens that would not be exposed to elevated temperatures.

After a one-day conditioning period in which the specimens were held at 149°C in each of their respective ovens to remove excess water, the temperatures of each of the ovens were slowly increased so the test temperatures of the 260 and 540°C were reached in approximately 24 hr and the test temperatures of 816 and 1093°C were reached in approximately 48 hr. Temperatures were maintained at these levels throughout the test duration, with a maximum deviation of ±10°C, which occurred in the oven at 1093°C.*

After lengths of exposure of 3, 7, 14, 28, and 94 days, one specimen from each oven was removed, placed immediately into insulation to slow the rate of cooling, permitted to cool to room temperature, and then stored in the laboratory environment until testing. After all specimens had been removed from the ovens, 6.35-mm-gage-length strain

---

*The only exception is that, on days when specimens were to be removed from the 816 and 1093°C ovens, their temperatures were permitted to drop to 260°C to facilitate specimen removal.

gages were applied to two opposite faces of each of the 51-mm cube specimens. The two gages on each cube were then connected in series so that bending effects during testing would be averaged, should they occur. Specimens were then loaded to failure in compression, with load and strain outputs continuously recorded throughout the test.

The effect of length of exposure on the stress-strain behavior of the polymer-silica material system exposed to test temperature of 25 (room), 260, 538, 816, and 1093°C are presented in Figs. 81, 82, 83, 84, and 85, respectively. Figures 86, 87, 88, 89, and 90 present the effect of temperature on the stress-strain behavior of the material after lengths of exposure of 3, 7, 14, 28, and 94 days, respectively. A summary of strength and moduli of elasticity results relative to room temperature control specimens is presented in Table 9.

Test results indicate that the material had a tendency to lose strength (soften) for prolonged exposures at 260 and 538°C, initially

Table 9. Polymer-silica elevated-temperature test results

Exposure temperature (°C)	Length of exposure at test temperature				
	3-day	7-day	14-day	28-day	94-day
	Relative compressive strength values[a] (%)				
260	111	114	117	101	96
538	67	58	49	51	64
816	64	82	118	124	136
1093	164	*b*	*b*	*b*	*b*
	Relative moduli of elasticity[a] (%)				
260	76	102	95	85	63
538	21	24	18	20	25
816	27	41	40	49	125
1093	140	*b*	*b*	*b*	*b*

[a]Relative to values obtained for specimens maintained at room temperature.

[b]Excessive material flow for exposure times in excess of three days.

decrease strength and then increase strength with length of exposure at 816°C, and increase in strength significantly for short exposure to 1093°C; however, the material supplied could not withstand extended exposure at this temperature. Athough these results indicated that the material tended to soften (decrease strength) around 538°C, these values appear to be improvements relative to conventional concretes.* Also, the supplier has since developed improved formulations. Results obtained for one such formulation suitable for use at temperatures up to 980°C are contained in Appendix B.

3.3 Bench-Scale Corrosion Studies

A bench-scale corrosion study was conducted to verify the corrosion-inhibiting capability of grout in the presence of identified deleterious substances[16] (chlorides, nitrates, and sulfides) which were present in concentrations much greater than would normally be encountered. This phase of the investigation was conducted in two sections: stressed tendons and nonstressed tendons. Only a summary of test procedures and results will be included. If a more explicit description of this phase is desired, it may be obtained from a subsequent report.[17]

3.3.1 Stressed tendon

Test specimens utilized in this series of tests were 305-mm segments obtained from the central straight wire of seven-wire strand material originally obtained for fabrication of the nongrouted tendon beams. The specimens were prepared by (1) degreasing the wires with acetone, (2) inspecting for flaws, (3) applying the corrosion-inhibiting

*Availability of data on elevated-temperature behavior of concrete is limited. In-house results for a 19.1-mm maximum-aggregate-size concrete tested after 14 days exposure to temperatures of 177, 566, and 760°C exhibited strengths relative to room temperature of 73, 38, and 3, respectively. However, these values only show a trend because an aggregate was included in these mixes and one was not contained in the polymer-silica material.

compound* to the wire surface over the 50.8-mm gage length (if required for the particular test), (4) placing the wire through a rubber stopper in the bottom of a polyethylene bottle so the gage length was centrally located in the bottle (wire portions outside the gage length were protected by a polyurethane insulator point), (5) filling the bottle with demineralized water, (6) slowly bubbling hydrogen sulfide gas through the water for approximately 15 min (3000 ppm H_2S, pH $\sim$4), and (7) sealing the bottle with a rubber stopper (Fig. 91). The test procedure included (1) calibrating the 44.5-kN testing machine, (2) placing the specimen in the testing machine (216-mm wire length between grips), (3) loading the specimen to the desired percentage of wire ultimate strength (60% of wire failure strength unless noted otherwise), and (4) maintaining the load at this level. If the specimen did not fail within 24 hr, it was unloaded, the water resaturated with hydrogen sulfide, and the specimen reloaded to the previous level. This procedure was repeated until either the specimen failed or a minimum of six days lapsed. If failure due to corrosion did not occur within this time interval, the specimen was removed from its corrosive environment and loaded to failure at a rate of 0.51 mm/min. The only corrosive medium investigated† in the stressed tendon test series was hydrogen-sulfide-saturated water because NH_4NO_3 and NaCl solutions have been shown to not produce corrosion-induced failures within a reasonable time frame (less than one week). These tests were all conducted at room temperature [24 (±5°C)]. Figure 92 presents the stressed tendon corrosion test setup.

---

*These commercially available corrosion-inhibiting compounds are of the type that would be used for (1) temporary protection of strand, (2) protection of circumferential prestressing of a high-temperature gas-cooled reactor, and (3) protection of the tendons in the secondary containment of a pressurized-water reactor. Grout and grout-containing-known-flaw widths were also investigated.

†One uncoated wire specimen was tested in 0.2 *M* NH_4NO_3 while tensioned to 60% of wire failure load. No failure was produced in seven days, so the specimen was removed and reloaded to failure. No degradation in failure load occurred as a result of the exposure. Similarly, a specimen subjected to 0.1 *M* NaCl for 60 days while tensioned to 60% of wire failure load did not fail as a result of the exposure.

Variables in the stressed tendon corrosion test series were stress level (unprotected wire only) and type of corrosion-inhibiting compound (three commercially available types and grout). A limited number of tests were also conducted using a test specimen similar to that shown in Fig. 93 to identify a limiting flaw size that could be contained in the grout without decreasing its corrosion-inhibiting effectiveness. As a counterpart to the flawed grout tests, a few test specimens were tested in which the commercially available corrosion-inhibiting compound was deliberately removed from a section of the wire by scraping it with another piece of tendon wire.

Average times to failure and range in times to failure for uncoated wire tensioned to different percentages of a control specimen (no corrosive environment) failure load are presented in Fig. 94. Results indicate that, as the percent failure load was increased, both the times to failure and the range of failure times decreased. No wire failures or noticeable loss of strength occurred in the group of wires exposed to the hydrogen sulfide environment while being protected by either the commercial corrosion-inhibiting compounds or grout (12.7-mm-diam by 38-mm-long cylindrical sections cast around a pretensioned wire). Figure 95 presents the effect of grout flaw size on time to failure. Average failure times obtained for the grout-protected wire specimens in which flaws were cast in the grout to simulate grout cracking were 34.6, 48.1, and 118.3 hr for flaw widths of 3.2, 1.6, and 1.3 mm, respectively. Of the five specimens protected by grout with flaw widths of 0.8 mm, two failed after an average exposure time of 146 hr, and three did not fail after an average exposure of 228 hr; on reloading to failure, they averaged a 5% loss in strength relative to the control specimens. No failures occurred in the specimens having flaw grout widths of 0.3 mm during an exposure time of 168 hr; on reloading to failure, there was a 3% loss in strength relative to the control specimens. After an exposure of 264 hr, no failure or loss of strength occurred in the specimen protected by grout containing a 0.1-mm flaw. Average failure times obtained for the two commercially available corrosion-inhibiting compounds in which part of the corrosion-inhibiting compound was removed by scraping were 14 and

65.7 hr. To determine the self-healing capability of one of the commercial corrosion-inhibiting compounds, one specimen was scraped, permitted to stand 33 days so the material could flow to coat the scraped region, and then exposed to the hydrogen sulfide solution for 168 hr. No failure occurred during this exposure, and, on reloading to failure, no decrease in ultimate strength resulted.

3.3.2 Nonstressed tendons

A companion series of corrosion tests was conducted using the central straight wire of the seven-wire strand obtained for the nongrouted tendon beam test series. In this test series, the tendons were not stressed while subjected to the corrosive environments. Four corrosive environments, three of which were much more severe than would normally be encountered, were investigated: water saturated with hydrogen sulfide (3000 ppm), 0.2 *M* NH_4NO_3 at 66°C, 0.1 *M* NaCl, and the outdoor environment of Oak Ridge.* Variables in the test series were (1) type of corrosion-inhibiting agent (none, commercially available products, grout with and without flaws, and polymer-silica cement) and (2) length of exposure.

Hydrogen sulfide environment. Wire sections to be subjected to the hydrogen-sulfide-saturated water solution were prepared by thoroughly cleaning with acetone, inspecting for surface flaws, and applying the particular corrosion-inhibiting compound to a 25.4-mm section (gage length) of wire. The wires were then placed through holes that had been drilled diametrically through a 63.5-mm-diam polyvinyl chloride pipe at spacings of 36.8 mm. The wires were positioned so their gage lengths were inside the pipe. Rubber stoppers were used both to maintain wire positions throughout the test and to seal the pipe so the hydrogen-sulfide-saturated water solution would not leak from the pipe. The test was initiated by filling the pipe with demineralized water, elevating one end of the pipe approximately 150 mm, bubbling hydrogen sulfide gas slowly for 15 min through the water from the lower end of the pipe so the gas was forced to percolate through the water, and sealing the pipe.

*Only unprotected wire was considered for the outdoor exposure.

Water level in the pipe and resaturation of the water with hydrogen sulfide were done routinely on Mondays, Wednesdays, and Fridays throughout the duration of the test. Figure 96 presents the test setup.

Specimens that had been either unprotected, protected by commerical corrosion inhibitors, or protected by grout were removed from the polyvinyl chloride pipe after periods of exposure of 33, 77, and 120 days. The specimens were tested by loading to failure at a rate of 0.51 mm/min in the testing machine shown in Fig. 92. The relative effectiveness of the various corrosion inhibitors was evaluated by comparing their ultimate loads and times to failure both to the unprotected specimens and to control specimens that had not been subjected to the corrosive environment.* After 33 days of exposure, no detrimental effects were noted from hydrogen sulfide exposure in the grout and commercial corrosion-inhibiting compound protected tendons; however, for the unprotected specimens, there was an 8% decrease in load capacity and a 62% decrease in ductility (time to failure). Results obtained after 77 days of exposure indicate no detrimental effects of corrosion in the specimens protected by either grout or commercial corrosion-inhibiting compounds; however, unprotected specimens exhibited an 8% decrease in load capacity and a 60% decrease in ductility. Finally, after 120 days exposure, (1) the unprotected wire exhibited decreases in load capacity of 11% and ductility of 70%, (2) wires with the temporary commercial corrosion-inhibiting agent exhibited decreases in load capacity of 14% and ductility of 75%, (3) one set of specimens protected by a commercial corrosion-inhibiting agent exhibited no loss of load capacity but a 14% decrease in ductility, and (4) the grout-protected specimens exhibited no loss of load capacity but a decrease in ductility of 12%.

A second test series was conducted to evaluate the corrosion-inhibiting capability of the polymer-silica candidate grout material and to investigate the effect of flaws contained in either grout or the commercial corrosion-inhibiting compounds on their corrosion-inhibiting capability. After lengths of exposure of 30, 74, and 127 days, the

*A significant effect is arbitrarily defined as decreases in load capacity of more than 3% and time to failure of more than 6% from control values.

polymer-silica protected specimens exhibited ultimate load decreases of 1, 1, and 10% and decreases in time to failure of 14, 32, and 30%, respectively. Specimens protected by grout-containing flaws were tested after lengths of exposure of 35 and 119 days. For 35 days exposure and flaw widths ranging from 0.01 to 0.76 mm, there was no significant decrease in either failure loads or times to failure; however, for 119 days exposure, reductions in load ranged from 7 to 11% and reductions in time to failure from 4 to 8% for the extremes in flaw widths. Companion scraped commercial corrosion-inhibiting compounds exhibited 5 and 15% average load reductions and 56 and 63% average reductions in time to failure (or 35 and 119 days exposure, respectively).

Nitrate environment. The second corrosive environment investigated in the nonstressed tendon test series was 0.2 *M* NH_4NO_3. Specimens were prepared for exposure using the same techniques as for the hydrogen sulfide tests except that, instead of being placed through a pipe, the specimens were inserted through the bottom of a stainless steel pan and held in position by rubber stoppers. After filling the pan with the NH_4NO_3 solution, it was placed into an oven maintained at 66°C to increase the severity of nitrate attack.[18] One set of specimens prior to insertion into the oven is shown in Fig. 97.

Specimens were either unprotected, protected by commercial corrosion-inhibiting compounds, or protected by grout. Lengths of exposure were 42, 78, and 132 days. Specimens protected by commercially available corrosion-inhibiting compounds exhibited no significant decreases in either load capacity or ductility for exposures of 42, 78, and 132 days. After 38 days exposure, the grout-protected specimens exhibited no decrease in strength and ductility; however, after 87 days exposure, there was a 22% decrease in time to failure, and, after 122 days exposure, there was a 26% decrease in time to failure, even though there was no decrease in wire strength after these exposure times.* Corresponding with this,

*It is interesting to note that 50.8-mm grout cubes placed in the NH_4NO_3 solution at 66°C exhibited strength decreases of 37 and 57% relative to control specimens cured in limewater for exposure periods of 35 and 60 days, respectively. For an exposure of 101 days, the specimens deteriorated to the point that they could not be tested. Similar specimens placed in the hydrogen sulfide and chloride solutions did not exhibit significant strength changes for exposure times up to 100 days.

unprotected wire after exposure periods of 42, 78, and 132 days exhibited strength reductions of 14, 6, and 9% and decreases in ductility of 67, 58, and 66%, respectively.

A companion set of specimens was prepared and exposed to the NH_4NO_3 solution at 66°C to demonstrate the corrosion-inhibiting capability of the polymer-silica candidate grout material and to investigate the effect of flaws contained in the grout and in the commercial corrosion-inhibiting compounds on the corrosion-inhibiting ability of these materials. Periods of exposure were for 33, 84, and 130 days, and flaw widths ranged from 0.03 mm to 3.18 mm. No significant strength reductions occurred in the polymer-silica cement-protected specimens for 33- and 84-day exposures, but, after 130 days, there was a 9% decrease in strength. Decreases in ductility after 33-, 84-, and 130-day exposures were 7, 13, and 27%. For exposures of 33 and 84 days, there were no decreases in strength for the grout specimens containing flaws except for the specimen protected by grout with a 3.18-mm flaw, which showed a 9% strength decrease after 84 days. After the 130-day exposure, all the grout specimens with flaws exhibited ∿9% reduction in strength. Ductility decreases for these specimens were ∿3% after 33 days exposure for all flaw widths, and, after 84 days exposure, ∿13% for flaw widths up to 0.13 mm, 17% for a flaw width of 0.25 mm, 22% for a flaw width of 0.76 mm, and 38% for a flaw width of 3.18 mm. After an exposure period of 130 days, ductility decreases for flaw widths from 0.03 to 3.18 mm ranged from 28 to 44%. The corresponding scraped commercial corrosion inhibitors for the three exposure periods exhibited strength decreases of 1, 5, and 7% and decreases in ductility of 2, 0, and 2%, respectively.

Chloride environment. The effect of 0.1 *M* NaCl on the effectiveness of the various corrosion-inhibiting agents was also evaluated. Specimens were prepared for testing using the same techniques as for the nitrate test series. The specimens after preparation were placed in a stainless steel pan such as shown in Fig. 97. After filling the pan with the chloride solution, the solution was maintained in the laboratory environment.

As for the previous test series, specimens were either unprotected, protected by commercial corrosion inhibitors, or protected by grout.

Periods of exposure were 30, 71, 107, and 164 days. After a 30-day exposure period to the NaCl solution, one unprotected wire was tested and there was no decrease in load capacity; thus, no additional specimens were tested at this exposure age. No decreases in strength and ductility occurred after 71 days exposure in either the specimens protected by the commercially available materials or those protected by grout; however, the unprotected specimen after this exposure period exhibited a 4% decrease in strength and a 49% decrease in ductility. Exposure of 107 days to the NaCl solution produced 3 to 6% strength decreases in the commercially available corrosion inhibitors and a 4% strength decrease in the grout-protected wires. Corresponding ductility decreases for the commercial products ranged from 11 to 24%, while there was a 4% decrease in the grout-protected specimens. Strength and ductility decreases for the unprotected specimens were 8 and 60%, respectively. Strength decreases in the commercial product protected wires after 164 days exposure were 8%, while the ductility reductions ranged from 5 to 29% (temporary coating material). Grout-protected specimens exhibited a 9% strength decrease and a 35% ductility decrease for this exposure. Corresponding strength and ductility decreases obtained for the unprotected wire after 164 days exposure were 13 and 64%, respectively.

As in the previous test series, a companion set of specimens was prepared and exposed in the NaCl solution to demonstrate the corrosion-inhibiting capability of the polymer-silica candidate grout material and to investigate the effect of flaws contained in the grout and in the corrosion-inhibiting compounds on the corrosion-inhibiting ability of these materials. After exposure periods of 71, 107, and 164 days, strength decreases for the polymer-silica-protected wires were 0, 4, and 9%, respectively; corresponding ductility decreases were 2, 30, and 35%. Specimens having corrosion barriers containing flaws were exposed to the NaCl solution for periods of 64, 110, and 153 days. After 64 days exposure, there was no reduction in strength detected for any of these specimens; however, there was an average ductility decrease of 3% for the commercial corrosion inhibitors, which had been scraped, and, as the flaw size in the grout increased from 0.03 to 3.18 mm, the ductility

reductions were from 0 to 34%. Strength and ductility reductions for corresponding unprotected specimens were 7 and 32%, respectively. Strength reductions of approximately 2% and ductility reductions of 6 to 24% occurred in the flawed commercial corrosion-inhibiting compounds after 110 days exposure. Decreases in strength in the flawed grout specimens after the same exposure period were approximately 2 and 8% for flaw widths up to 0.76 and 3.18 mm, respectively. Corresponding ductility decreases ranged from 10% for the 0.03-mm flaw to 67% for the 3.18-mm flaw. Decreases in strength and ductility for an unprotected wire were 5 and 36%, respectively. After 153 days exposure, strength decreases for the flawed commercial corrosion-inhibiting compounds were 11%, with ductility decreases of 13% obtained for one specimen and 0% for a second specimen. The flawed grout-protected specimens exhibited strength decreases from 7 to 18% for flaw widths ranging from 0.03 to 3.18 mm. Corresponding ductility decreases ranged from 9 to 75%.

Outside environment. The last corrosive environment to be investigated was the outside environment of Oak Ridge. Previous results indicated that the likelihood of corrosion occurring in a specimen protected by a corrosion inhibitor and subjected to the relatively mild outside environment was remote. Therefore, only unprotected wire was investigated to demonstrate the need for continuous corrosion protection of prestressing steel. Test specimens from the same material source as used in the previous studies were prepared by cutting to length (305 mm) and thoroughly cleaning with acetone. After cleaning, they were placed in a rack and stored outside.

Specimens were removed from the test rack at exposure ages of 38, 79, and 114 days and loaded to failure. Strength decreases for these exposure times were 3, 8, and 11%, respectively. The ductility decreased 4% for an exposure of 38 days, but there was no change for 79 and 114 days exposure.

3.4 Applicability of Acoustic Emission to Concrete Material Systems

Current philosophy in PCPV design requires that there should be available a means for evaluating the functional capability of the structure

during its lifetime.[2] This has resulted in a requirement to develop in-service inspection programs. Because nongrouted tendons may be retensioned to eliminate losses, replaced, removed for inspection, and readily evaluated for level of prestressing, they have almost always been selected for the prestressing system. If a technique can be developed for in-service monitoring of grouted tendons, their advantages may be incorporated into PCPVs. One potential inspection technique for grouted-tendon monitoring is acoustic emission.

3.4.1 Acoustic emission

Acoustic emissions are small-amplitude elastic stress waves generated during material deformation resulting from a mechanical or thermal stimulus. The stress waves are detected by transducers as small displacements on the specimen surface. The emissions are classified as being either continuous or burst. Continuous acoustic emissions are low-level, high-signal-density emissions such as might be observed during tension testing of unflawed specimens. Burst acoustic emissions are generated when a plastic zone or microcracks form at a crack tip or when crack extension occurs. Characterization of these stress wave emissions provides an insight into the type of inelastic deformation that is occurring. Amplitude of the stress wave emission indicates the magnitude of flaw extension, rate of stress wave emission indicates the rate of flaw propagation, and the total acoustic emission energy generated is proportional to the loss of structural integrity.

Instrumentation systems for acoustic emission monitoring generally include transducers, preamplifiers, filters, processors, and recorders. Transducers (sensors), when stimulated by stress waves, transform the mechanical excitations into electrical signals. Piezoelectric crystals are generally used as transducers because of their high sensitivity and stability. The signal from the transducer is fed to a preamplifier, which is located as close as possible to the transducer to provide a good signal-to-noise ratio and to match impedances (long cables may be used without adversely affecting signal-to-noise ratio). Emerging from the preamplifier, the electrical signals are processed by signal conditioners, such as filters (enable selective rejection of certain unwanted

signals), main amplifiers (provide a variable and calibrated gain), and discriminators (selectively reject signals having certain spatial or temporal characteristics). After conditioning, the electrical signals generally exceed 1 V and are ready for processing. Several processing techniques are available, including those that (1) count the number of times the signal crosses a preset threshold value (the number of crossings is proportional to magnitude of the acoustic emission signal and thus an approximate measure of the energy or severity of the event), (2) extract electrical energy by an energy module (compares count and energy), (3) count number of events and not threshold crossings, (4) perform spectral analysis, and (5) perform amplitude distribution. Presentation of the data may be by punched tape, printed tape, magnetic tape or disk, cathode ray oscilloscope display, or graphic plotters.

Flaws may be located by use of data from an array of three or more coupled transducers (two or more for one-dimensional source location). Location of an acoustic source is usually established through analysis of differences in time of propagation of the stress wave emissions to the multiple sensor array. A typical sequence of events for flaw location on a two-dimensional surface may be described as follows.

1. An acoustic event produces an expanding spherical wave, which impacts one of the transducers, starting a clock.
2. The time of arrival of the stress wave to the other transducers of the array is established.
3. When the rate of propagation of the stress wave in the material and the arrival times are known, a locus of points (a circle for two-dimensional case) may be established for each transducer to indicate possible locations of the source.
4. The intersection of the circles identifies the flaw location.

Commercially available flaw location systems use analog or digital computers to perform all analyses. Statistical methods may be incorporated into the system for data processing to develop probability maps for the structure being investigated so that areas with a high probability of containing flaws may be identified. Tentative advantages of acoustic emission are that access to the entire vessel is not required; 100% of

the vessel volume may be inspected; the vessel may be monitored in service; the system possesses the capability to detect, locate, and categorize the approximate severity of a growing defect; and the technique requires minimal time. Potential disadvantages or problem areas of the system, which must be overcome, are that background noise, which may mask defect emissions, will have to be filtered out; hydrotest stresses (proof tests) are not truly representative of in-service stresses; time-temperature annealing effects may influence results; the vessel should be continuously monitored so all events may be identified; and, unless the instrumentation is permanently mounted, downtime is required for instrumentation and calibration before each test.

3.4.2 Applications of acoustic emission to PCPVs

The state of the art of acoustic emission has advanced very rapidly in the last few years through numerous applications. The applicability of acoustic emission for monitoring of metallic materials and components and the corrosion of metallic materials has been well established.[19,20] In fact, at least one company has developed an acoustic emission system that is being used to inspect nuclear power plant coolant systems and metallic containment vessels. However, only limited applications of acoustic emission have been made to concrete material systems.

The limited results obtained from acoustic emission applications to concrete material systems indicate that onset and failure progression can be detected, stress wave emission characteristics may be correlated to material modulus of elasticity, loading levels can be evaluated nondestructively, flaws may be located, and the sensitivity of acoustic emissions for detection of failure processes and deformation in materials is superior to conventional techniques.[21,22] These results are sufficiently encouraging to indicate that acoustic emission may be feasible for in-service monitoring of the structural integrity of PCPVs; however, fundamental laboratory characterization studies on concrete material behavior are required prior to implementation of acoustic emission techniques for monitoring of structures as complex as a PCPV.

3.4.3 Acoustic emission laboratory investigation

Because developing acoustic emission to the point that its techniques may be implemented in the field for grouted tendon monitoring was not practicable in the current study, only limited tests were conducted to demonstrate the feasibility of acoustic emission for monitoring concrete and simple concrete models. Two series of tests were conducted: (1) monitoring of plain concrete compression cylinders and flexure members and (2) monitoring of several of the grouted-nongrouted tendon 0.15-m by 0.30-m by 3.1-m beam structural models.

Monitoring of plain concrete specimens. Three sets of concrete cylinders (0.15 m diam by 0.54 m long) and flexure prisms (0.15 by 0.15 by 0.91 m) fabricated according to ASTM C192-76 were cast to obtain acoustic emission data on concrete under compressive and tensile loadings. Four compression cylinders and three flexure specimens were contained in each specimen set. The basic mix design used for specimen fabrication is presented in Table 3. The variable between mixes was the water content, which was adjusted so that acoustic emission data could be obtained from low-, medium-, and high-strength concretes.

After curing for five months, the compression specimens were prepared for testing by instrumenting with two 0.10-m gage-length strain gages placed at 180° intervals on the circumference of each cylinder in the direction of loading.* Two 50-kHz resonant-frequency transducers were attached to the specimen to be tested at a longitudinal spacing of 0.30 m, and two additional 50-kHz transducers were attached to the upper and lower loading platens to minimize noise from the platen-cylinder interface (Fig. 98). The testing procedure followed for three of the cylinders in each set included: (1) adjusting the amplifier gain of the active acoustic emission transducers for an equal level of background noise of approximately 0.8 V (gains of active transducers labeled T and B in Fig. 98 were 91 and 92 dB, respectively), (2) setting the threshold voltage for detecting an acoustic emission event approximately 0.4 V above the background noise, (3) zeroing and calibrating strain and load

*The strain gages on each cylinder were wired in series to minimize the effects of bending, should they occur.

transducer responses, (4) programming the multisensor source location acoustic emission system shown in Fig. 99 for one-dimensional source location, and (5) loading the cylinder to failure with load-strain and acoustic emission data obtained throughout. The fourth cylinder of each set was prepared for testing in the same manner as the three previous cylinders of each set. Specimen testing was different because the specimens were loaded to failure in cycles, with each succeeding load cycle after an initial cycle to 20% of failure load being incremented by 10% of the average failure stress obtained for the first three cylinders tested of each set. After completion of a load cycle, the load was reduced to 22.2 kN prior to initiation of a new cycle. Results obtained for the three low- (19.5-MPa), medium- (36.8-MPa), and high-strength (50.8-MPa) cylinders loaded to failure in one cycle are presented in Figs. 100, 101, and 102, respectively. The figures present acoustic-emission-event histograms, cumulative acoustic-emission-event counts,* and normalized strain as a function of percent failure stress. The effects of load cycling on acoustic emission activity for the low-, medium-, and high-strength concrete are summarized in Tables 10, 11, and 12, respectively. Results indicate that, for the specimens loaded to failure in one cycle, there was good correlation between acoutic emission and stress-strain curves for low- and medium-strength concrete; that is, from 0 to 30% ultimate strength, the stress-strain curve was essentially linear and acoustic emission activity was small; from 30 to 70% ultimate strength, the stress-strain curve started to deviate from linearity due to an increase in bond cracks between the aggregate and matrix and the acoustic emission activity increased; and above ∿70% ultimate failure strength, there was a rapid deviation of the stress-strain curve from linearity due to a rapid increase in matrix cracking and there was an associated sharp increase in acoustic emission activity. The high-strength concrete specimens exhibited relatively uniform activity from initiation of loading until approximately 85 to 90% ultimate strength, when the activity increased sharply. Results obtained for the

*Dashed line for cumulative event count is a smoothed curve that has eliminated initial noise resulting from platen-cylinder interaction.

Table 10. Number of events by load interval for increasing load cycling of low-strength concrete

Load range (kN)	Number of valid events per load range interval for cycle									
	1	2	3	4	5	6	7	8	9	10
0.0–71.2	10	0	0	0	0	0	0	0	0	0
22.2–106.8		2	2	0	0	0	0	1	0	0
22.2–142.3			0	2	0	0	0	0	0	0
22.2–177.9				4	1	0	0	0	0	0
22.2–213.5					3	0	0	0	0	0
22.2–249.1						4	0	0	1	0
22.2–284.7							6	0	0	0
22.2–320.3								5	0	0
22.2–355.9									8	1
22.2–438.2										81

Table 11. Number of events by load interval for increasing load cycling of medium-strength concrete

Load range (kN)	Number of valid events per load range interval for cycle							
	1	2	3	4	5	6	7	8
0.0–133.4	18	1	0	0	0	0	0	0
22.2–200.2		4	0	0	0	0	0	0
22.2–266.9			7	0	0	0	0	0
22.2–333.6				2	0	0	0	0
22.2–402.6					6	0	0	0
22.2–469.7						5	3	1
22.2–536.9							10	2
22.2–604.1								26[a]

[a]Floppy-disc error after this number of events.

specimens cyclically loaded to failure with each succeeding load cycle being to a higher load level indicate that the Kaiser effect (once a load has been applied to a member and the associated acoustic emission activity resulting from its application ceased, no more emission will occur

Table 12. Number of events by load interval for increasing load cycling of high-strength concrete

Load range (kN)	Number of valid events per load range of interval for cycle								
	1	2	3	4	5	6	7	8	9
0.0–186.8	37	0	0	0	0	0	0	0	0
22.2–302.5		7	5	0	0	0	0	0	0
22.2–373.7			6	0	0	0	0	0	0
22.2–467.1				3	3	2	0	0	1
22.2–560.5					14	5	2	0	3
22.2–653.9						11	3	1	3
22.2–742.9							22	17	18
22.2–836.3								113	82
22.2–851.8									85

until the load level is exceeded, even if the load is completely removed)[23] apparently applies to concrete material systems.

After curing for five months, the 0.15-m by 0.15-m by 0.91-m flexure specimens were prepared for testing by applying a 0.10-m gage-length strain gage to one face of each of the three specimens cast for the low-, medium-, and high-strength concretes. Just prior to testing, two acoustic emission transducers (50-kHz resonant frequency) were attached to the specimens at a spacing of 0.50 m on the same surface as the strain gage. The specimen was then placed in the flexure test setup (ASTM C78-75) shown in Fig. 103 with the surface containing the acoustic emission transducers and strain gage placed down so that they were located on the tensile surface of the specimen. Major and minor spans for the flexure tests were 0.25 and 0.75 m, respectively. After placing in the fixture, amplifier gains for the acoustic emission transducers were adjusted as described previously (gains for the transducers were 91 and 92 dB), load and strain outputs were zeroed and calibrated, and the acoustic emission system was programmed for one-dimensional source location. The specimens were then loaded in flexure to failure with stress-strain and acoustic emission data obtained throughout loading. Stress-strain curves obtained for all the flexure specimens were essentially linear up to failure. As a result,

acoustic emission activity was absent until just prior to failure, when a few (<10) events occurred.

Monitoring of prestressed concrete beam members. The composite behavior of the concrete prestressing strand material system that made up the posttensioned grouted and nongrouted beam structural models described in Section 3.1 was also investigated with acoustic emission. Selected beams of the grouted-nongrouted tendon test series were monitored by acoustic emission as they were tested to failure. Specimen fabrication and testing procedures were as described earlier, except for inclusion of acoustic emission monitoring. Prior to testing, six 50-kHz acoustic emission transducers were attached to the bottom surface of the beam to be tested. Two were attached near the major span reaction points and used as slave transducers to lock out localized reaction noises. The remaining four transducers were spaced at 0.6-m increments to monitor the central 1.80 m of the beam and thus provide data on flexural crack locations. Transducer amplifier gains were adjusted for equal background noise output (as described previously), and the detection threshold voltage was adjusted so that it was approximately 0.4 V above ambient background noise. The acoustic emission system was programmed for one-dimensional source location and the beam loaded in flexure to failure with acoustic emission source location data obtained throughout the test. Figure 104 presents the acoustic emission grouted-nongrouted tendon beam test setup.

Seventeen of the grouted and nongrouted tendon beams were monitored by acoustic emission while they were tested to failure.* Because the results are too voluminous to be contained in this report, only results from one grouted tendon and one nongrouted tendon beam, which are typical of the other results obtained, will be presented. Figures 105 and 106

---

*One of these beams containing a grouted tendon was fabricated in which a 0.15-m length of tendon in the constant-moment region of the beam was deliberately unbonded by coating it with grease and wrapping it with electrician's tape prior to grouting. It was hoped that acoustic emission might provide a technique of locating voids or regions of unbonding in grouted tendon elements; however, during grouting, the grout pressure was apparently sufficient to force the tape to one end of the beam so that the beam acted as a continuously grouted beam. Tape location was verified by sawing the beam after testing.

present typical acoustic emission data in the form of event activity as a function of location along the length of the beam for a nongrouted and grouted tendon beam, respectively. Superimposed above the acoustic emission activity plots are photographs of the beams after testing so that the agreement between crack locations and acoustic emission active areas may be noted. Results indicate that, for nongrouted tendon beams where only one or two major cracks occurred during testing to failure, acoustic-emission-determined crack locations and actual crack locations correlated very well. In grouted tendon beams tested to failure, four or more major cracks generally formed, and the correlation between acoustic-emission-identified crack locations and actual crack locations was not as definite. (Locational accuracy of the first crack in the beam was accurate, but the accuracy decreased as more cracks formed.) This "smearing" of acoustic emission active regions was related to development of several cracks so that a source-initiated stress wave had to travel around cracks to go from transducer to transducer, as required for source location, and, as noted in Fig. 106, the initial main cracks branched and propagated horizontally as the cracking matured.

3.5 Groutability of Large Posttensioned Prestressing Tendon Systems

The preliminary test plan initially proposed that two full-scale static-flexure tests be conducted using beams 0.36 m wide by 0.81 m deep by 12.19 m long. Prestressing contained in the beams was to have been thirty-eight 6.35-mm-diam grade 240 wires. One beam was to contain a nongrouted tendon and the second a grouted tendon. The purpose of the test was to provide information on both the groutability of large tendon systems and relative behavior of grouted and nongrouted beams containing a more representative prestressing material. Analysis results contained in Appendix A indicate that performance would be merely a scaled-up version of that obtained from the 0.15-m by 0.30-m by 3.1-m beam models previously investigated and that fabrication and testing of such large elements would be very difficult and costly. In addition, the prestressing system, which was sized so that testing could be conducted in the

laboratory, was still not representative of the large tendon prestressing systems such as listed in Table 1, which are of the type presently considered for PCPV fabrication. Groutability thus remains the primary question on large tendon prestressing systems.

Two primary problem areas encountered in the grouting of large tendon systems are (1) ensuring there is complete encapsulation by grout* of the prestressing at locations of sharp curvature where tendons have a tendency to bunch and (2) bleeding of the grout mix water to produce sedimentation. To provide insight into these problems, extensive groutability studies were conducted in conjunction with the Oyster Creek Nuclear Electric Generating Station[4] and the Robinson Nuclear Power Plant.[24]

The objective of the Oyster Creek test program was to demonstrate conclusively if normal grouting procedures would be effective in achieving penetration of grout into a packed group of tendon elements at the inside radius of the duct for a curved tendon. If the normal grouting procedures were not satisfactory, then effective grouting procedures were to be developed. Reproducibility of results for field applications was also to be demonstrated. To accomplish this objective, a variety of prestressing systems (BBR, Freyssinet, SEEE, VSL, and WCS) was employed in a test structure designed to simulate a tendon draped around a 6.1-m-radius equipment hatch. Test results indicate that normal grouting procedures are effective in grouting strand tendons but special techniques are required for parallel-wire tendons to ensure effective grout penetration. Reproducibility of effective grouting was demonstrated for the strand tendons.

In the early stages of grout consideration for the Robinson Nuclear Power Plant, it was noted that sedimentation of the cement grout could produce free water at the top of the tendon conduit to a depth in the vicinity of 1/2 to 1% of its height.[25] To eliminate this bleed phenomenon, admixtures were added to the grout and grouting procedures were investigated. Using an admixture containing a water reducer, gelling

---

*Whether or not complete encapsulation with continuous contact is required is a subject of debate.

agent, and an expansive agent and using procedures developed, it was demonstrated that a 42-m-high tendon can be effectively grouted with no detrimental sedimentation.

The groutability of a 54-m-long vertical tendon consisting of fifty-four 12.7-mm-diam strands in a 152-mm-diam smooth-wall heavy-duty pipe was also investigated in conjunction with the Oyster Creek Nuclear Station. The addition of a grouting aid to the grout enabled the tendon to be successfully grouted. To verify this, one month after testing, the tendon was cut and sectioned to reveal no settlement and an excellent grout material. Thus, with the proper choice of grout aids and procedures, it has been demonstrated that vertical tendons in excess of 50 m high can be successfully grouted without sedimentation problems.

ORNL-DWG 79-4358 ETD

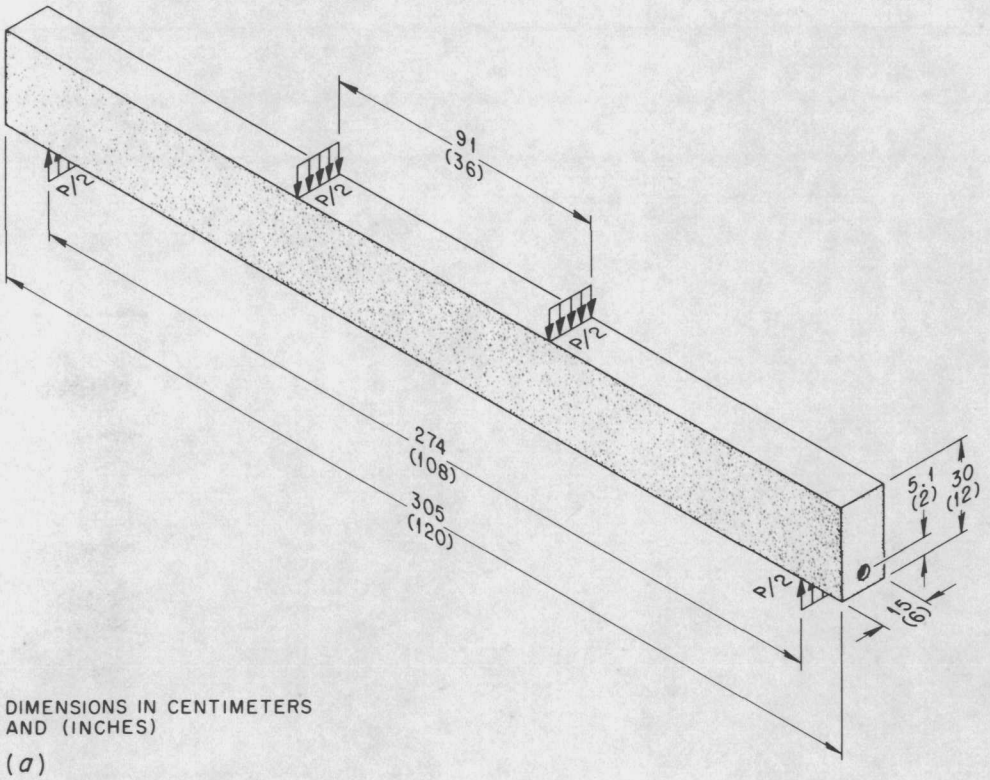

DIMENSIONS IN CENTIMETERS
AND (INCHES)

(*a*)

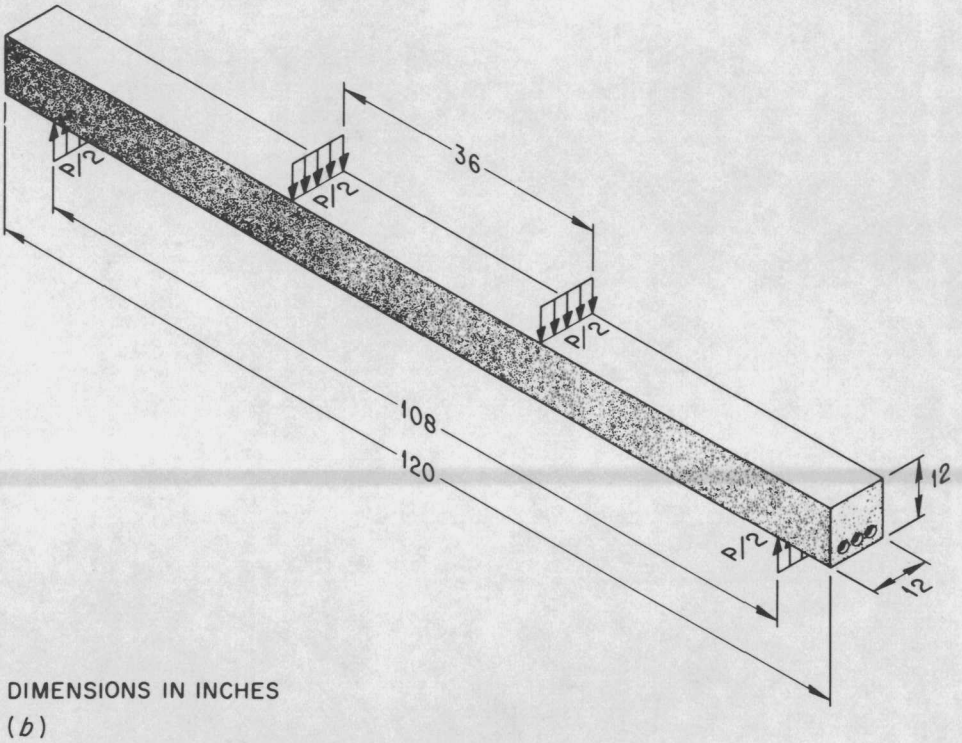

DIMENSIONS IN INCHES

(*b*)

Fig. 1. Flexure test specimen geometries. (a) 0.15 m wide, 0.30 m deep, 3.1 m long; (b) 0.30 m wide, 0.30 m deep, 3.1 m long.

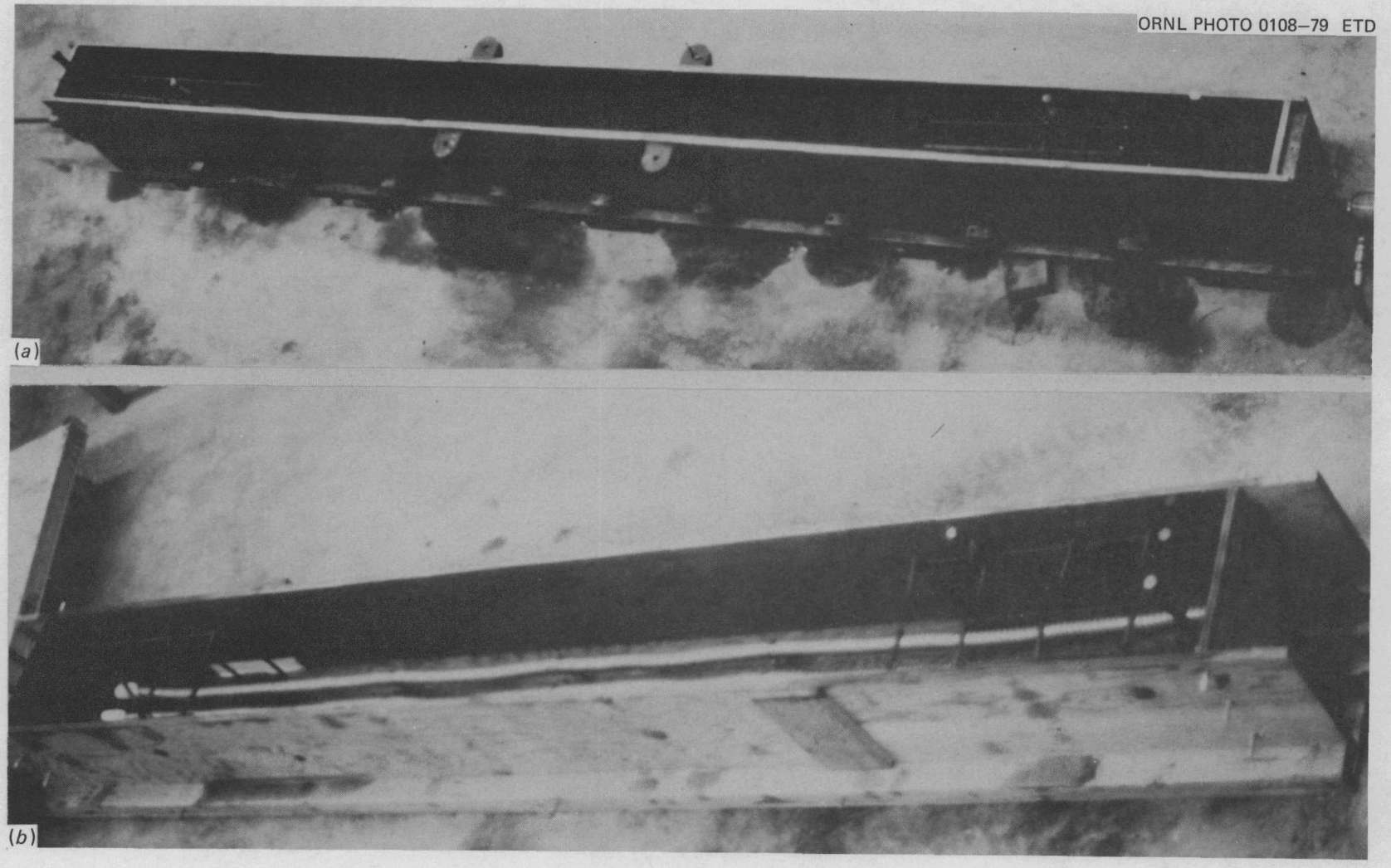

Fig. 2. Molds for flexure specimen fabrication. (a) 0.15-m-wide, 0.30-m-deep, 3.1-m-long specimens; (b) 0.30-m-wide, 0.30-m-deep, 3.1-m-long specimens.

Fig. 3. Concrete mixer.

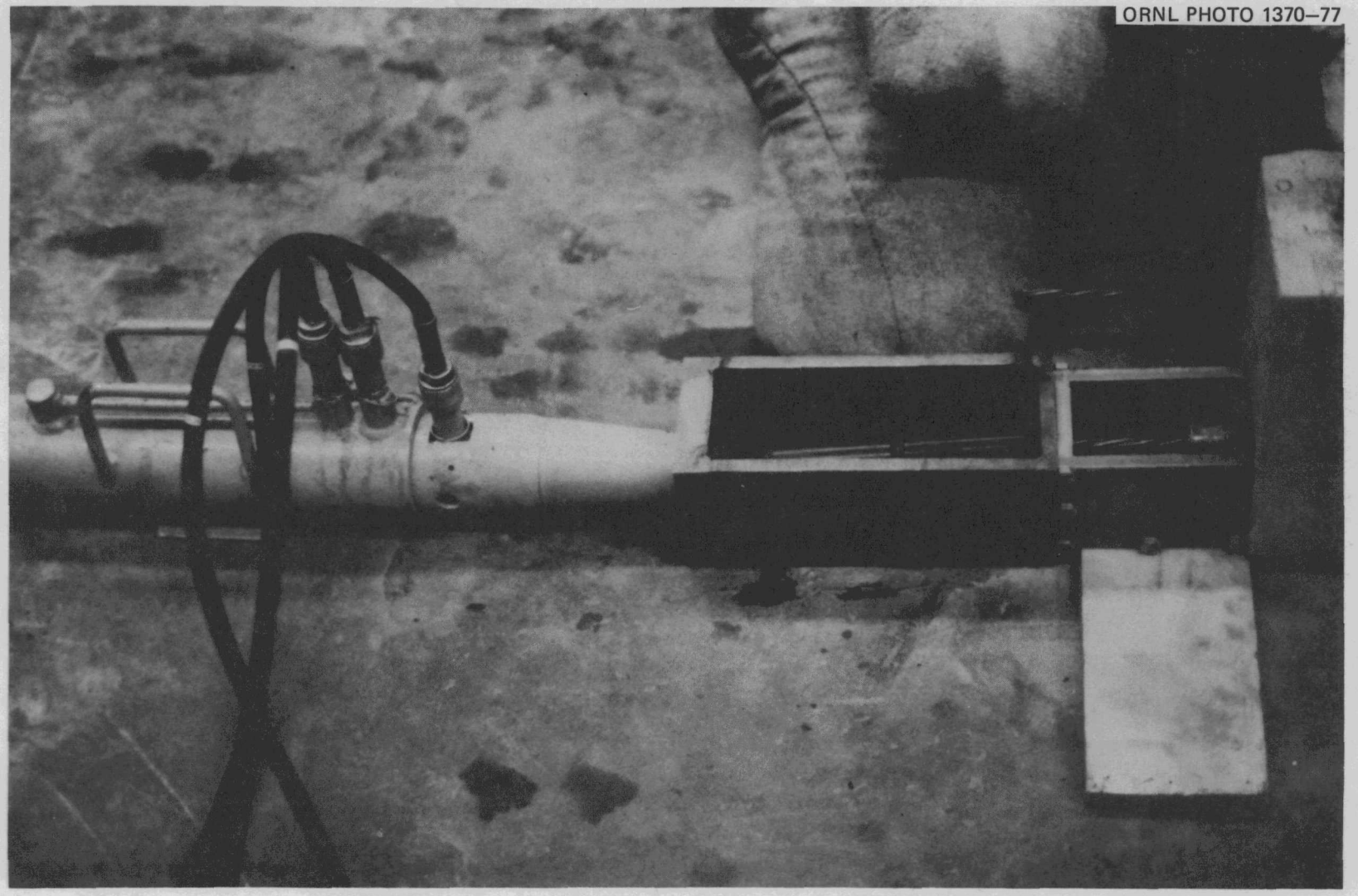

Fig. 4. Prestressing strand posttensioning setup.

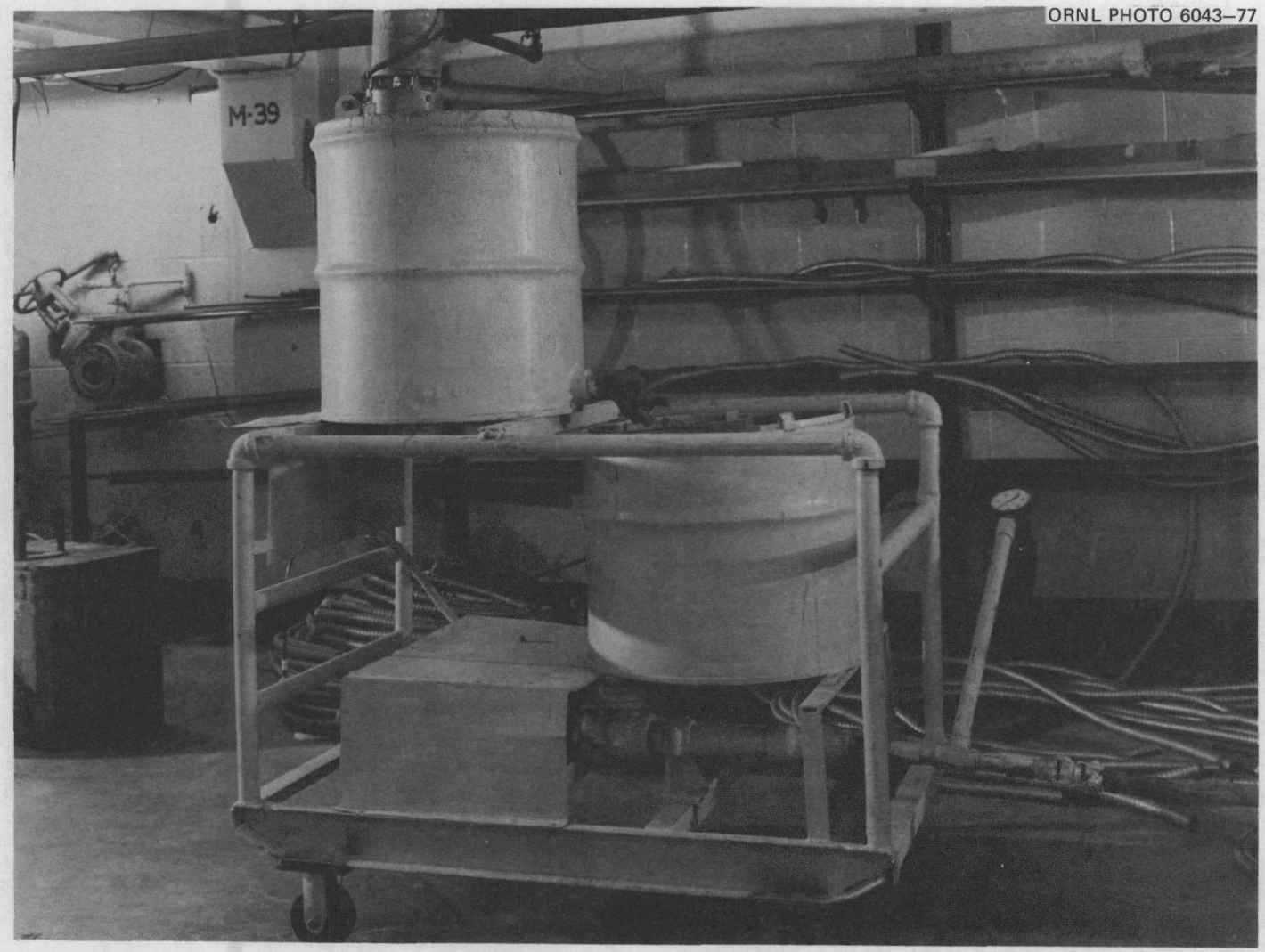

Fig. 5. Grout pump.

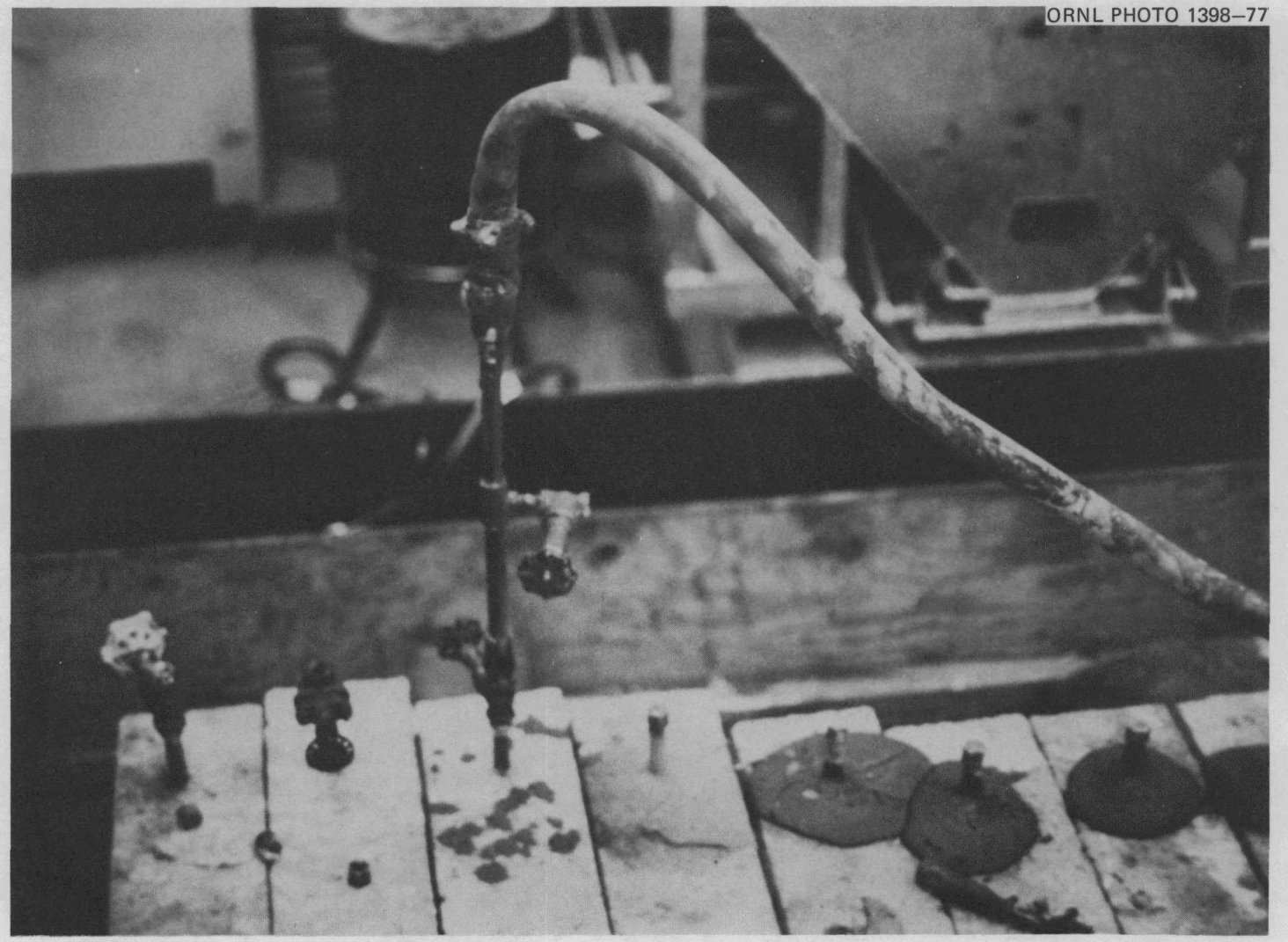

Fig. 6. Grouting of prestressed concrete beam.

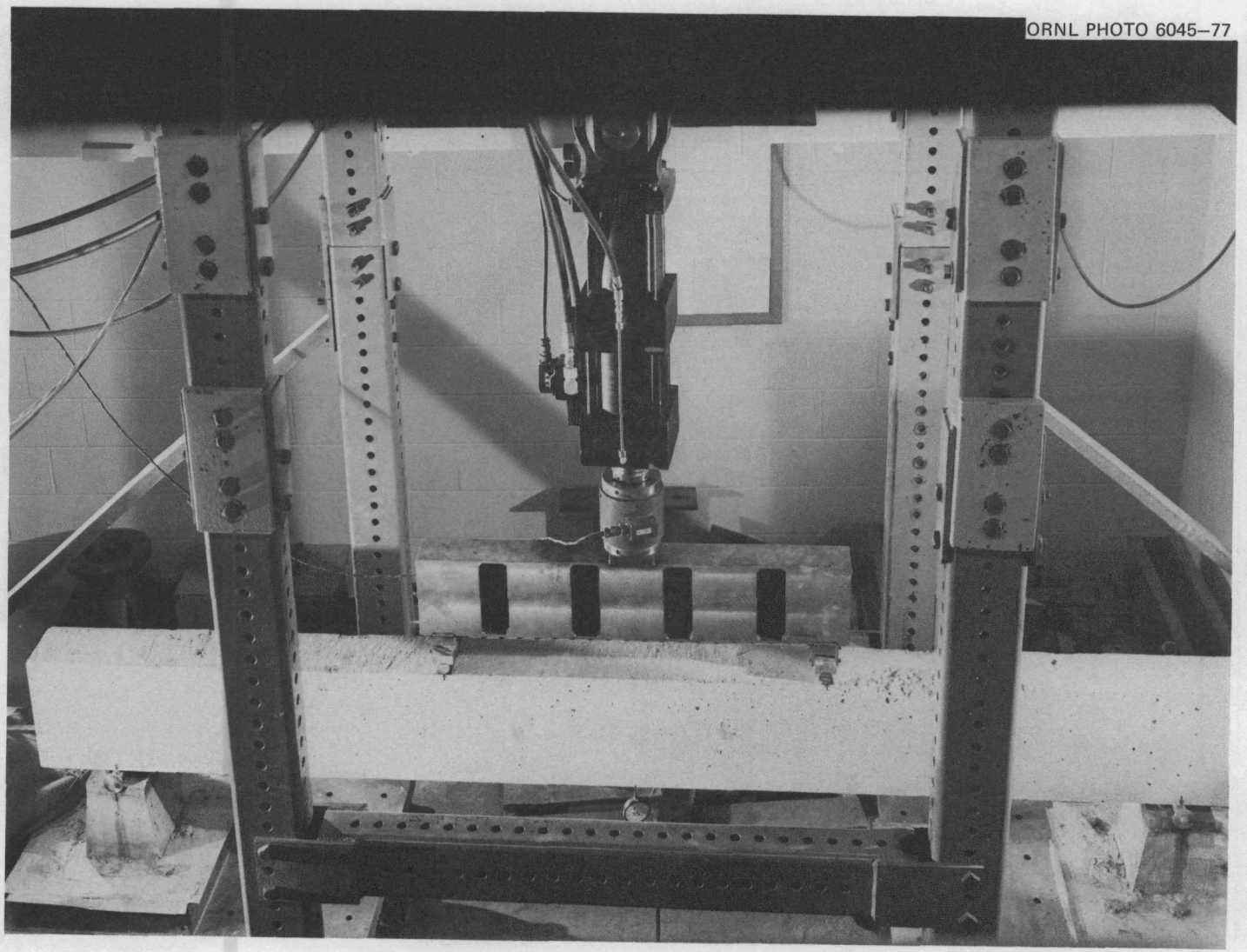

Fig. 7. Flexure test setup.

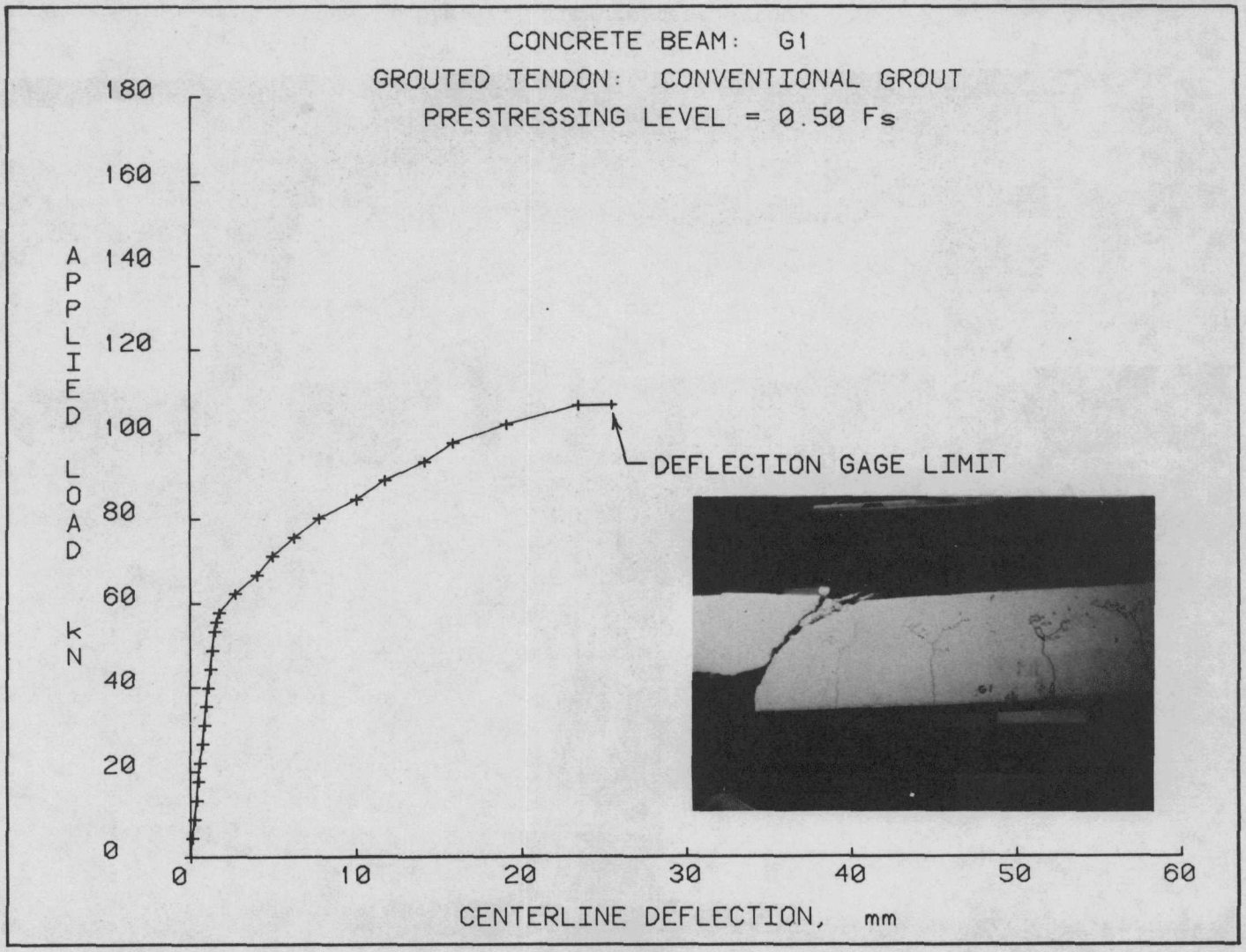

Fig. 8. Load vs centerline deflection — Beam G1.

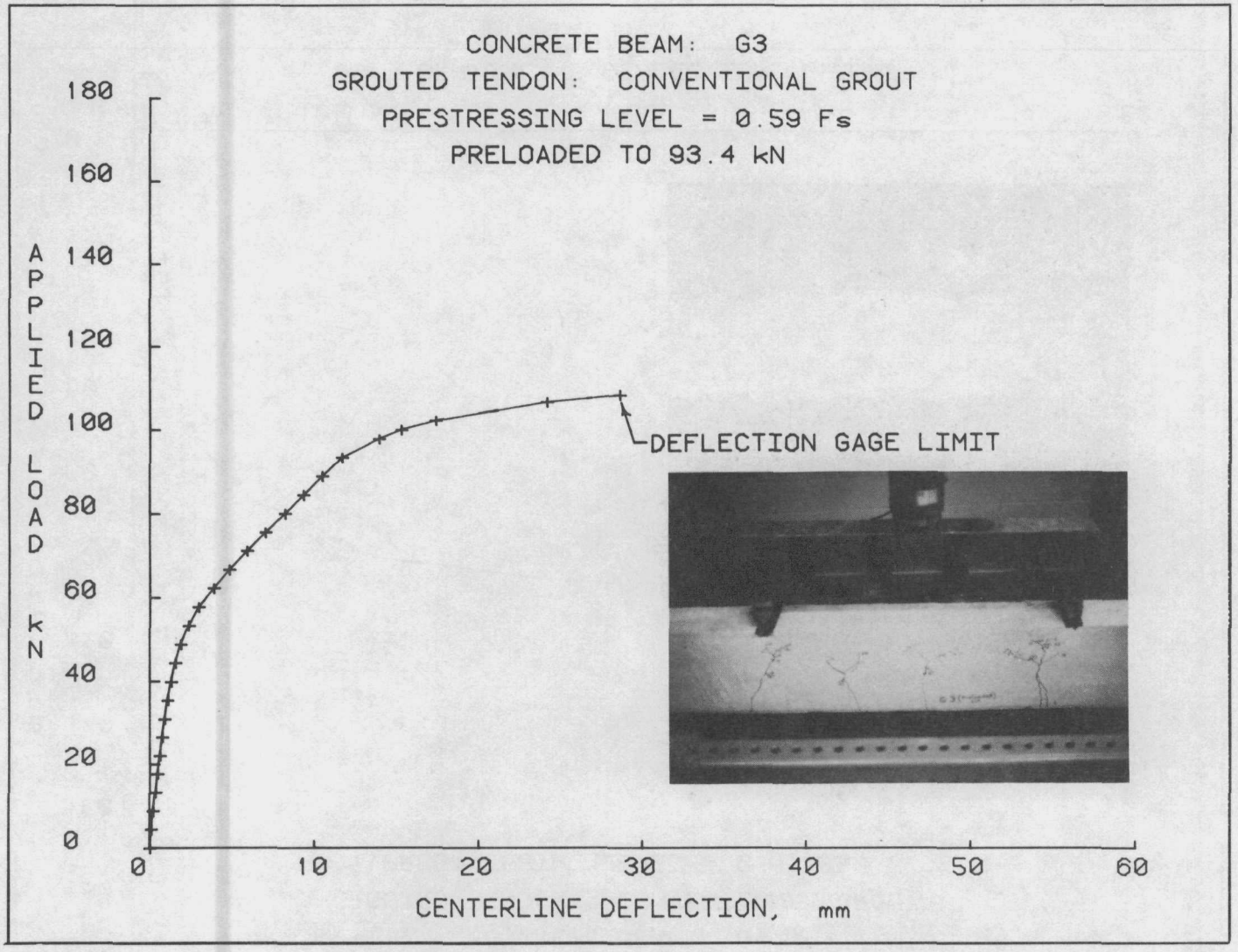

Fig. 9. Load vs centerline deflection — Beam G3.

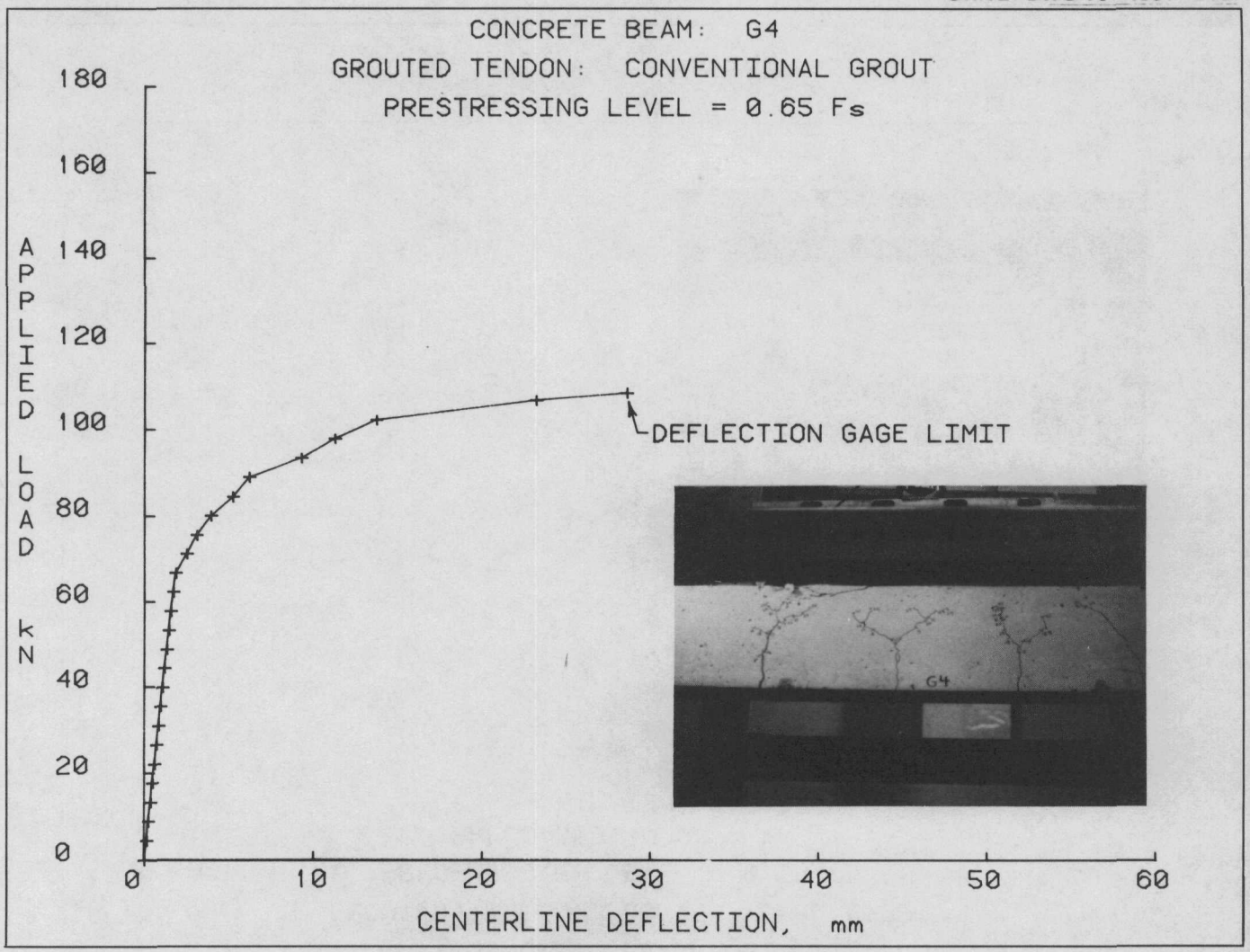

Fig. 10. Load vs centerline deflection — Beam G4.

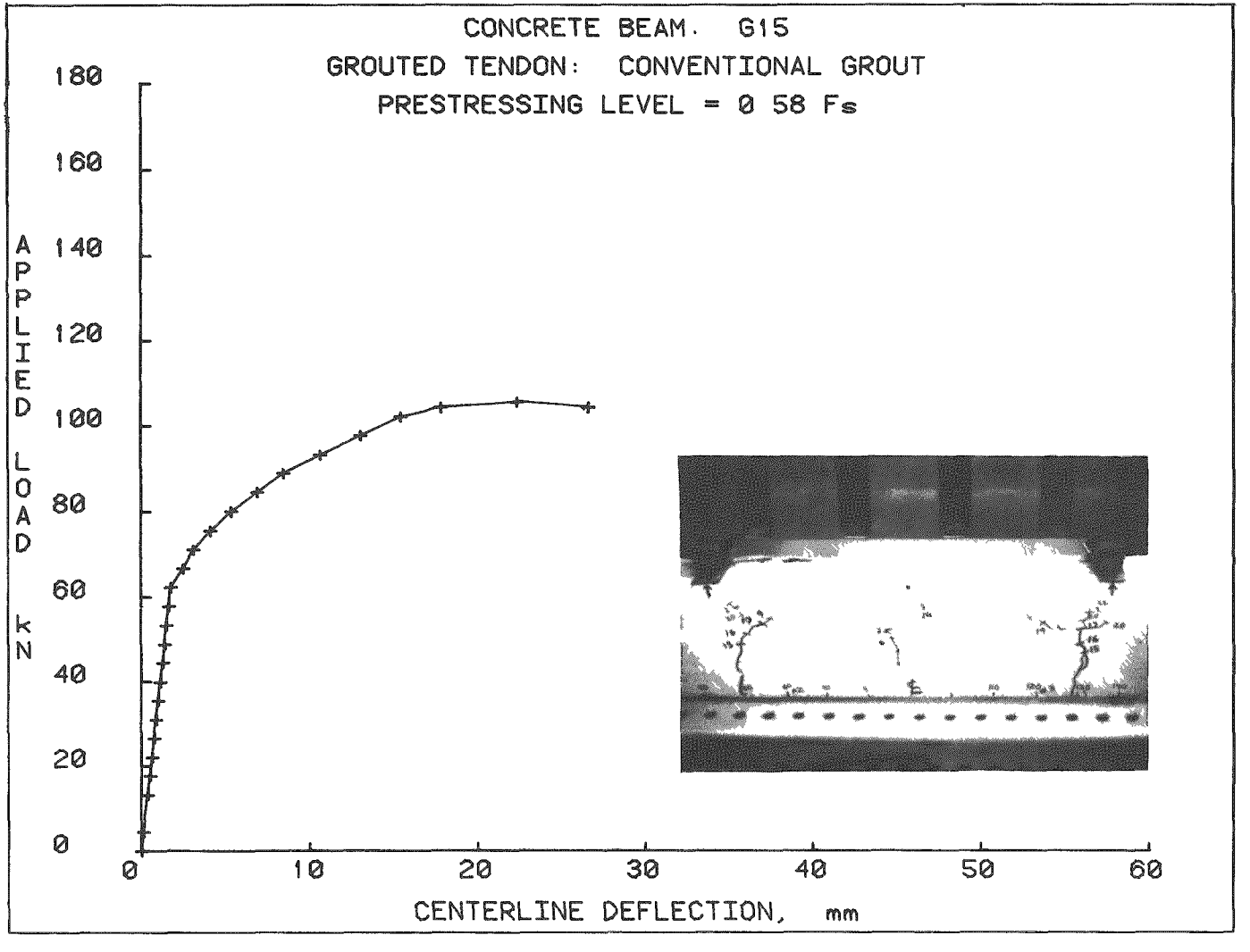

Fig. 11. Load vs centerline deflection — Beam G15.

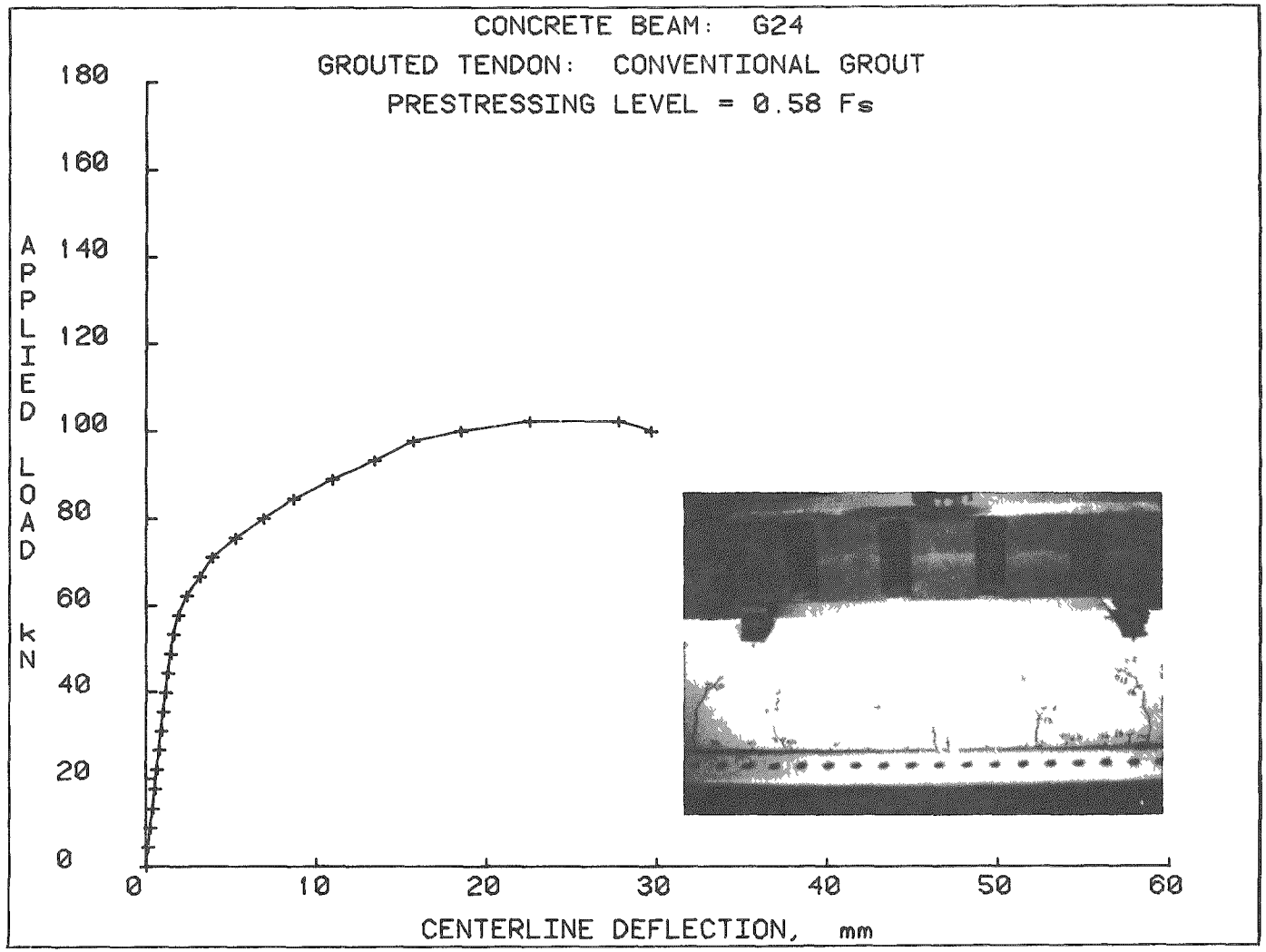

Fig. 12. Load vs centerline deflection — Beam G24.

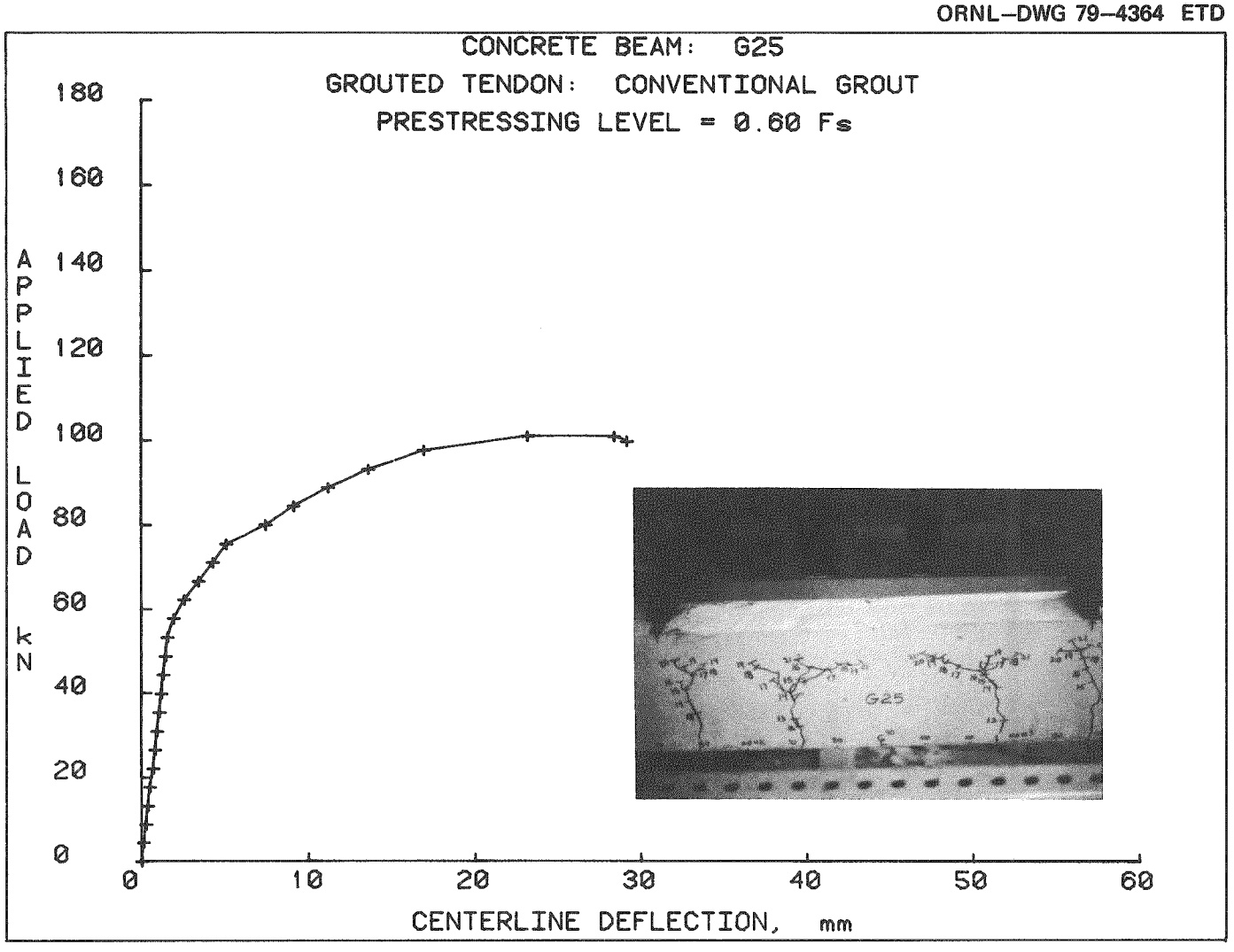

Fig. 13. Load vs centerline deflection — Beam G25.

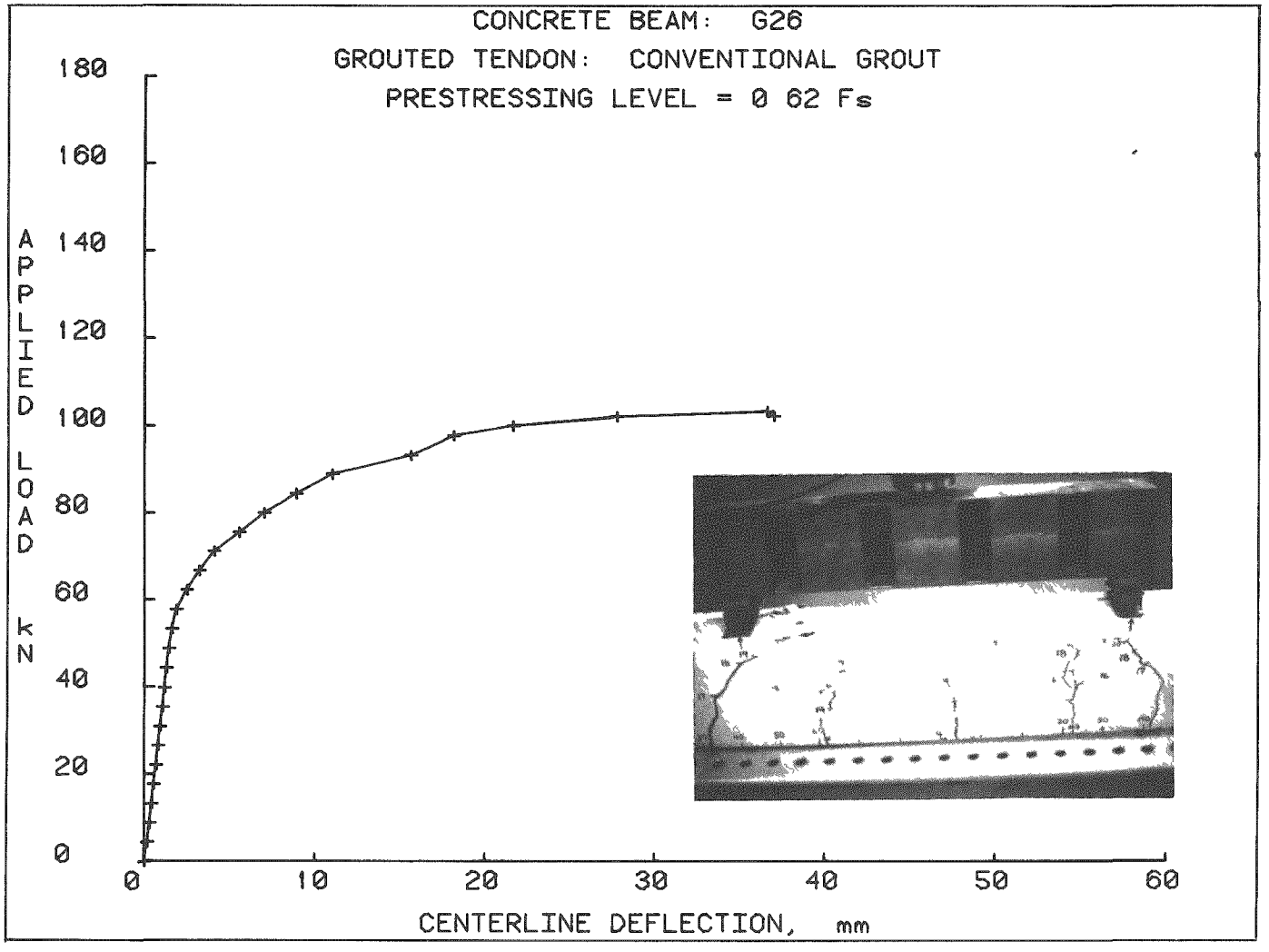

Fig. 14. Load vs centerline deflection — Beam G26.

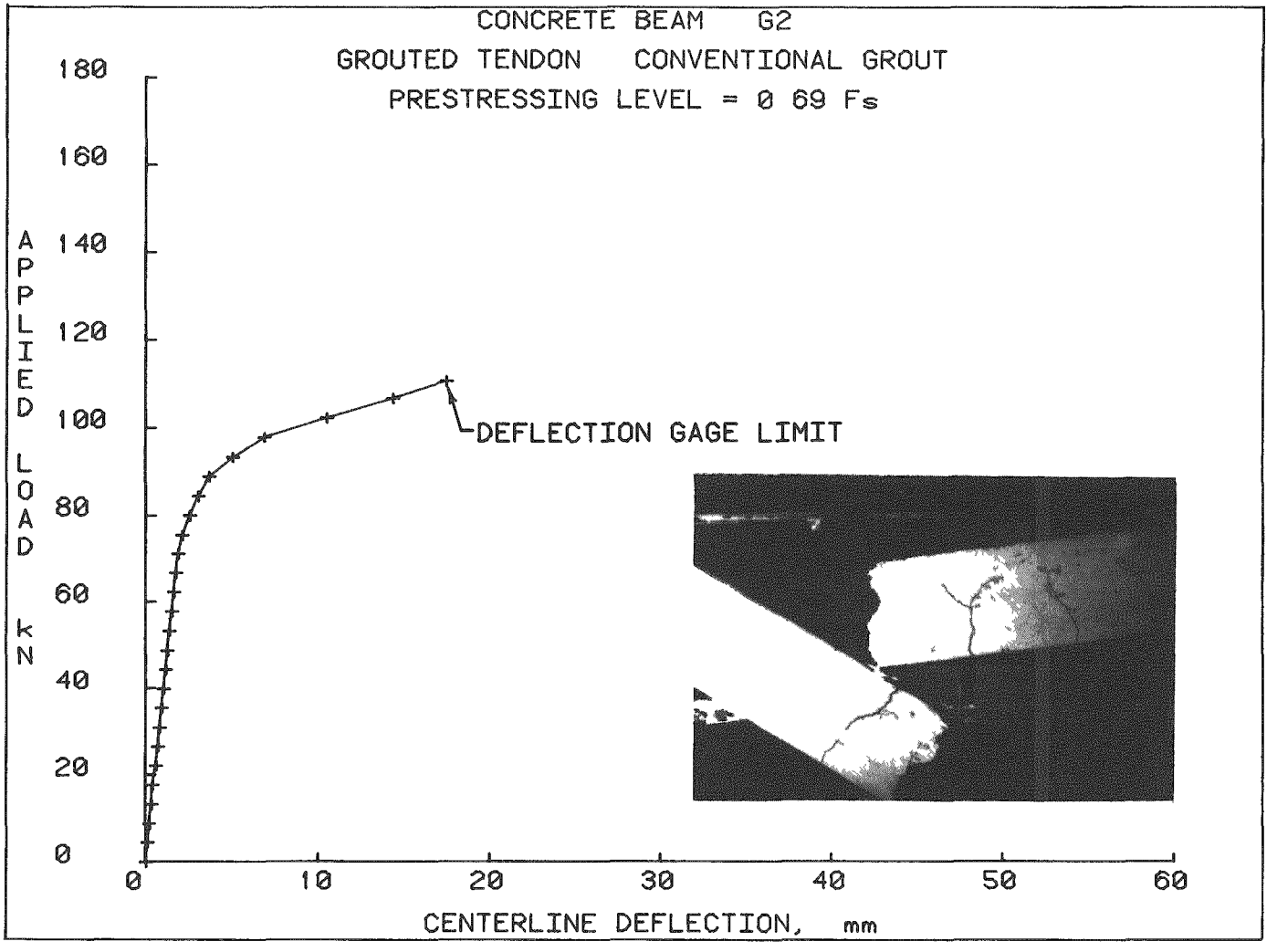

Fig. 15. Load vs centerline deflection — Beam G2.

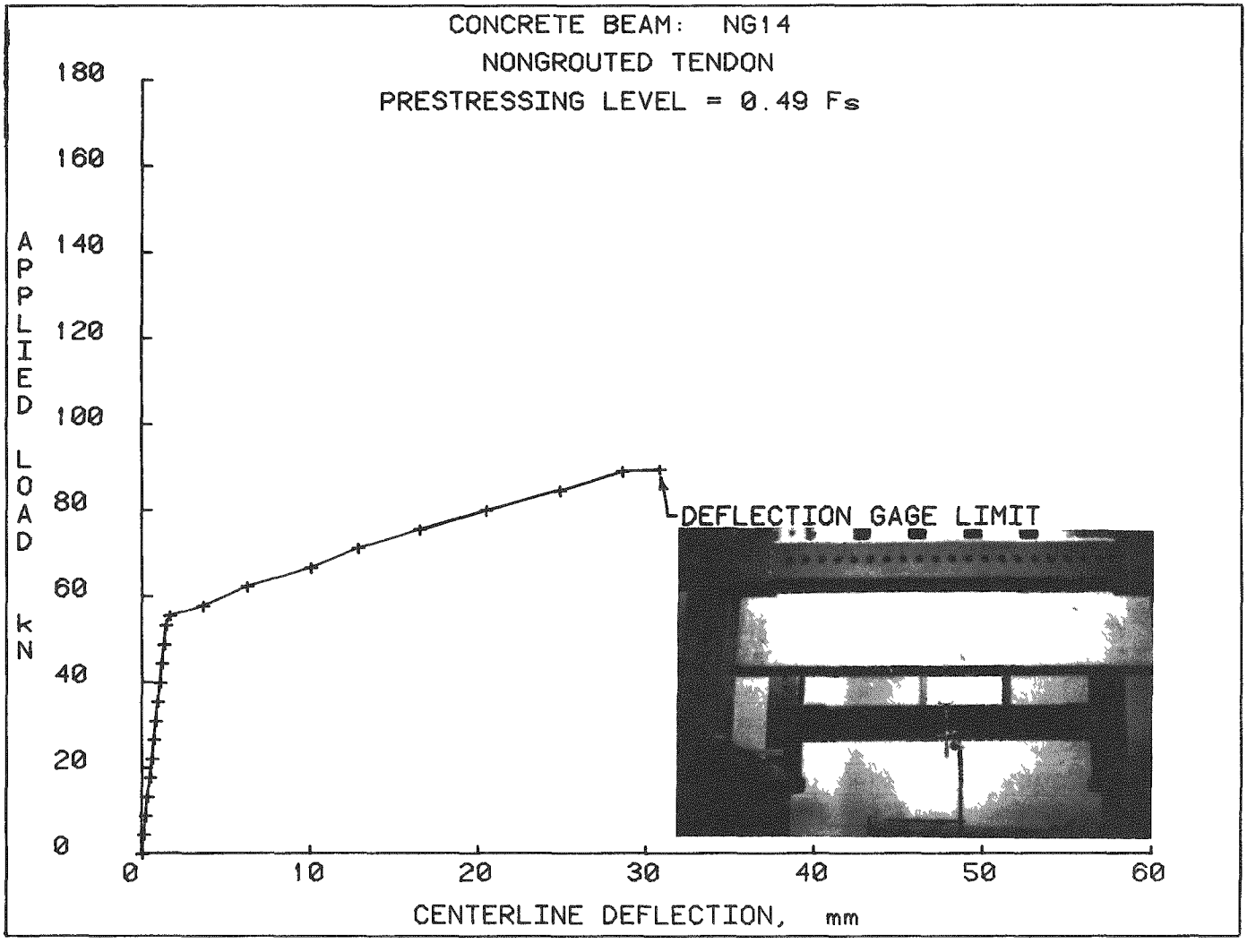

Fig. 16. Load vs centerline deflection — Beam NG14.

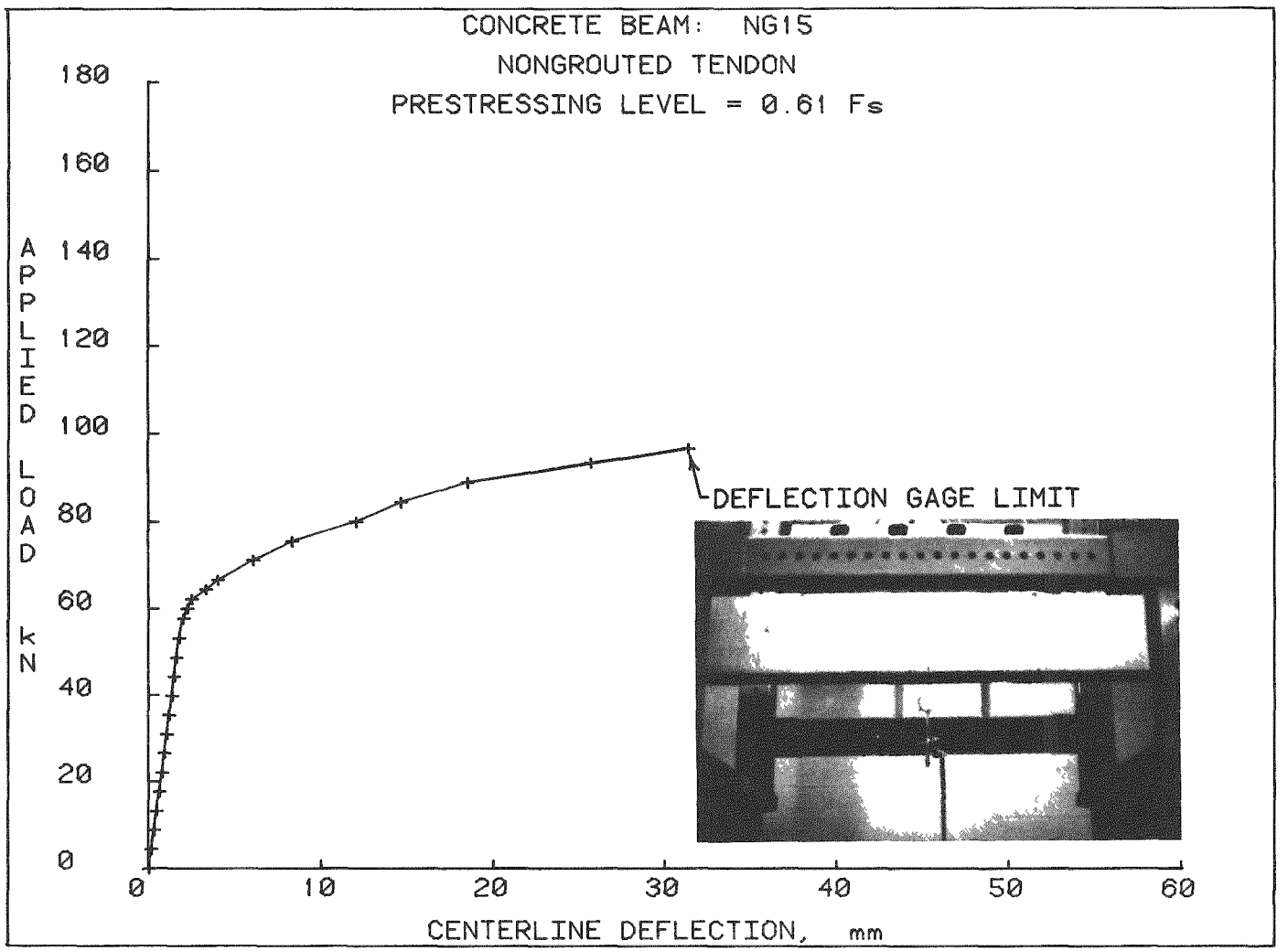

Fig. 17. Load vs centerline deflection — Beam NG15.

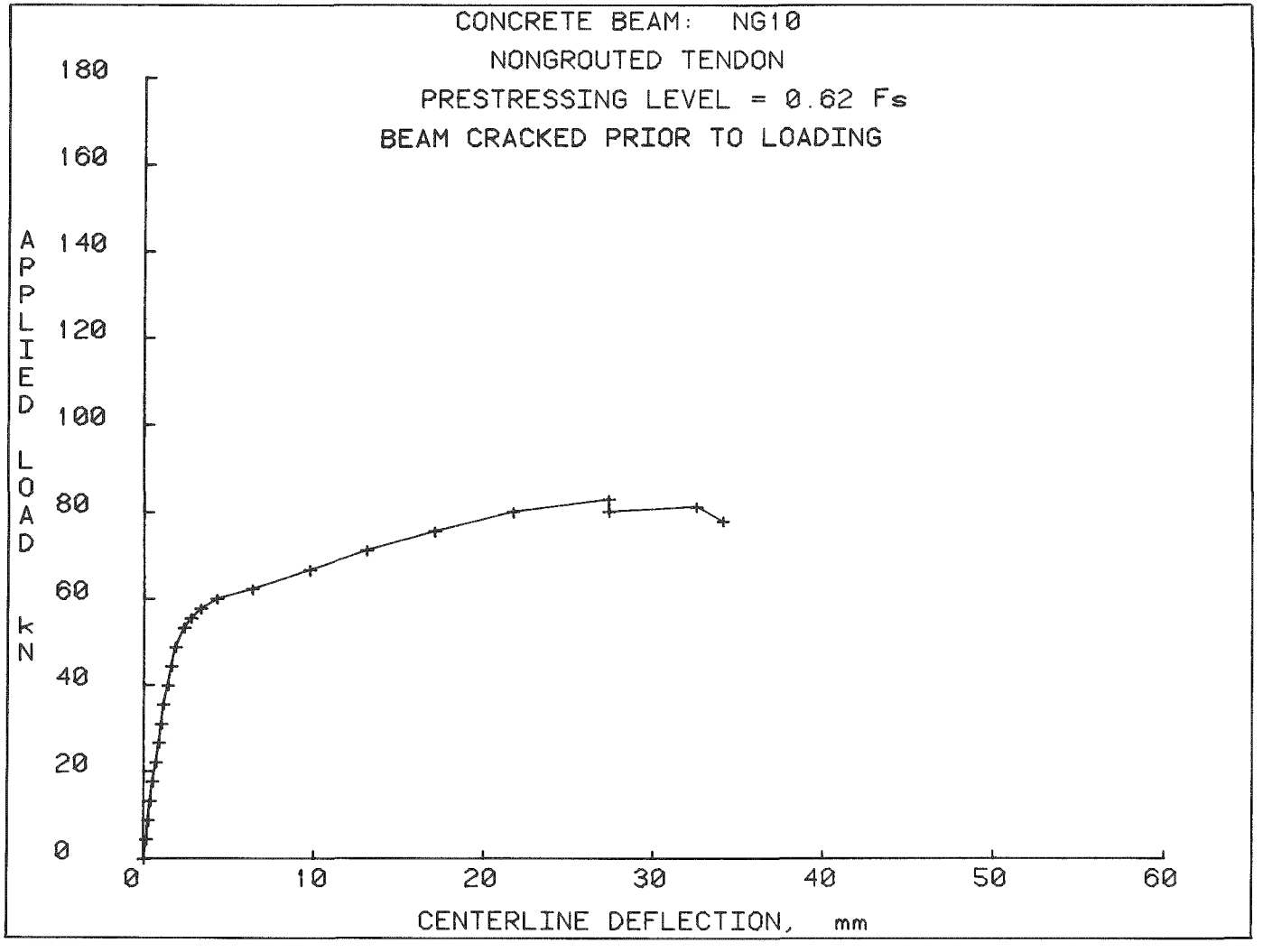

Fig. 18. Load vs centerline deflection — Beam NG10.

ORNL–DWG 79–4370 ETD

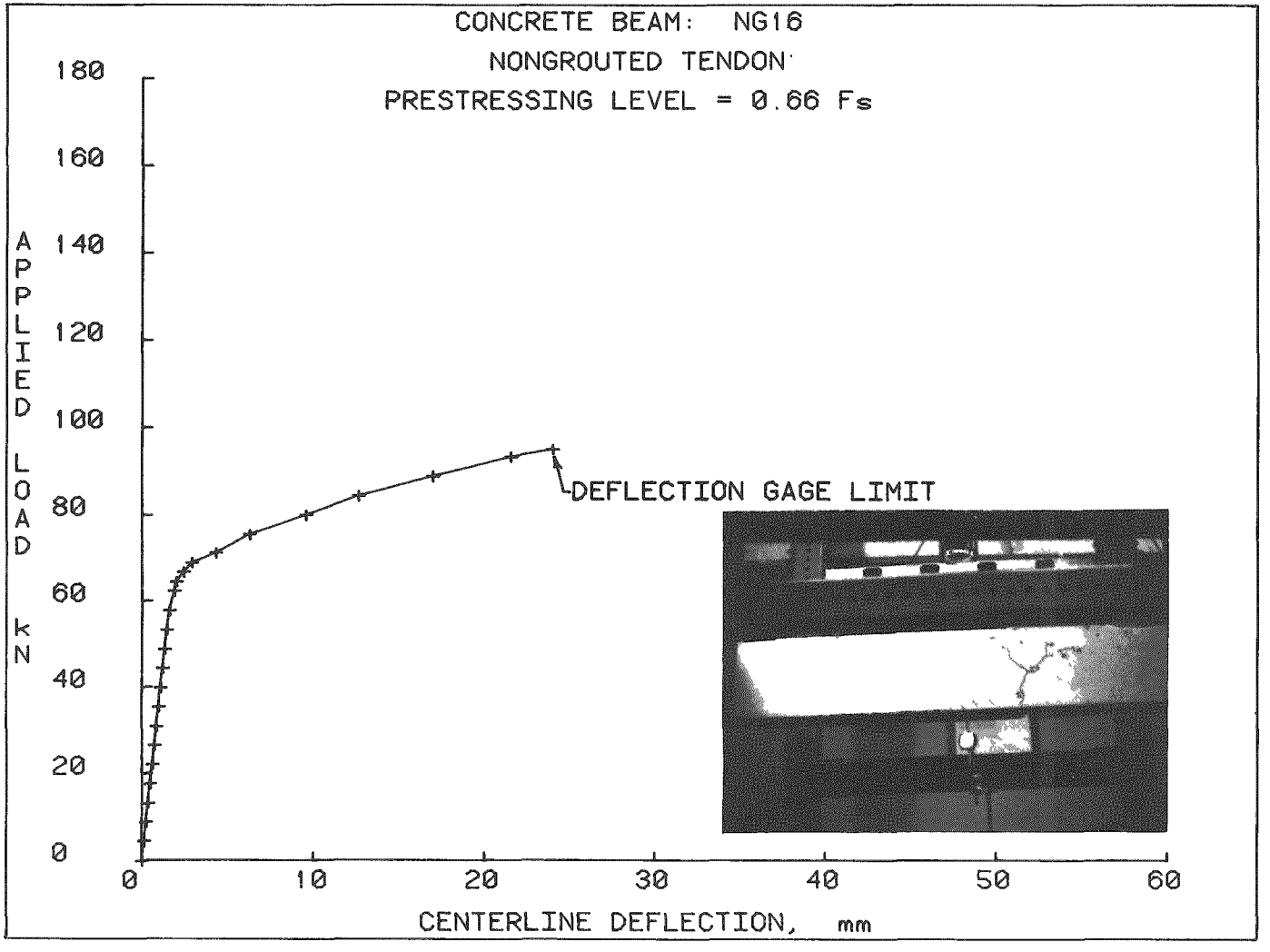

Fig. 19. Load vs centerline deflection — Beam NG16.

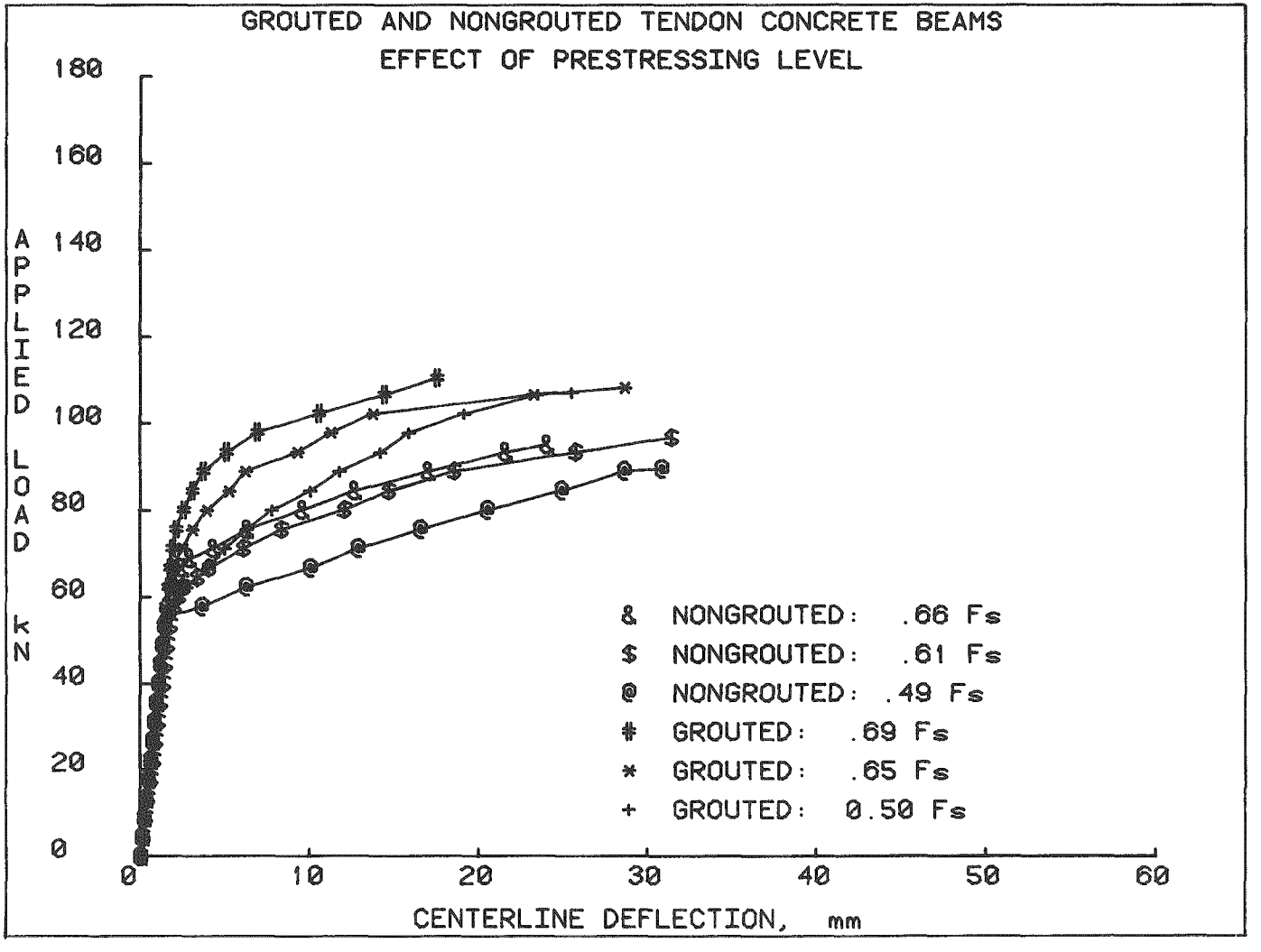

Fig. 20. Effect of prestressing level on beam performance.

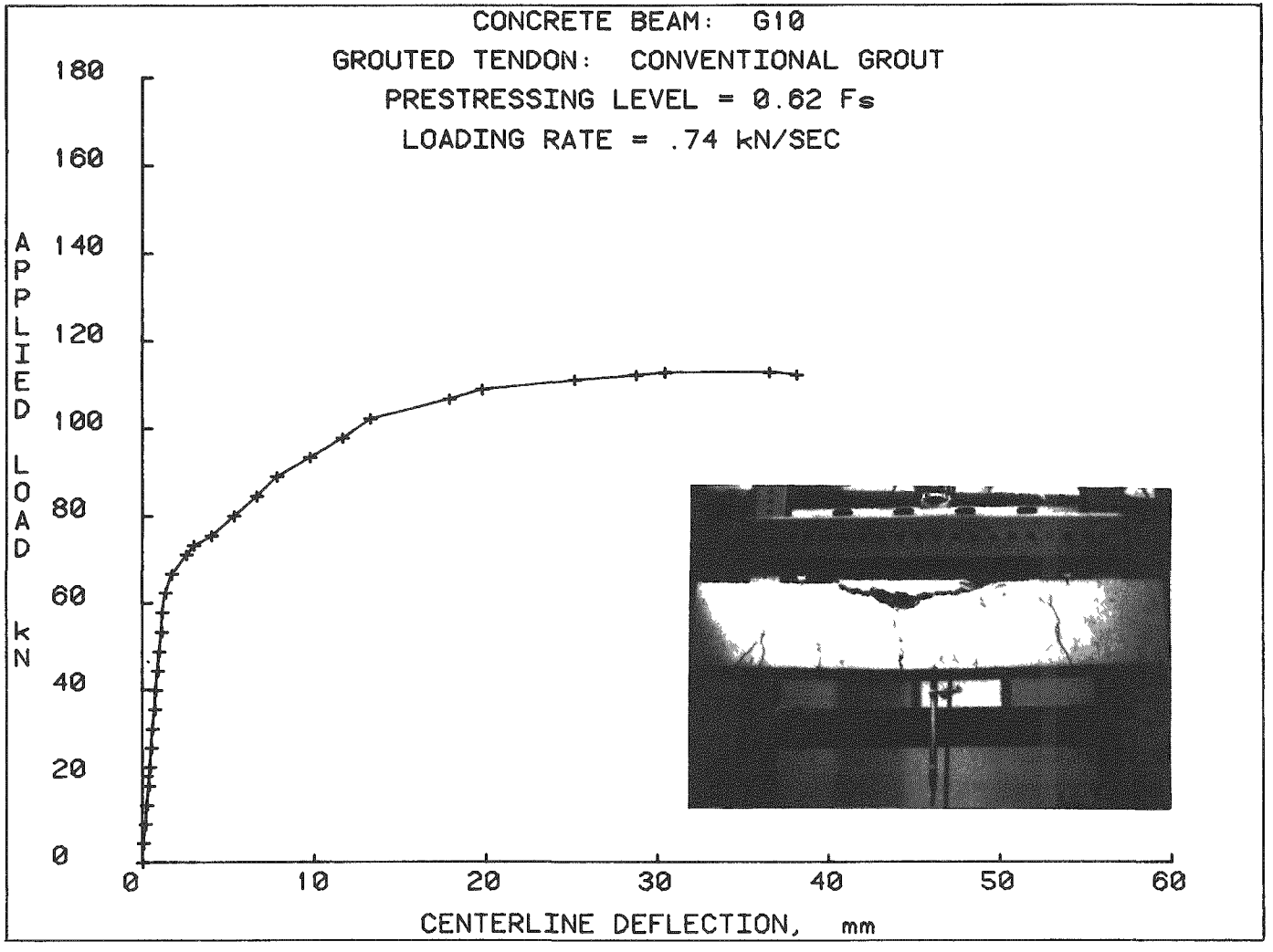

Fig. 21. Load vs centerline deflection — Beam G10.

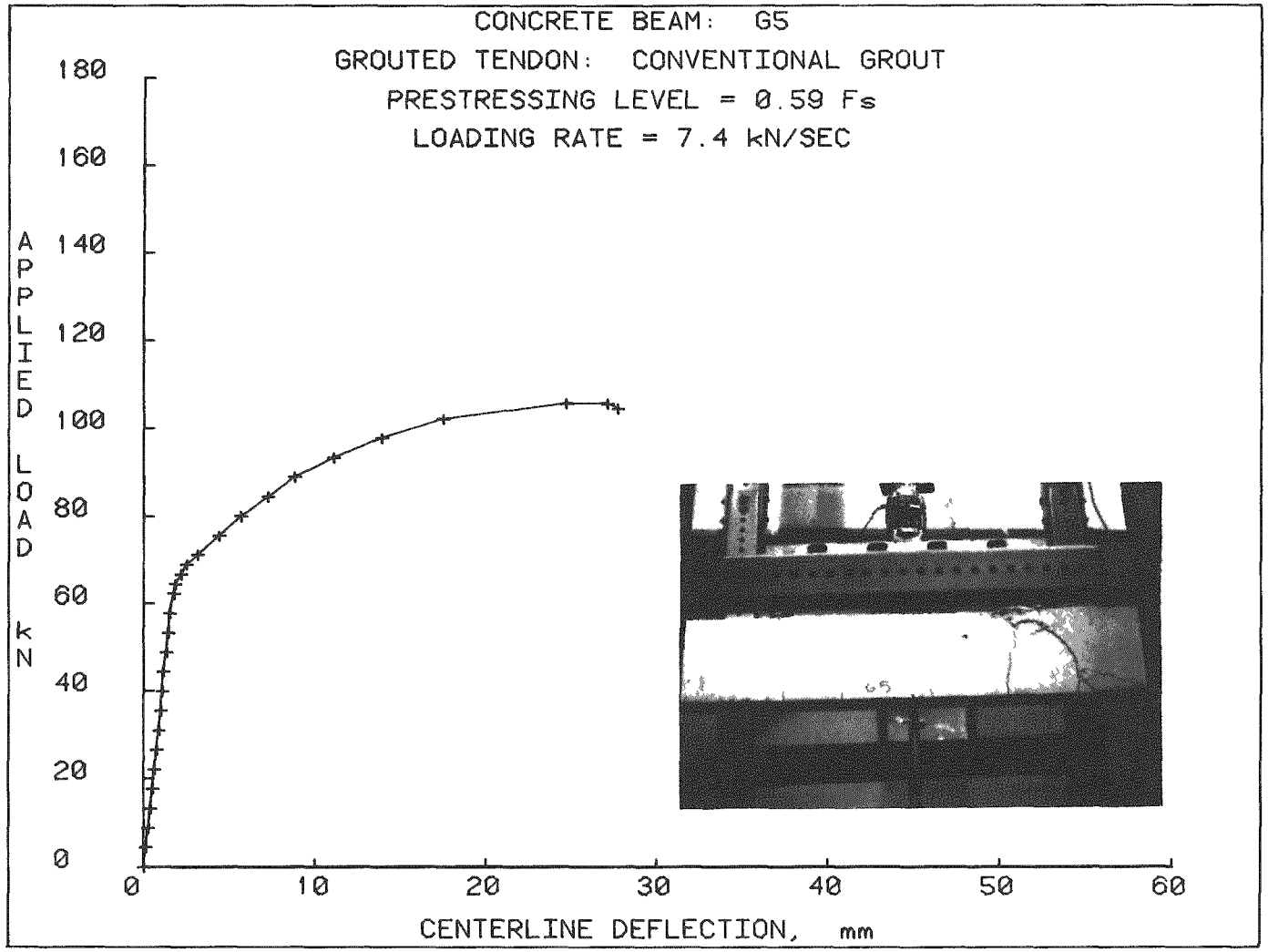

Fig. 22. Load vs centerline deflection — Beam G5.

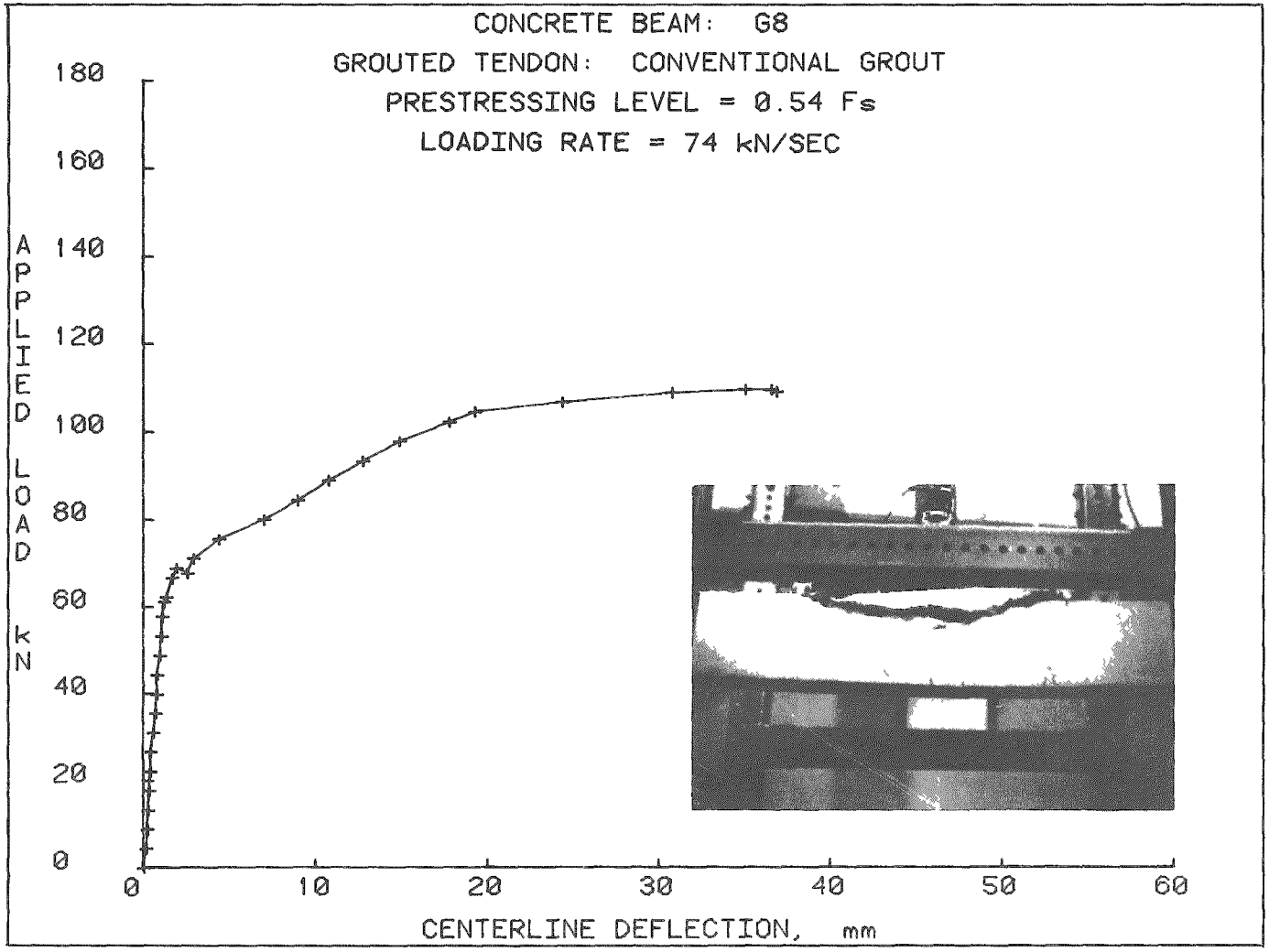

Fig. 23. Load vs centerline deflection — Beam G8.

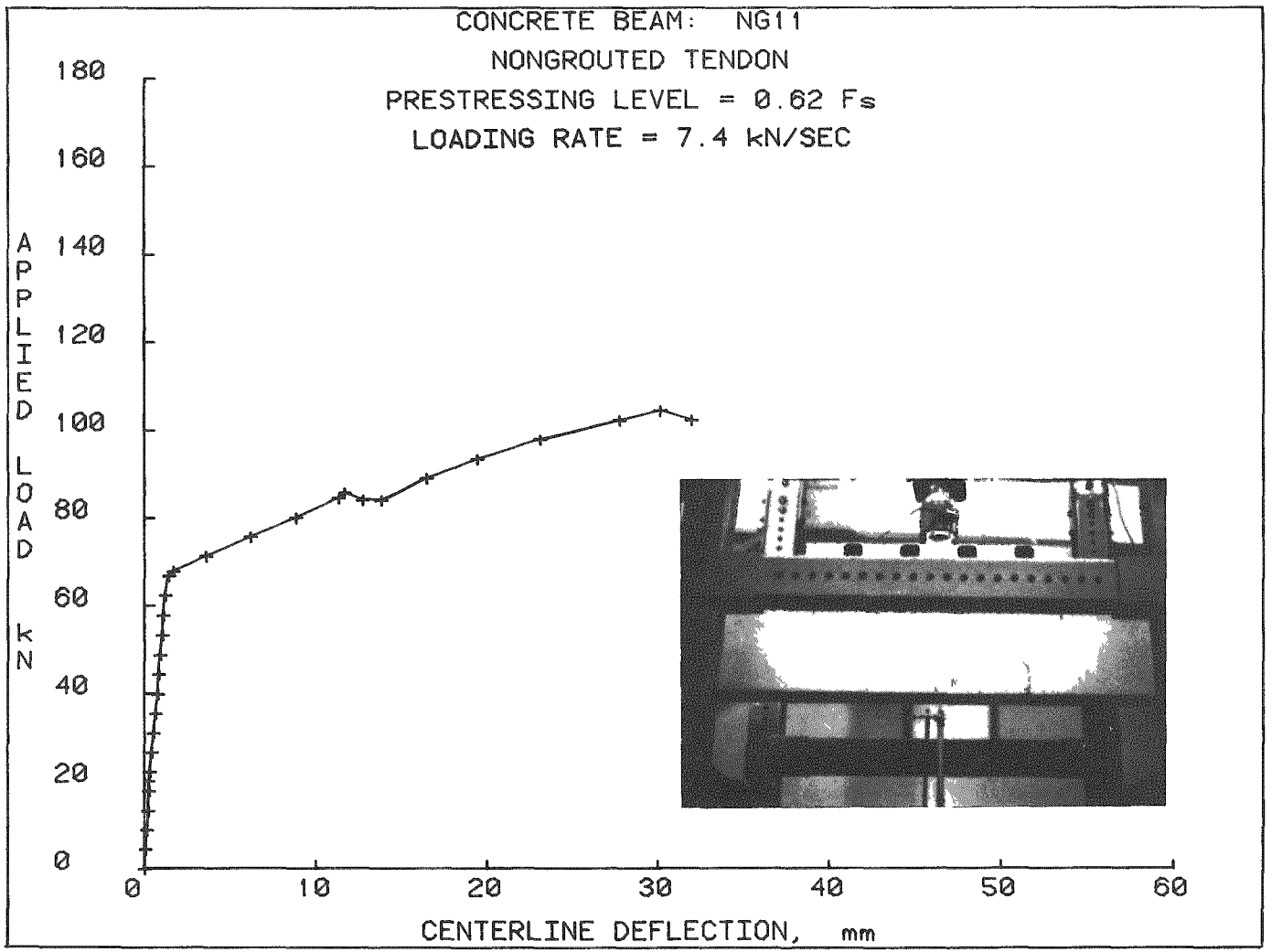

Fig. 24. Load vs centerline deflection — Beam NG11.

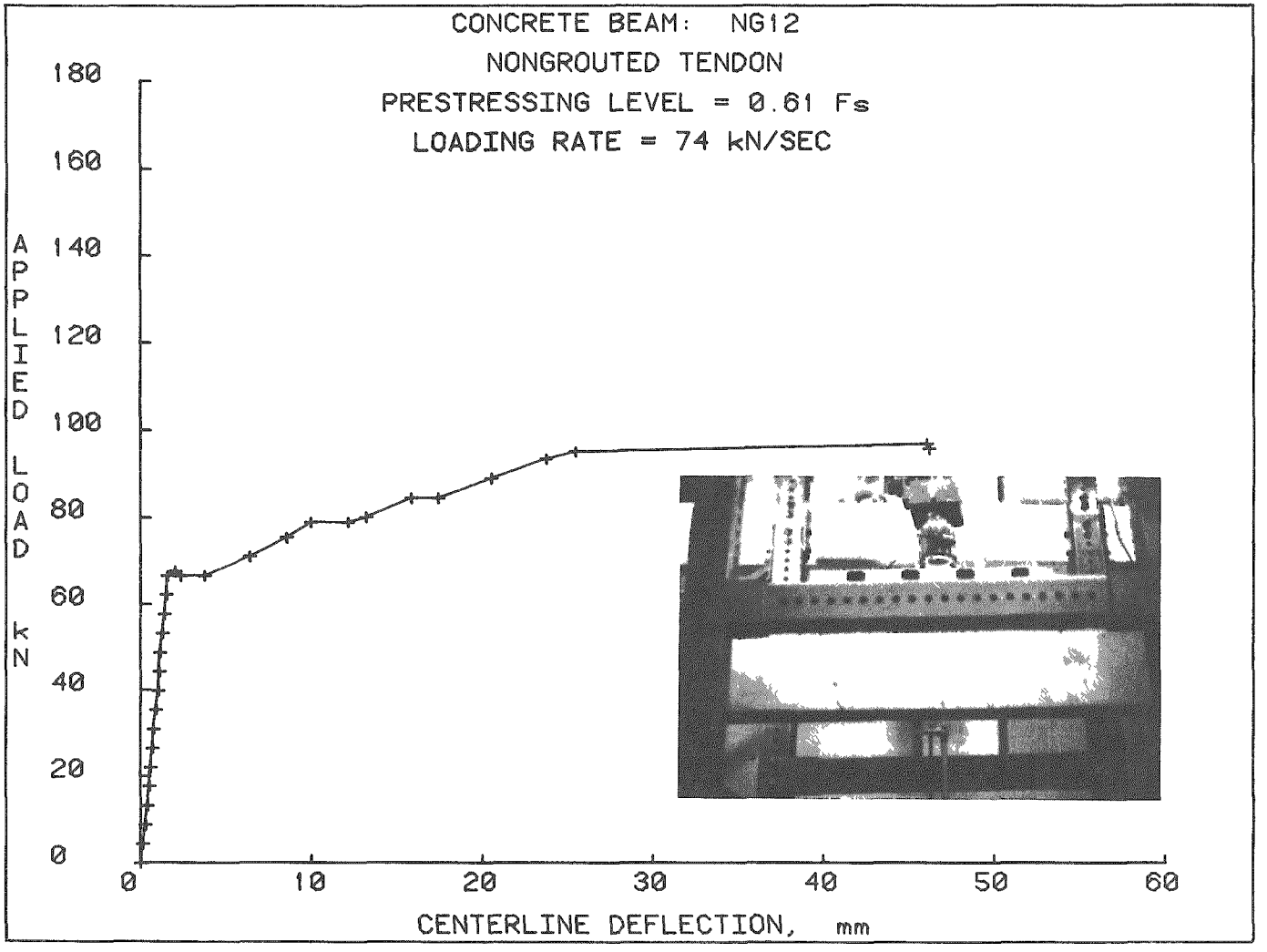

Fig. 25. Load vs centerline deflection — Beam NG12.

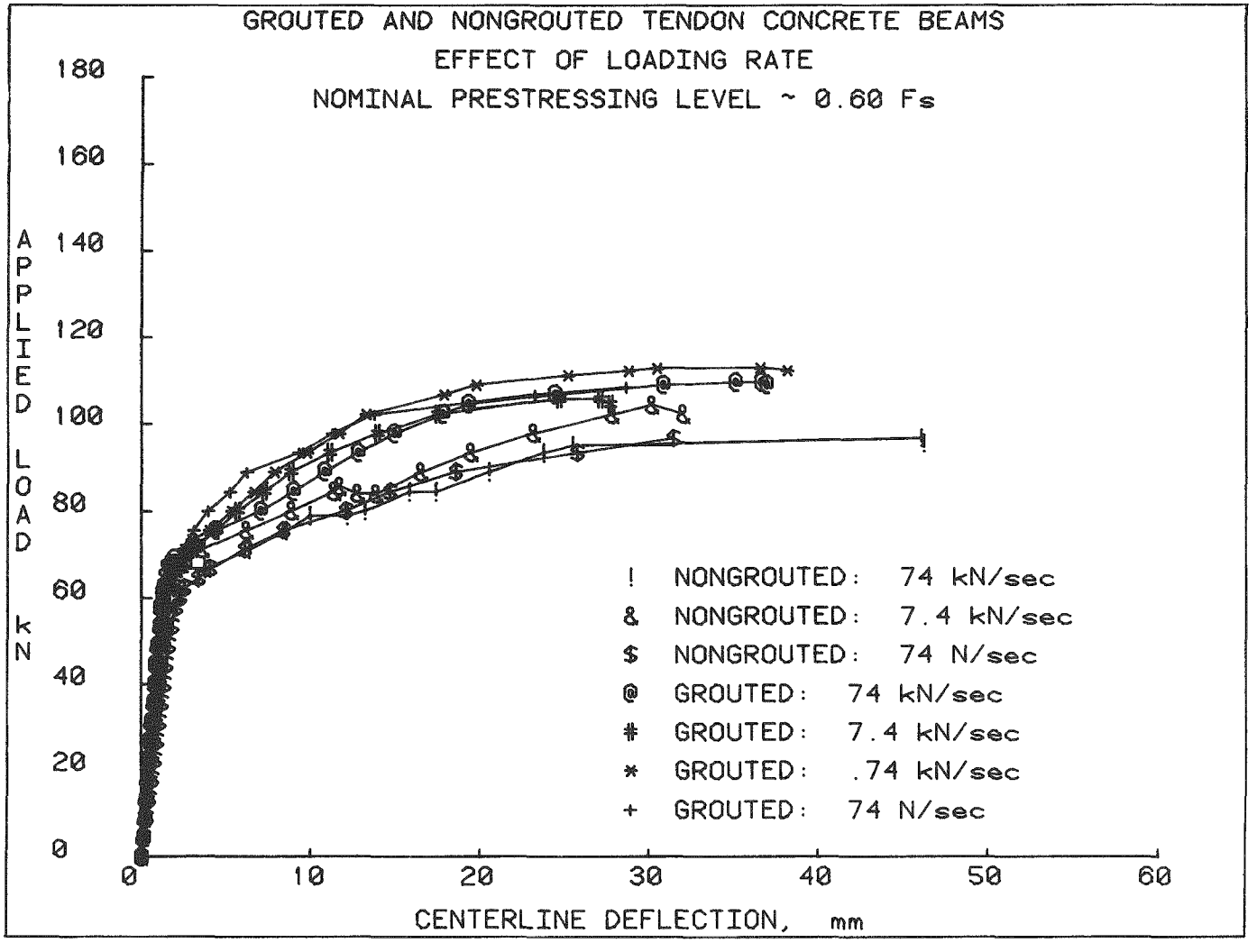

Fig. 26. Effect of loading rate on beam performance.

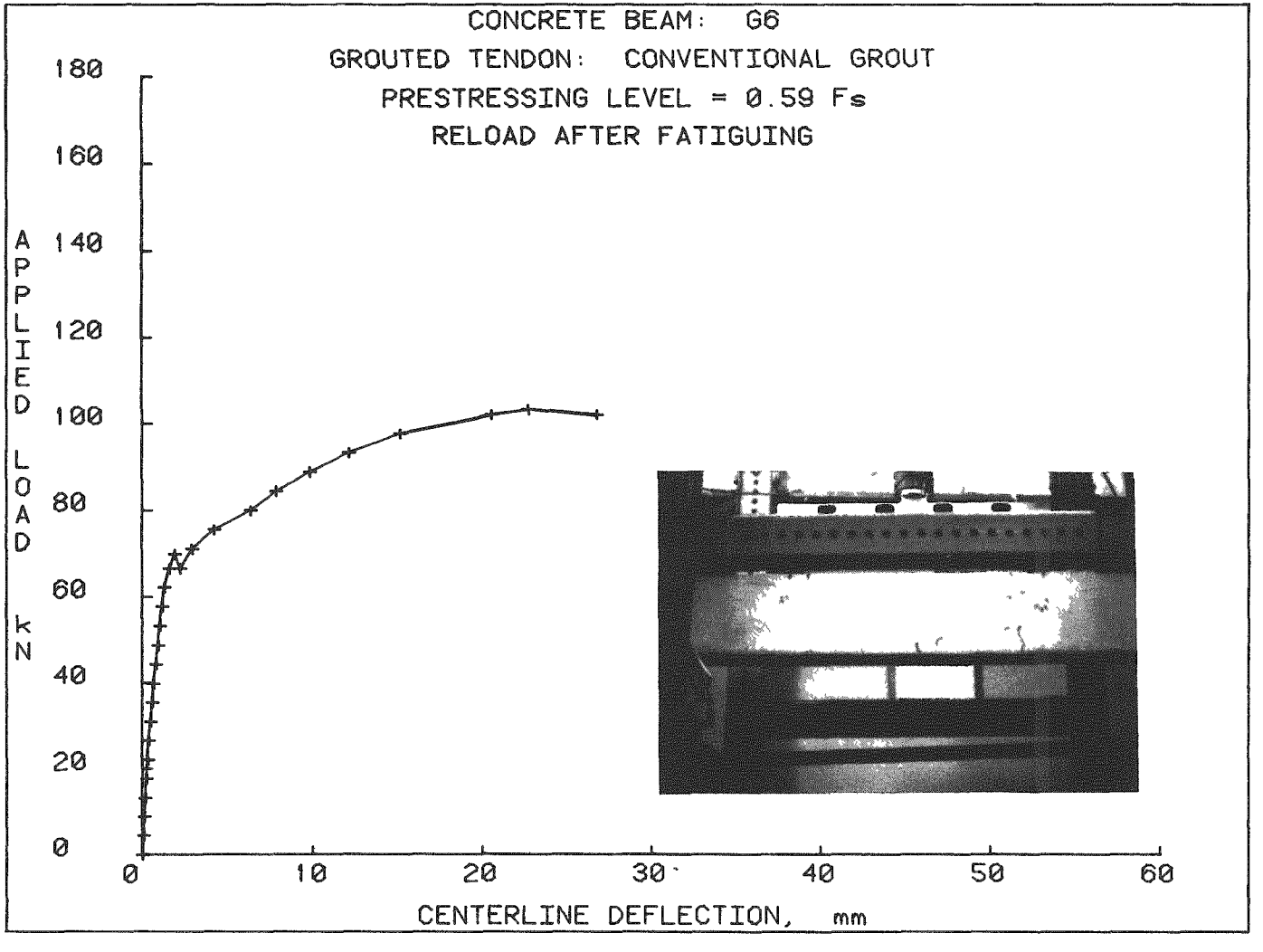

Fig. 27. Load vs centerline deflection — Beam G6.

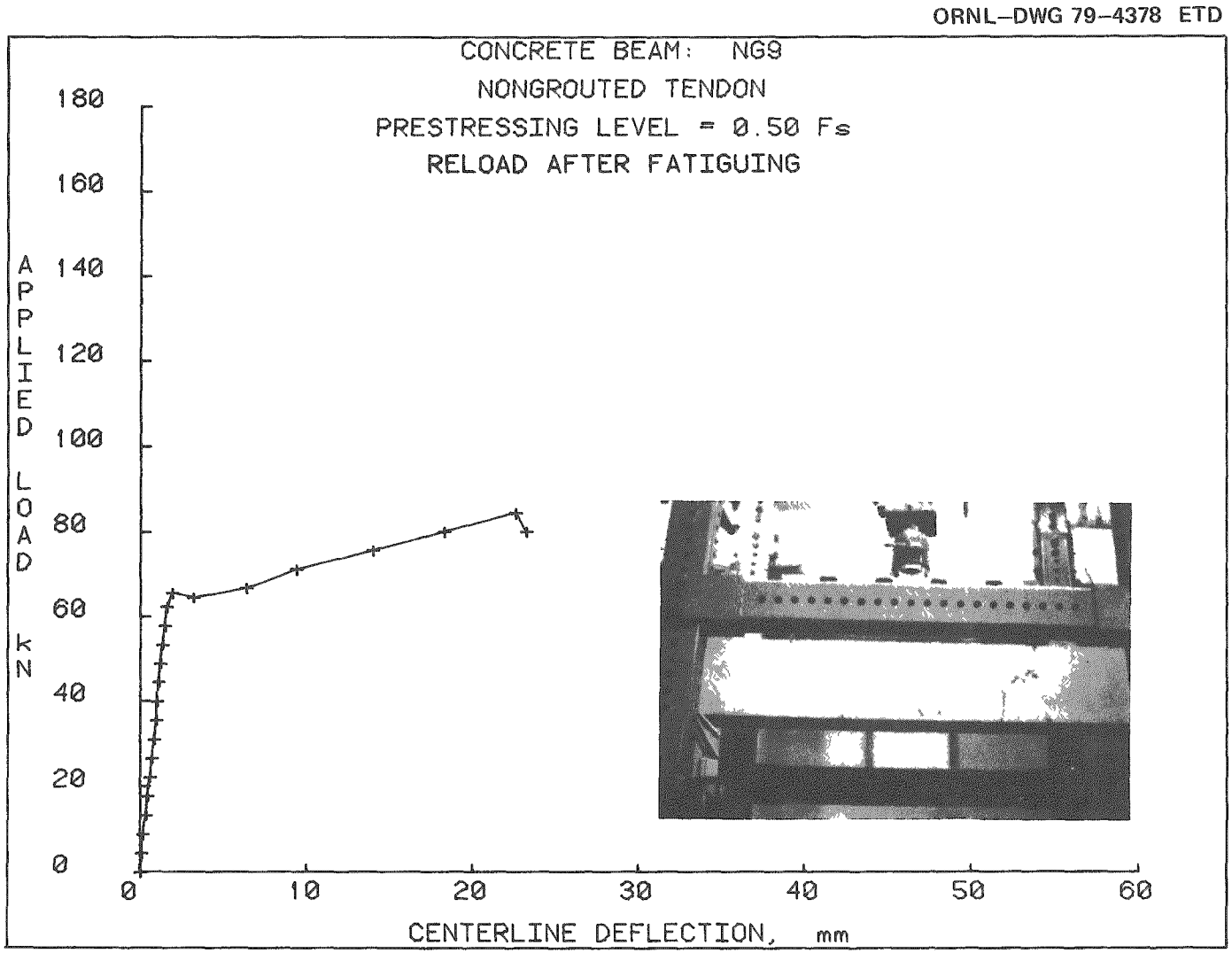

Fig. 28. Load vs centerline deflection — Beam NG9.

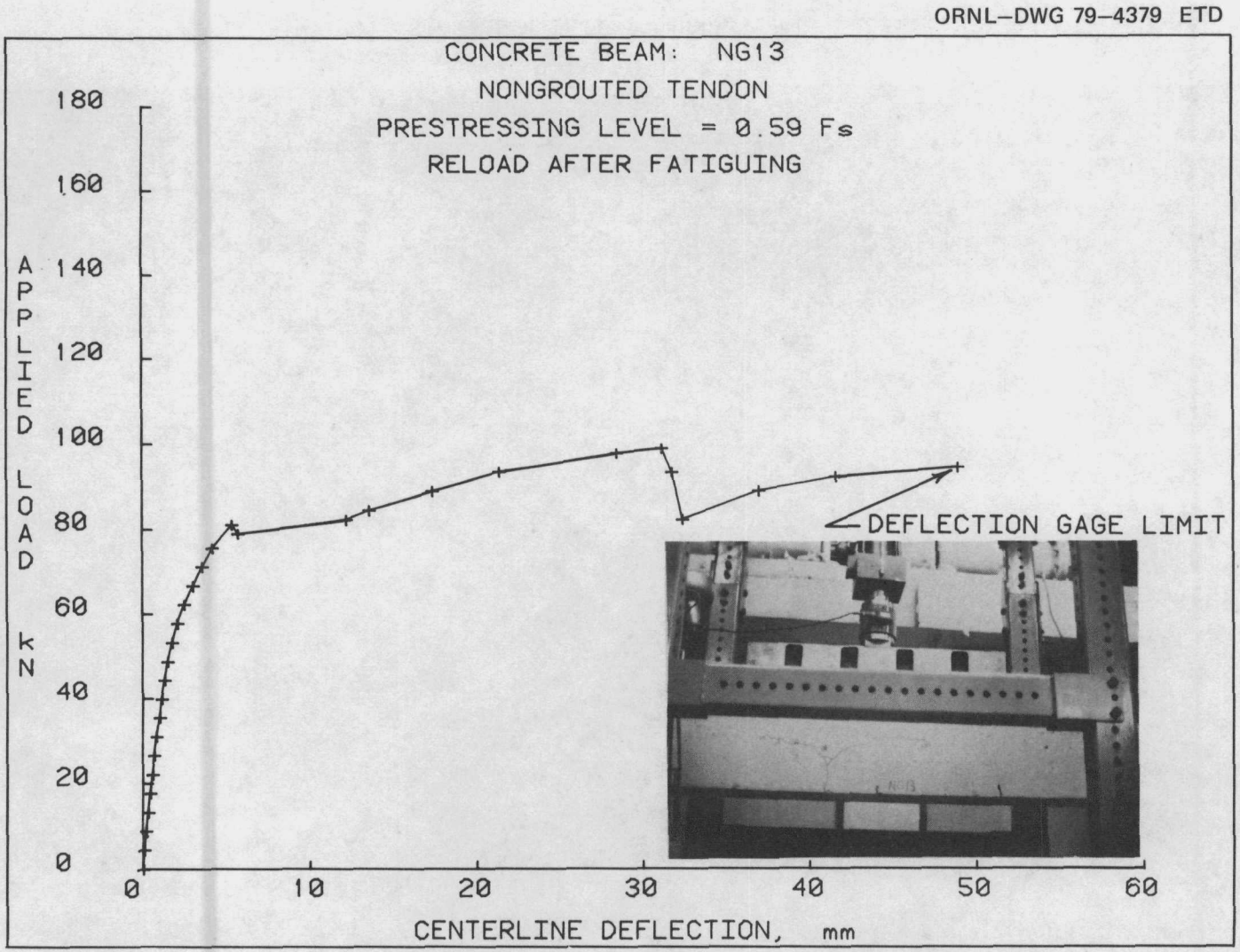

Fig. 29. Load vs centerline deflection — Beam NG13.

Fig. 30. Simulated failed tendon test specimen.

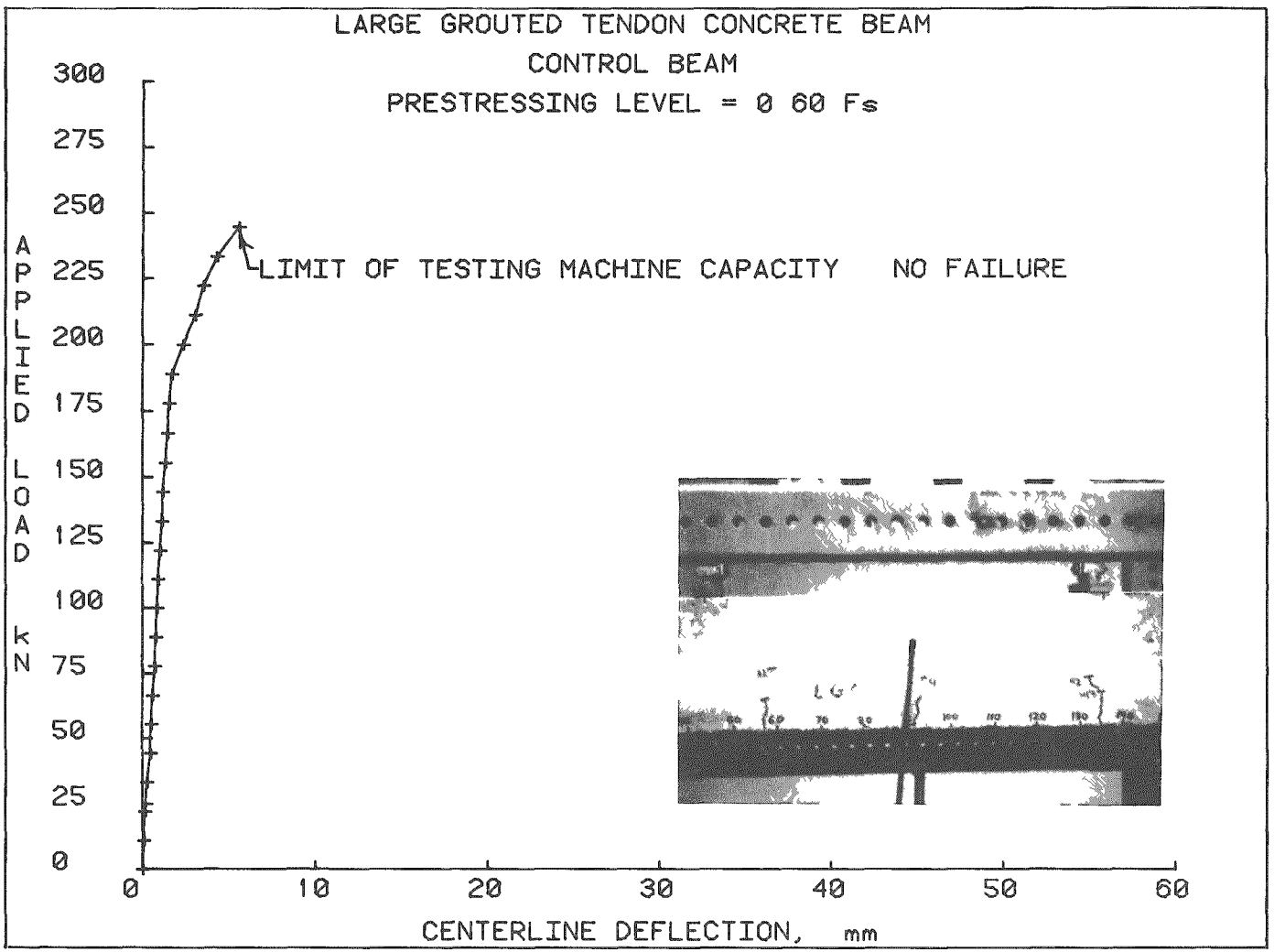

Fig. 31. Load vs centerline deflection — Beam LGC.

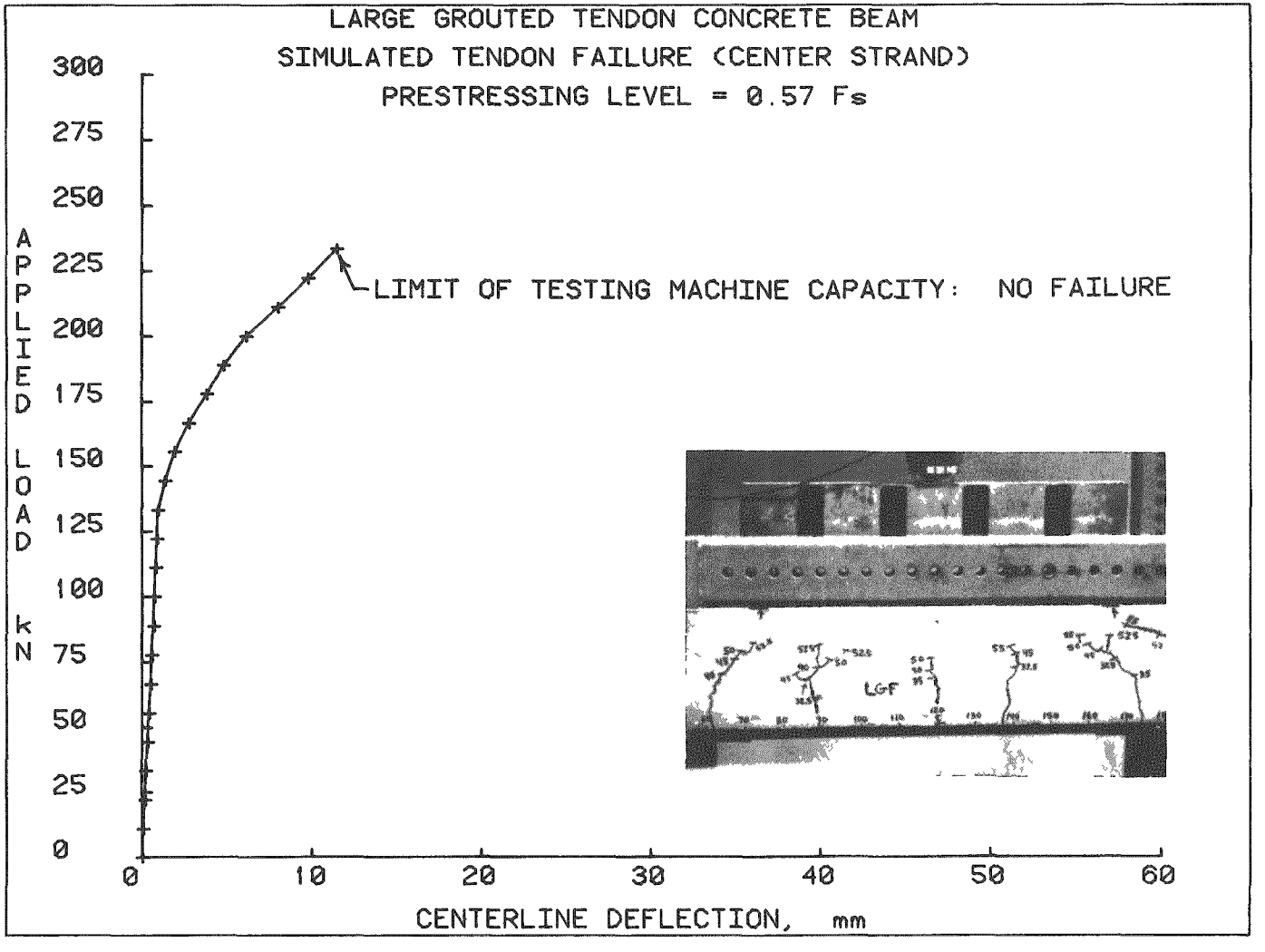

Fig. 32. Load vs centerline deflection — Beam LGF.

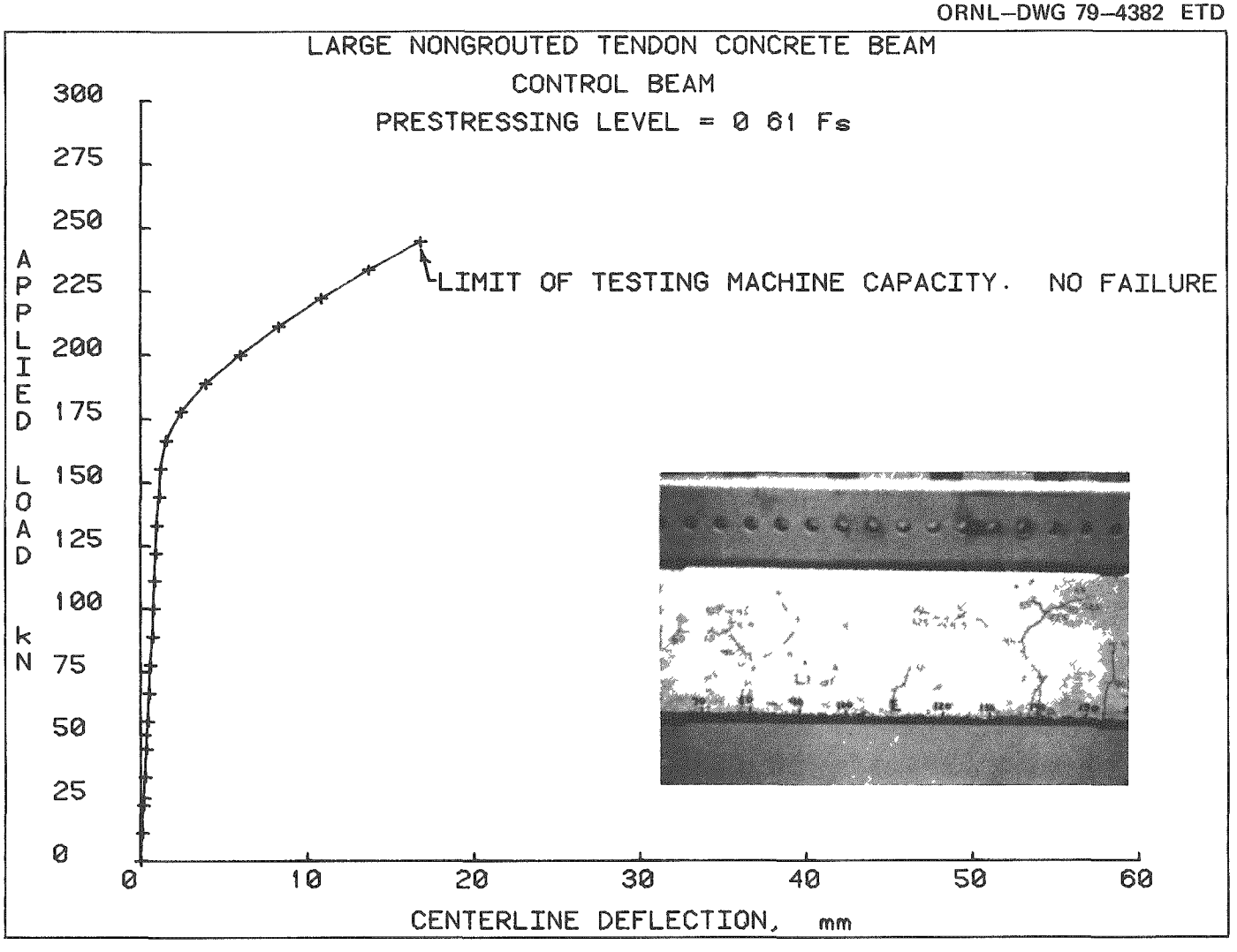

Fig. 33. Load vs centerline deflection — Beam LNGC.

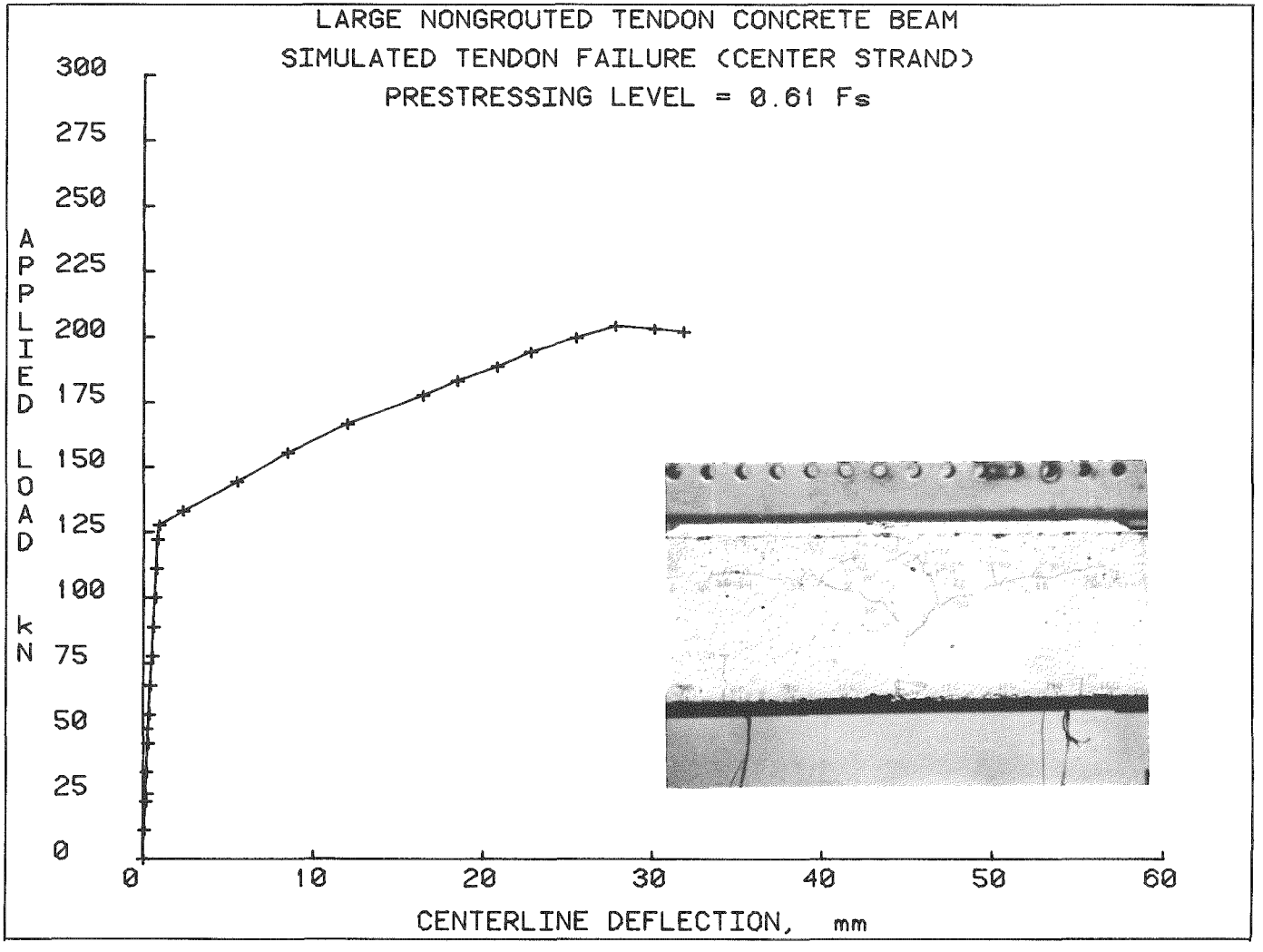

Fig. 34. Load vs centerline deflection — Beam LNGF.

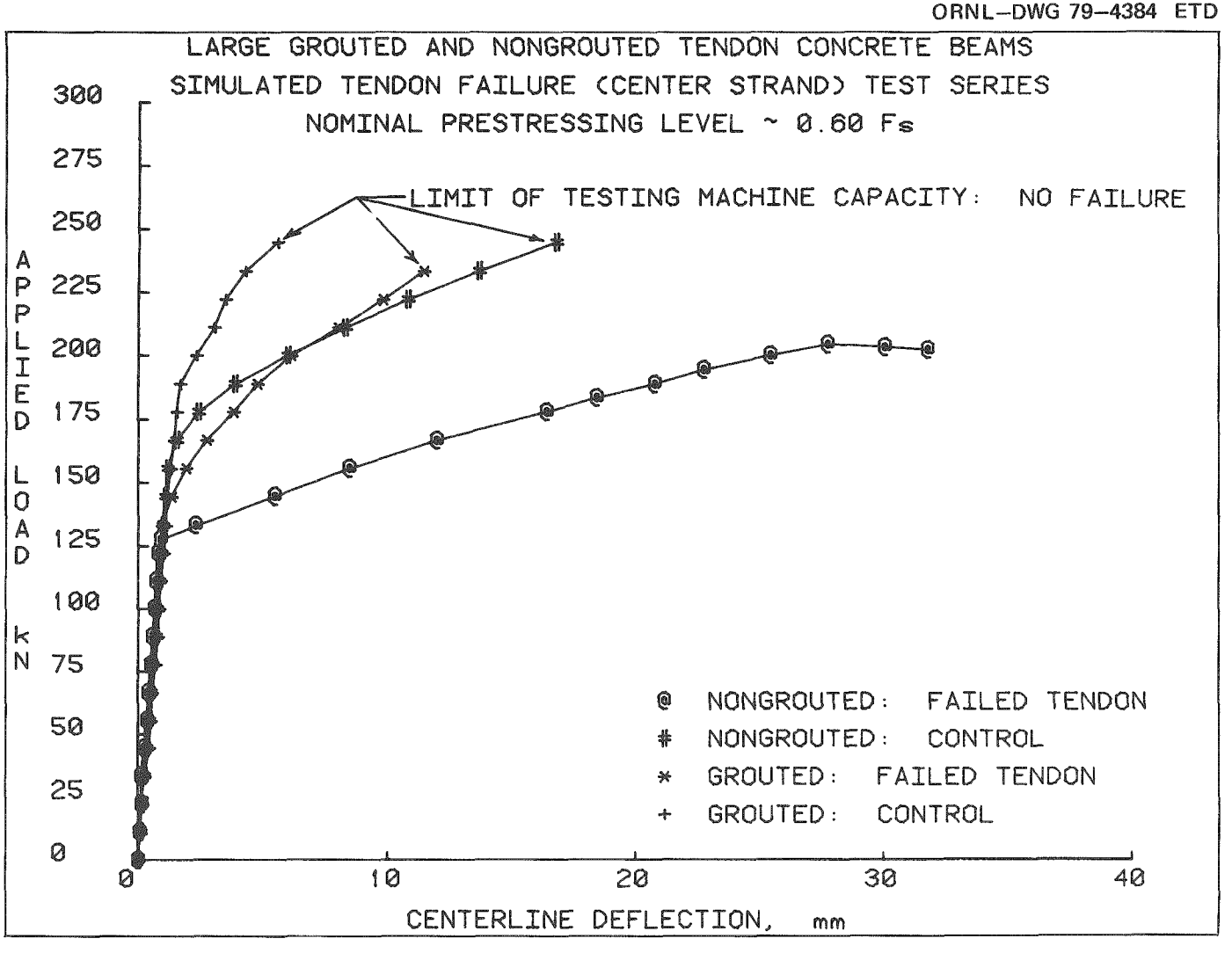

Fig. 35. Effect of simulated tendon failure on beam performance.

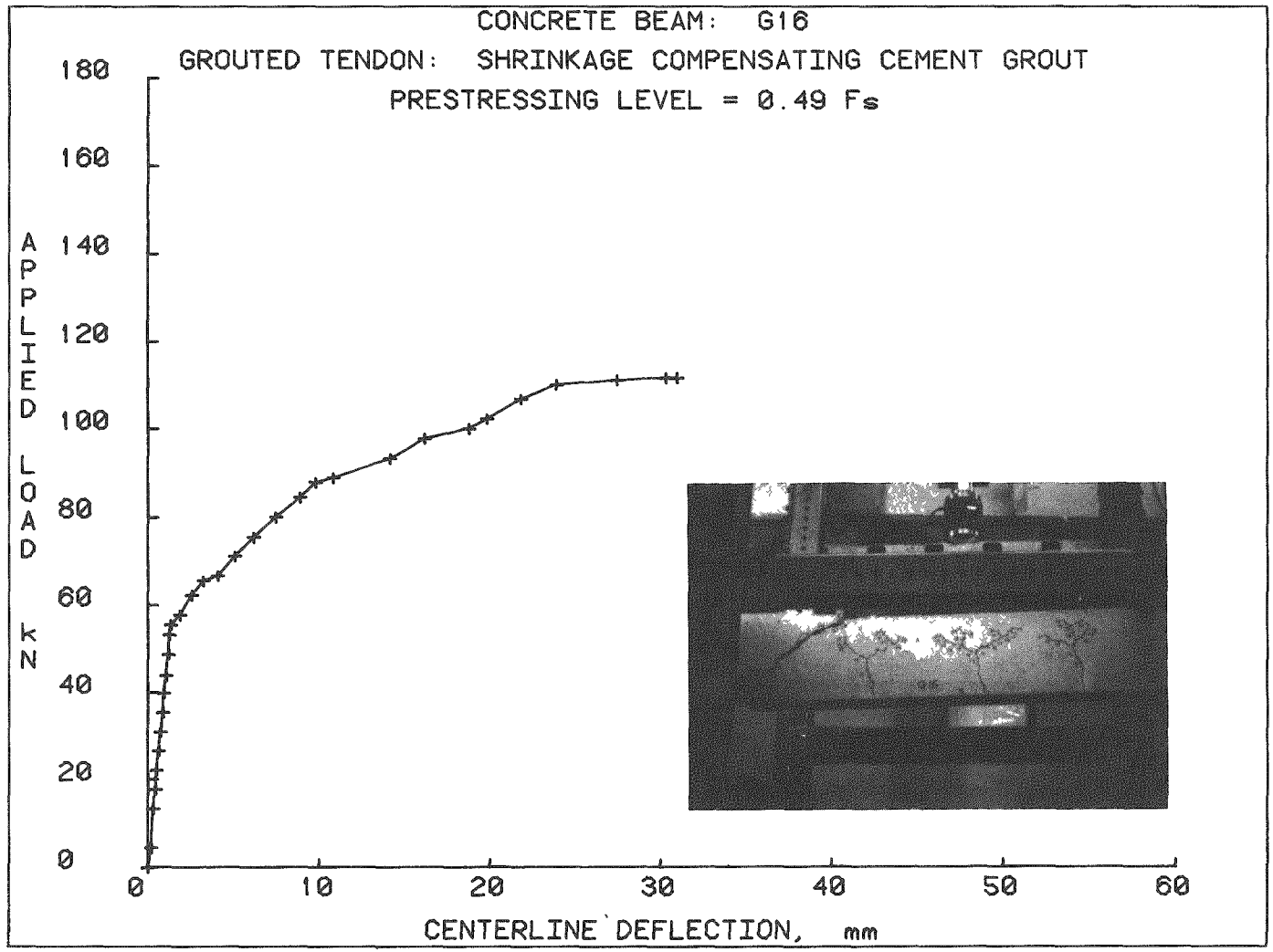

Fig. 36. Load vs centerline deflection — Beam G16.

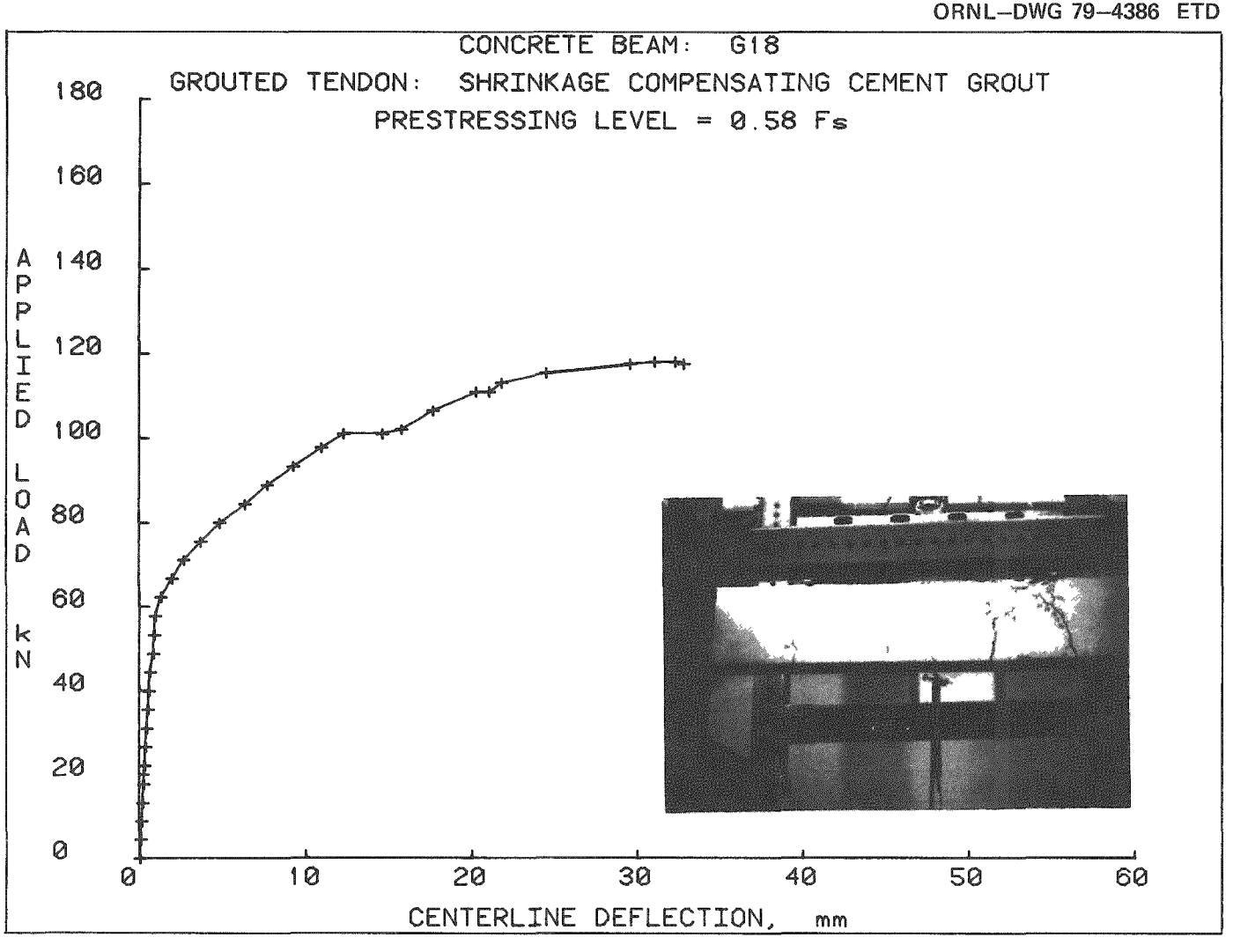

Fig. 37. Load vs centerline deflection — Beam G18.

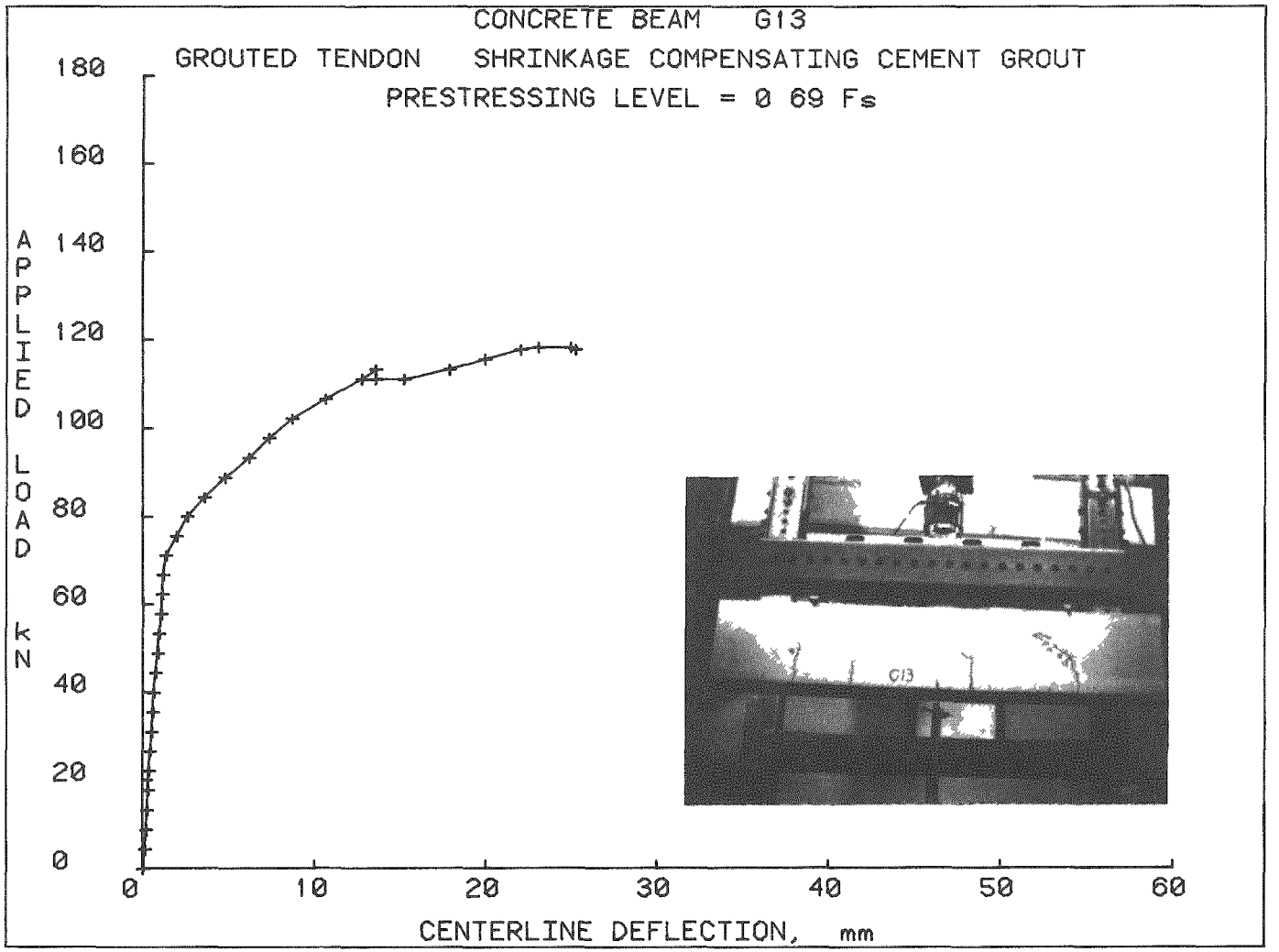

Fig. 38. Load vs centerline deflection — Beam G13.

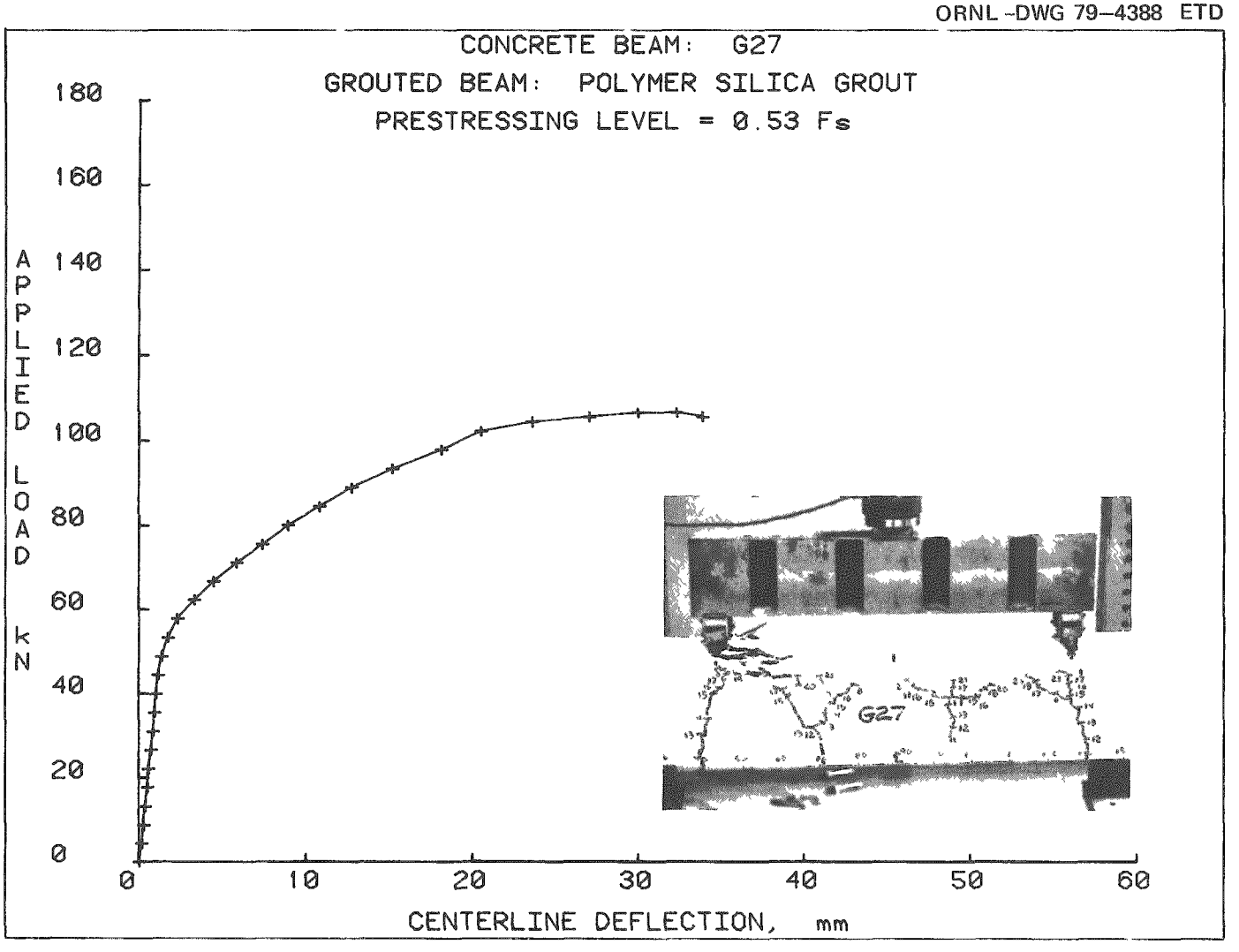

Fig. 39. Load vs centerline deflection — Beam G27.

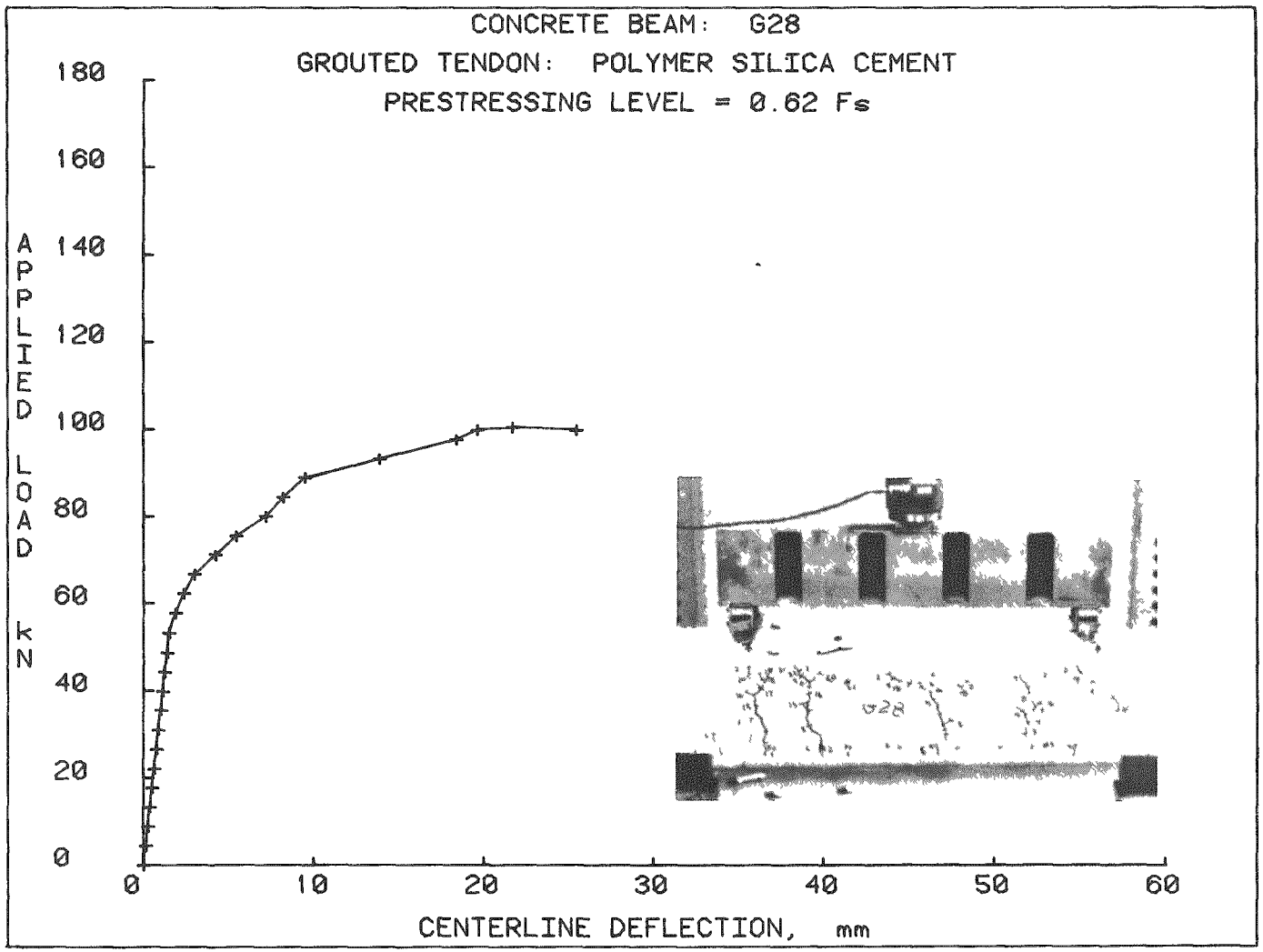

Fig. 40. Load vs centerline deflection — Beam G28.

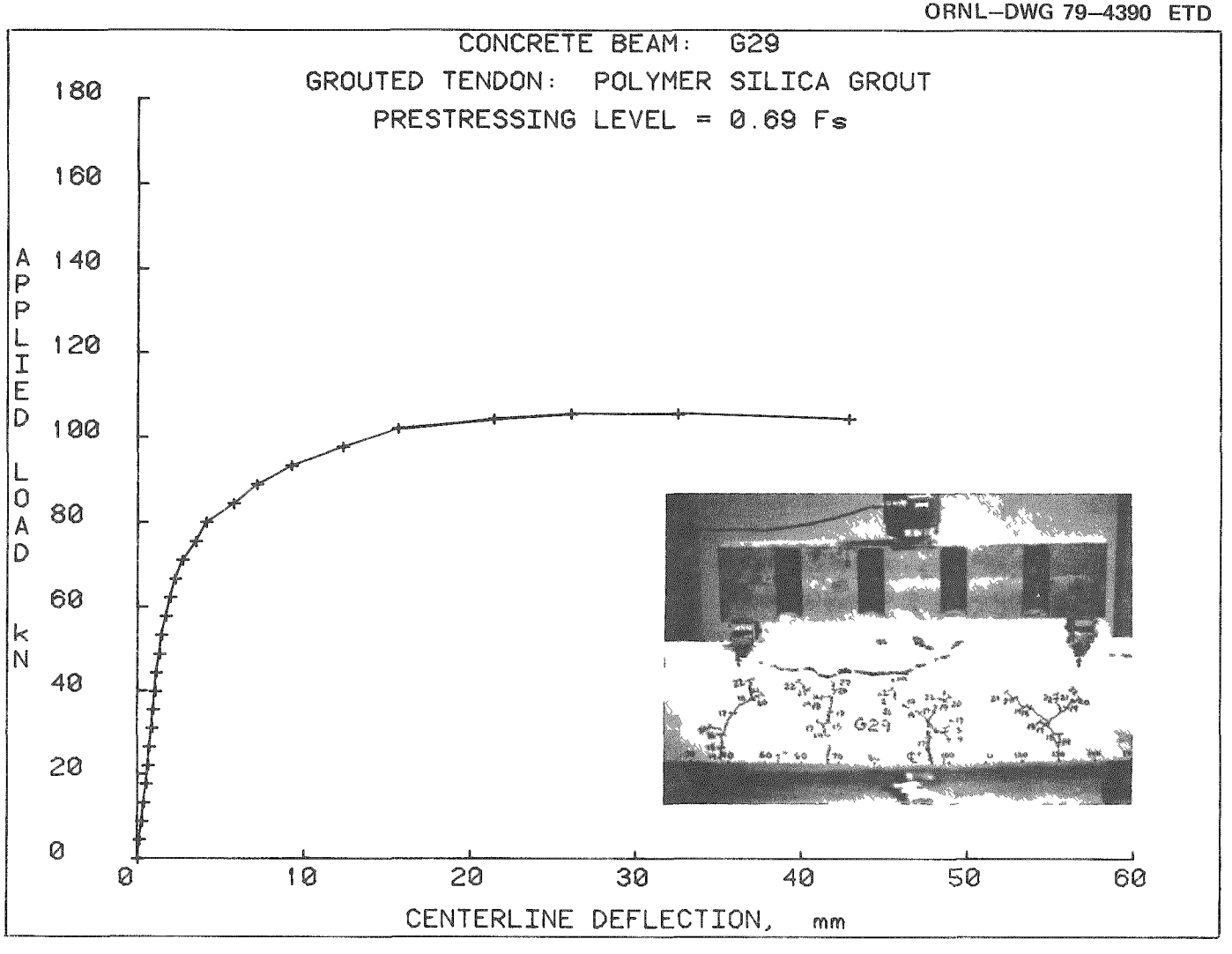

Fig. 41. Load vs centerline deflection — Beam G29.

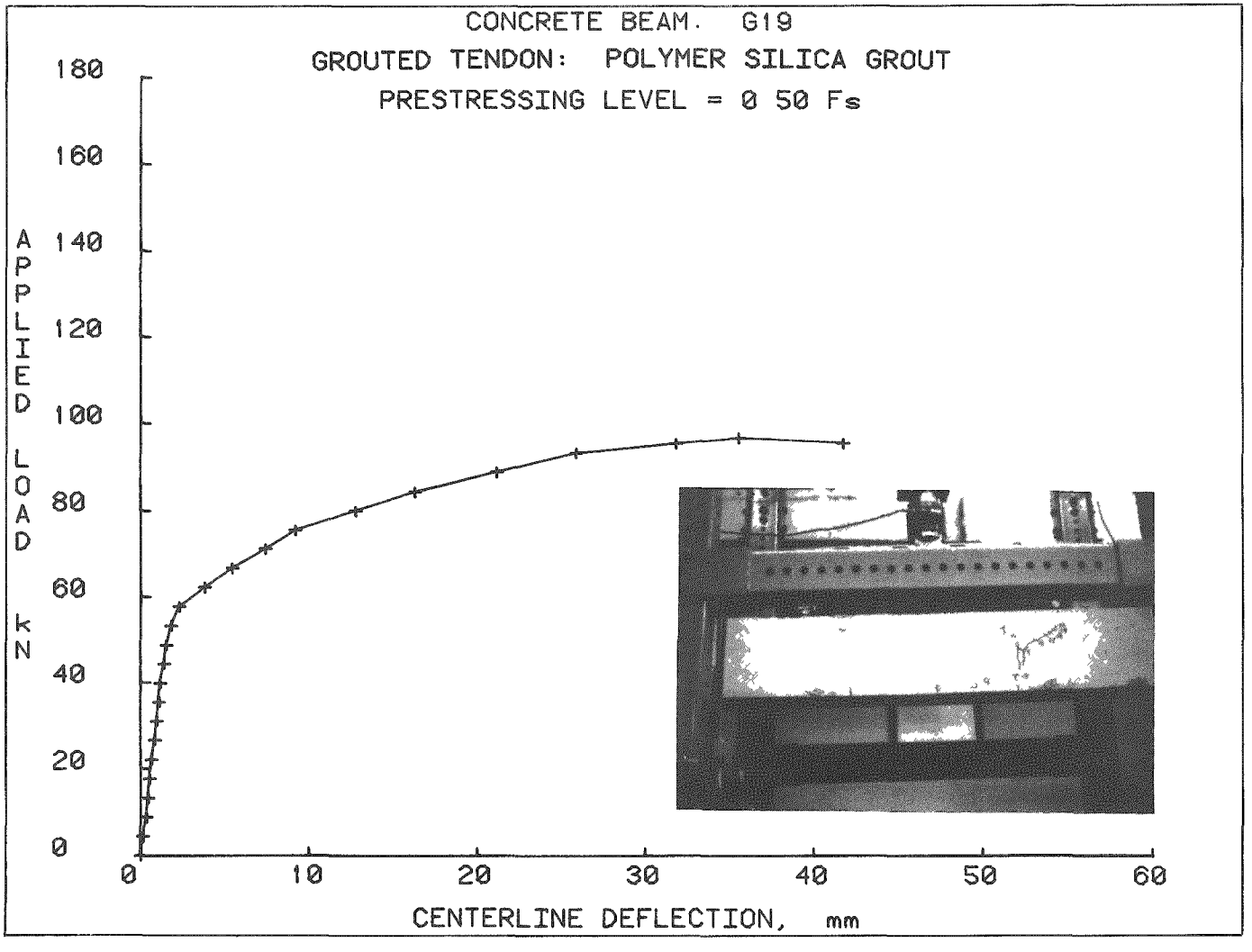

Fig. 42. Load vs centerline deflection — Beam G19.

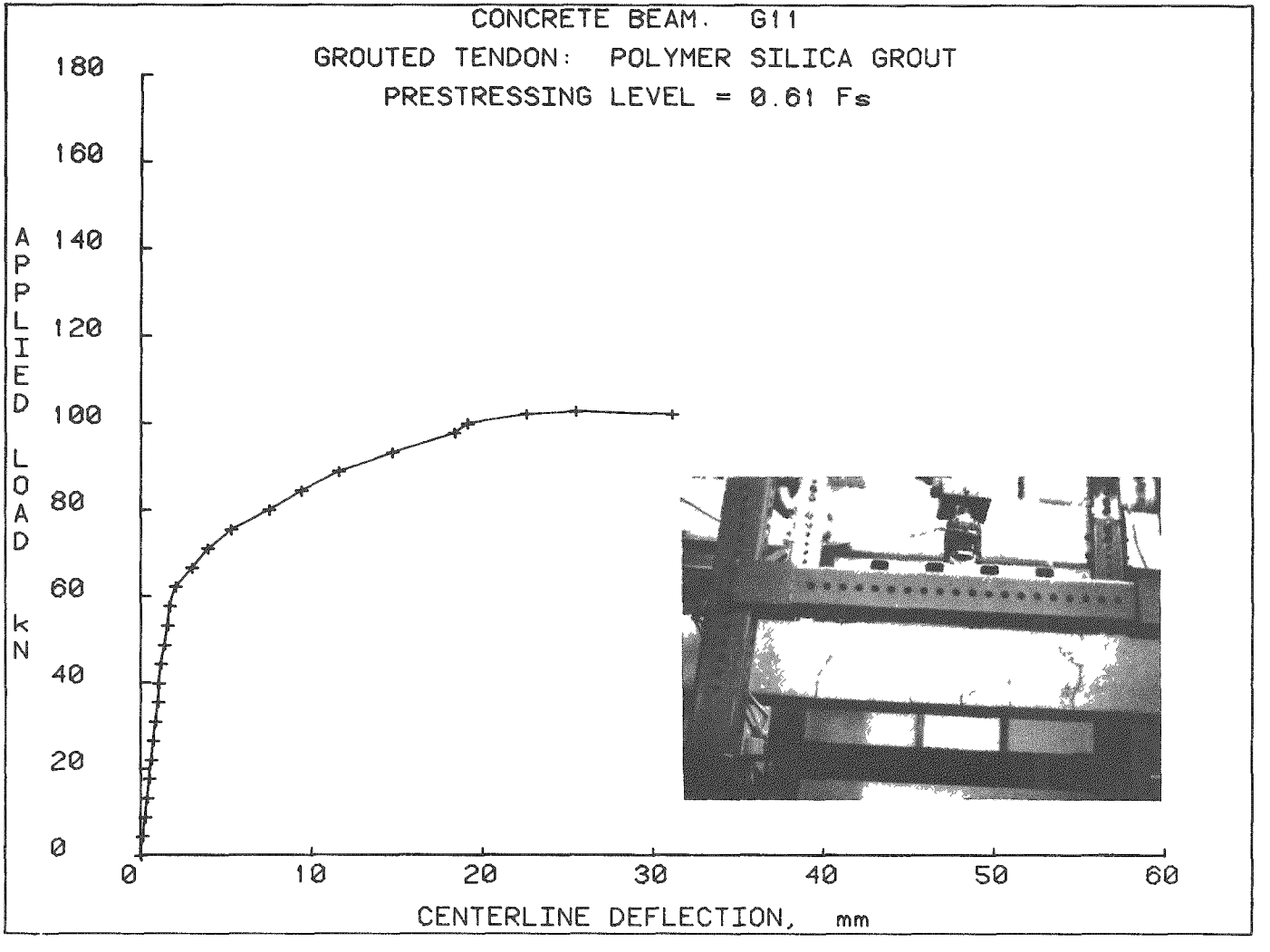

Fig. 43. Load vs centerline deflection — Beam G11.

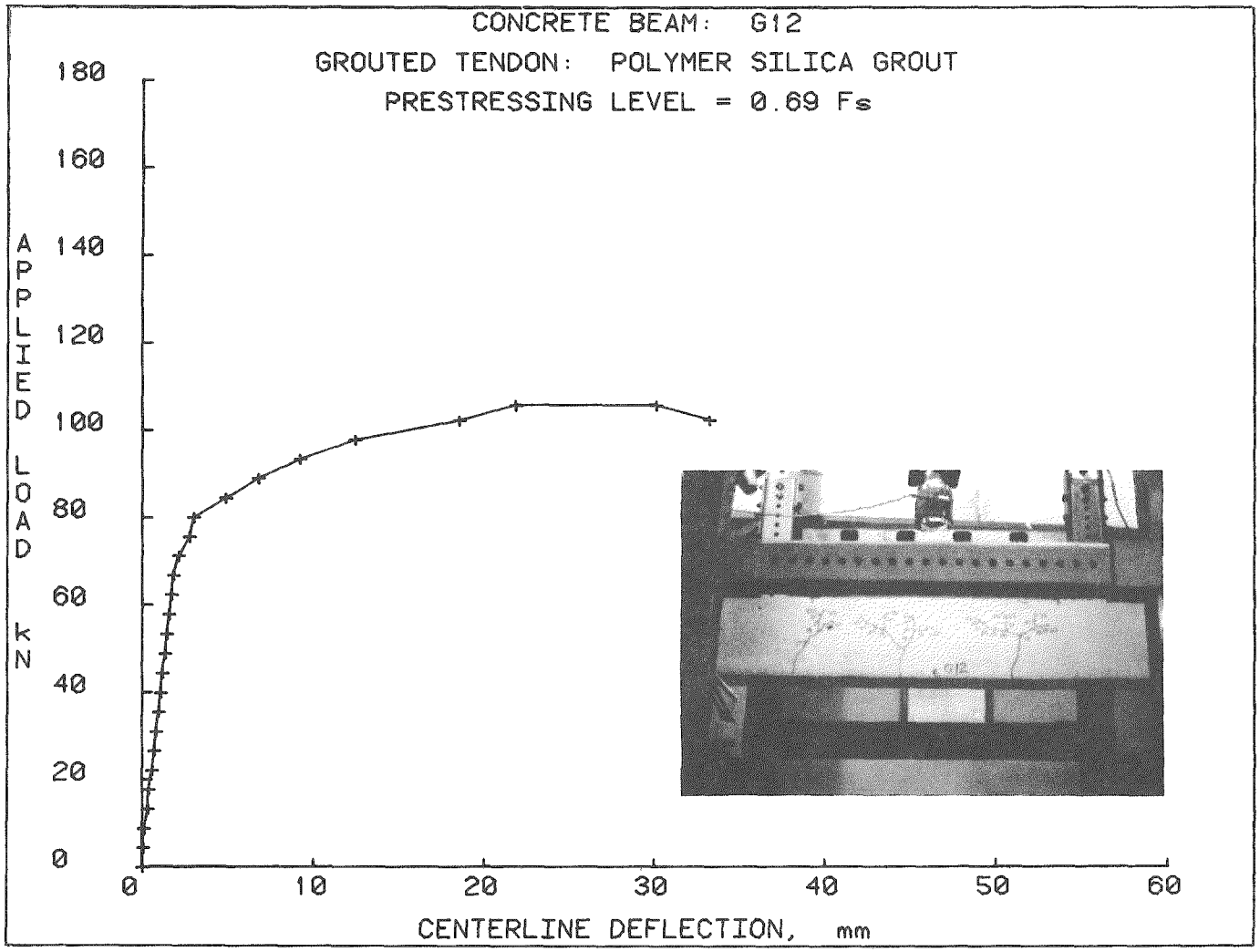

Fig. 44. Load vs centerline deflection — Beam G12.

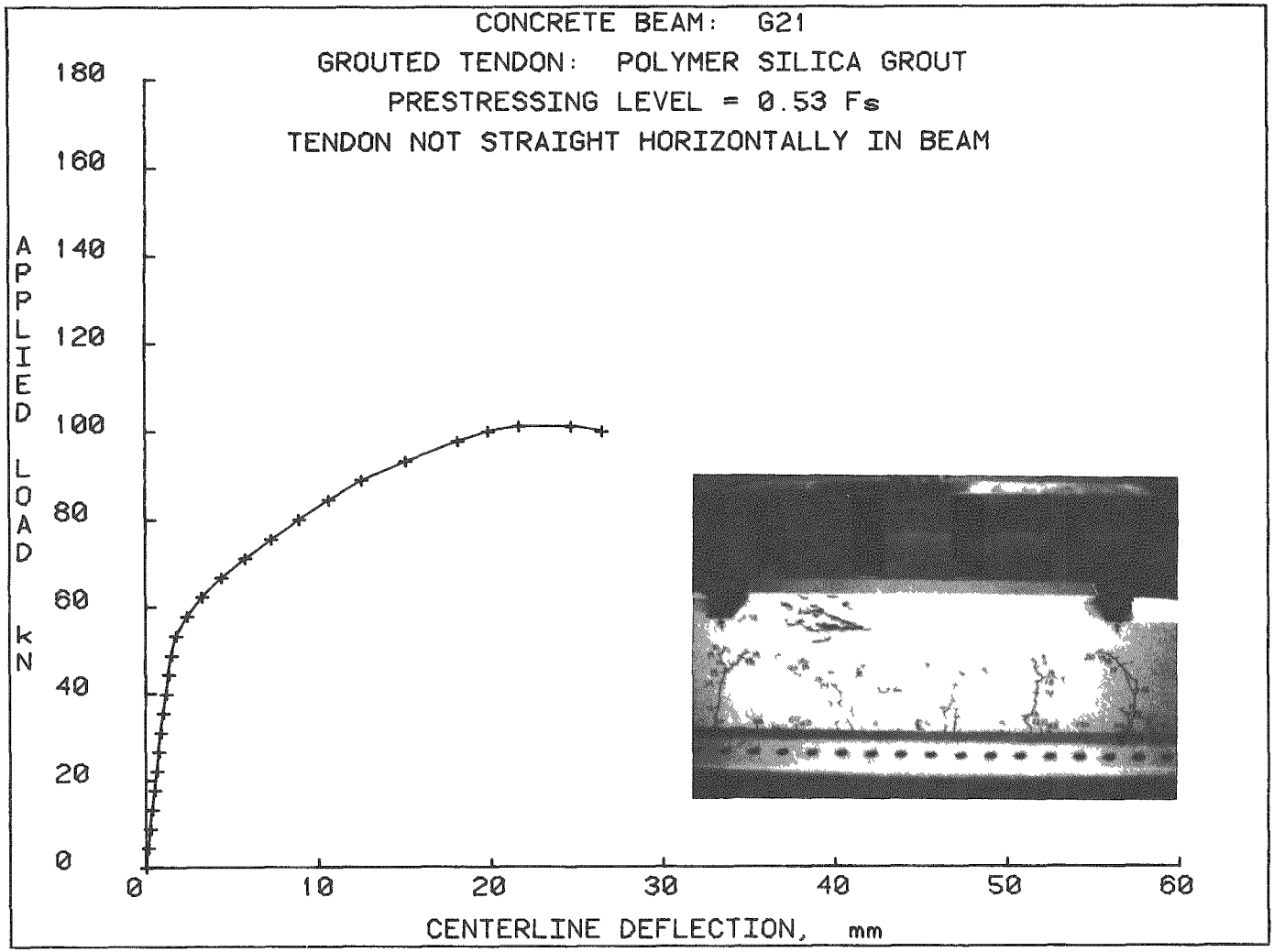

Fig. 45. Load vs centerline deflection — Beam G21.

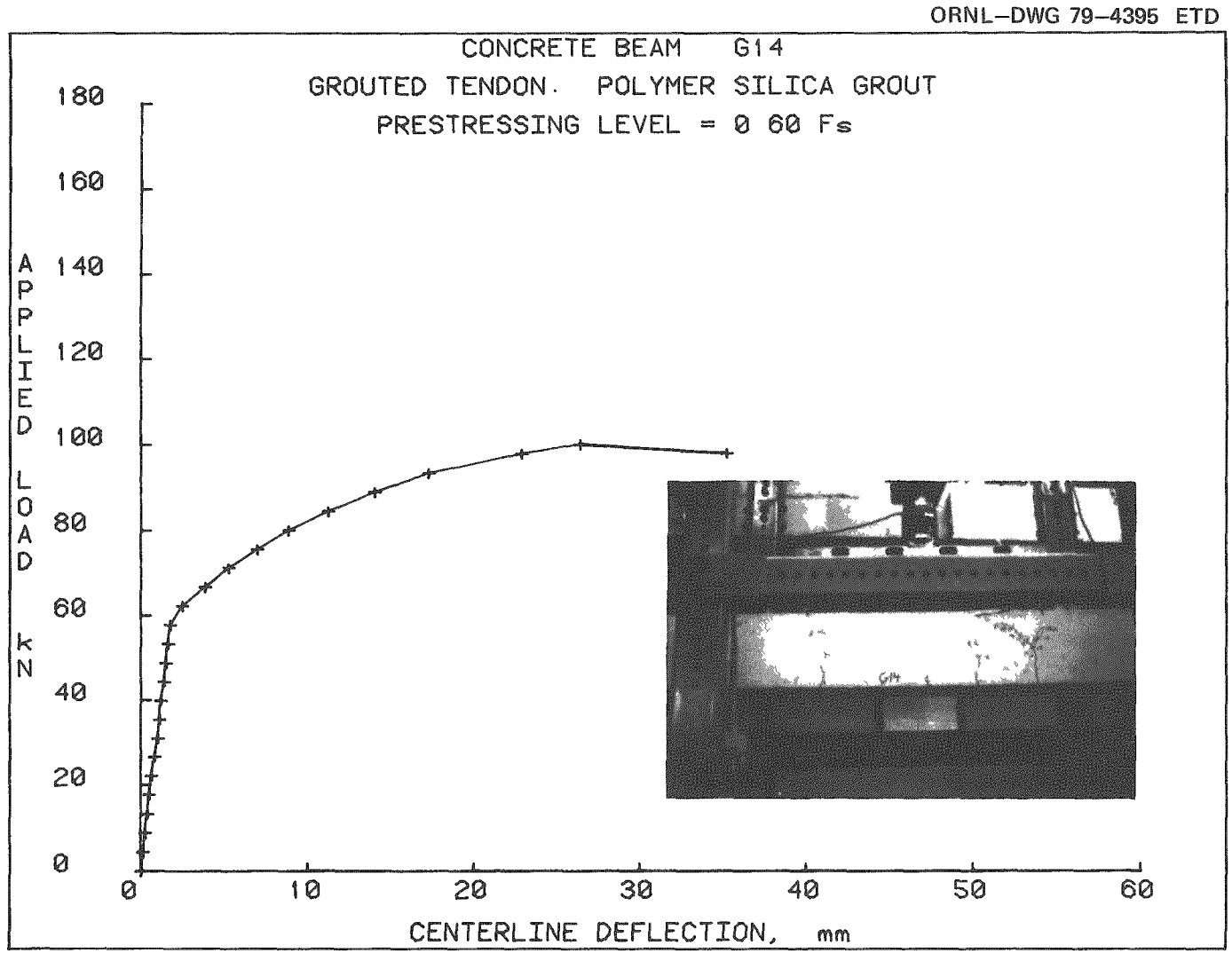

Fig. 46. Load vs centerline deflection — Beam G14.

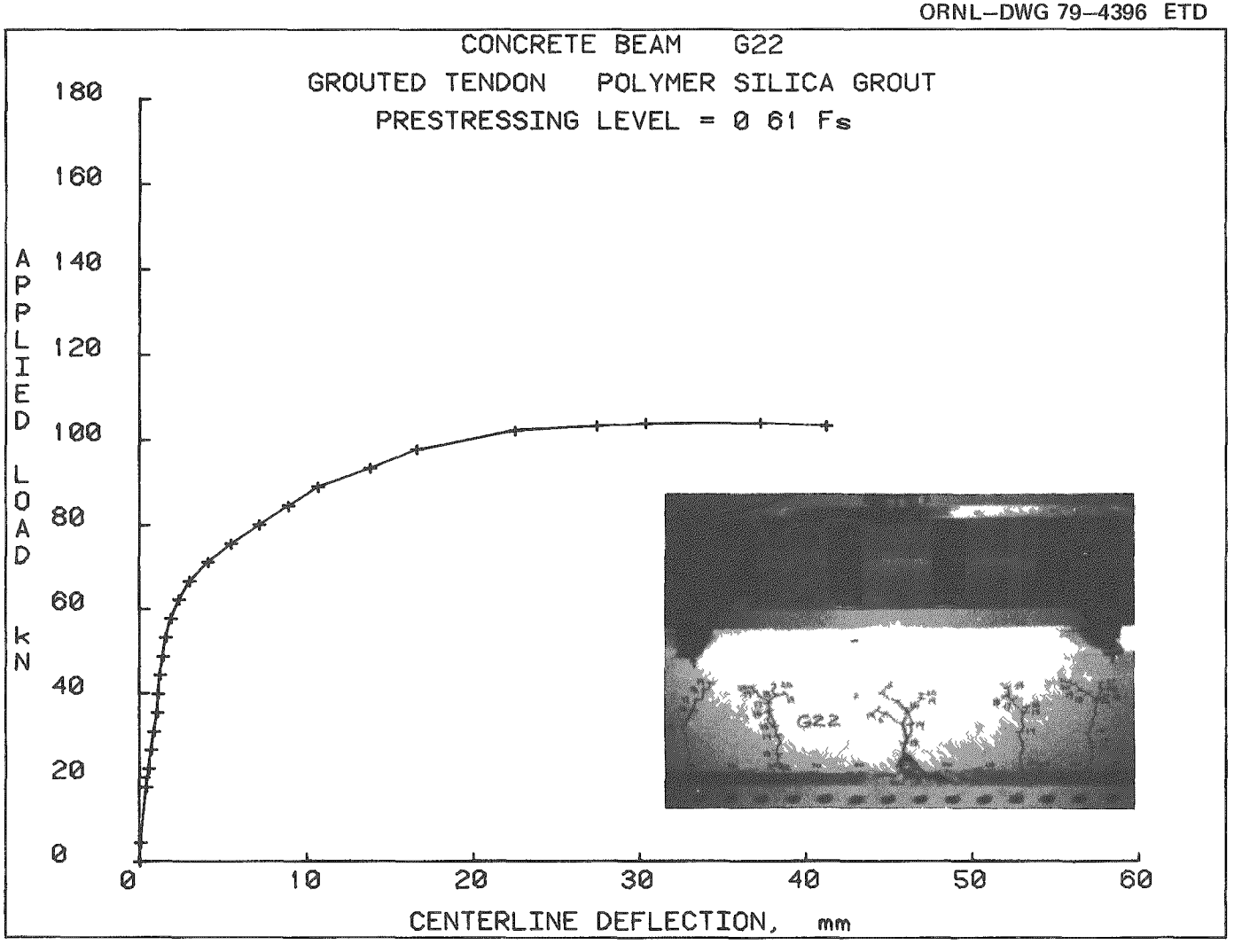

Fig. 47. Load vs centerline deflection — Beam G22.

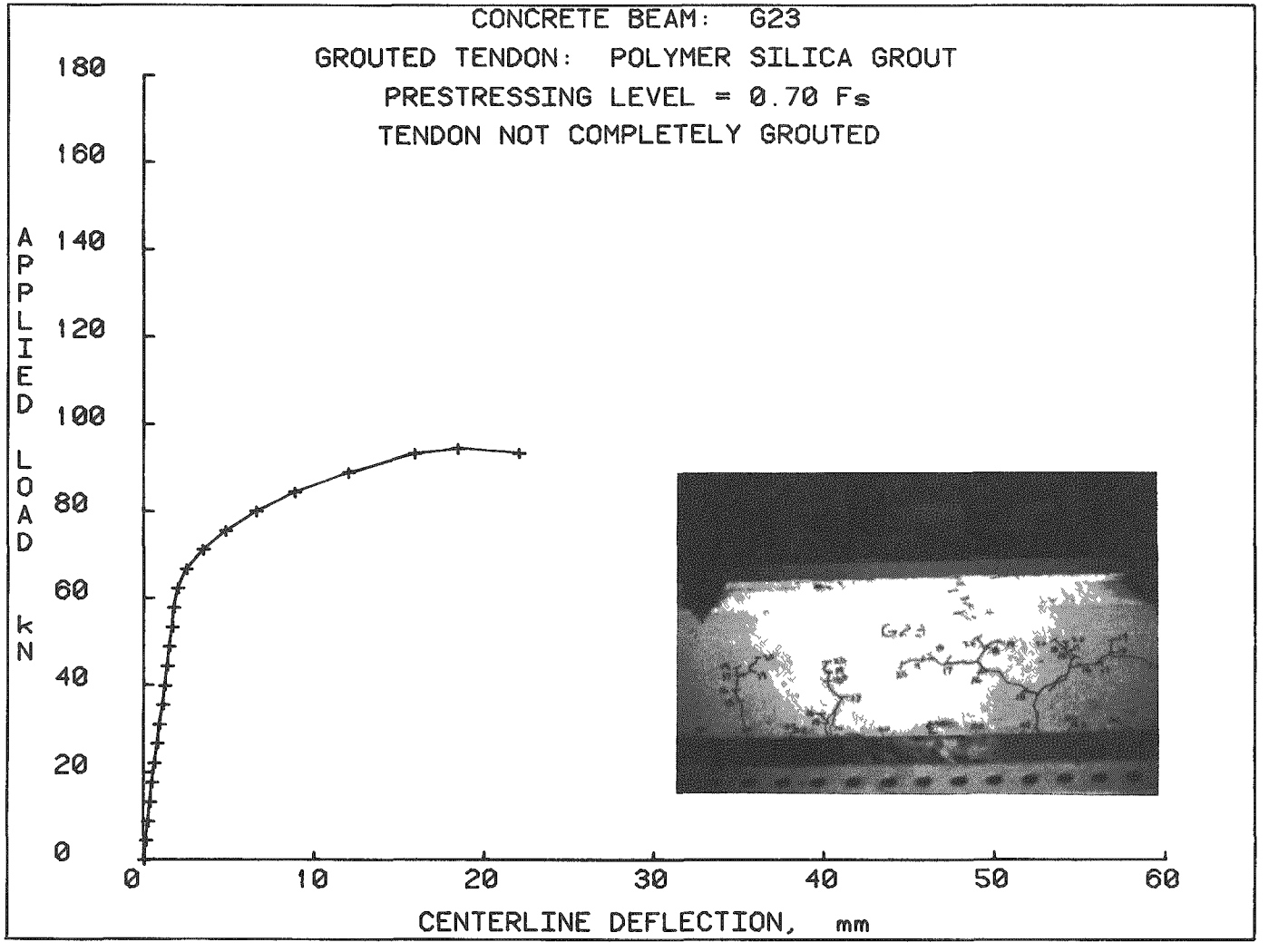

Fig. 48. Load vs centerline deflection — Beam G23.

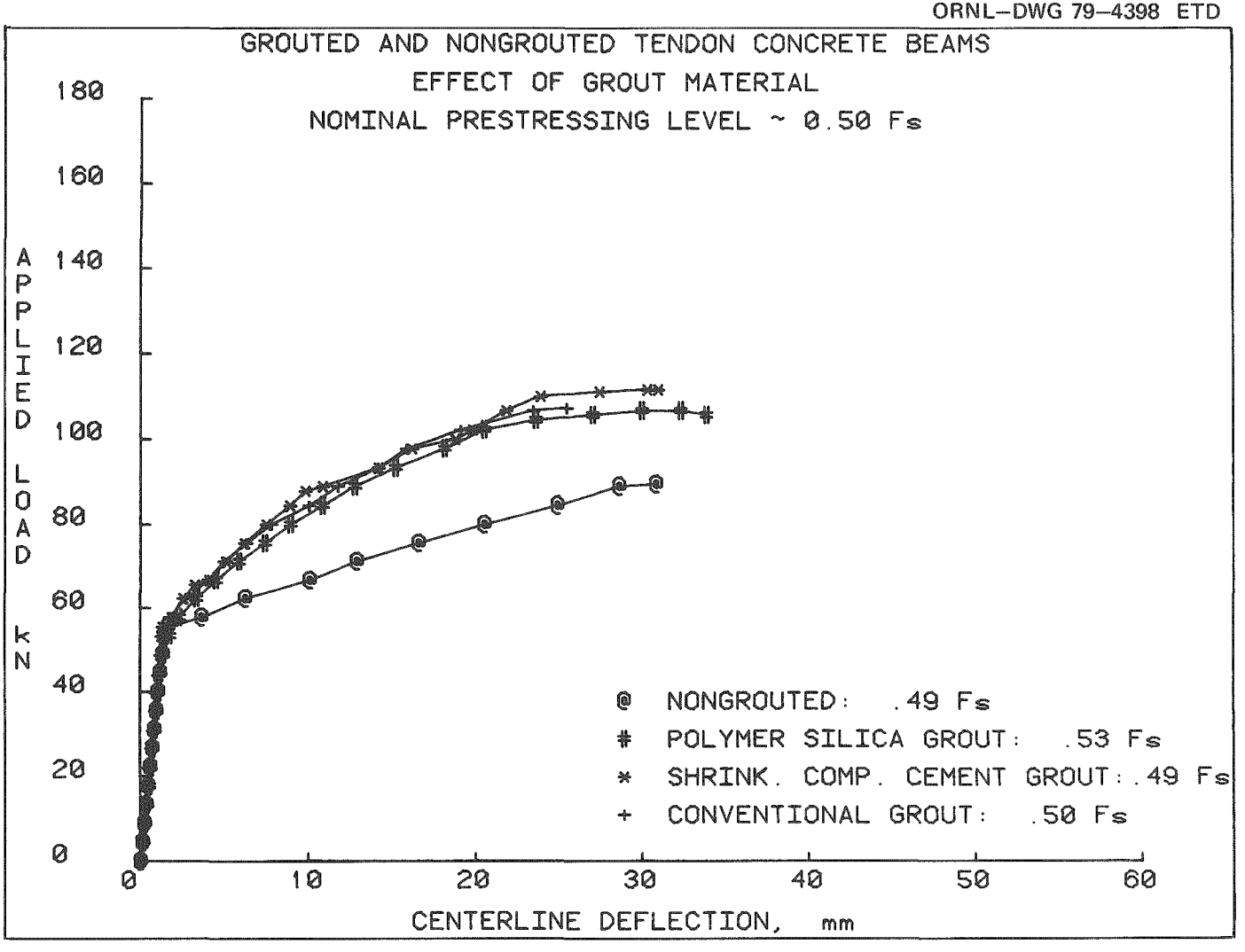

Fig. 49. Effect of grout material on beam performance — F_s = 0.50.

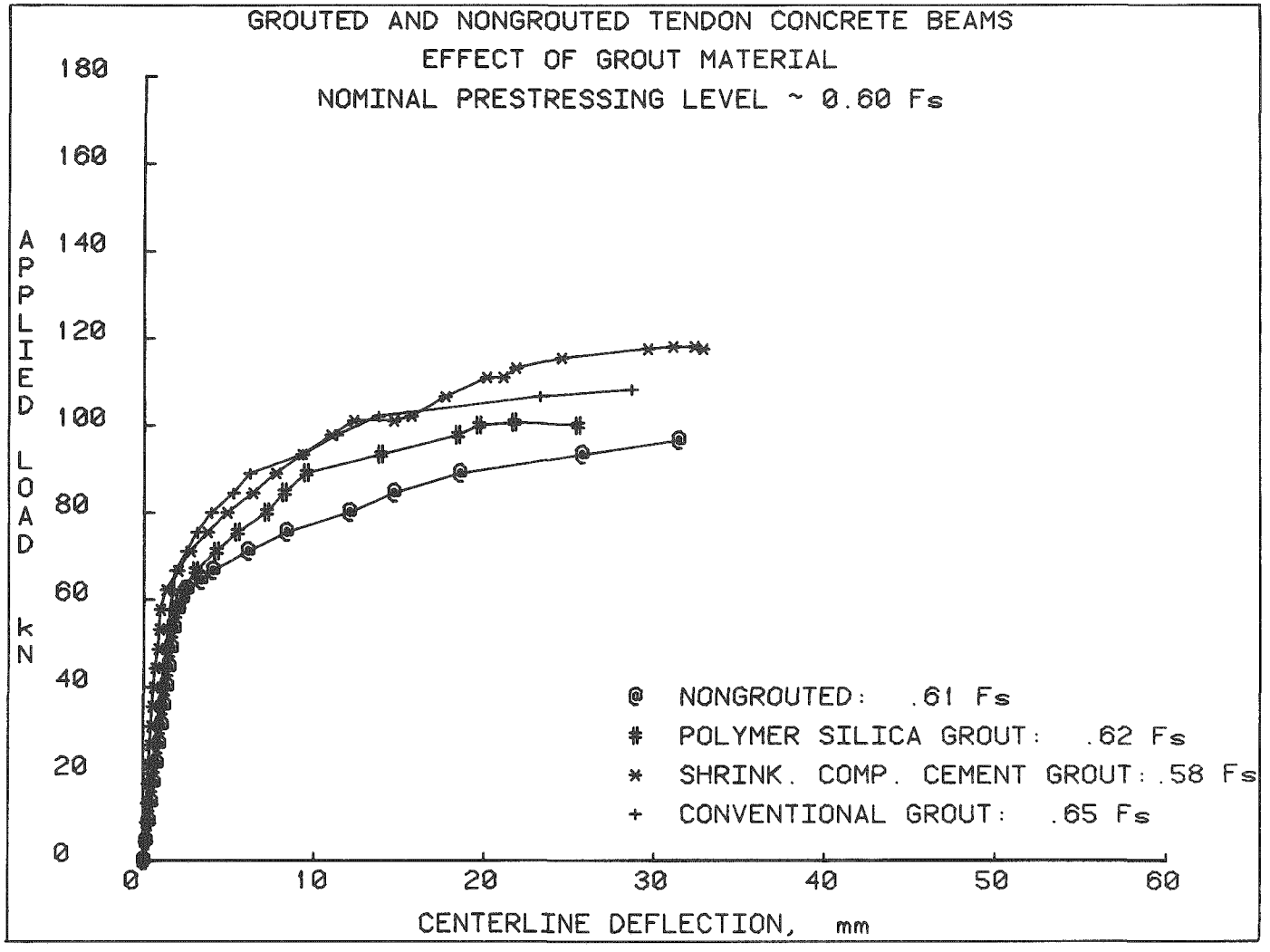

Fig. 50. Effect of grout material on beam performance — F_s = 0.60.

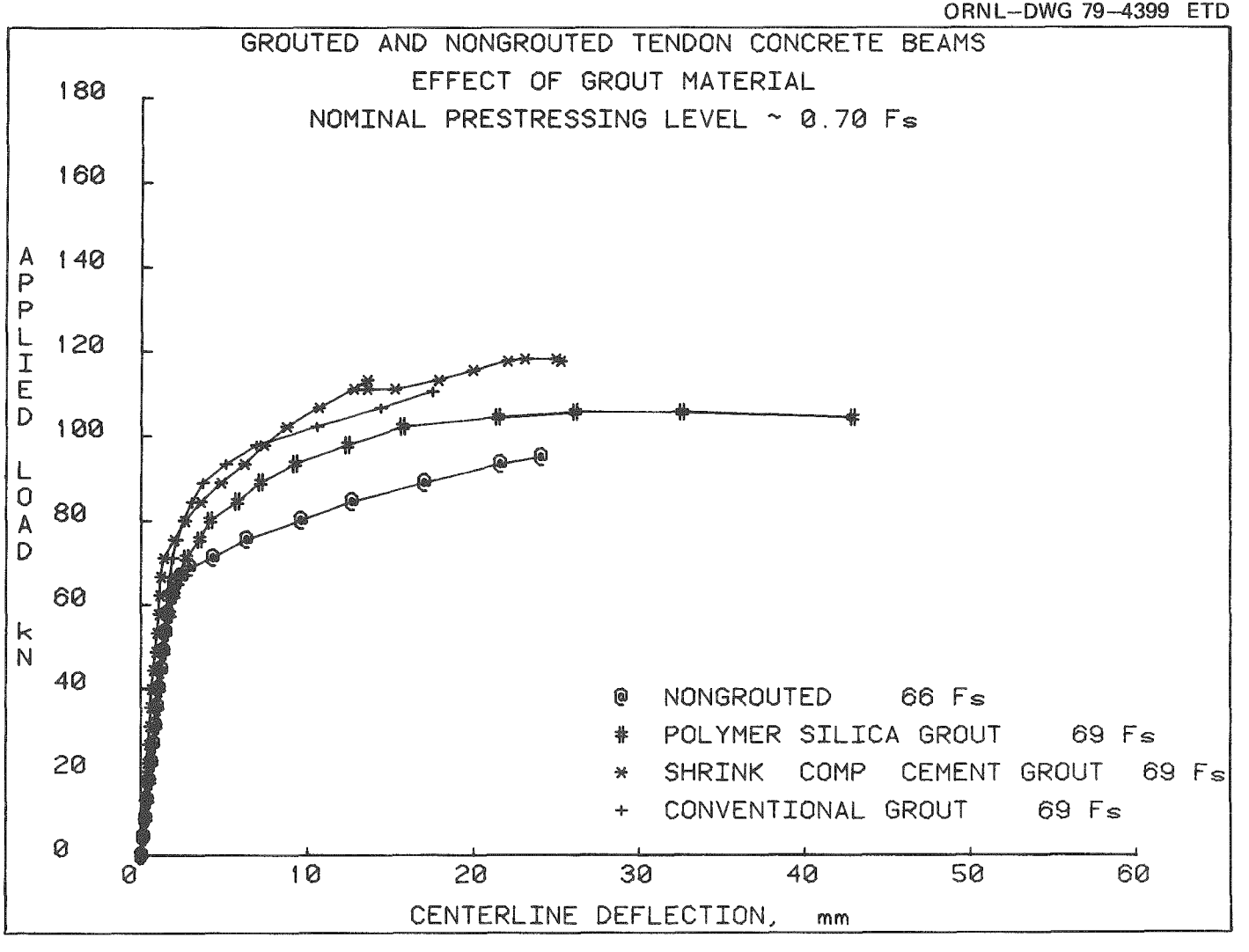

Fig. 51. Effect of grout material on beam performance — F_s = 0.70.

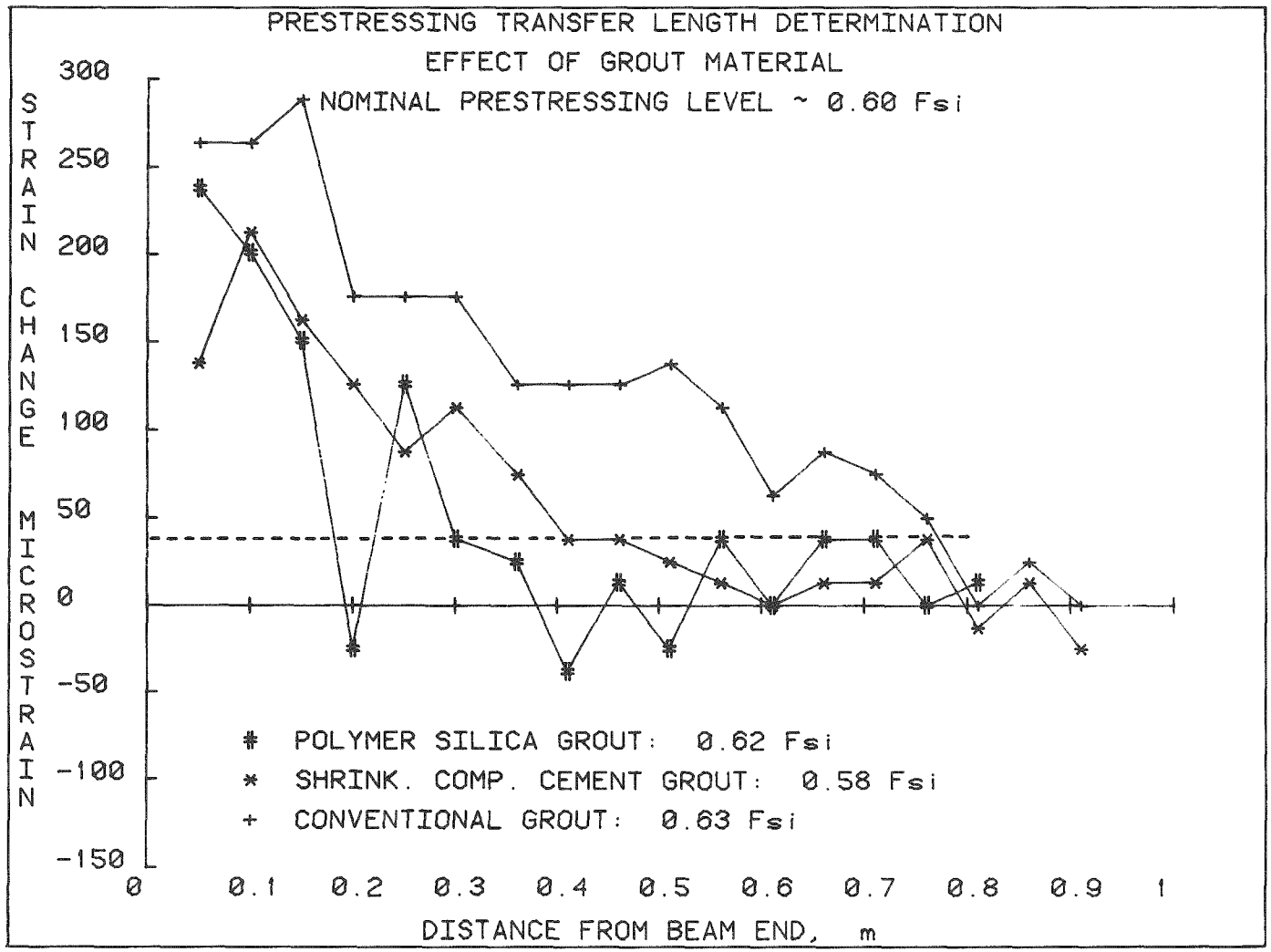

Fig. 52. Effect of grout material on prestressing transfer length.

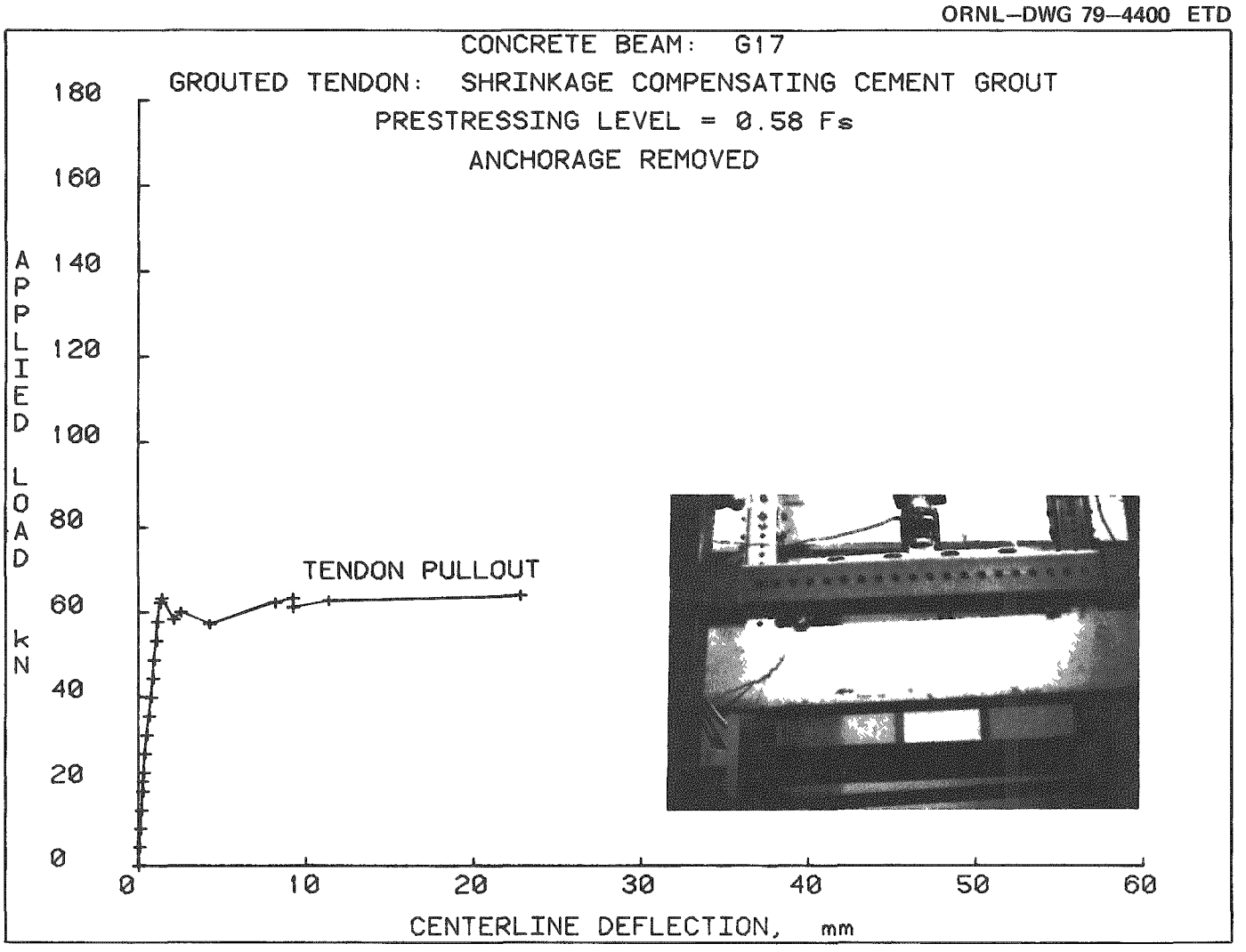

Fig. 53. Load vs centerline deflection — Beam G17.

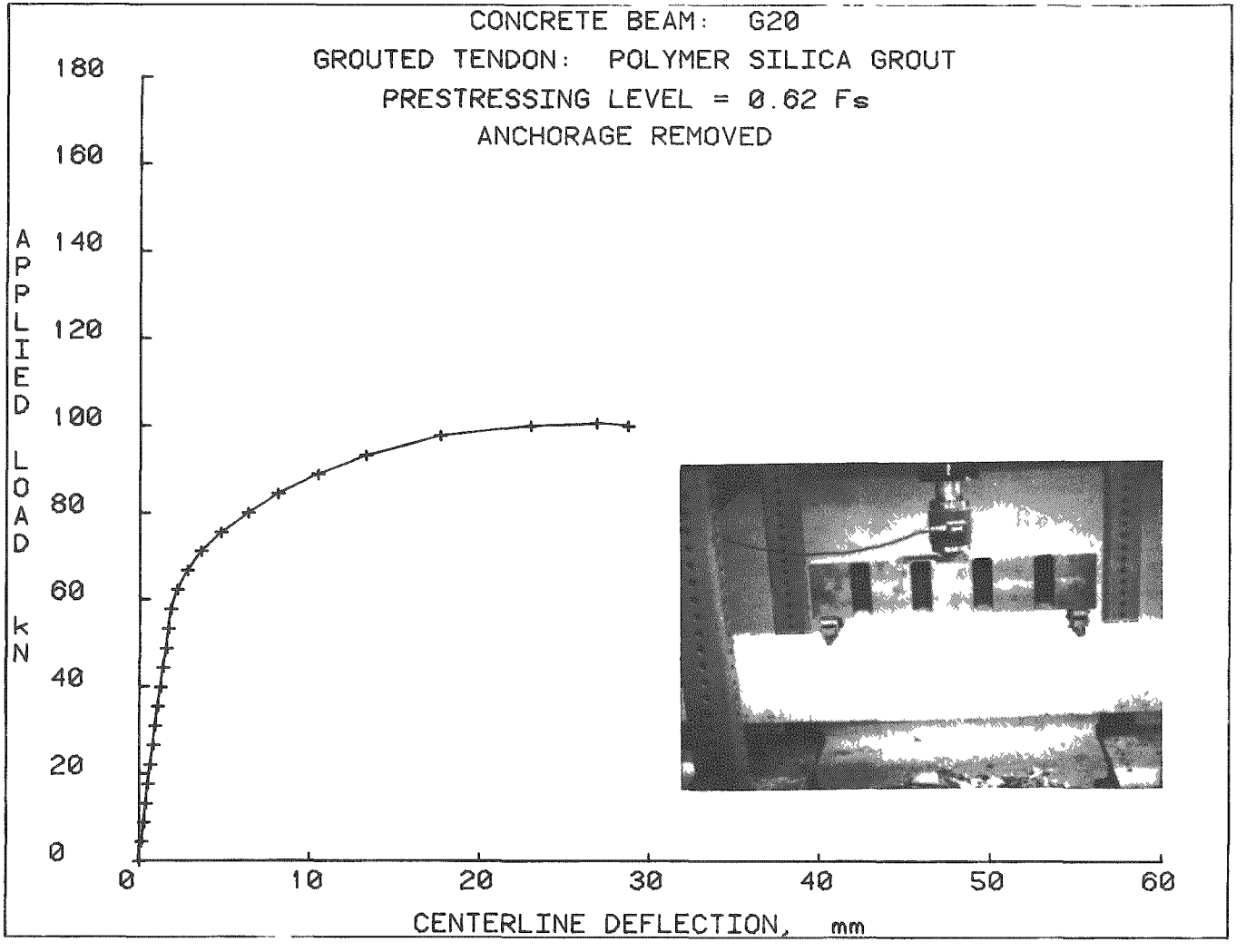

Fig. 54. Load vs centerline deflection — Beam G20.

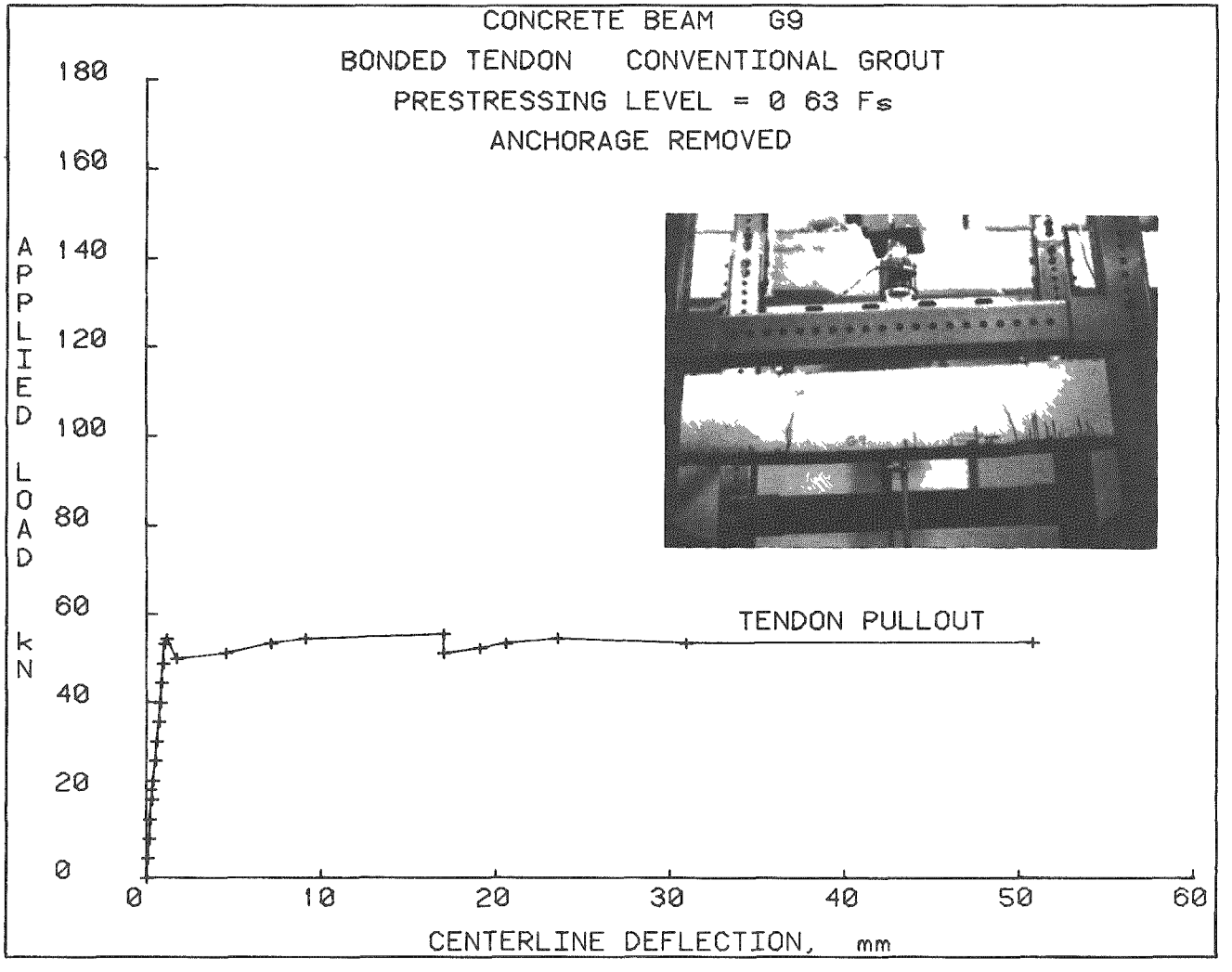

Fig. 55. Load vs centerline deflection — Beam G9.

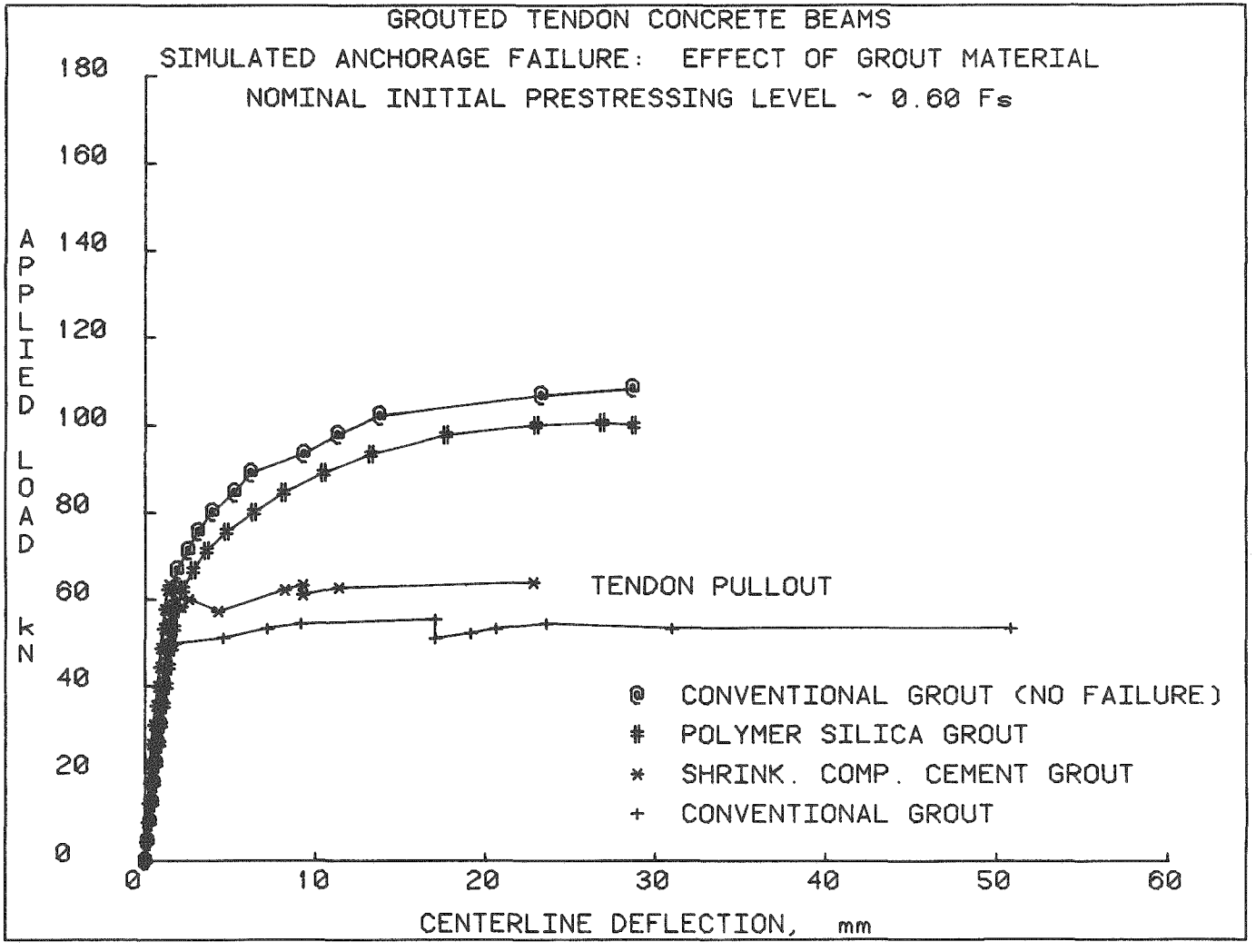

Fig. 56. Simulated anchorage failure: effect of grout material.

ORNL PHOTO 6044–78

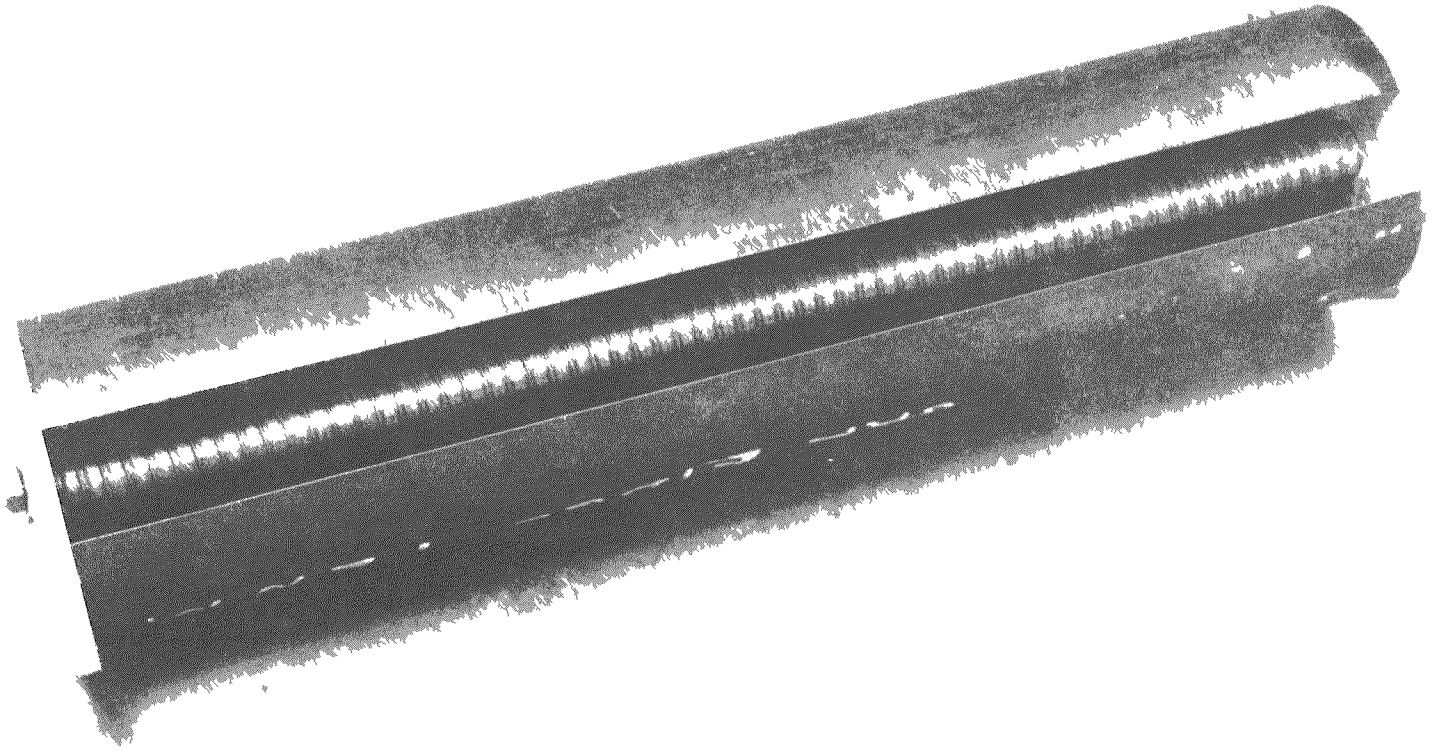

Fig. 57. Bond pull-out test specimen mold.

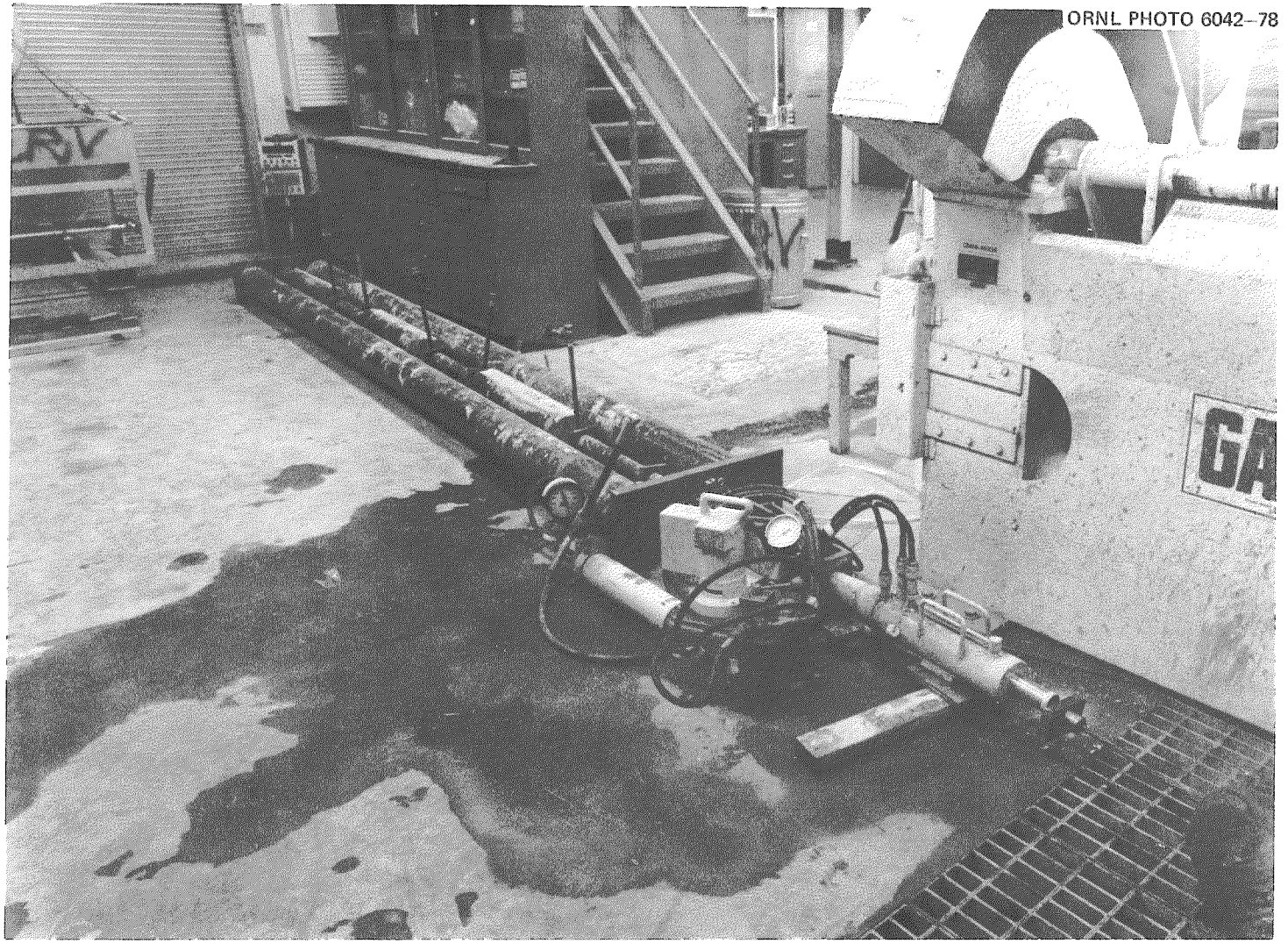

Fig. 58. Tensioning fixture for bond pull-out specimens.

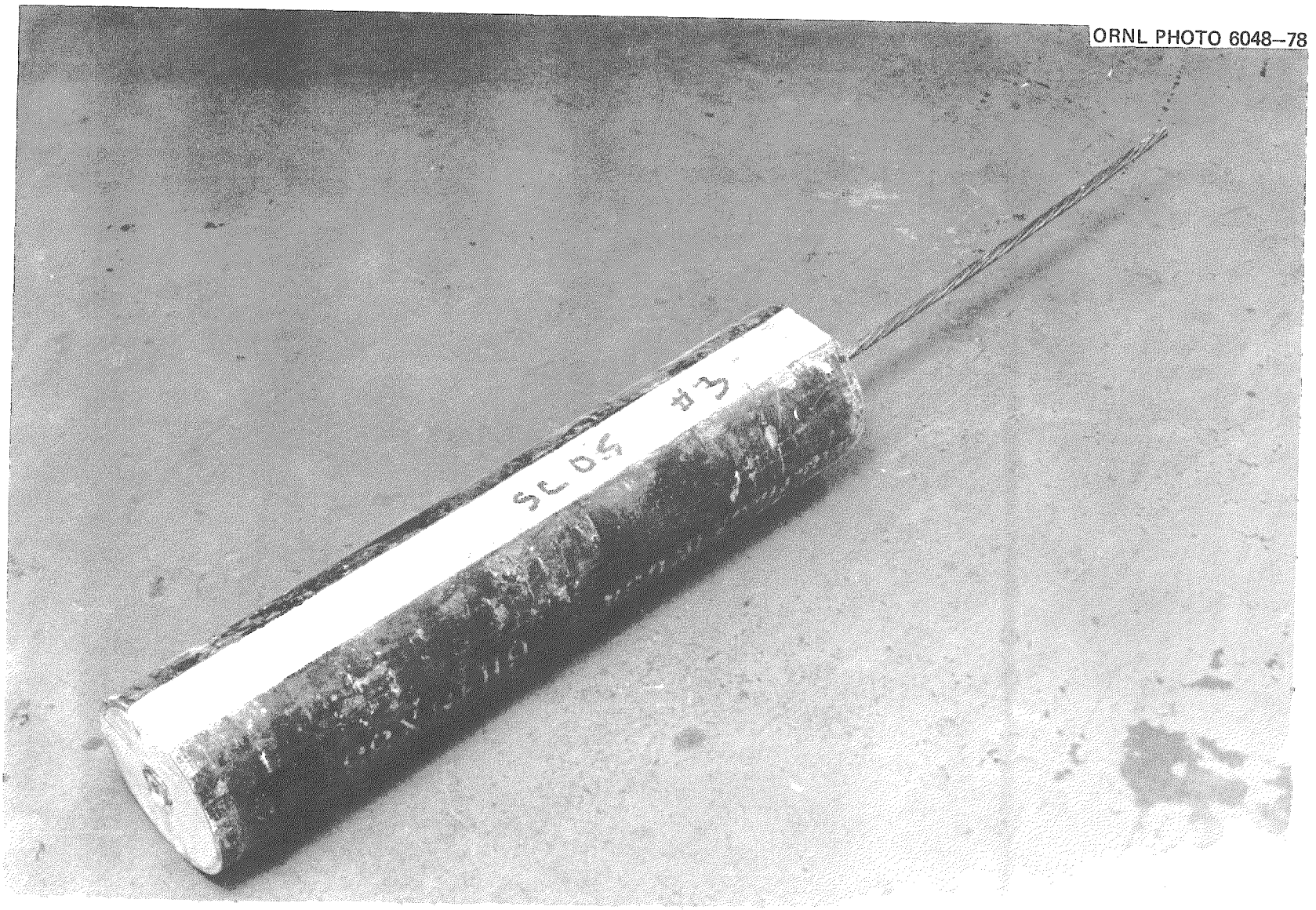

Fig. 59. Bond pull-out test specimen.

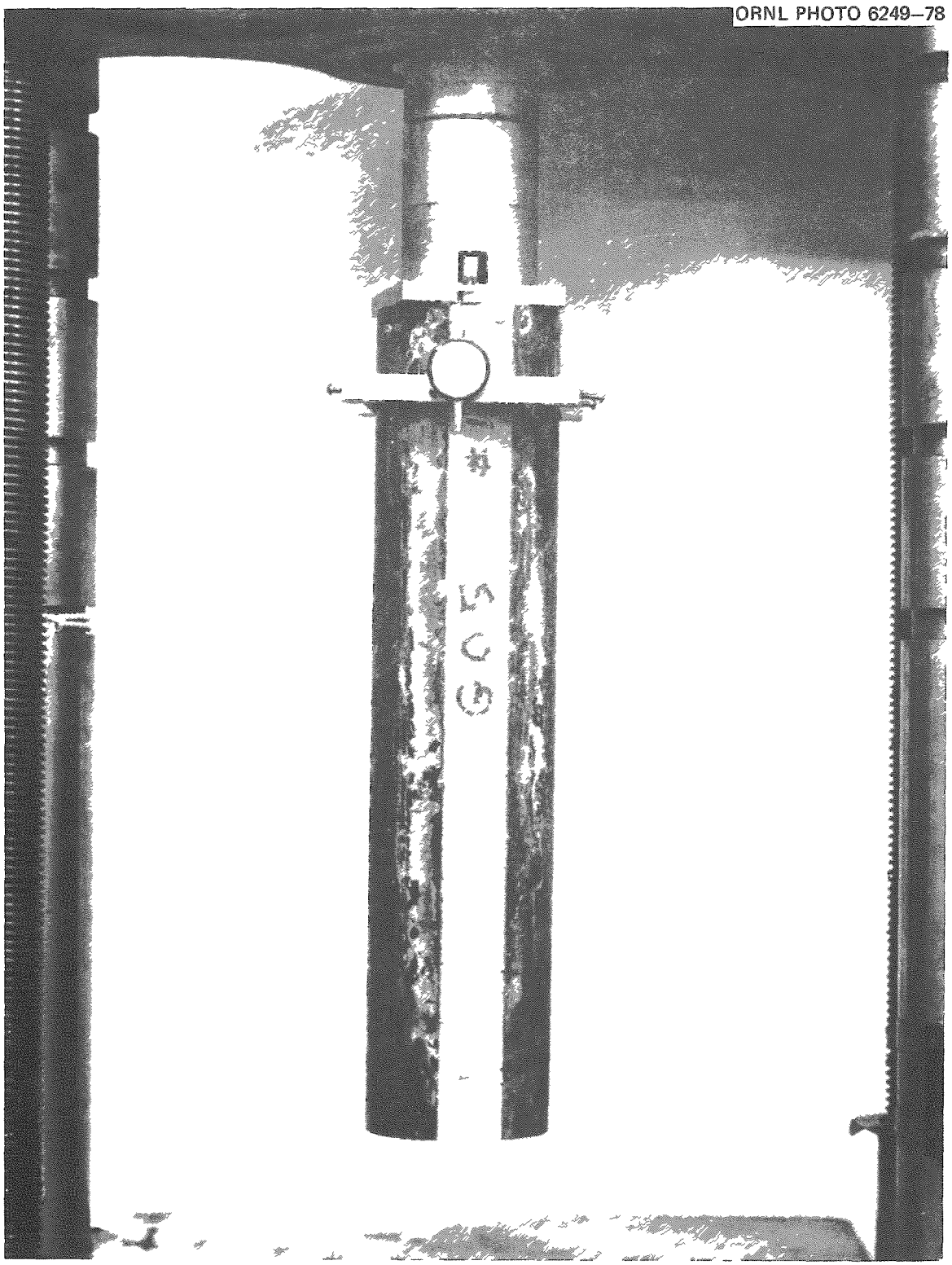

Fig. 60. Bond pull-out test setup.

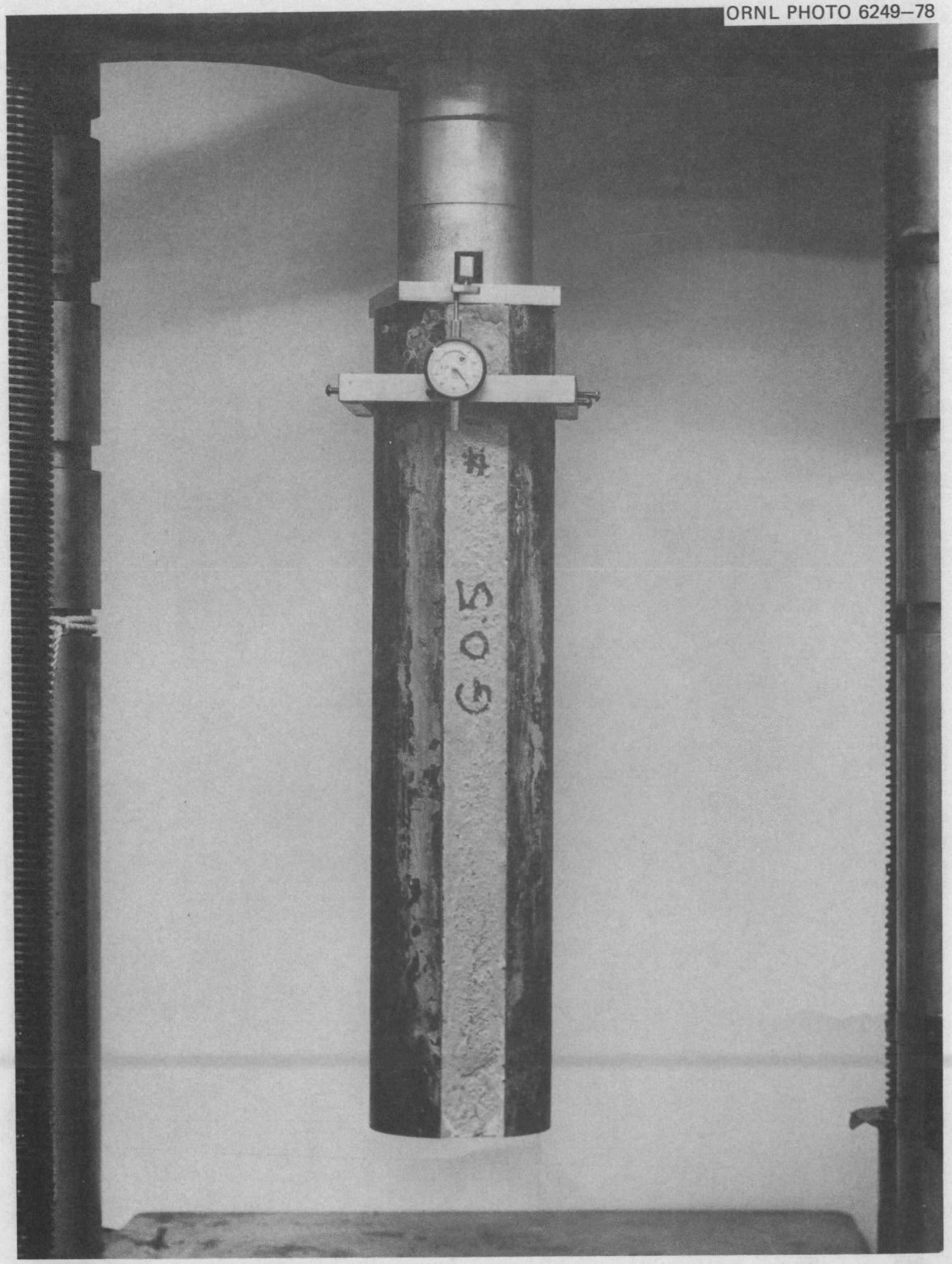

Fig. 60. Bond pull-out test setup.

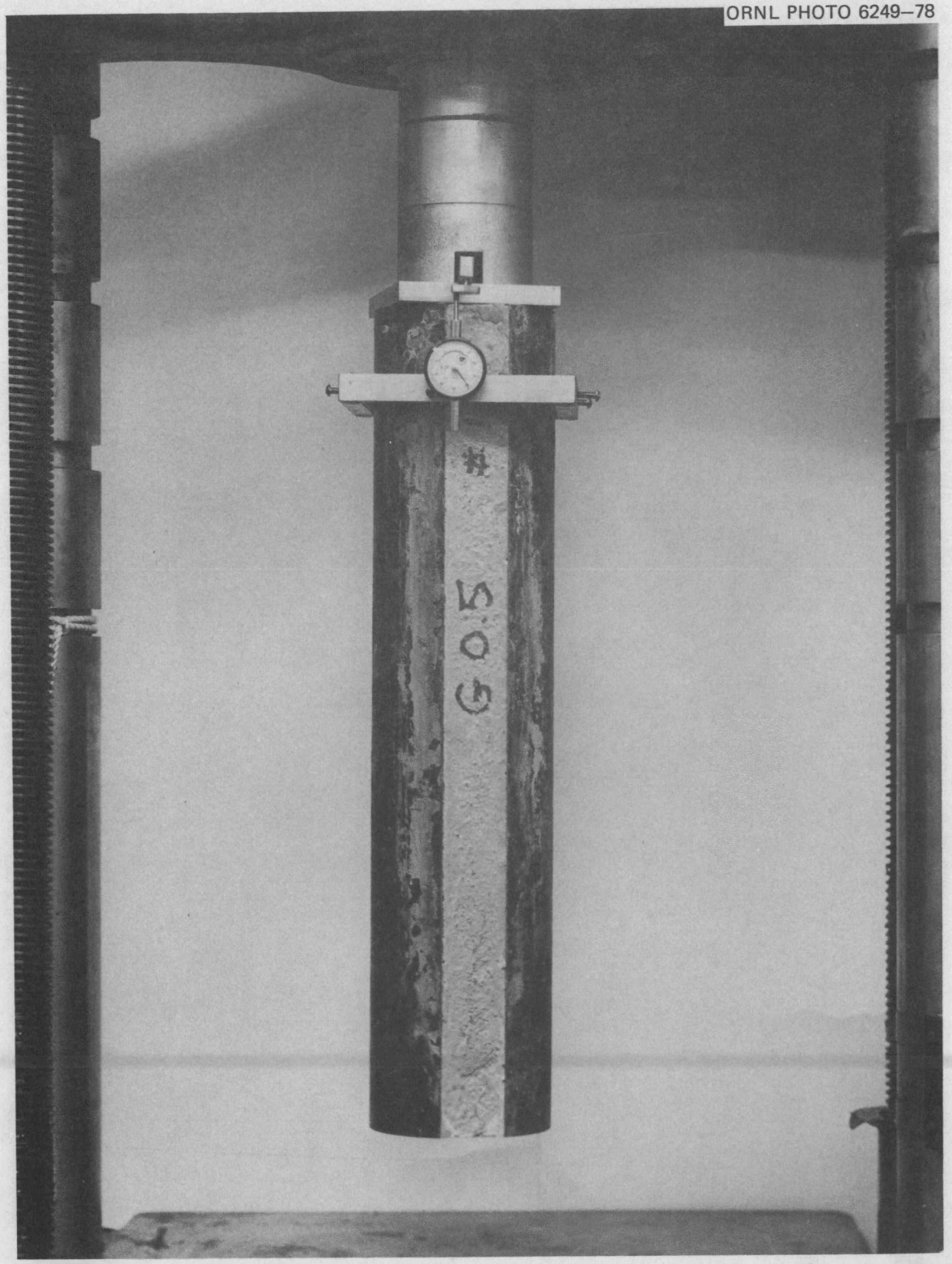

Fig. 60. Bond pull-out test setup.

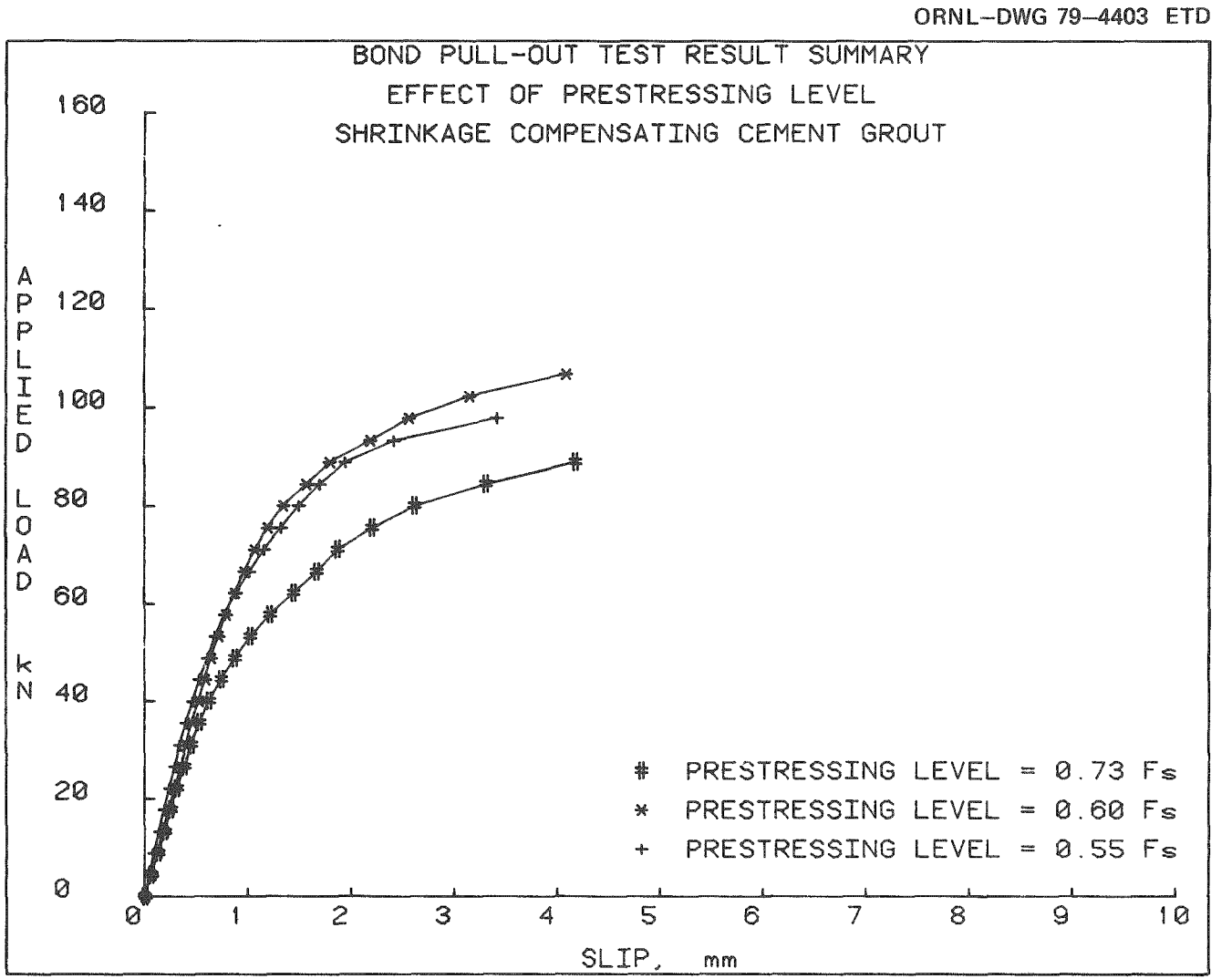

Fig. 61. Applied load vs slip: shrinkage-compensating cement grout.

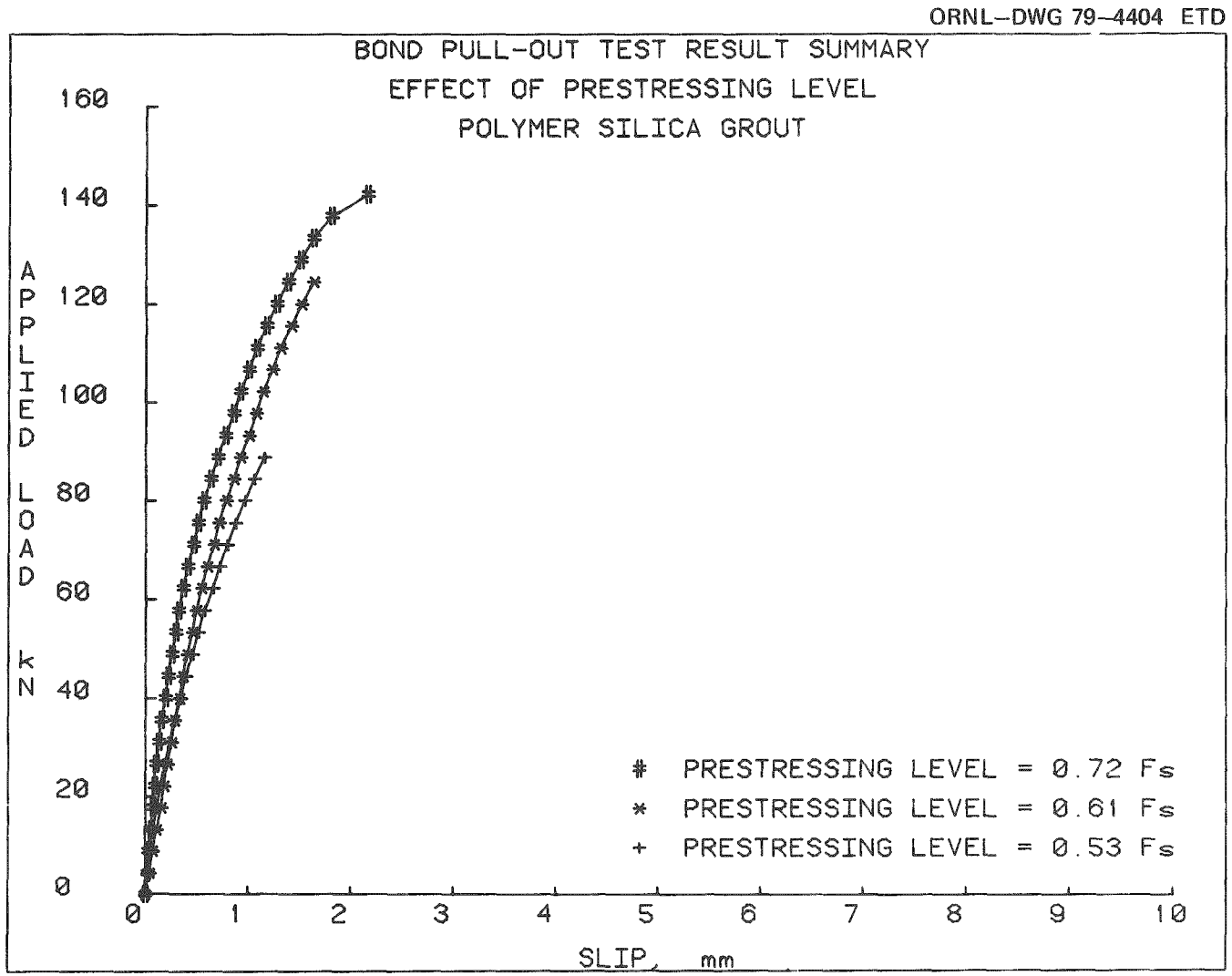

Fig. 62. Applied load vs slip: polymer-silica cement grout.

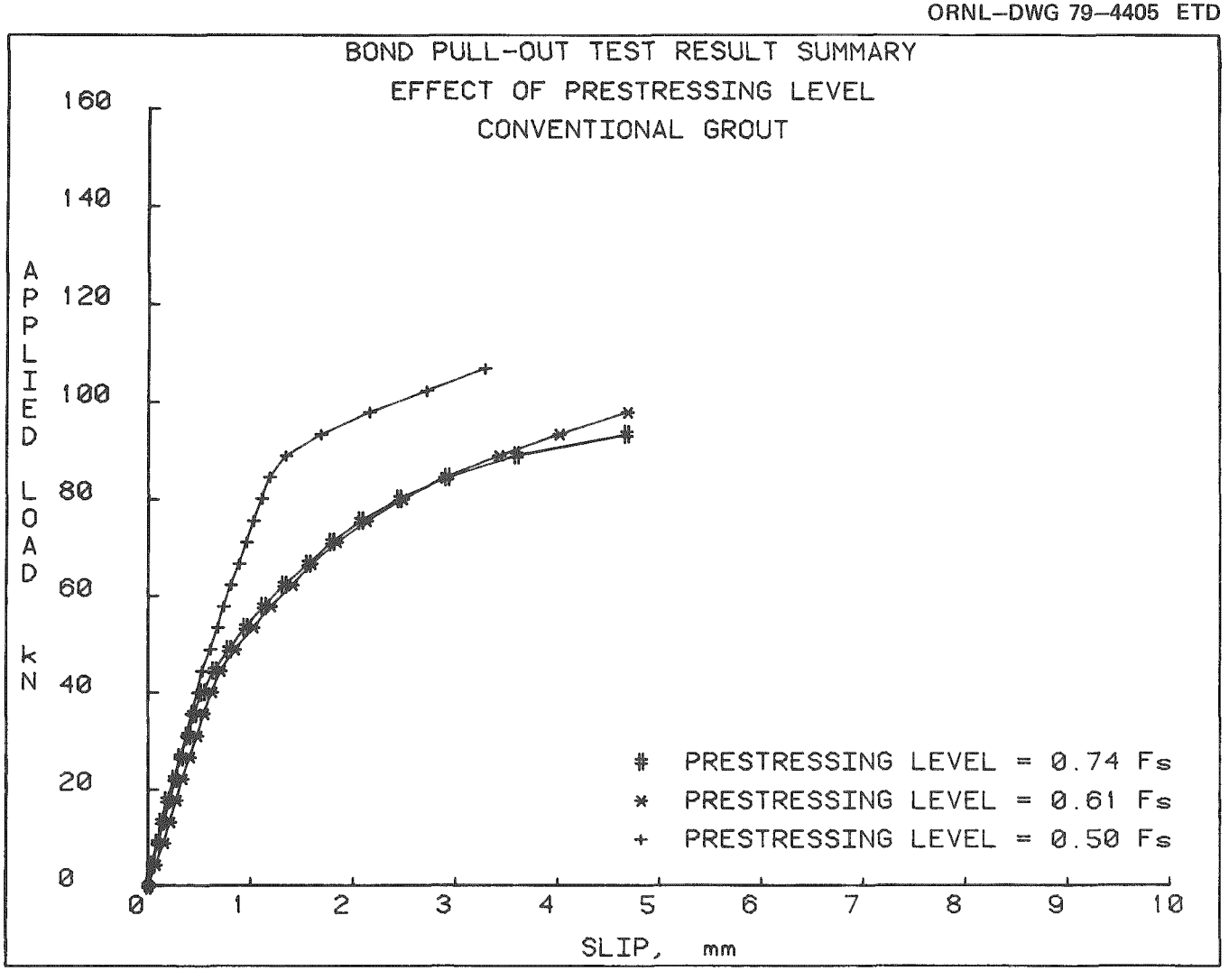

Fig. 63. Applied load vs slip: conventional grout.

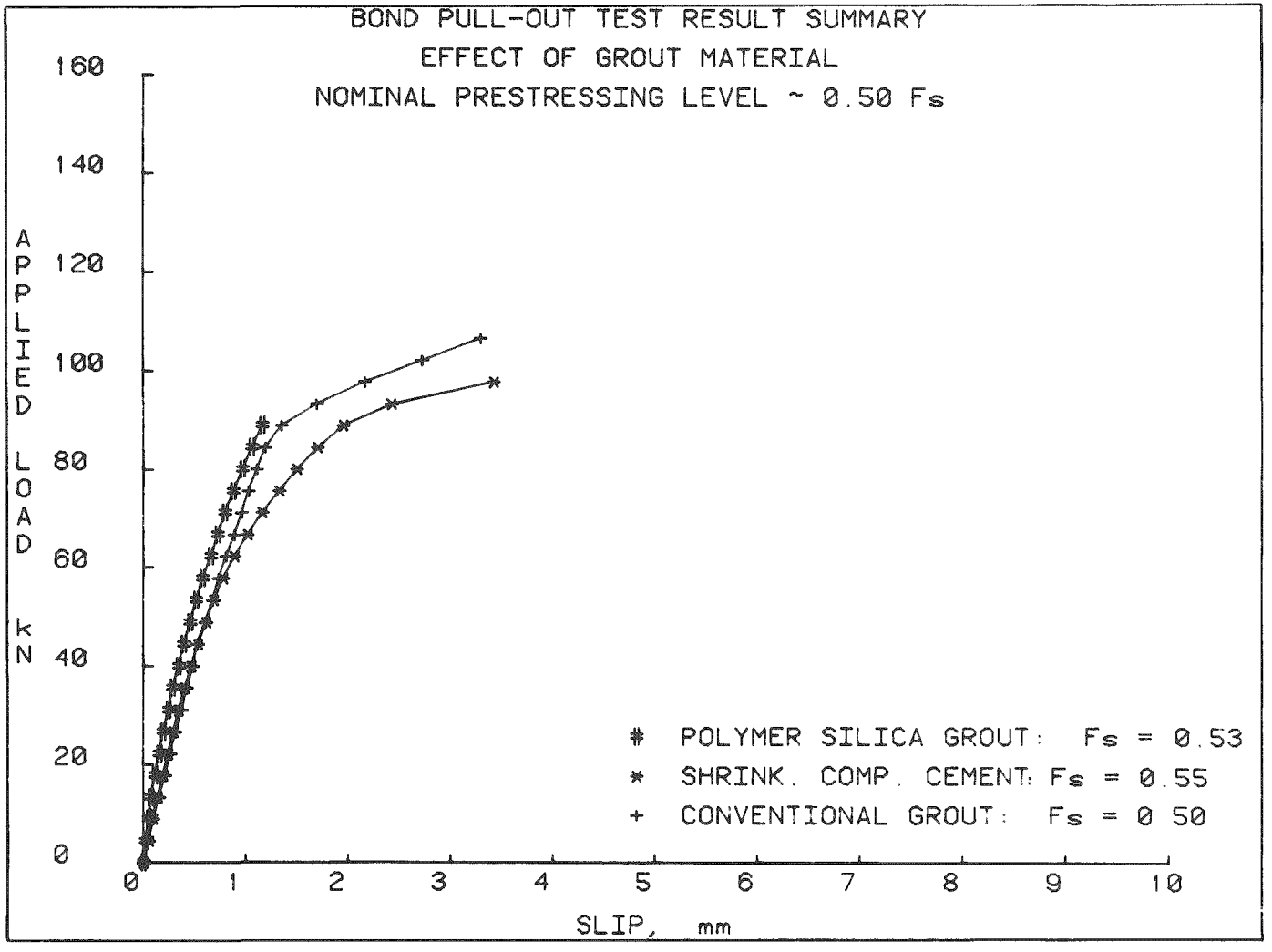

Fig. 64. Effect of grout material on load-slip behavior — F_s = 0.50.

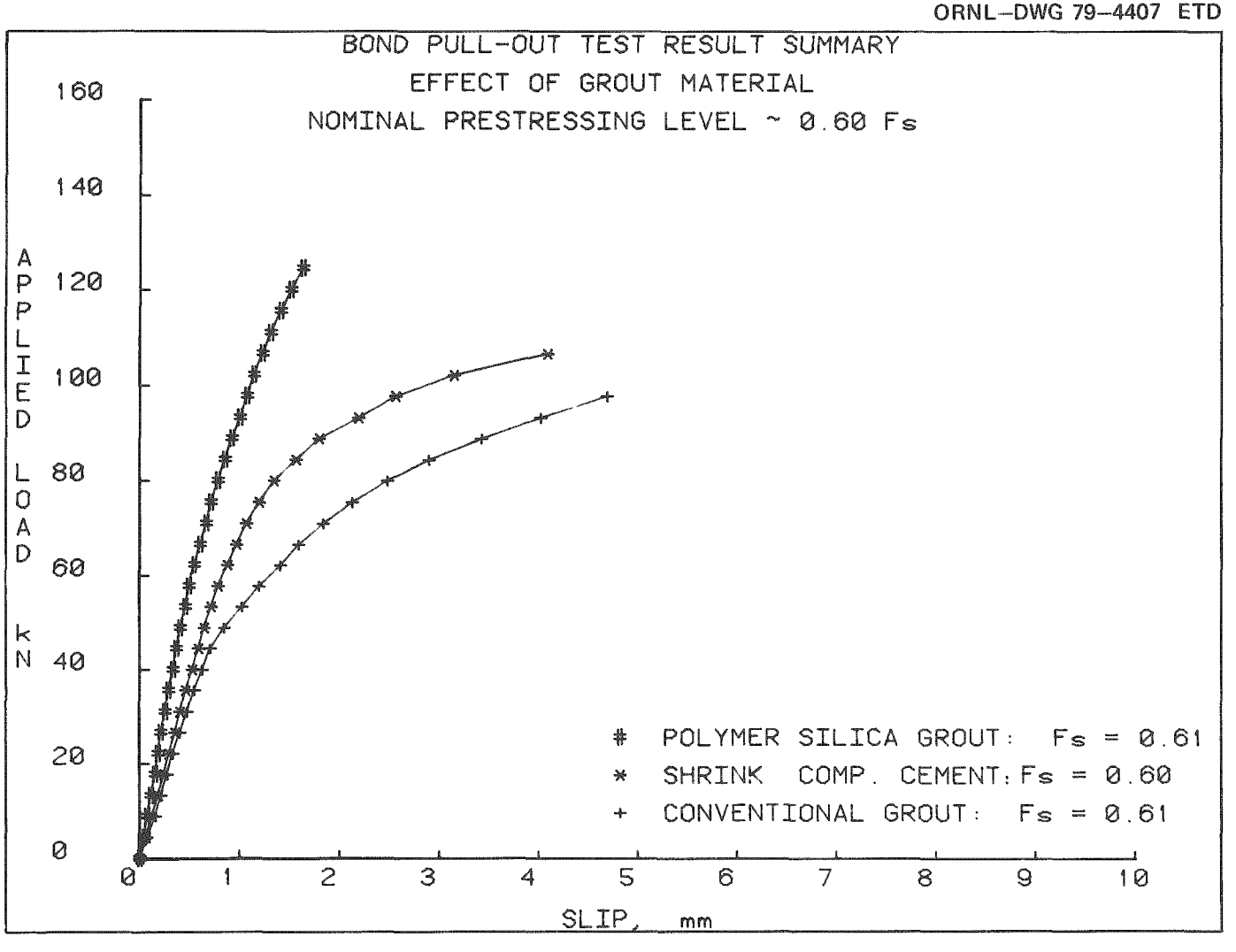

Fig. 65. Effect of grout material on load-slip behavior — F_s = 0.60.

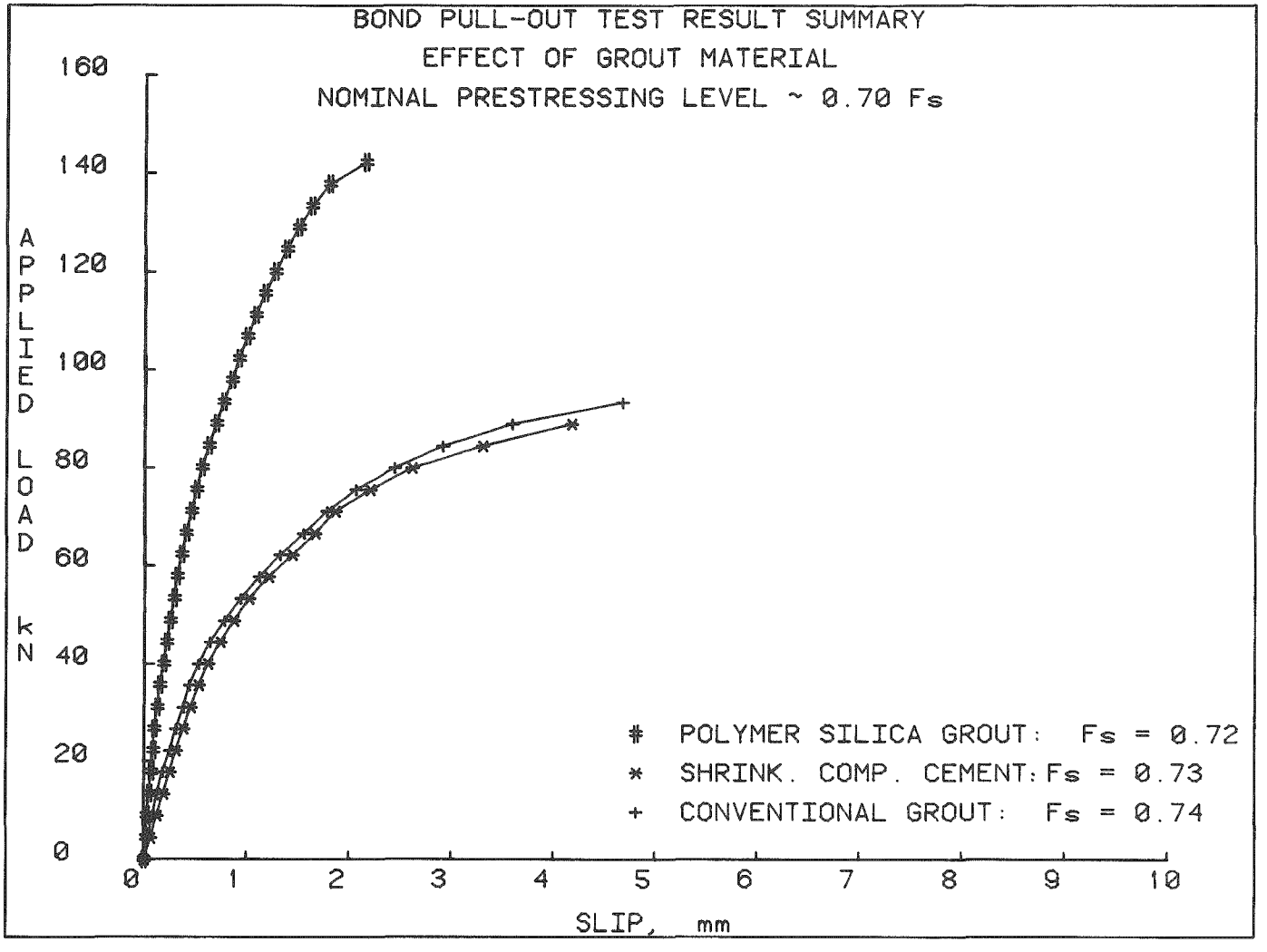

Fig. 66. Effect of grout material on load-slip behavior — F_s = 0.70.

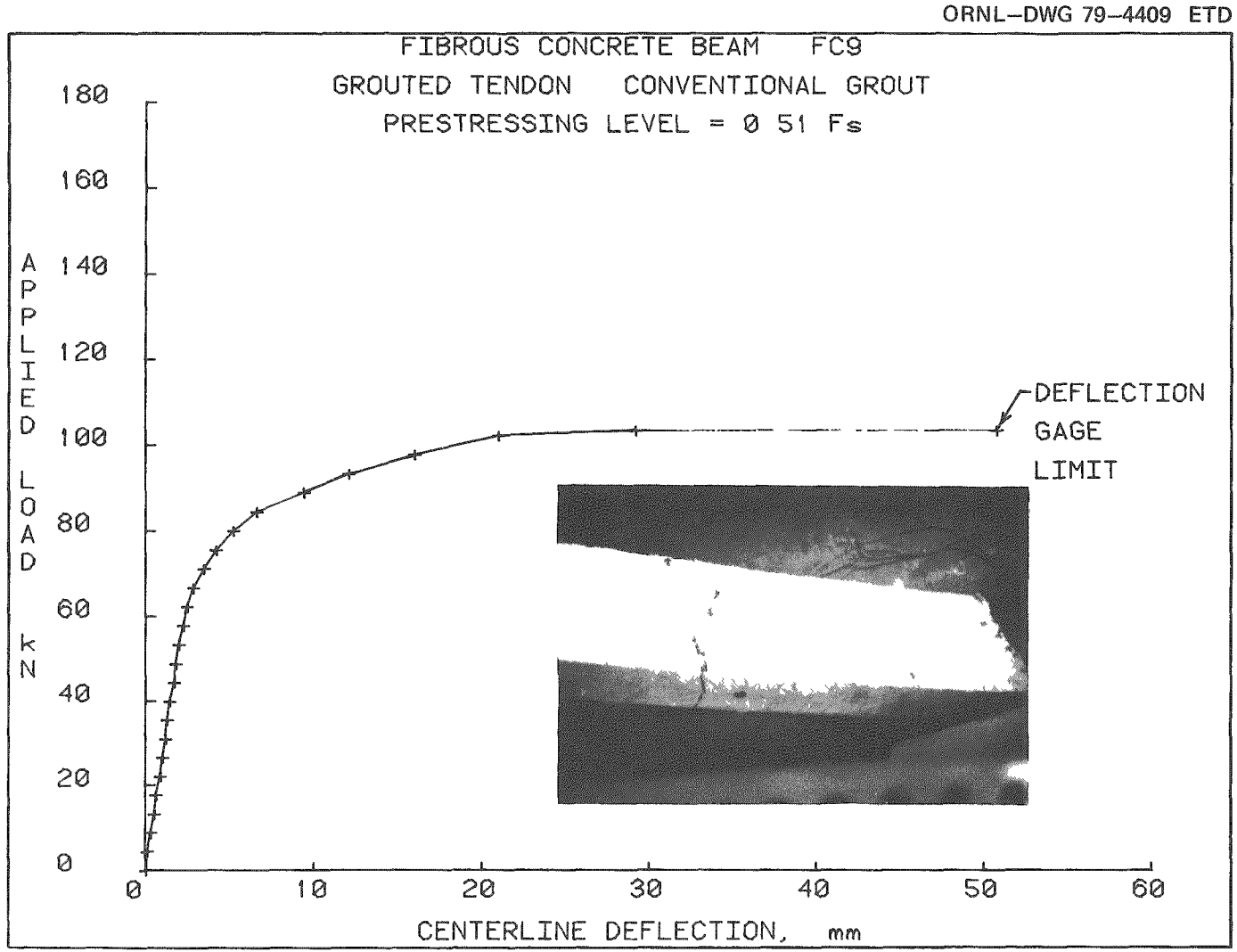

Fig. 67. Load vs centerline deflection — Beam FC9.

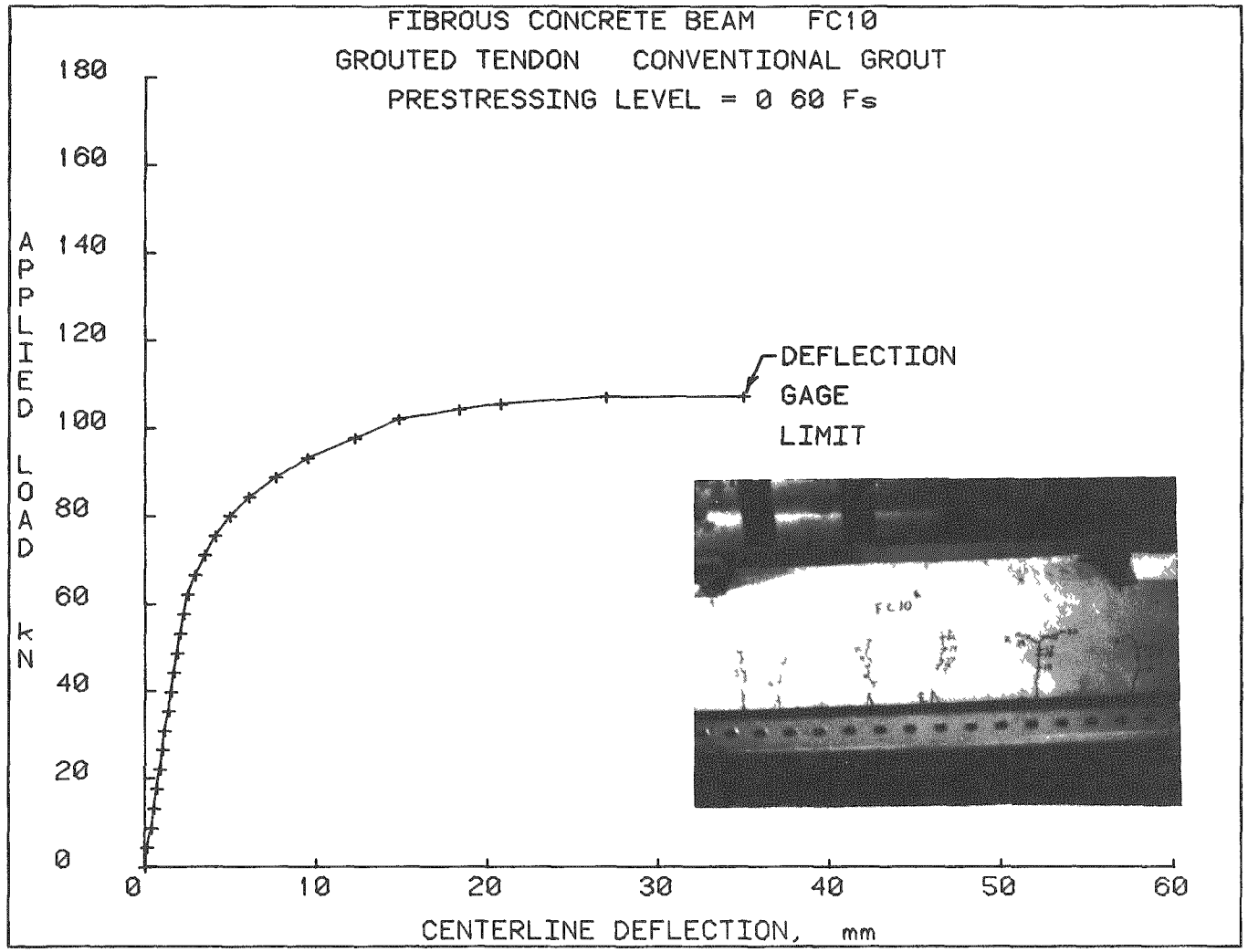

Fig. 68. Load vs centerline deflection — Beam FC10.

ORNL-DWG 79-4411 ETD

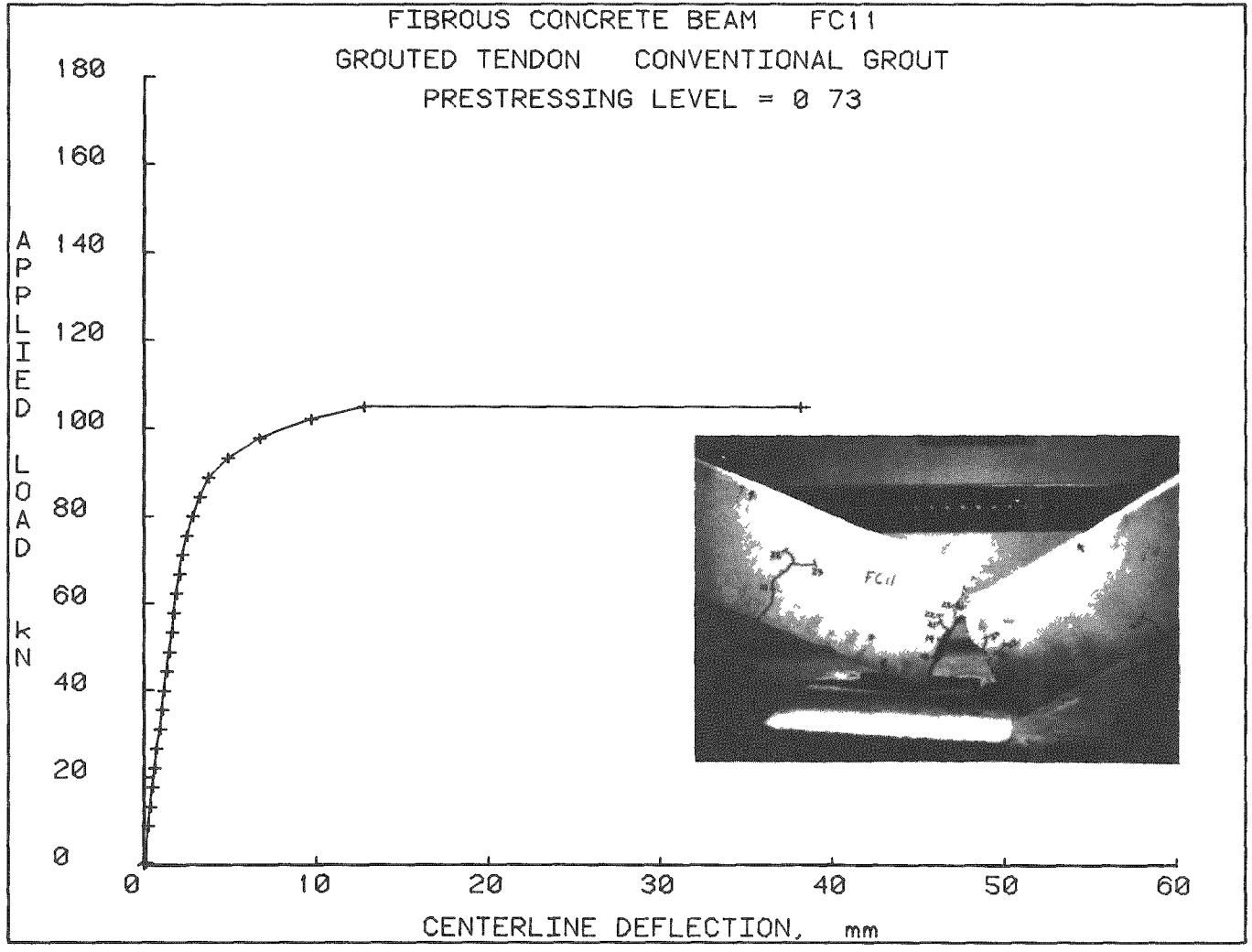

Fig. 69. Load vs centerline deflection — Beam FC11.

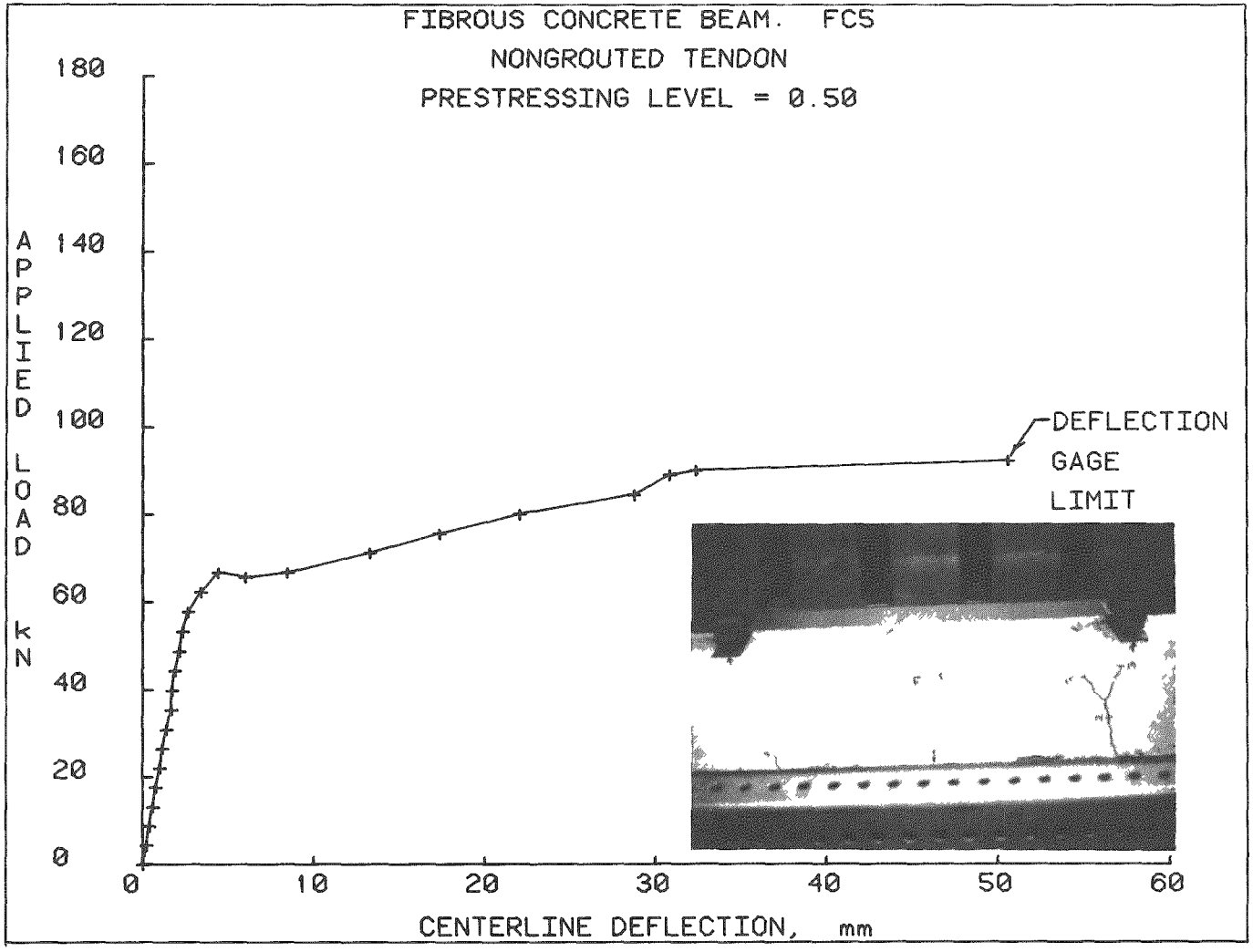

Fig. 70. Load vs centerline deflection — Beam FC5.

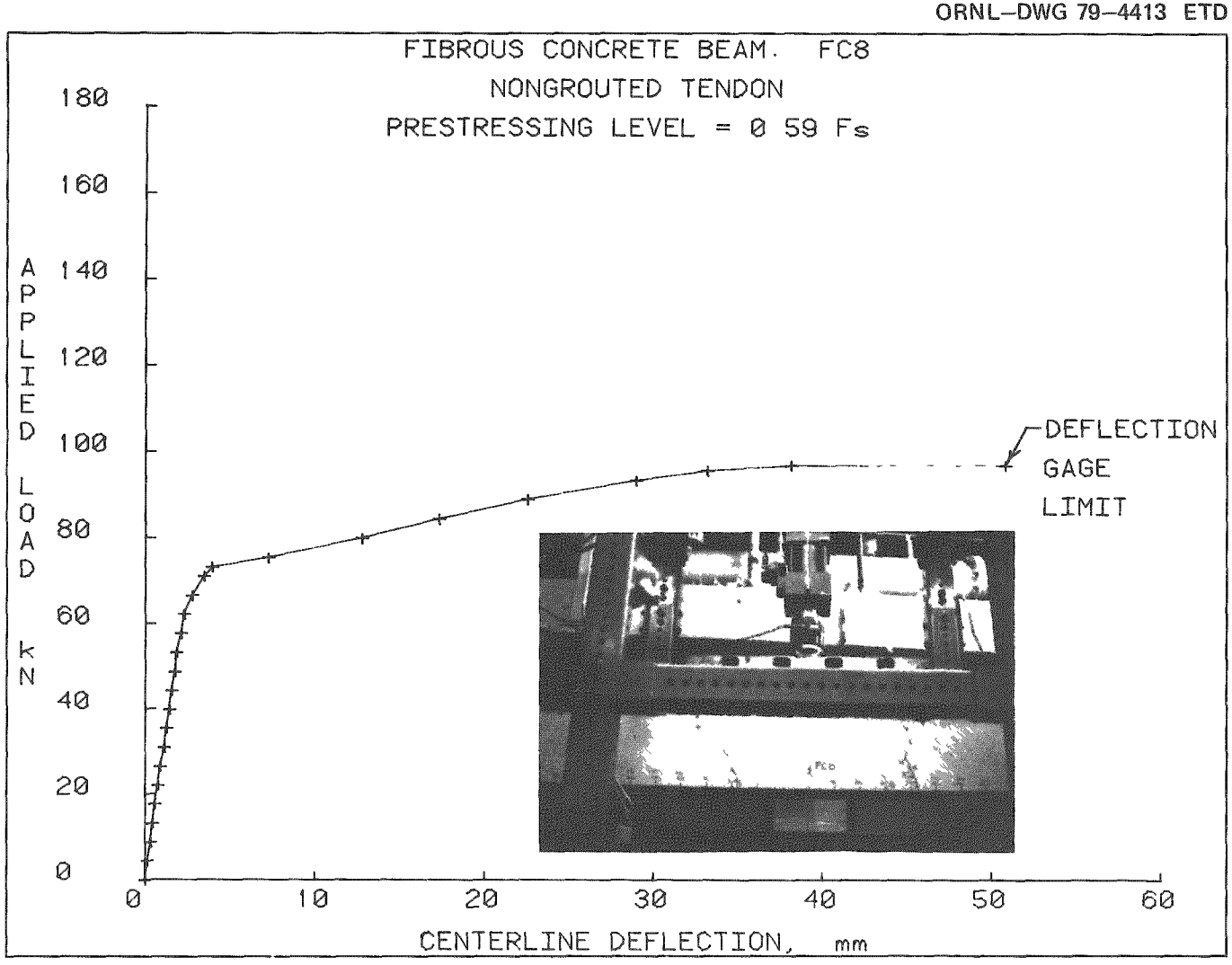

Fig. 71. Load vs centerline deflection — Beam FC8.

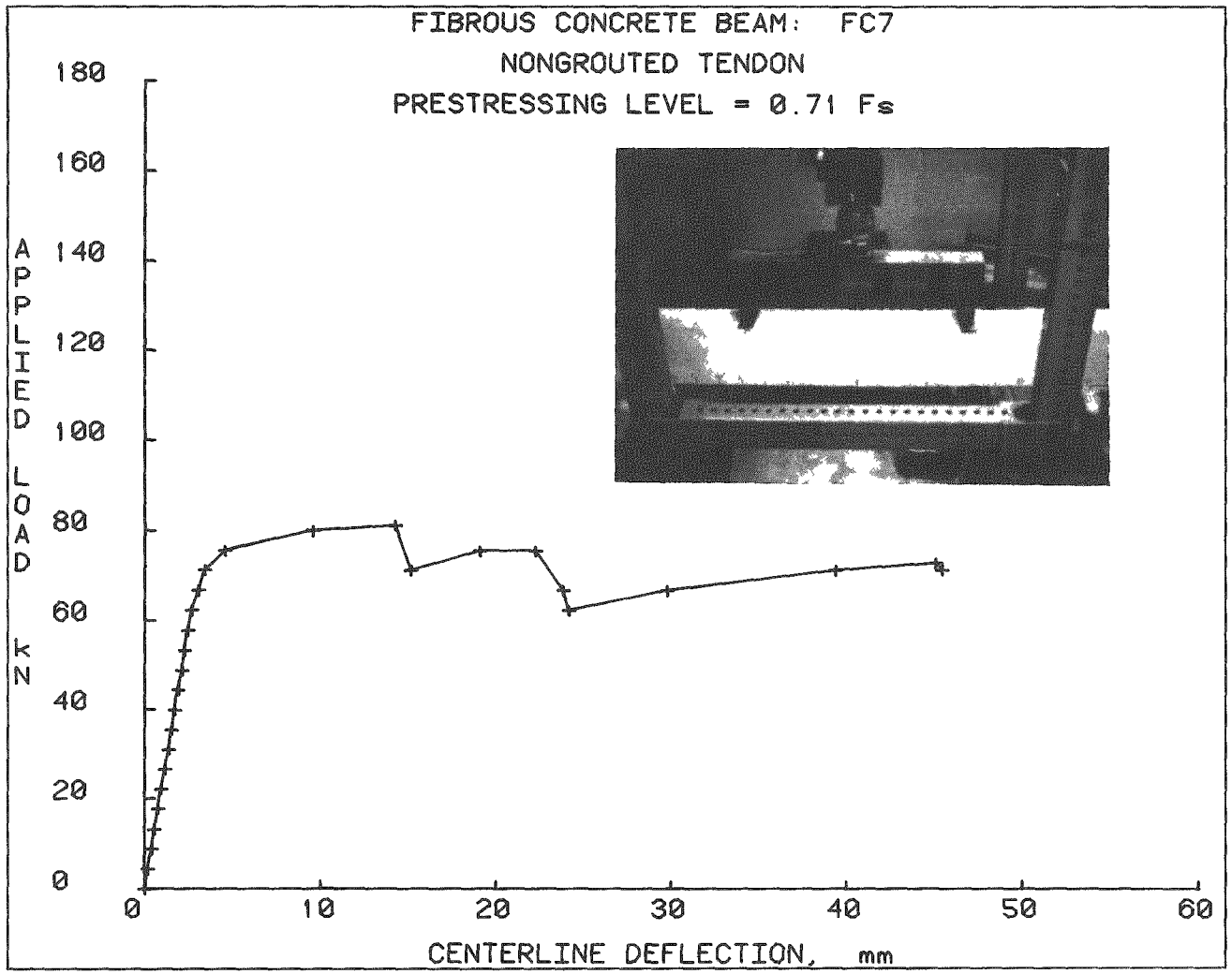

Fig. 72. Load vs centerline deflection — Beam FC7.

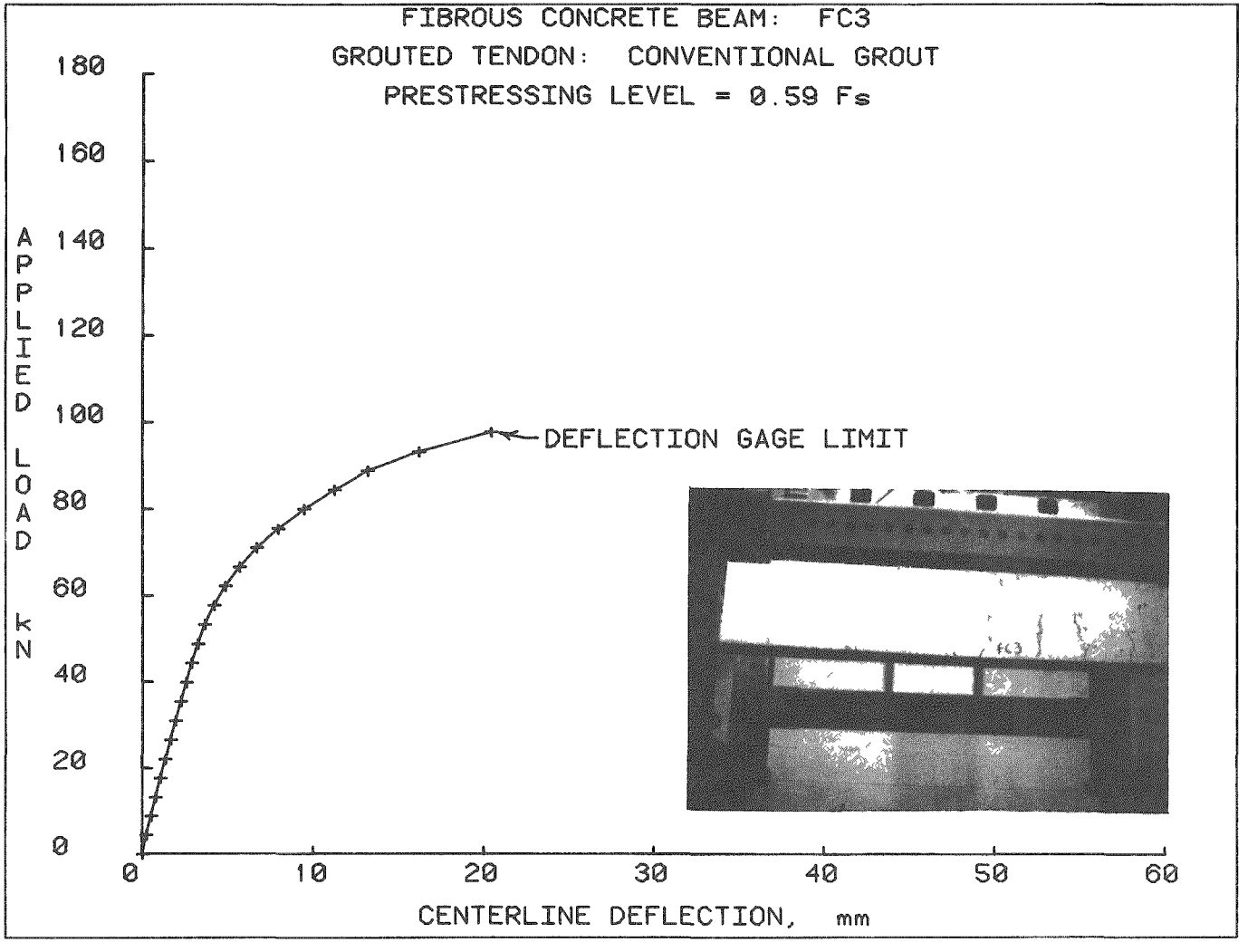

Fig. 73. Load vs centerline deflection — Beam FC3.

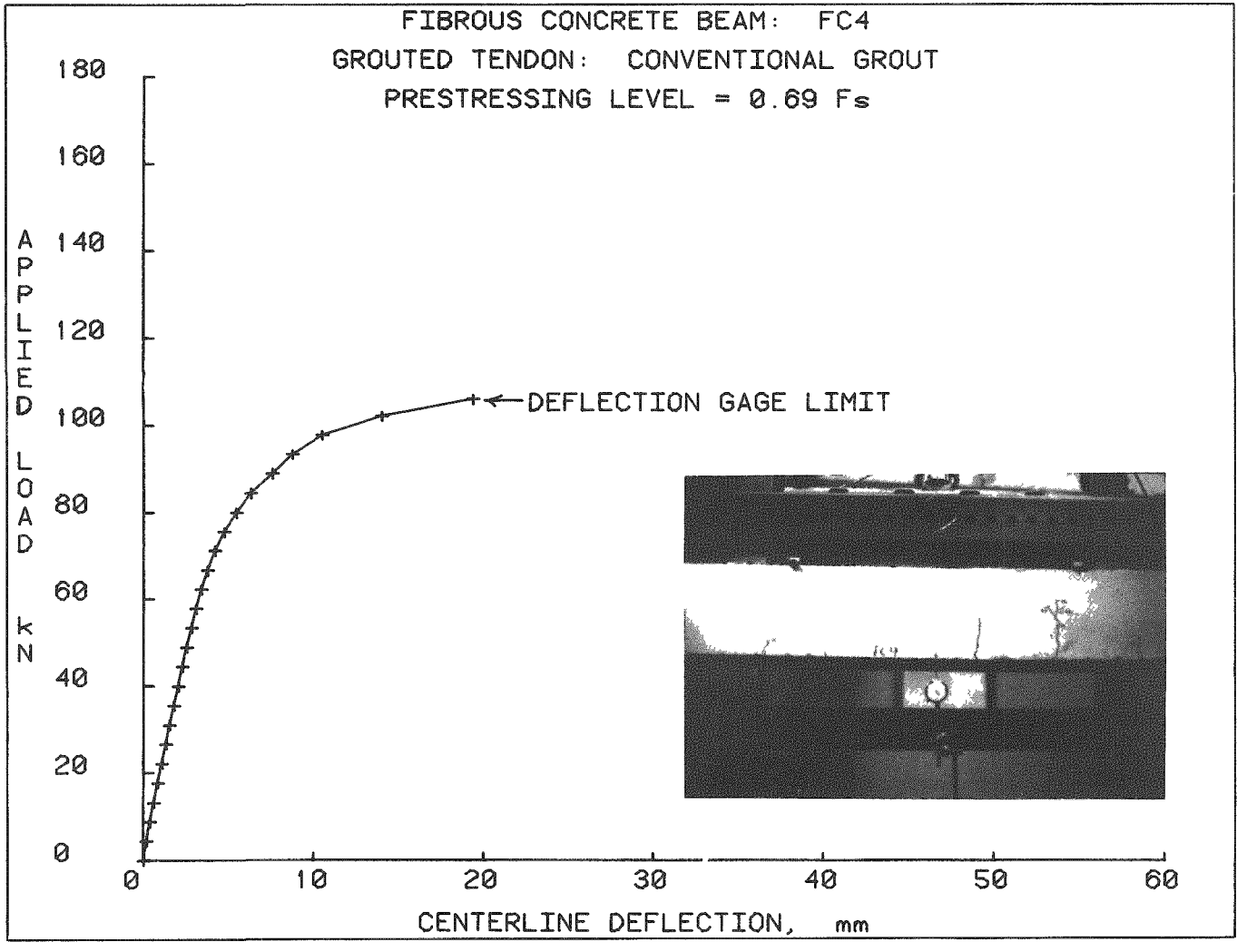

Fig. 74. Load vs centerline deflection — Beam FC4.

ORNL–DWG 79–4417 ETD

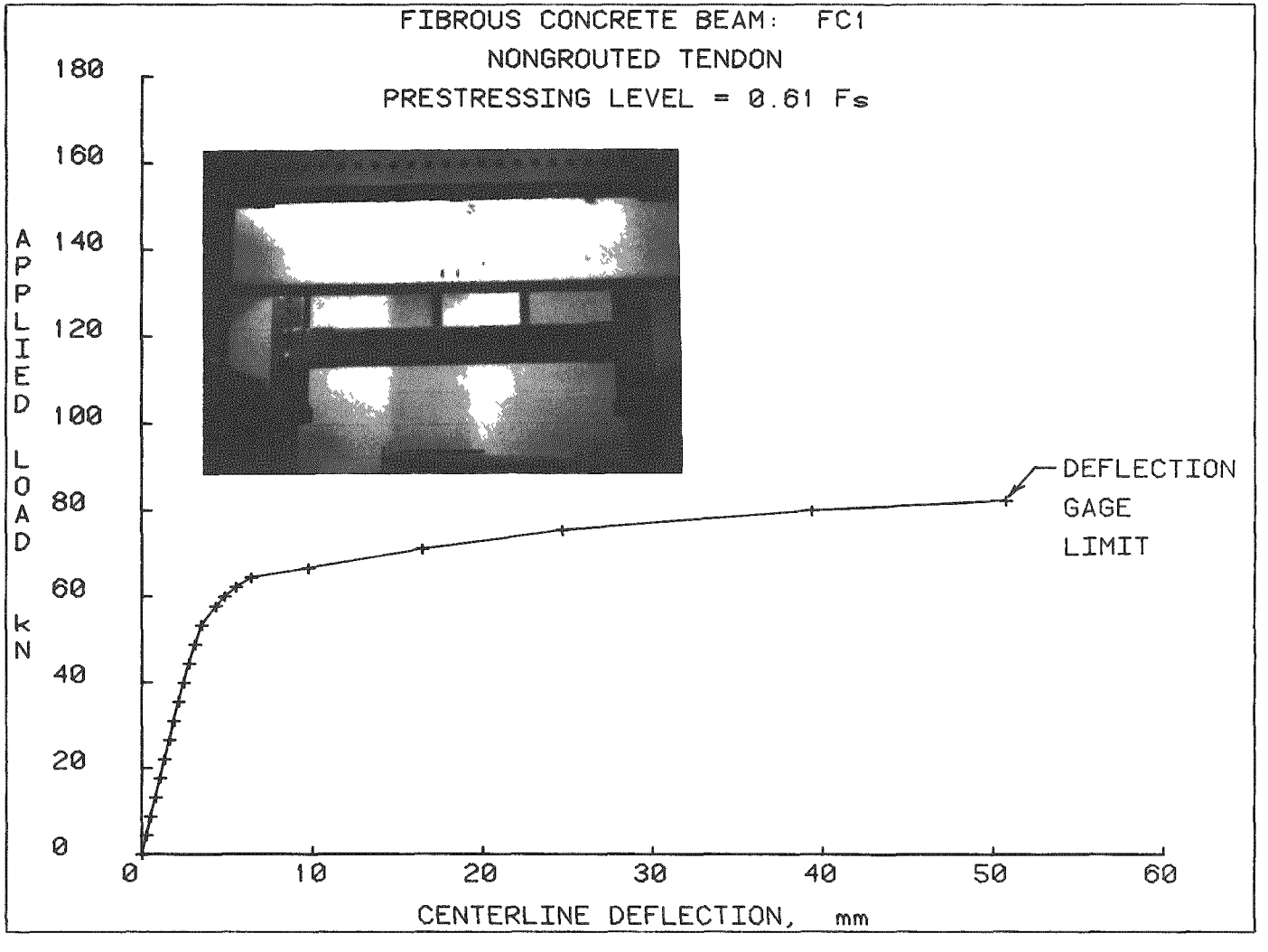

Fig. 75. Load vs centerline deflection — Beam FC1.

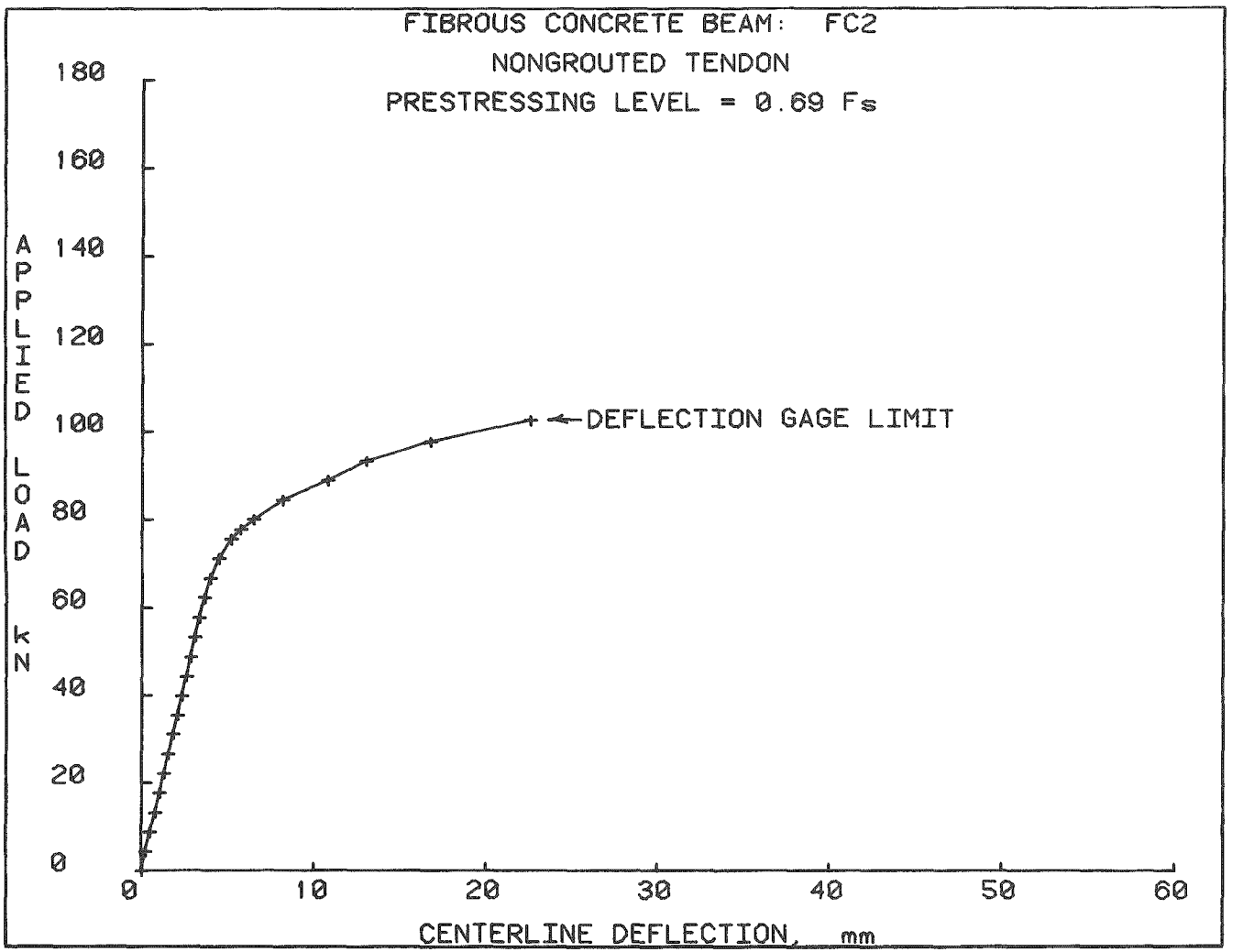

Fig. 76. Load vs centerline deflection — Beam FC2.

ORNL-DWG 79-4419 ETD

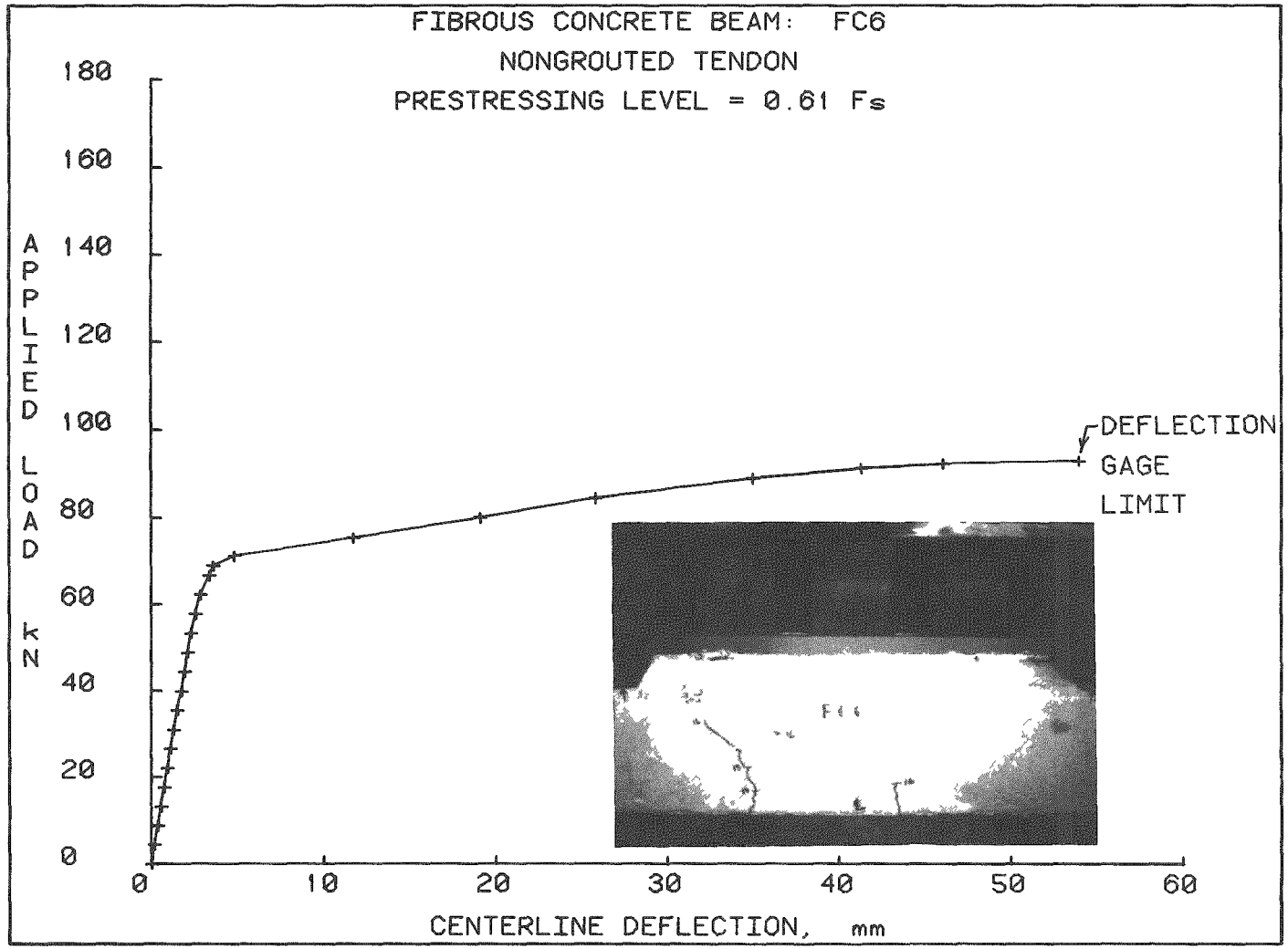

Fig. 77. Load vs centerline deflection — Beam FC6.

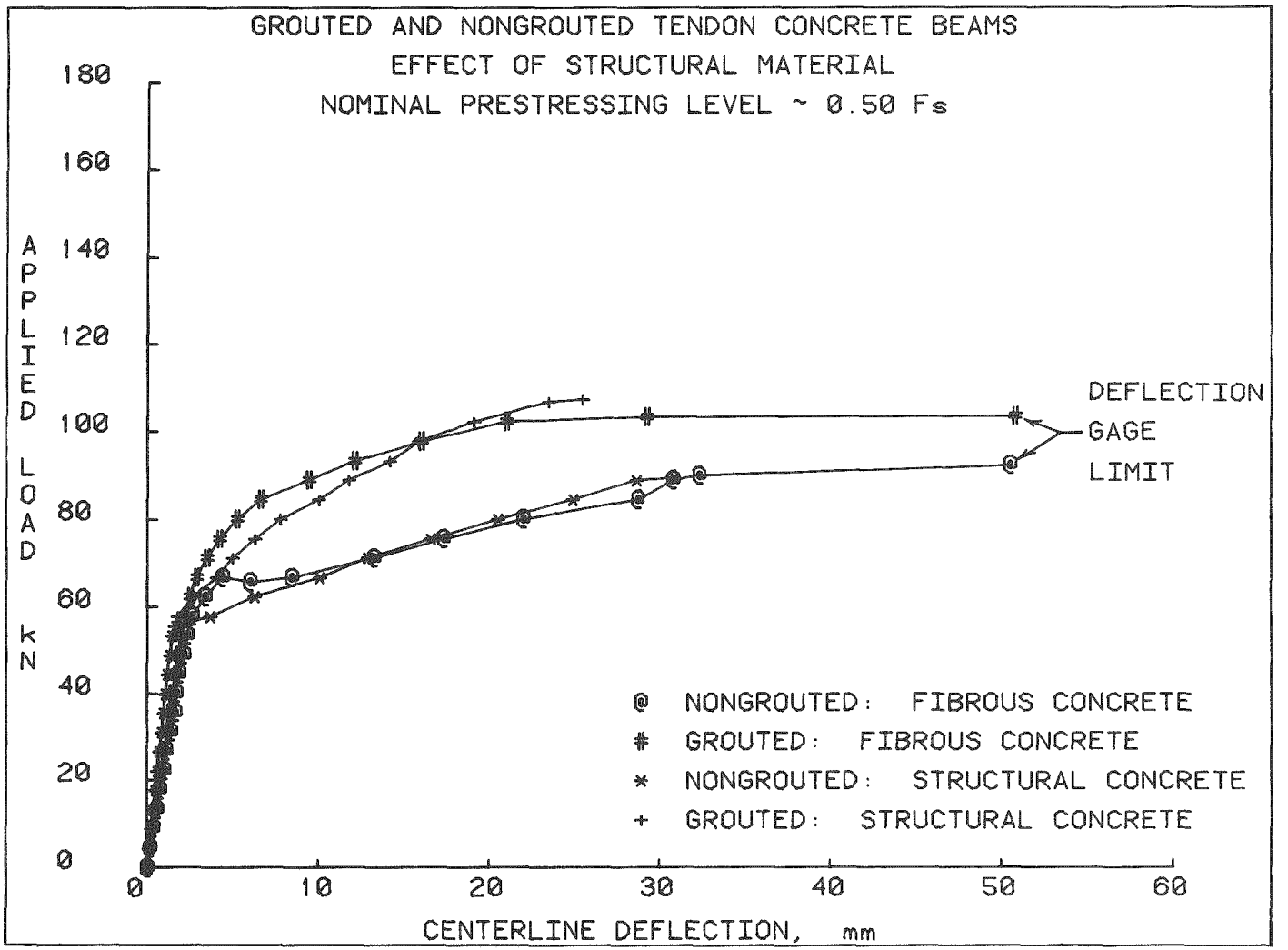

Fig. 78. Effect of structural material on beam performance — F_s = 0.50.

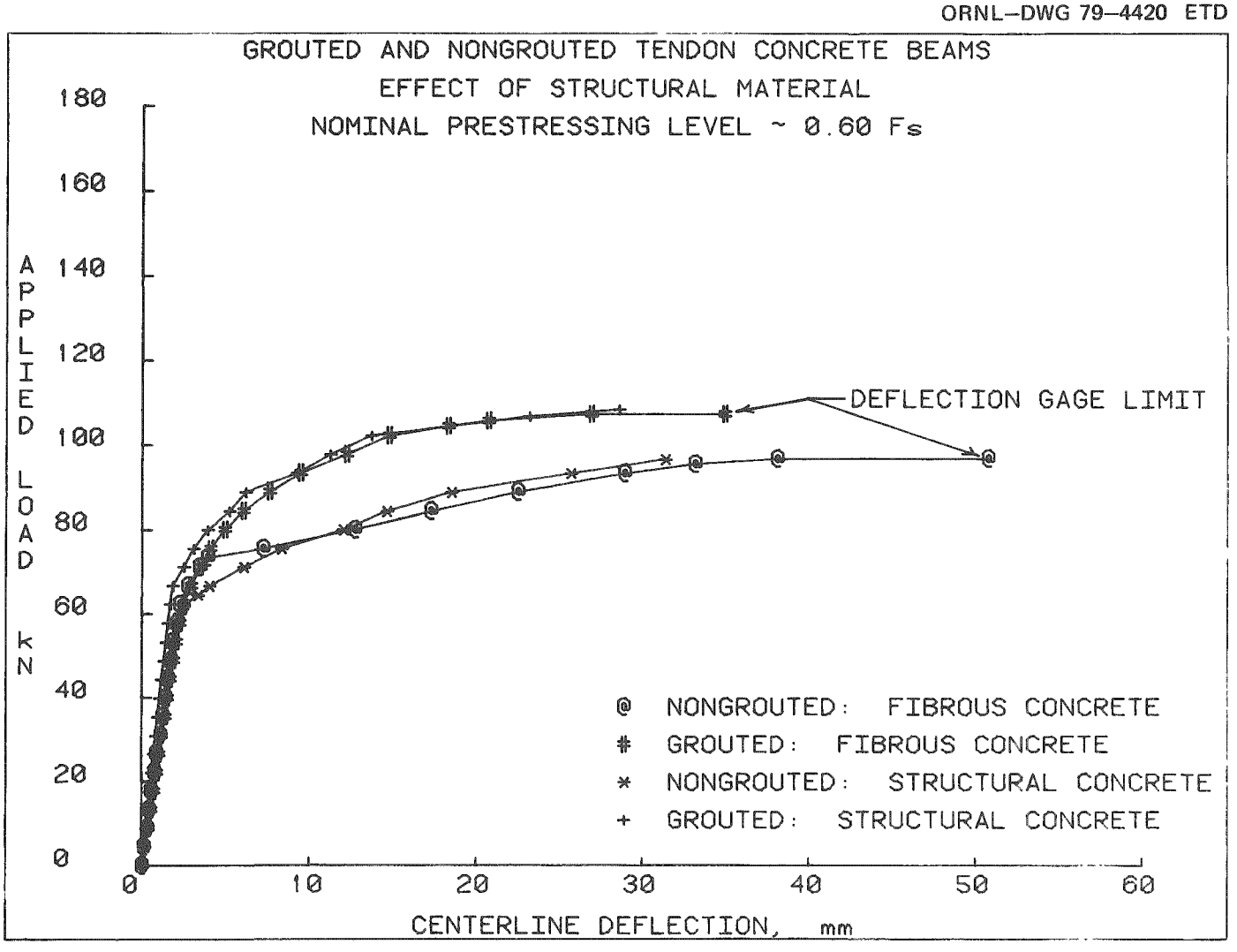

Fig. 79. Effect of structural material on beam performance — F_s = 0.60.

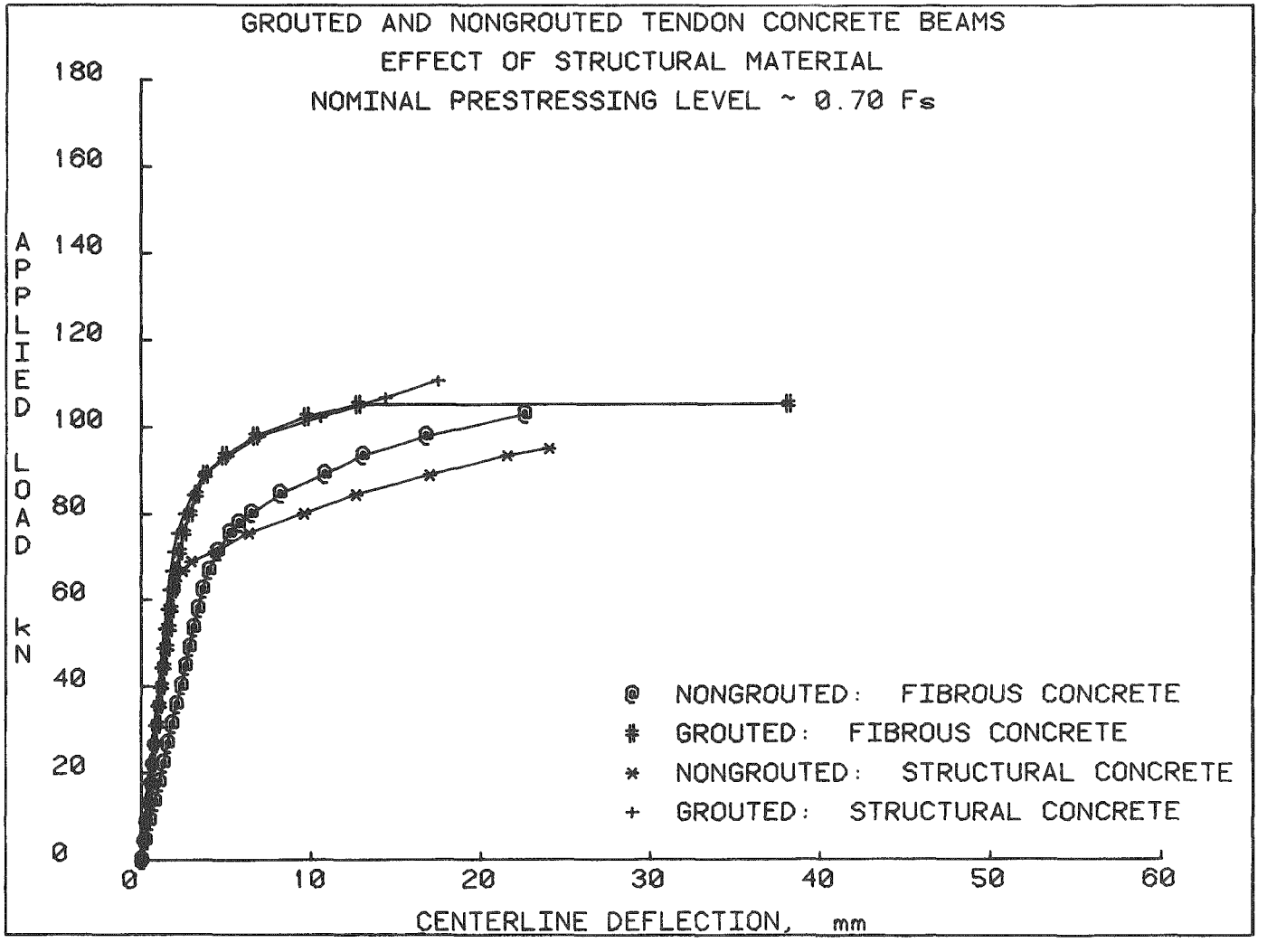

Fig. 80. Effect of structural material on beam performance — F_s = 0.70.

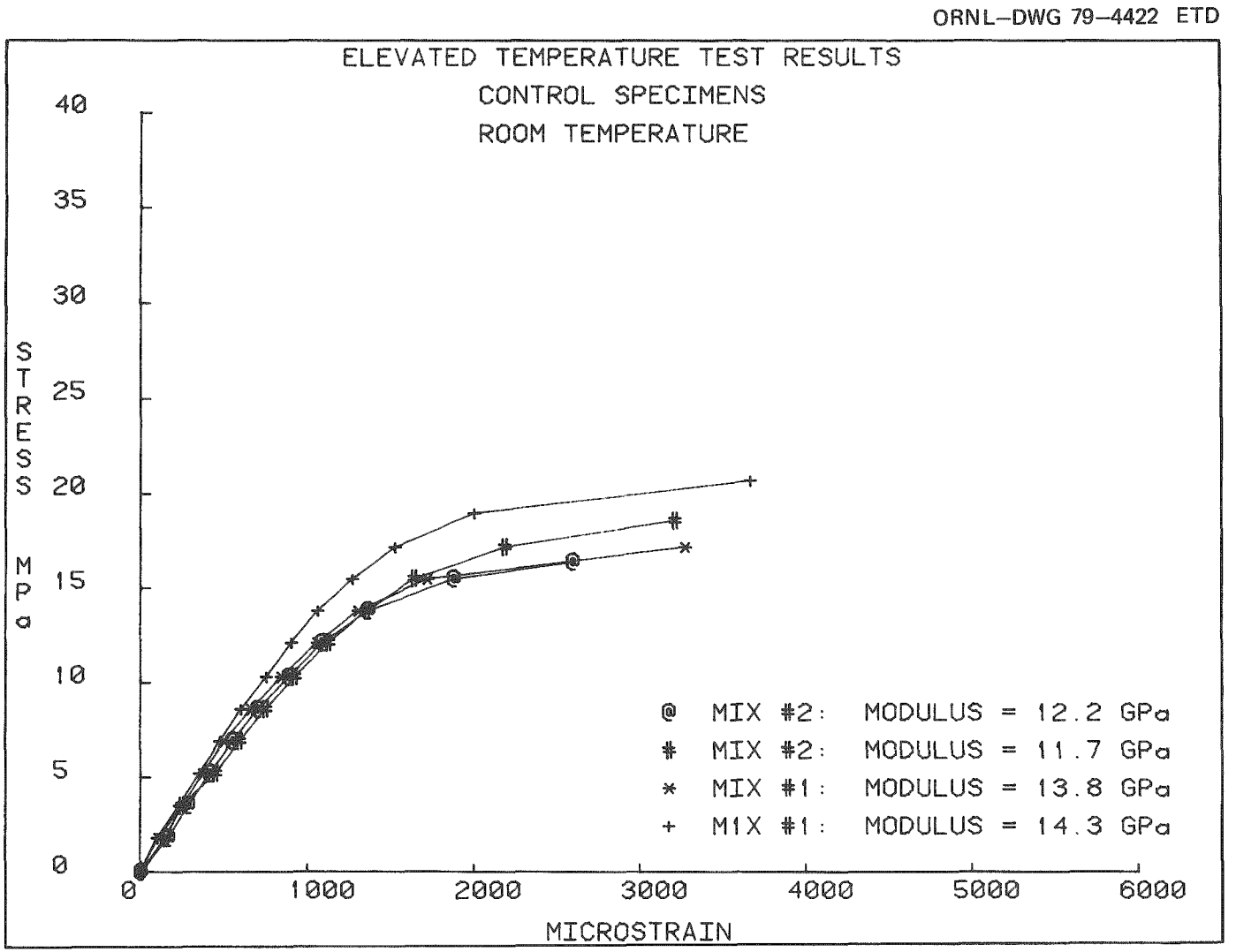

Fig. 81. Polymer-silica material stress vs strain: room temperature (25°C).

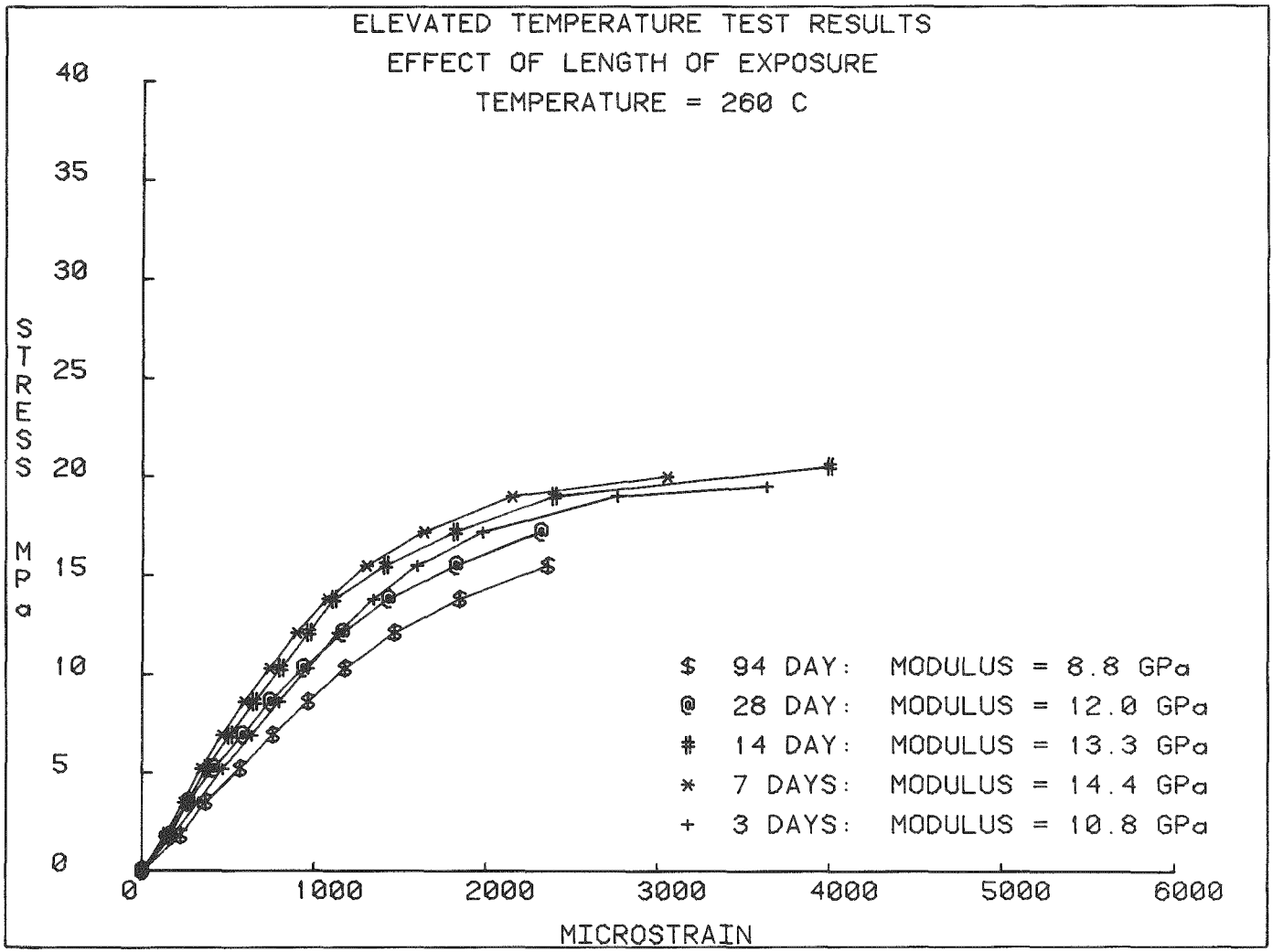

Fig. 82. Polymer-silica material stress vs strain: 260°C.

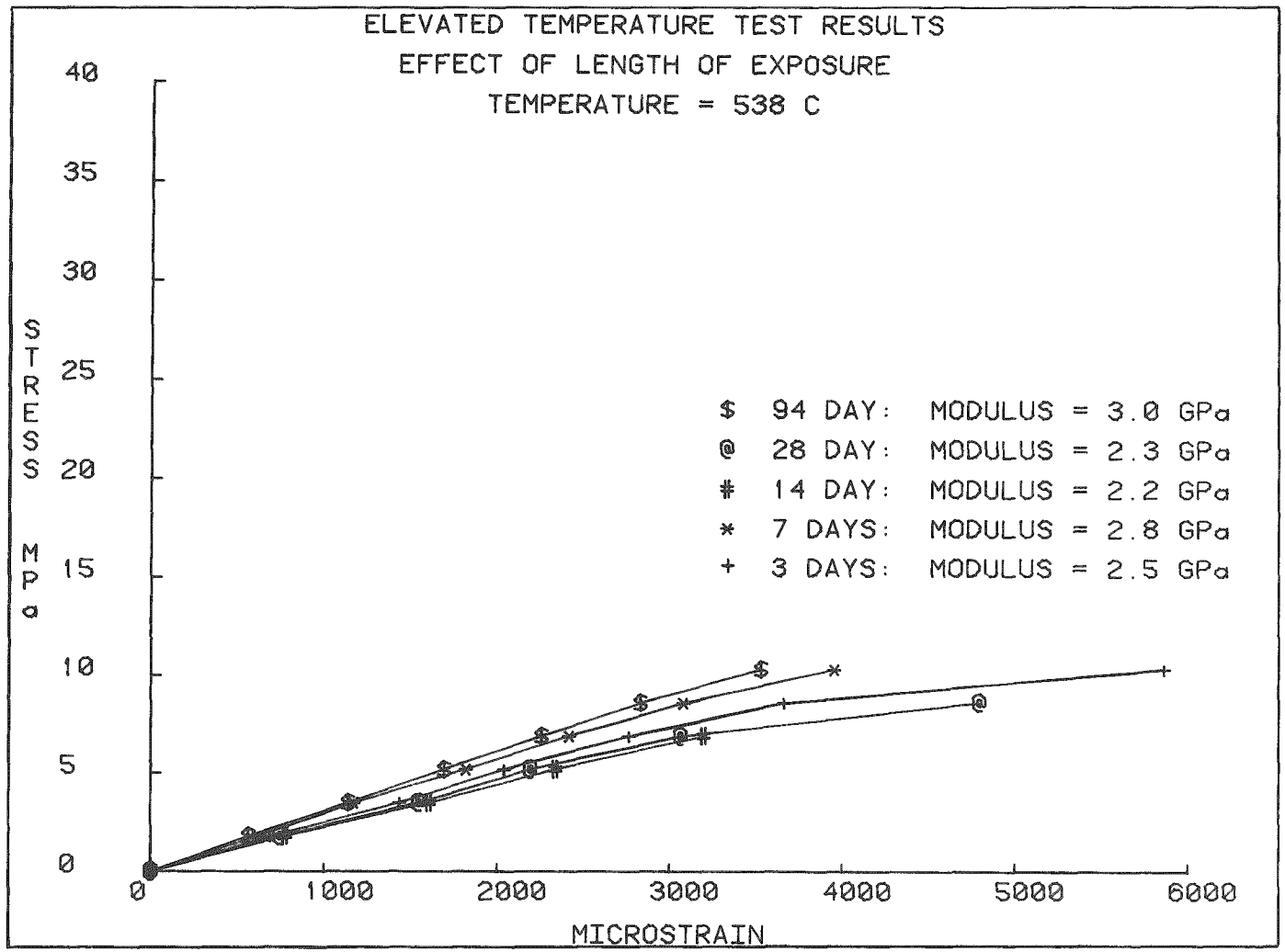

Fig. 83. Polymer-silica material stress vs strain: 538°C.

ORNL-DWG 79-4425 ETD

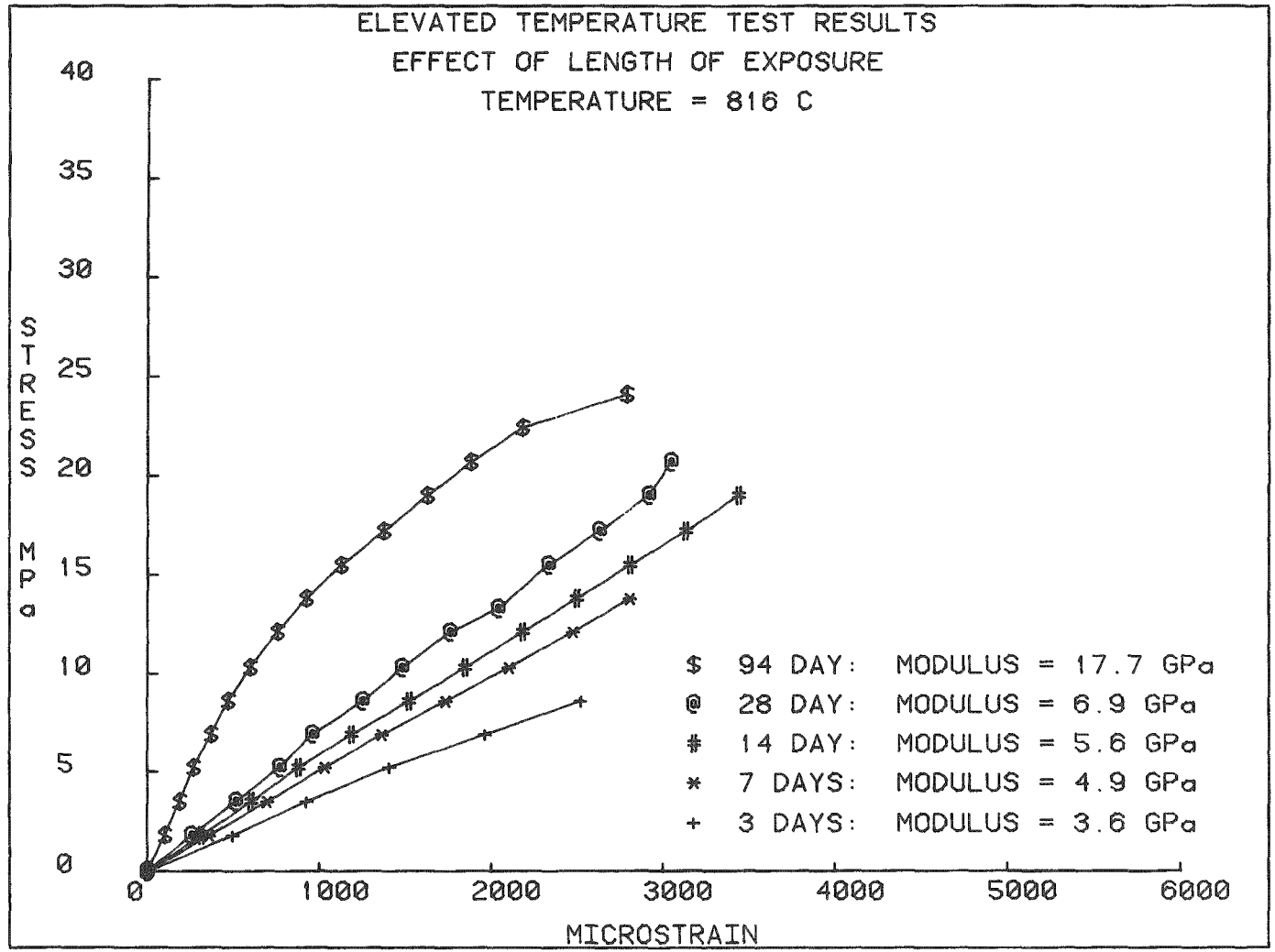

Fig. 84. Polymer-silica material stress vs strain: 816°C.

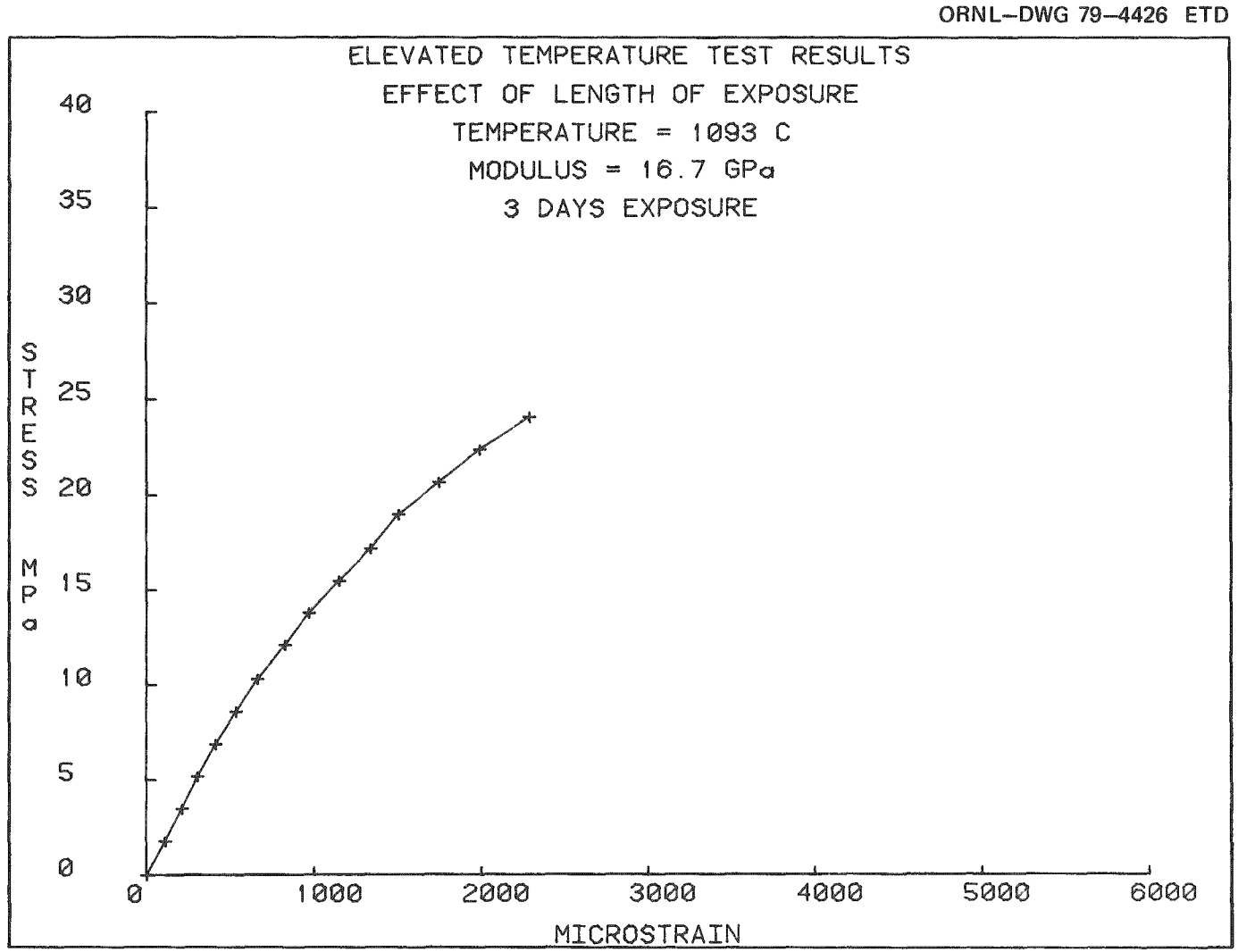

Fig. 85. Polymer-silica material stress vs strain: 1093°C.

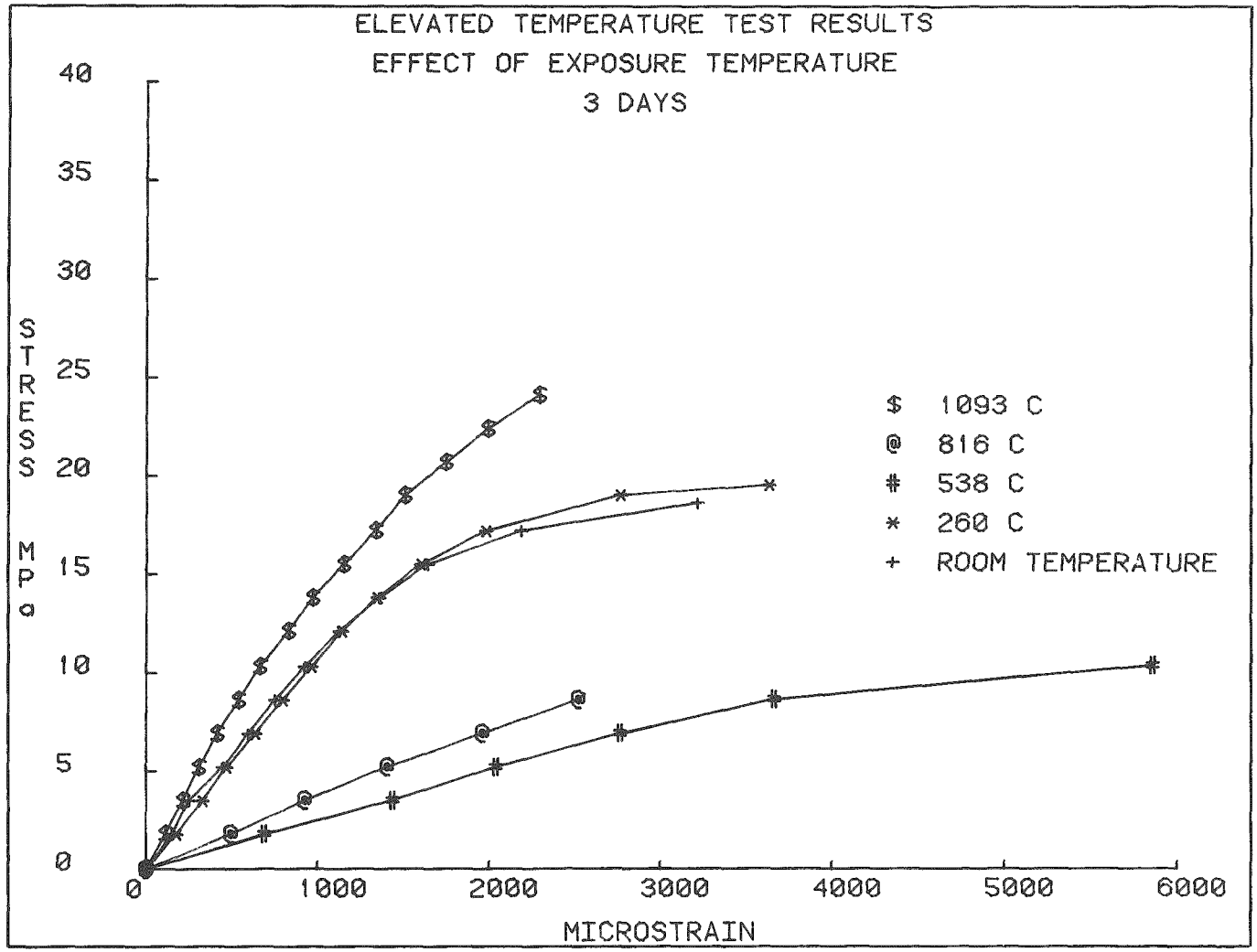

Fig. 86. Effect of temperature on polymer-silica material — 3-day exposure.

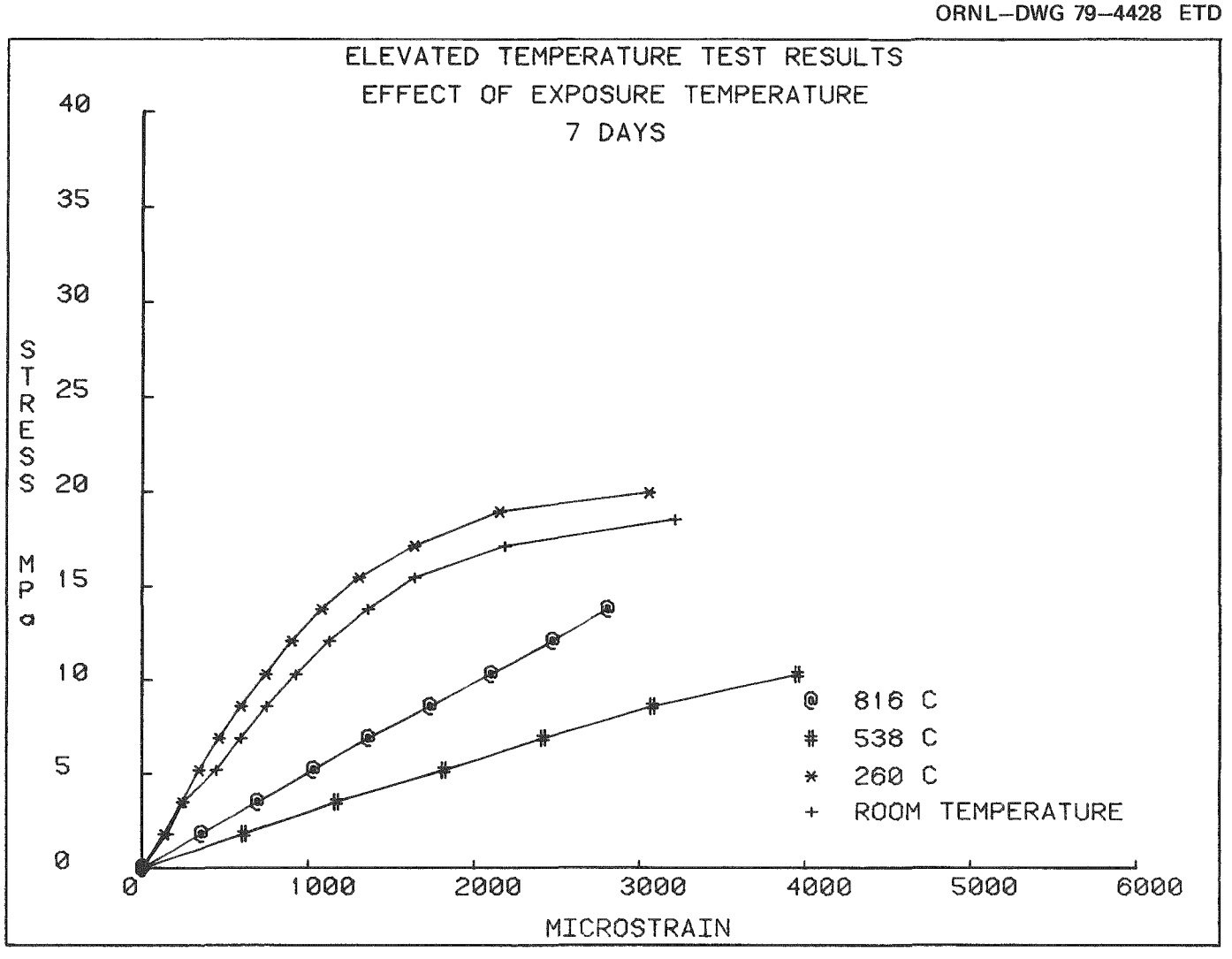

Fig. 87. Effect of temperature on polymer-silica material — 7-day exposure.

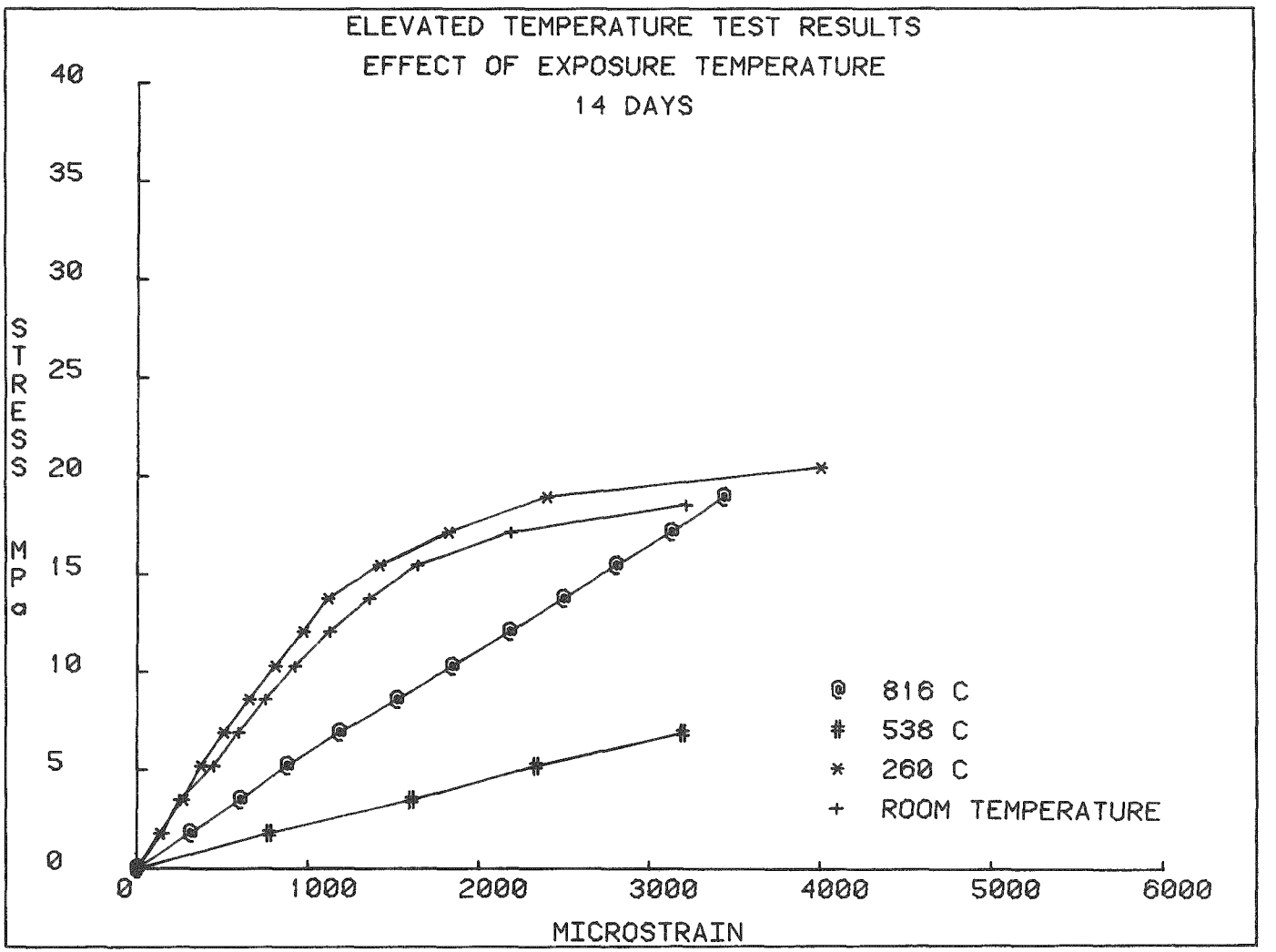

Fig. 88. Effect of temperature on polymer-silica material -- 14-day exposure.

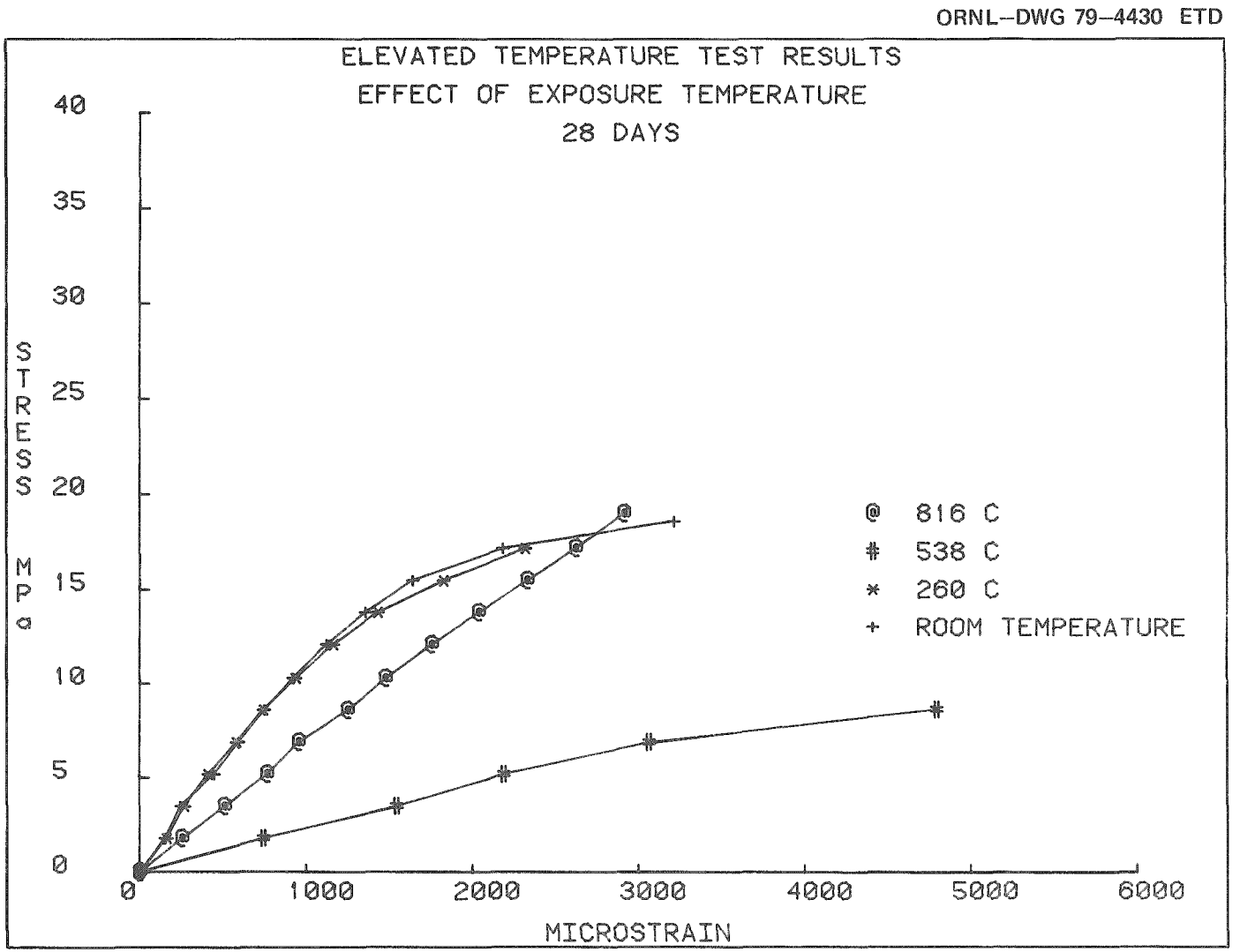

Fig. 89. Effect of temperature on polymer-silica material — 28-day exposure.

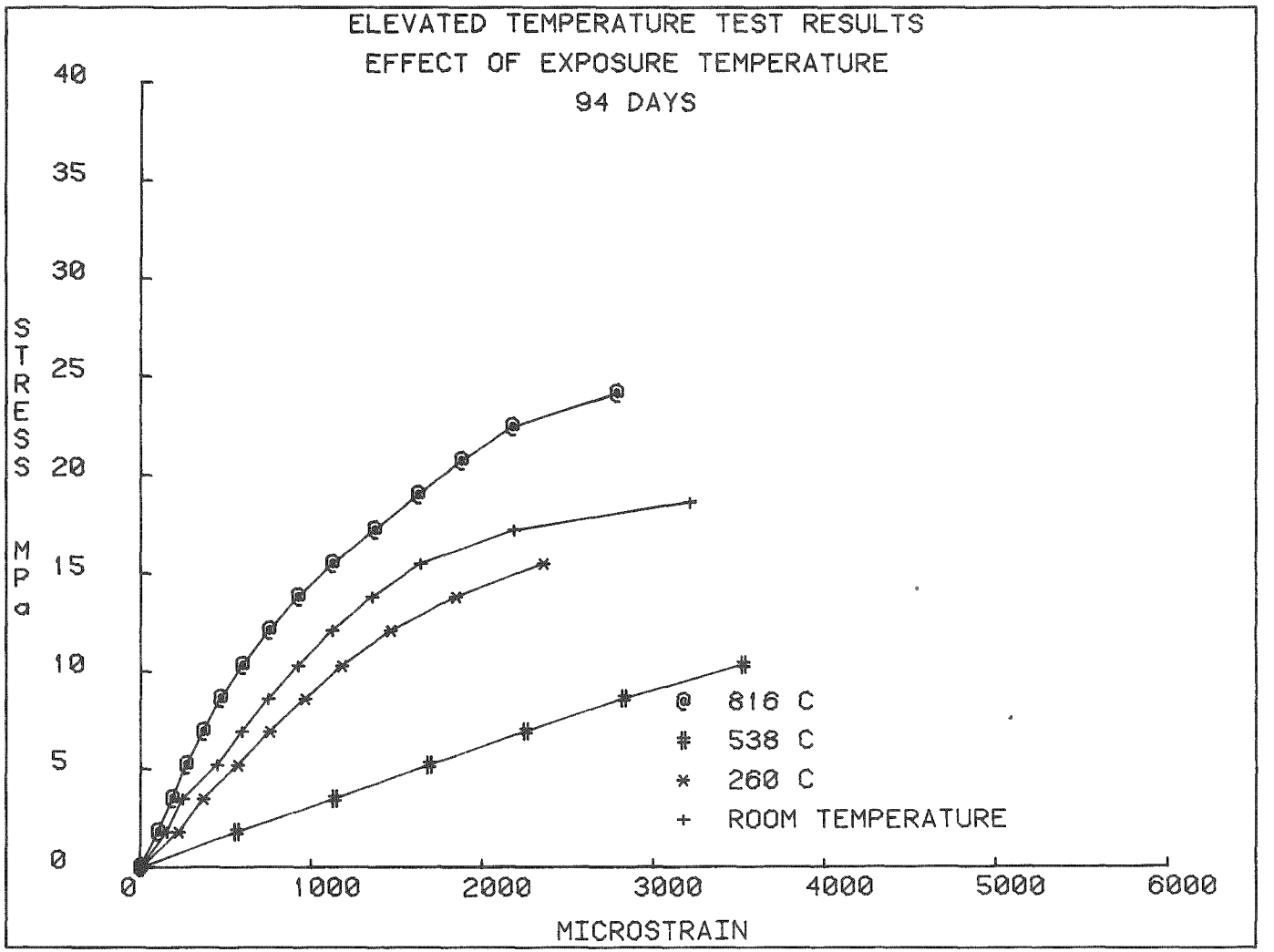

Fig. 90. Effect of temperature on polymer-silica material — 94-day exposure.

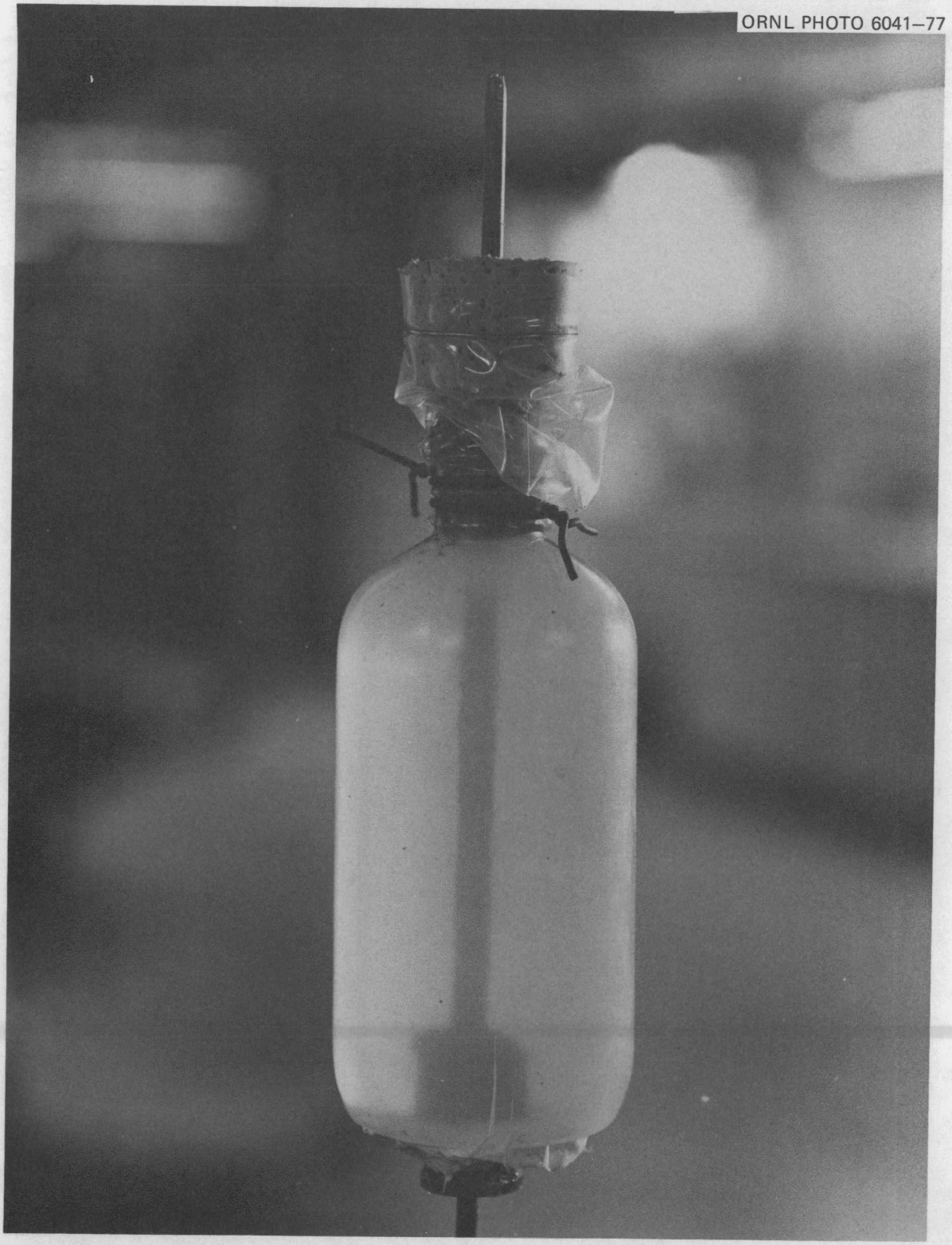

Fig. 91. Stressed tendon corrosion test specimen.

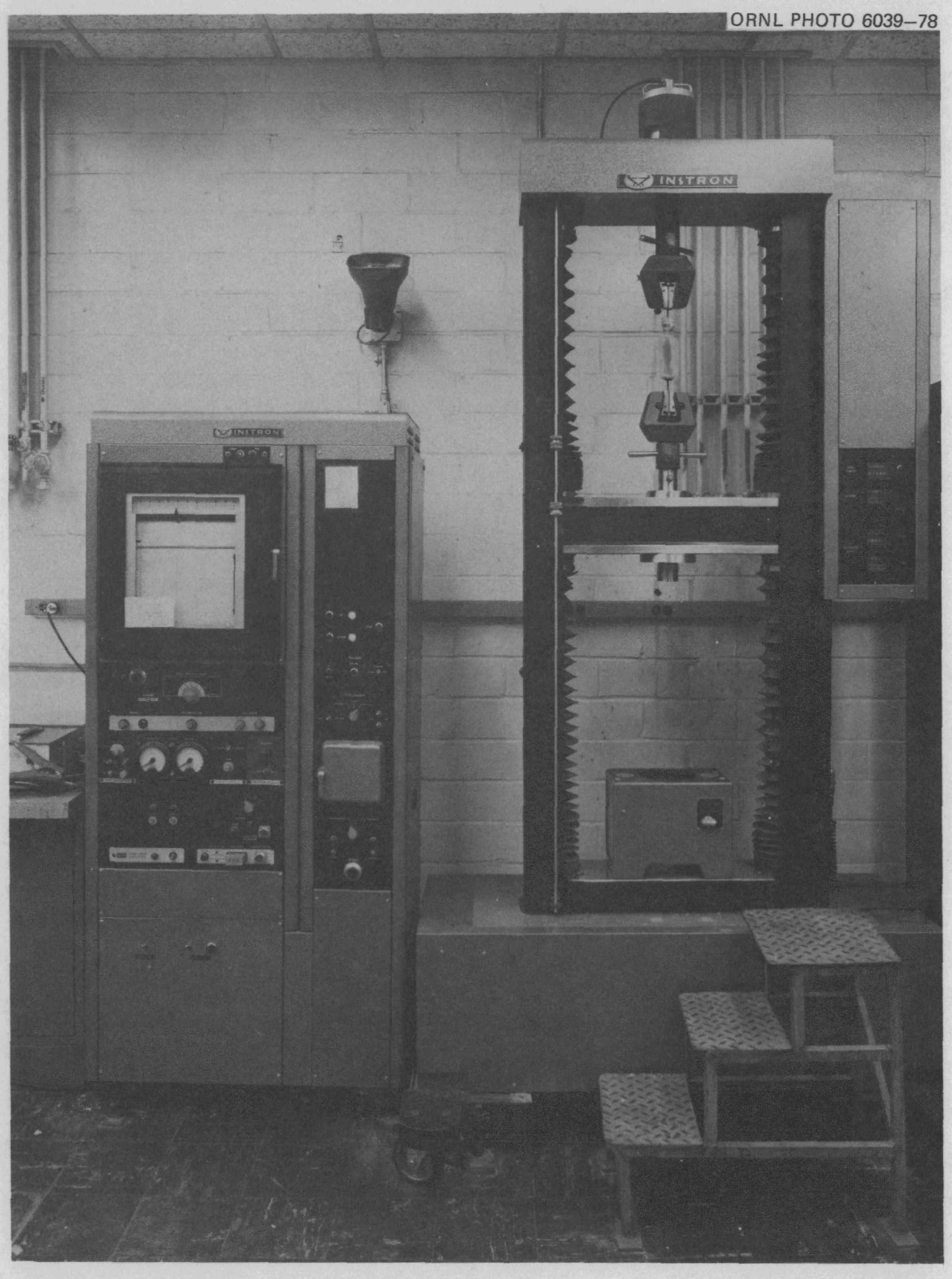

Fig. 92. Stressed tendon corrosion test setup.

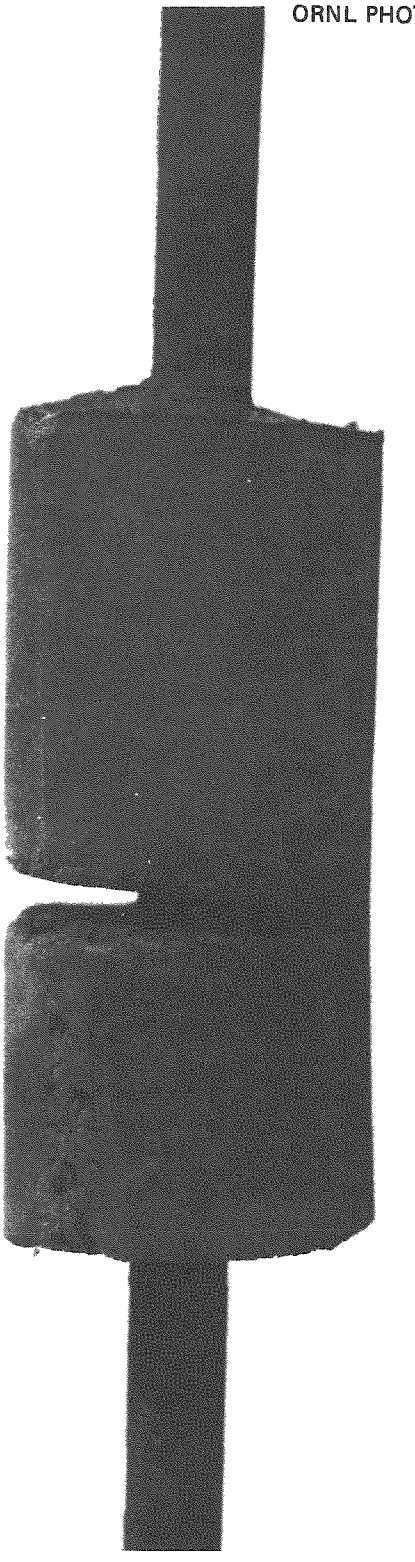

Fig. 93. Flawed grout corrosion test specimen.

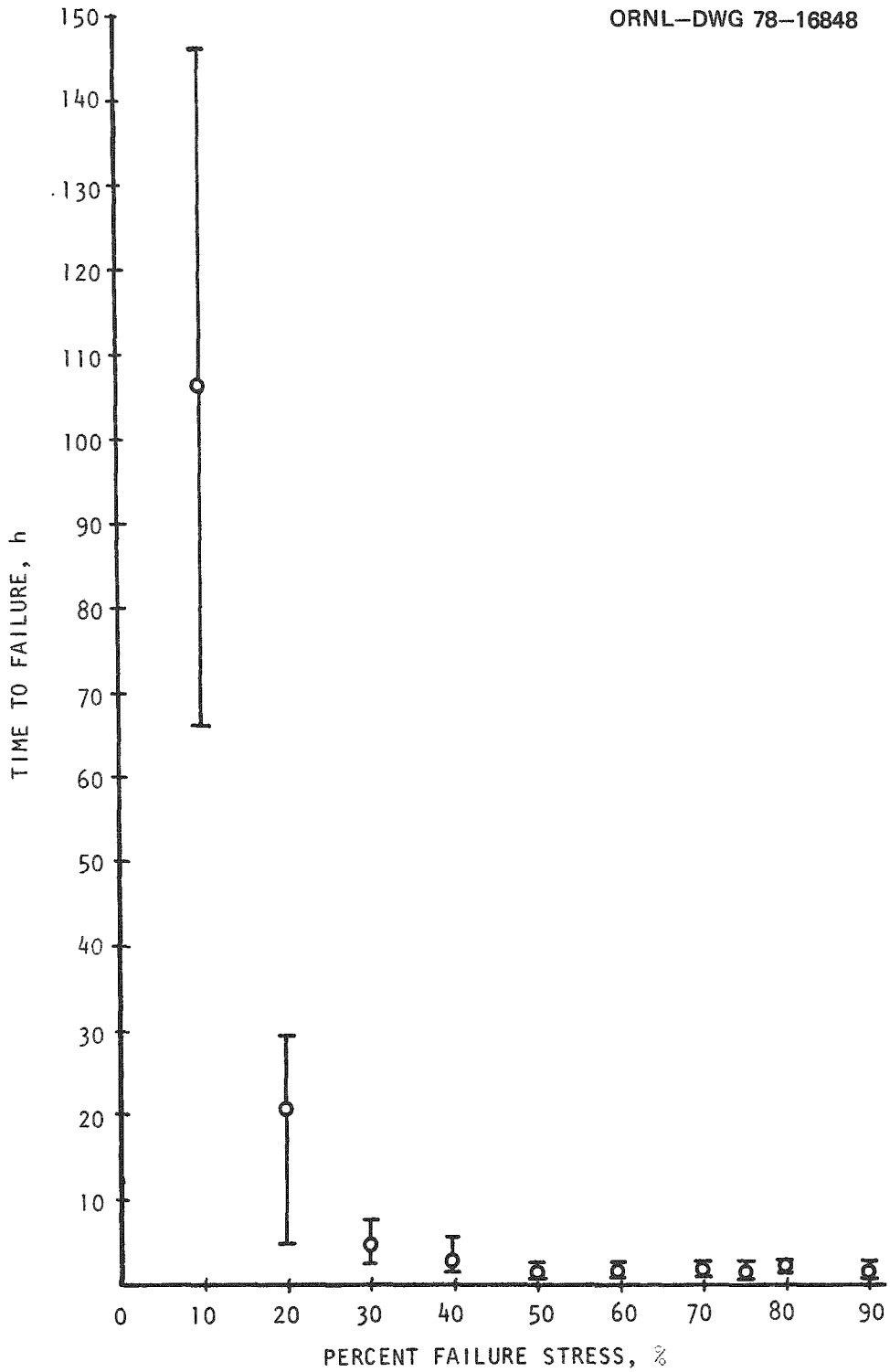

Fig. 94. Effect of percent failure load on failure time: $H_2S + H_2O$ environment.

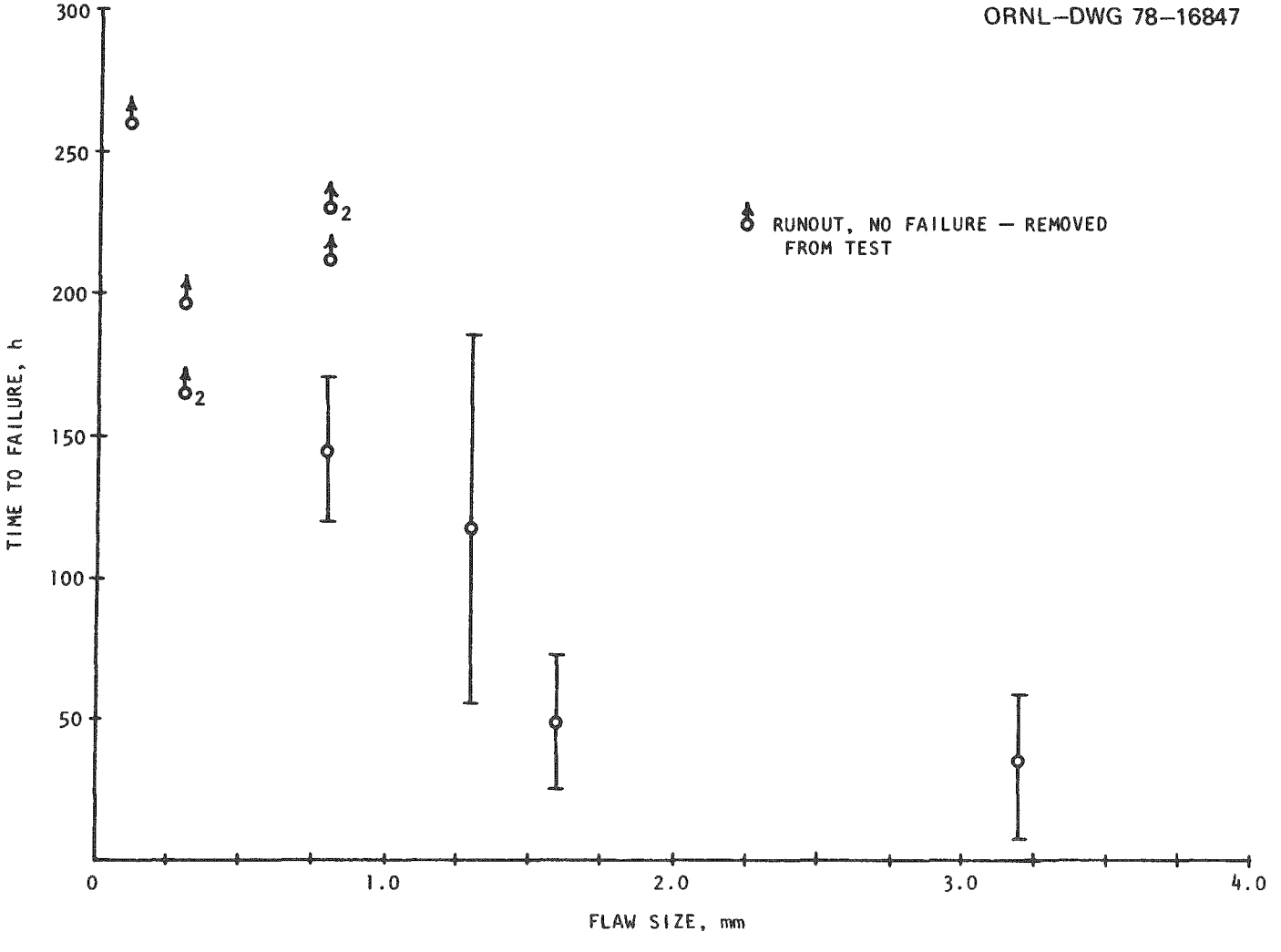

Fig. 95. Effect of flaw size on time to failure: tendons stressed to 60% failure in an H_2S environment.

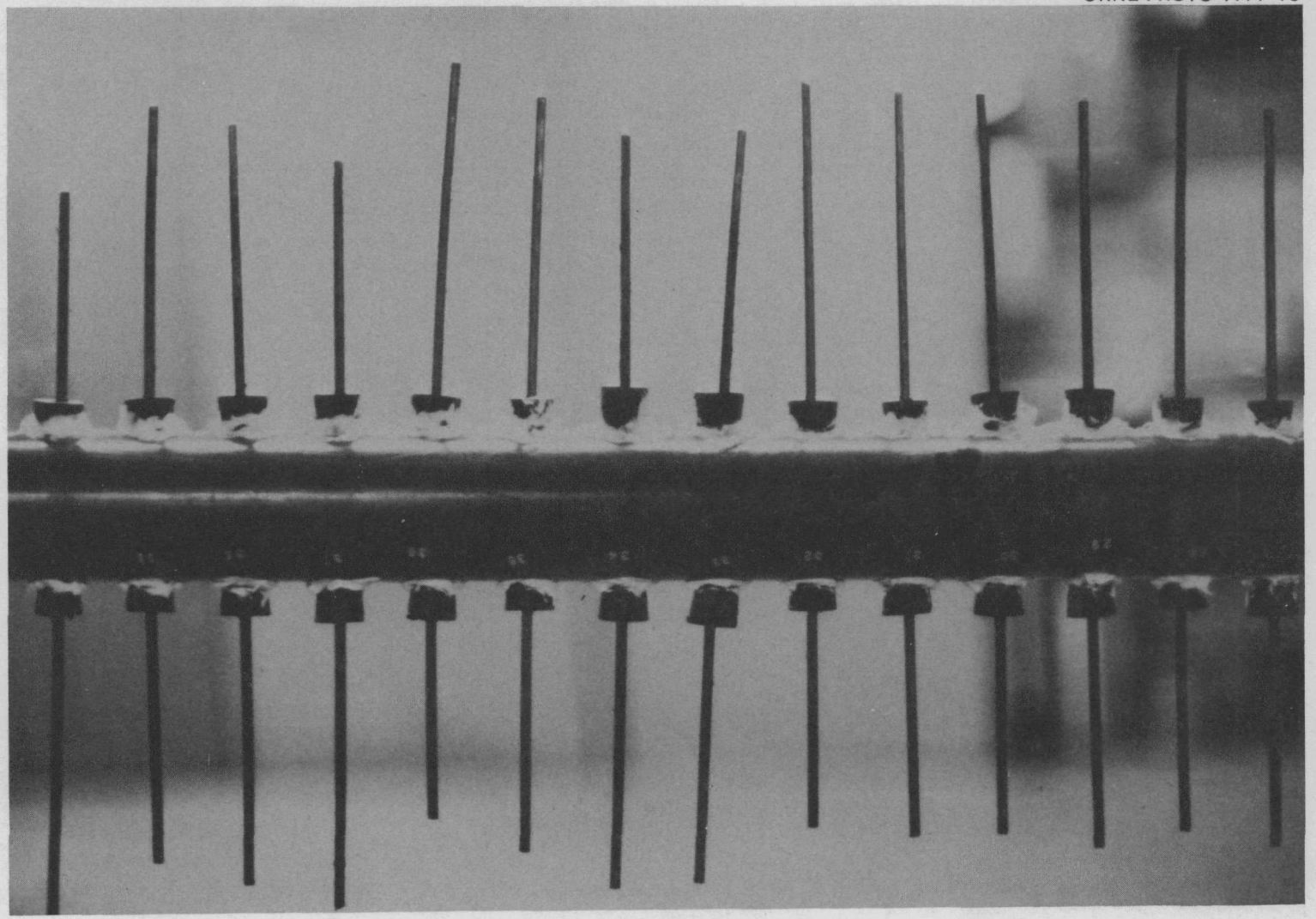

Fig. 96. Nonstressed tendon hydrogen sulfide exposure test setup.

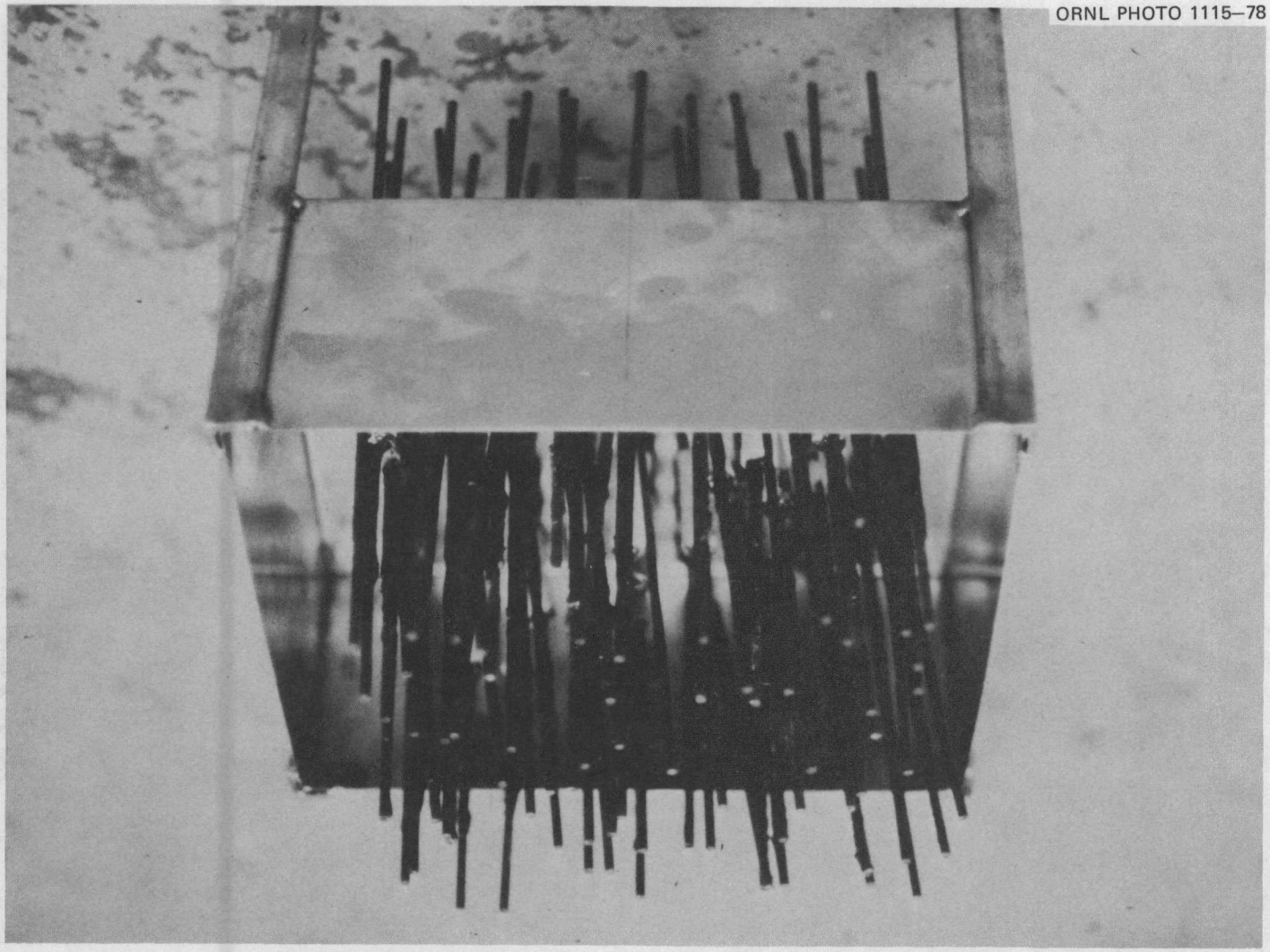

Fig. 97. Nonstressed tendon NH_4NO_3 and NaCl exposure test setup.

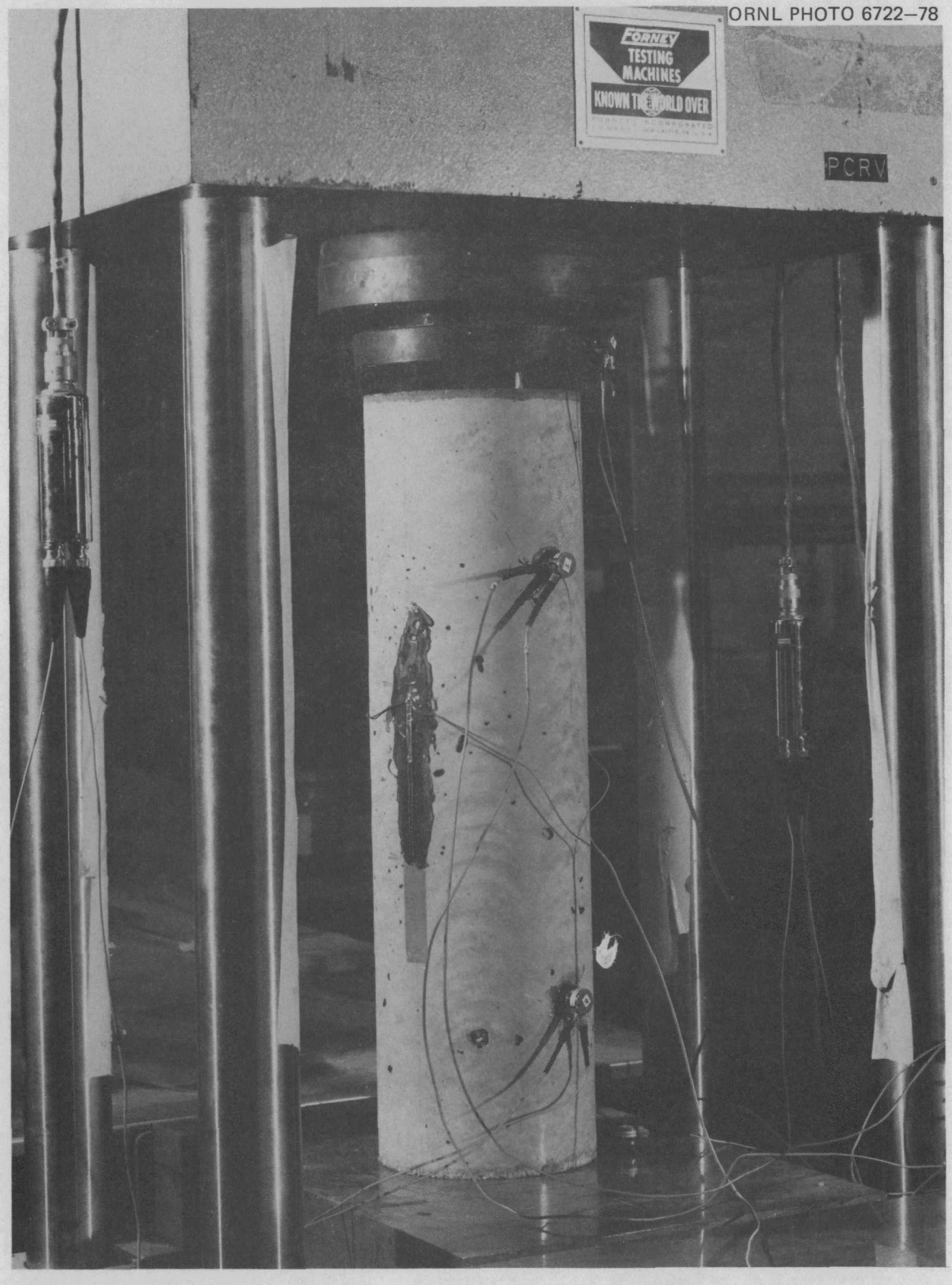

Fig. 98. Test setup for acoustic emission monitoring of plain concrete cylinders.

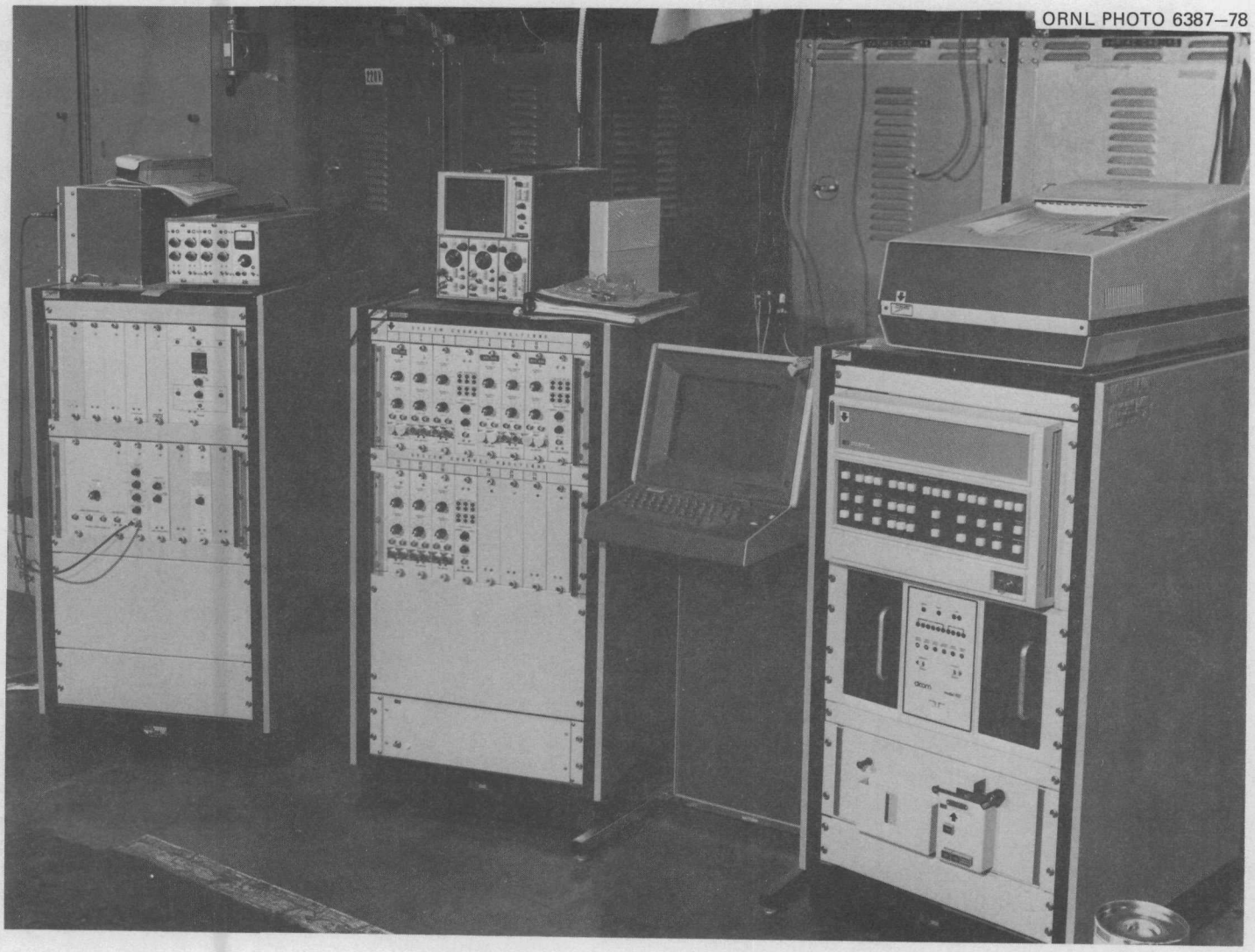

Fig. 99. Multichannel source location acoustic emission system.

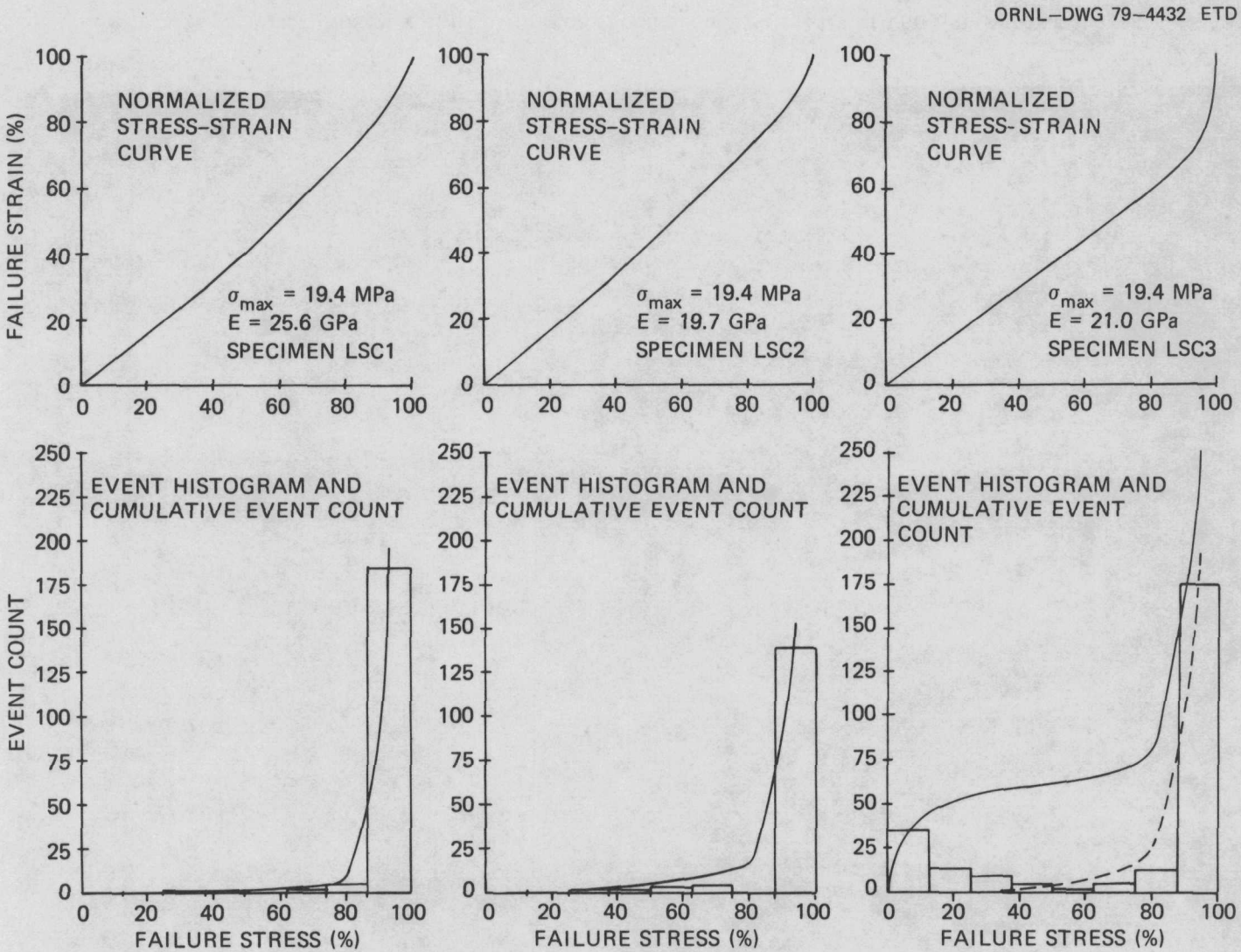

Fig. 100. Acoustic emission test results: low-strength concrete cylinders.

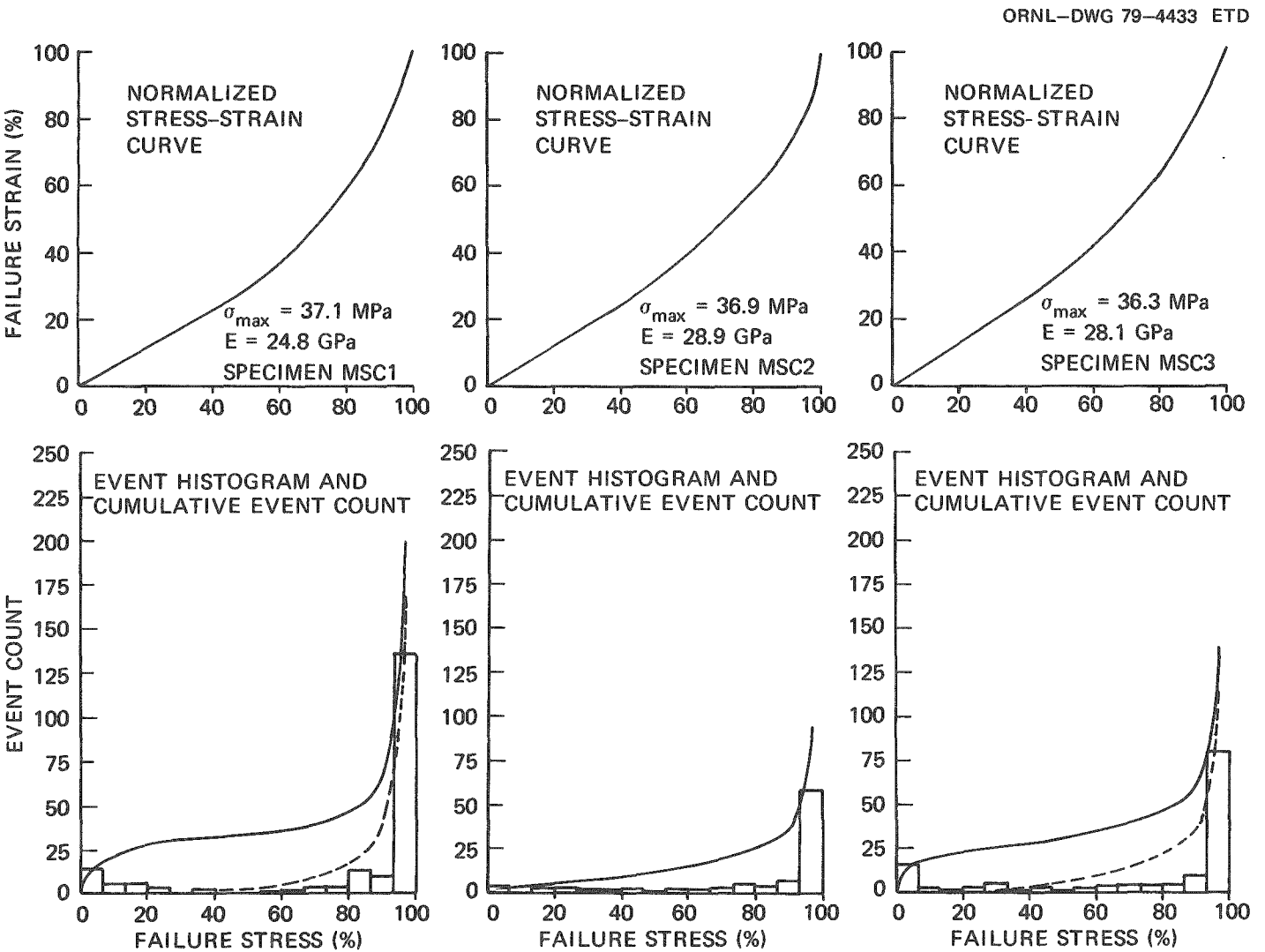

Fig. 101. Acoustic emission test results: medium-strength concrete cylinders.

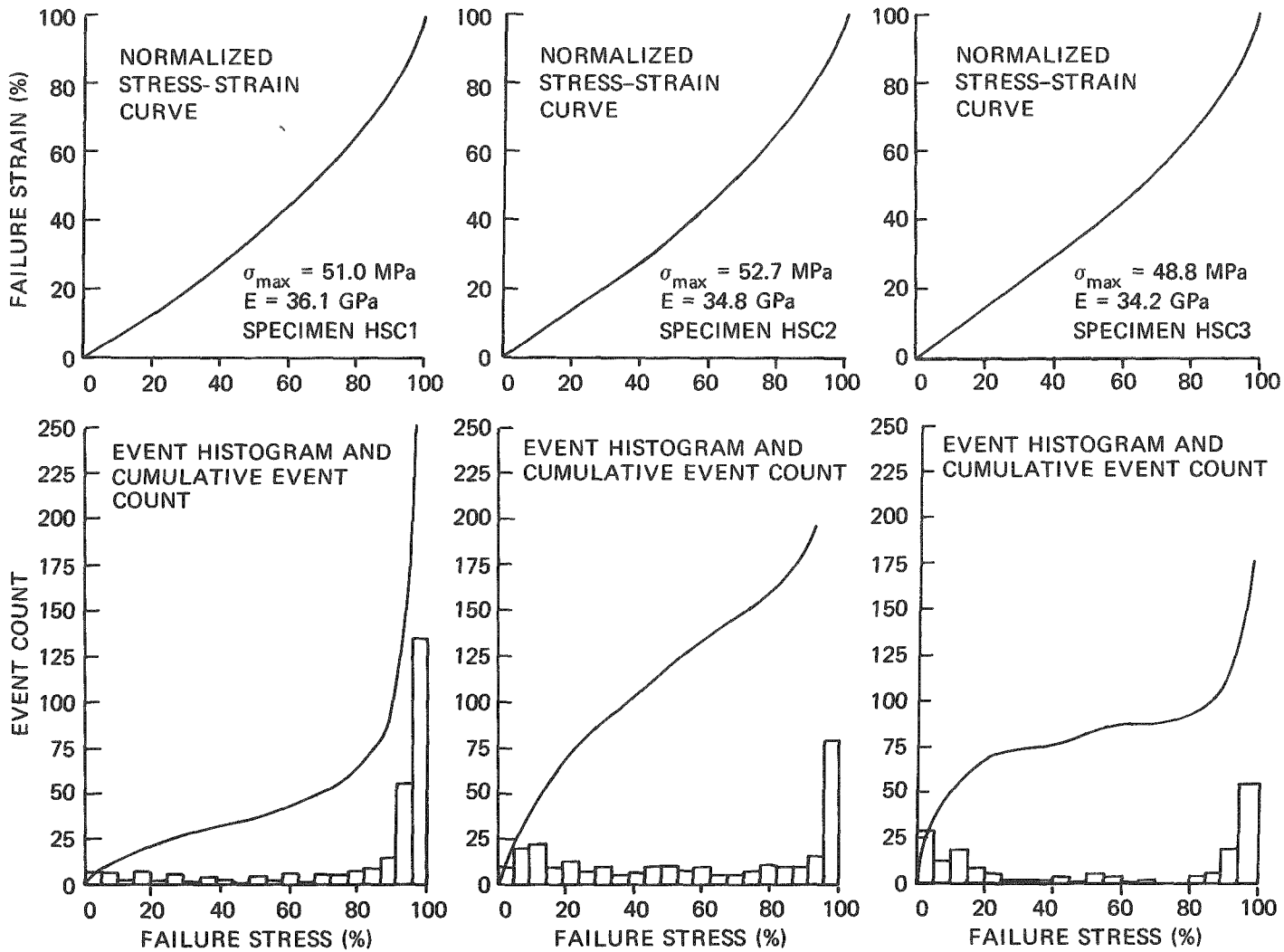

Fig. 102. Acoustic emission test results: high-strength concrete cylinders.

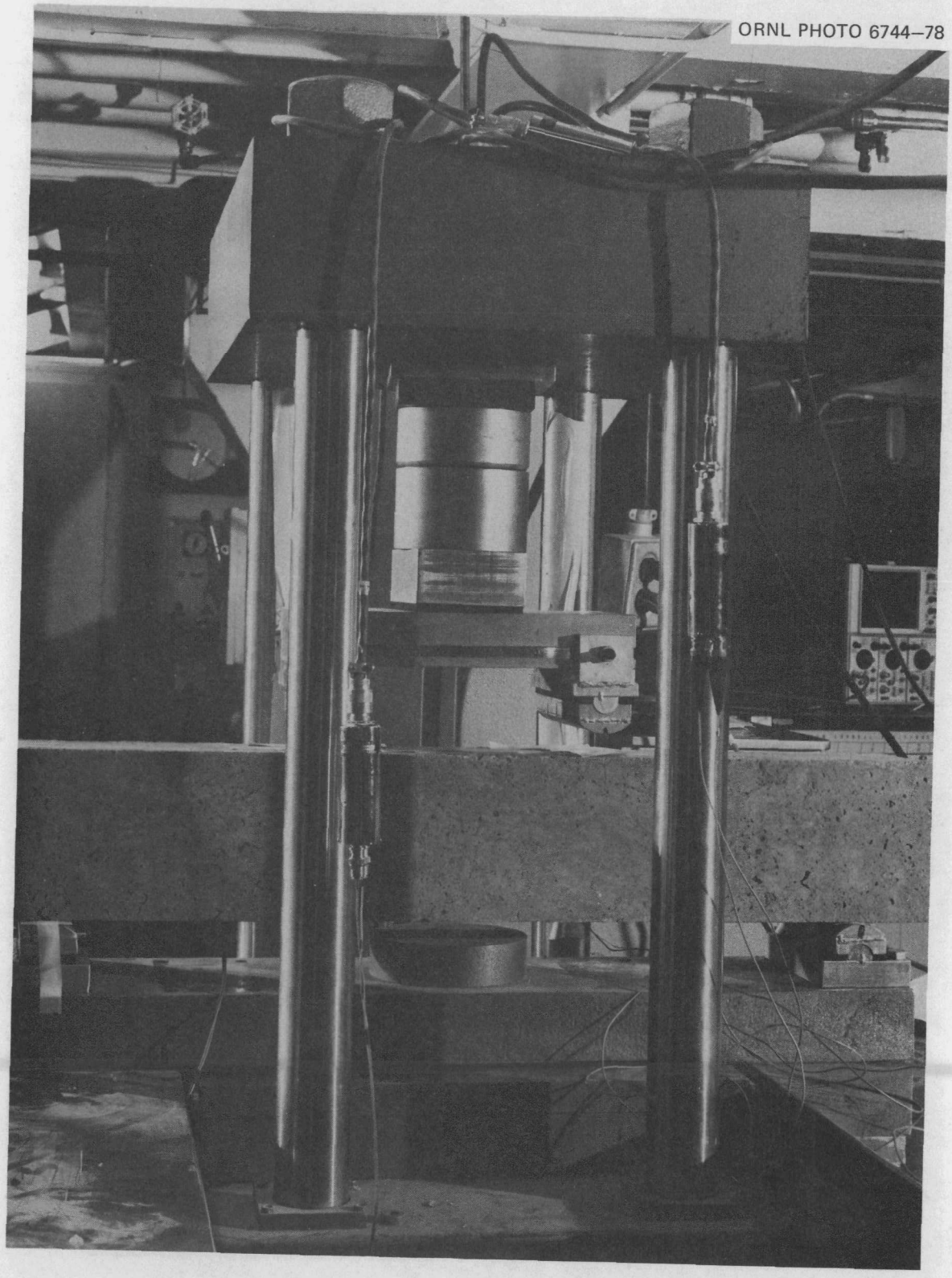

Fig. 103. Test setup for acoustic emission monitoring of plain concrete flexure specimens.

Fig. 104. Test setup for acoustic emission monitoring of posttensioned concrete beams.

ORNL–DWG 78–8434

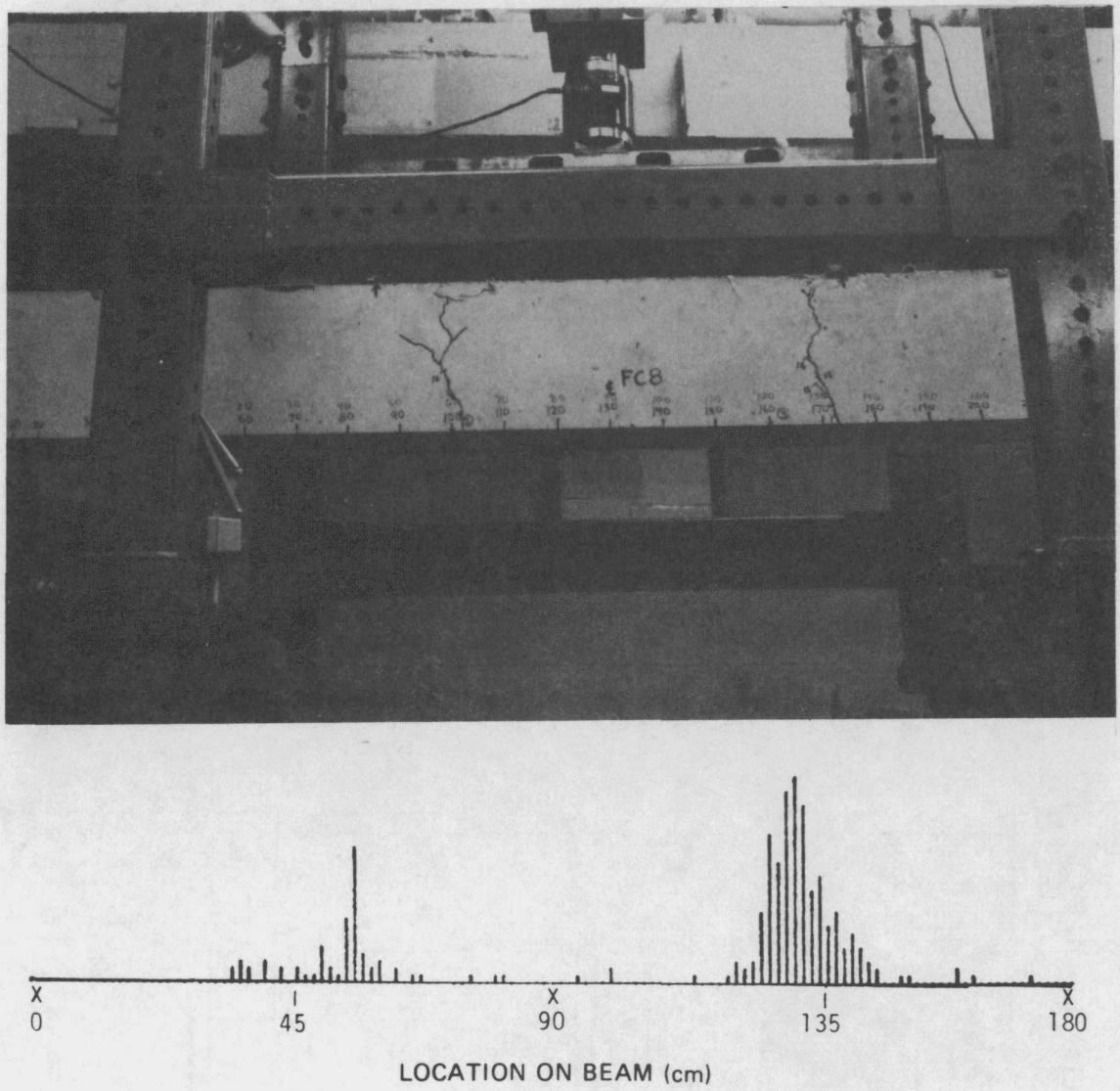

Fig. 105. Typical acoustic emission result: nongrouted-tendon beam.

ORNL–DWG 78–8435

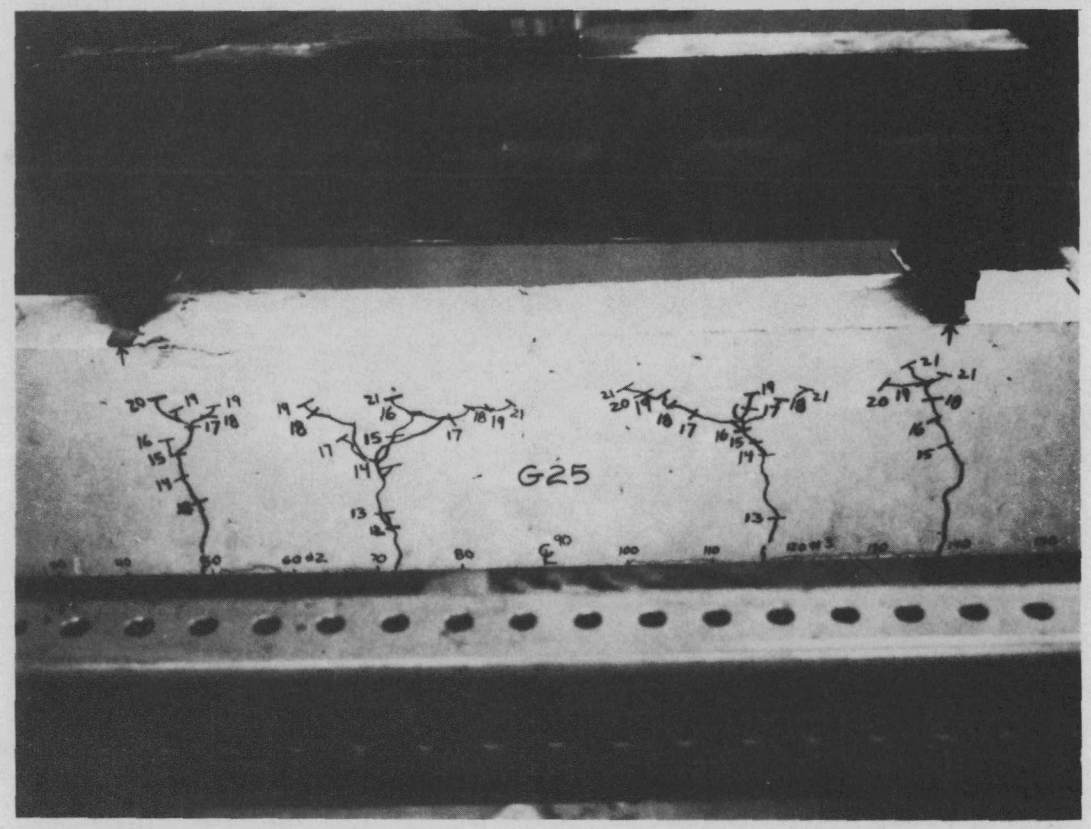

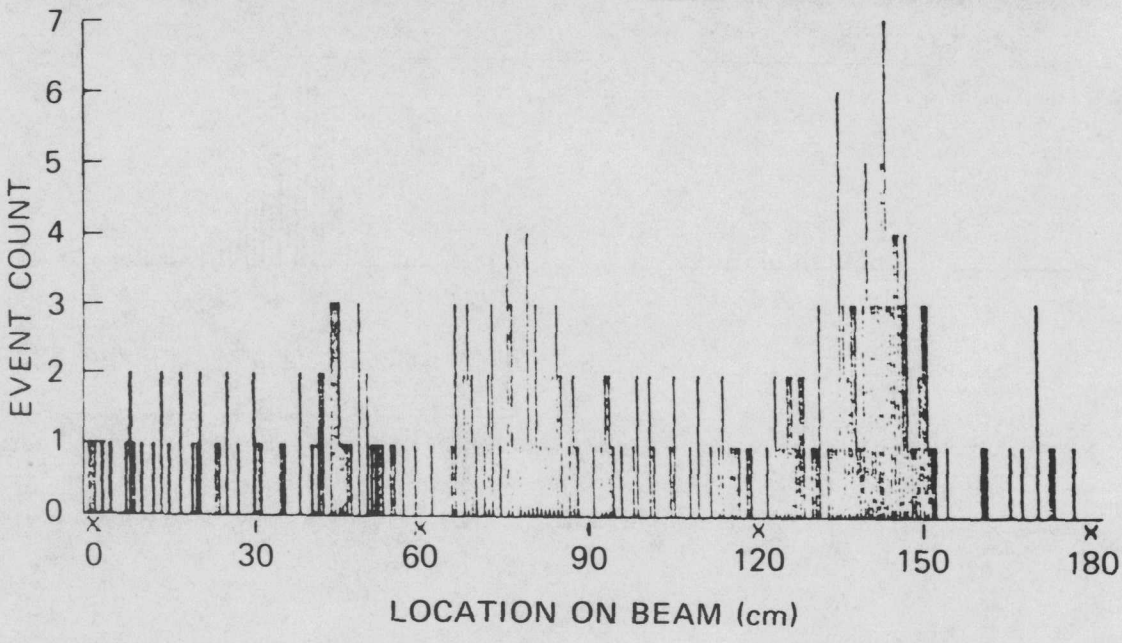

Fig. 106. Typical acoustic emission result: grouted-tendon beam.

4. SUMMARY AND CONCLUSIONS

Presently in this country, nongrouted tendons are exclusively used as the prestressing system for PCPVs; however, grouted tendon systems offer advantages, such as improved flexural load capacity and potentially reduced surveillance costs, which make them potentially cost effective for PCPV applications. To provide insight into this, an experimental investigation was conducted. The investigation was divided into four phases: (1) grouted-nongrouted tendon behavior, (2) selected "new" material system evaluations, (3) bench-scale corrosion studies, and (4) a preliminary evaluation of acoustic emission as a potential technique for monitoring the structural integrity of prestressed concrete pressure vessels. An overview was also conducted on the groutability of large tendon systems.

Specific conclusions that may be derived from the investigation are as follows:

1. The grouted tendon beam elements provide improved crack control (more cracks but much narrower), improved ultimate load capacities in flexure, and conservatism in seating and overall anchorage efficiency relative to the nongrouted tendon beam elements. (Anchorage failure is more critical for a nongrouted tendon than for a grouted tendon.)

2. The shrinkage-compensating cement grout material produced flexure members with slightly improved (<10%) ultimate load capacities, prestressing bond transfer lengths 47% less, and bond pull-out values equivalent to those of specimens grouted with conventional materials. Testing was limited; however, performance improvement trends were not significant enough to merit a recommendation for its use over conventional grouts in PCPVs as a general grout material.

3. The polymer-silica cement grout material produced flexure members with a slight reduction (<8%) in ultimate load capacities, prestressing bond transfer lengths 61% less, and bond pull-out values superior to those of specimens grouted with conventional materials. Results indicate that polymer-silica-based grouts have application where improved bond strengths are required (such as for anchorages) but are not presently recommended as a general PCPV grout because of their relatively high costs.

Elevated-temperature test results indicate that these materials also have application in regions of elevated temperature.

4. The flexural members fabricated from fibrous concrete demonstrated improved ductility and resistance to cracking relative to the conventional concrete prestressed members. These materials have potential application in areas of stress concentration such as at penetrations to reduce reinforcing steel requirements or in regions requiring improved impact resistance.

5. For the length of exposures investigated, the corrosion-inhibiting capability of grout for protecting prestressing steel materials has been demonstrated to be at least equivalent to that of commercial organic-based products in the presence of S^- and Cl^- environments. The corrosion-inhibiting capabilities of grout and commercial organic-based products in NO_3^- environments were equivalent for exposures of up to 38 days; however, for greater exposure periods, the NO_3^- environment produced ductility reductions with no decrease in load capacity for the grout-protected specimens. It should be noted,* however, that the ammonium nitrate solution was chosen as a worst case because it readily attacks both the grout and the prestressing steel.

6. Acoustic emission has been shown to be capable of monitoring plain concrete and performing one-dimensional source locations in simple concrete structures. A definite conclusion on the capability of acoustic emission to monitor grouted tendons in PCPVs cannot presently be made because it needs to be further investigated under more representative conditions (geometries).

7. A review of literature has demonstrated that large prestressing tendon systems may be effectively grouted in PCPVs.

---

*It is interesting to note that 50.8-mm grout cubes placed in the NO_3^- solution at 66°C exhibited strength decreases of 37 and 57% relative to control specimens cured in limewater for exposure periods of 35 and 60 days, respectively. For an exposure of 101 days, the specimens deteriorated to the point that they could not be tested. Similar specimens placed in the hydrogen sulfide and chloride solutions did not exhibit significant strength changes for exposure times up to 100 days.

REFERENCES

1. M. Schupack, "Large Post-Tensioning Tendons," *J. Prestressed Concr. Inst.* 17(3), 14–28 (1972).

2. U.S. Nuclear Regulatory Commission, Office of Standards Development, *Post-Tensioned Prestressing Systems for Concrete Reactor Vessels and Containments,* Regulatory Guide 1.103 (November 1975).

3. U.S. Nuclear Regulatory Commission, Office of Standards Development, *Inservice Inspection of Ungrouted Tendons in Prestressed Concrete Containment Structures,* Regulatory Guide 1.35, Rev. 2 (January 1976).

4. M. Schupack, *Report on the Performance of Post-Tensioning Tendons,* Appendix 5I, Docket No. 50-320, Three Mile Island 2, Jersey Central Power and Light Company, Parsippany, N.J., June 1968. Also, M. Schupack, "A Survey of the Durability Performance of Post-Tensioning Tendons, *J. Amer. Concr. Inst.* 75(10), 501–10 (1978).

5. R. F. D. Burrow, "Prestressing Tendon Systems," *Conference on Prestressed Concrete Pressure Vessels, London, 1968,* Group E, Paper 22, Institute of Civil Engineers.

6. J. R. Stoker, *A Progress Report of an Investigation of Methods of Inhibiting Corrosion of Prestressing Tendons,* Highway Transportation Agency, Department of Public Works, Materials and Research Department (October 1965).

7. M. Schupack, "Grouting of Post-tensioning Tendons," *Civ. Eng., Amer. Soc. Civ. Eng.* 48(3), 72–73 (1978).

8. J. R. Libby, *Modern Prestressed Concrete, Design Principles, and Construction Methods,* Van Nostrand Reinhold Company, New York, 1971, p. 151.

9. I. O. Oladapo, "Dynamic Loading of Prestressed Concrete Beams," *Mag. Concr. Res.* 14(40), 25–32 (1962).

10. W. A. Hamilton, "Dynamic Responses of Pretensioned Prestressed Concrete Beams," *J. Amer. Concr. Inst.* 65(10), 851–55 (1968).

11. J. D. Geddes, "The Effect of Grout Properties on the Structural Behavior of Posttensioned Concrete Beams," *Mag. Concr. Res.* 15(44), 67–76 (1963).

12. American Concrete Institute Committee 318, *Commentary on Building Code Requirements for Reinforced Concrete,* 1971, p. 61.

13. "State-of-the-Art Report on Fiber-Reinforced Concrete," *Amer. Concr. Inst. J.* 70(11), 729–44 (1973).

14. B. H. Gray et al., *Fibrous Concrete Construction Material for the Seventies*, Conference Proceedings M-28, Construction Engineering Research Laboratory, December 1972, p. 41.

15. G. Batson et al., "Steel Fibers as Shear Reinforcement in Beams," *Amer. Concr. Inst. J.* 69(10), 640–44 (1972).

16. U. S. Nuclear Regulatory Commission, Office of Standards Development, *Qualifications for Cement Grouting for Prestressing Tendons in Containment Structures*, Regulatory Guide 1.107, Rev. 1 (February 1977).

17. D. J. Naus, *An Evaluation of the Effectiveness of Selected Corrosion Inhibitors for Protection of Prestressing Steels in PCPVs*, ORNL/TM-6479 (to be published).

18. J. Flis, "Role of Temperature in Stress Corrosion Cracking of Iron in Nitrate Solutions," *Brit. Corros. J.* 10, 79–84 (1975).

19. American Society for Testing and Materials, *Acoustic Emission*, Special Technical Publication 505, 1972, p. 337.

20. American Society for Testing and Materials, *Monitoring Structural Integrity by Acoustic Emission*, Special Technical Publication 571, 1975, p. 289.

21. W. McCabe et al., "Acoustic Emission Behavior of Concrete Laboratory Specimens," *J. Amer. Concr. Inst.* 73(7), 367–71 (1976).

22. A. T. Green, *Stress Wave Emission and Fracture of Prestressed Concrete Reactor Vessel Materials*, Report 4190, Aerojet-General Corporation, June 1969, p. 105.

23. J. C. Spanner, *Acoustic Emission — Techniques and Applications*, Intex Publishing Company, Evanston, Ill. 1974, p. 3.

24. M. Schupack, "Grouting Aid for Controlling the Separation of Water for Cement Grout for Grouting Vertical Tendons in Nuclear Concrete Pressure Vessels," Paper 151/75, *International Conference on Experience in Design, Construction, and Operation of Prestressed Concrete Pressure Vessels and Containments for Nuclear Reactors, University of York, England, September 8–12, 1975*, pp. 251–60.

25. A. Wern, M. Schupack, and W. Larson, "Prestressing System for H. B. Robinson Nuclear Plant," *J. Power Div., Amer. Soc. Civ. Eng.*, pp. 539–66 (March 1971).

APPENDICES

APPENDIX A

The following contains calculations conducted by C. B. Oland for the 6 in. by 12 in. by 10 ft, 12 in. by 12 in. by 10 ft, and the 14 in. by 32 in. by 40 ft beam structural test models. These analyses were used for design of test fixtures and estimation of ultimate loads and deflections.

Nomenclature

A_c	concrete area
A_s	steel area
A_v	area of shear steel reinforcement
b	beam width
c	distance from beam neutral axis to tension or compression surface
d	effective beam depth
e	eccentricity
E_c	concrete modulus of elasticity
E_s	steel modulus of elasticity
f'_c	specified concrete compressive strengh
f_{cu}	compressive stress in concrete at ultimate
f_d	stress due to dead load
f_{pc}	compressive stress in concrete
f_{pe}	effective stress in concrete due to prestress only
f_r	concrete flexural strength
f'_s	steel tensile strength
f_{se}	steel stress after losses
f_{su}	steel stress at ultimate moment
f_x	stress at distance x above prestressing
f_y	yield strength of nonprestressed reinforcement
F_{se}	force in steel
h	beam height
I_c	beam moment of inertia
k_u	reinforcement index
ℓ	major span length
$M_{@\mathbb{C}}$	moment at centerline

M_{cr}	cracking moment
M_{max}	maximum bending moment at specified external loading
M_{ult}	ultimate moment
P_{cr}	cracking load
P_{ult}	ultimate load
S	shear stirrup spacing
T	tensile forces in vertical shear reinforcement in anchorage region
v_c	nominal permissible shear stress carried by concrete
v_{ci}	unit shear stress carried by concrete in vicinity of Type I cracking
v_{cw}	unit shear stress carried by concrete in vicinity of Type II cracking
v_u	nominal shear stress
V	shear force
V_{ci}	shear force carried by concrete in vicinity of Type I cracking
V_{cw}	shear force carried by concrete in vicinity of Type II cracking
V_ℓ	shear force at section occurring simultaneously with M_{max}
V_p	vertical component of effective prestressing force
w	beam weight per foot length
x	arbitrary horizontal distance from beam support
$\Delta_{\mathbb{Q}}$	centerline beam deflection
$\Delta_{\mathbb{Q}ult}$	ultimate deflection at beam centerline
ϵ_{ce}	concrete strain at the prestress steel level
ϵ_{cu}	useful limit of strain in the compressed concrete
ϵ_{se}	steel strain due to effective prestress
ϵ_{su}	steel strain at ultimate
φ_{cr}	curvature at cracking
φ_{ult}	curvature at ultimate moment

Calculations for 6 in. by 12 in. by 10 ft Concrete Beam

$A_s = (1)(0.153) = 0.153$ in.^{2} → One 1/2 in. strand grade 270

$f_s' = 270$ ksi

$f_{se} = 0.6\, f_s' = 162$ ksi

$F_{se} = f_{se}\, A_s = 24.79$ k

$b = 6$ in.

$d = 10$ in.

$h = 12$ in.

$e = 4$ in.

$A_c = 72$ in.^{2}

$I_c = 864$ in.^{4}

$w = (12)(6)(150)/144 = 75$ lb/ft

$\ell = 108$ in.

Initial Stresses After Prestressing Losses

$$\frac{F_{se}}{A_c} = \frac{24.79}{72} = -0.344 \text{ ksi} \rightarrow \text{Axial stress}$$

$$\frac{F_{se}\, e\, (h/2)}{I_c} = \frac{24.79(6)(4)}{864} = \pm 0.689 \text{ ksi} \rightarrow \text{Eccentric stress}$$

$$\frac{w\, \ell^2}{8}\,\frac{(h/2)}{I} = \frac{75}{8}\,\frac{(9)^2(12)(6)}{864} = \pm 0.061 \text{ ksi} \rightarrow \text{Dead load stress}$$

Initial Stress Distribution

$$-\frac{F_{se}}{A_c} \pm \frac{F_{se}\ e\ (h/2)}{I_c} \qquad -\frac{F_{se}}{A_c} \pm \frac{F_{se}\ e\ (h/2)}{I_c} \pm \frac{w\ \ell^2}{8}\frac{c}{I}$$

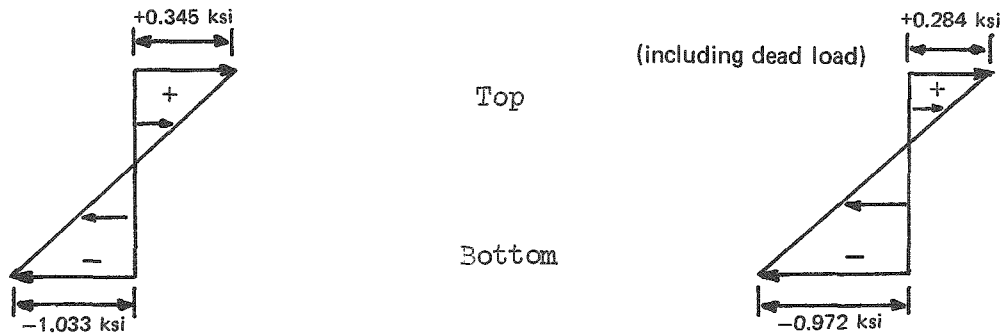

Cracking Moment

$$M_{cr} = \frac{I}{c}\left[f_r + \frac{F_{se}}{A_c} + \frac{F_{se}\ e\ (h/2)}{I_c}\right] = \frac{864}{6}\ (0.605 + 0.344 + 0.689)$$

$$= 236 \text{ in.-k}$$

$$\sum M_{@\mathcal{L}} = \frac{P_{cr}}{2}\left(\frac{\ell}{2} - \frac{\ell}{6}\right) + \frac{w\ \ell}{2}\left(\frac{\ell}{2} - \frac{\ell}{4}\right) - M_{cr} = 0$$

$$P_{cr} = 2\,\frac{\left[M_{cr} - (w\ \ell^2/8)\right]}{\ell/3} = \frac{6}{108}\ (236 - 9) = 12.6 \text{ k}$$

$$\varphi_{cr} = \frac{M_{cr}}{E_c\ I_c} = \frac{236}{4600(864)} = 5.93 \times 10^{-5} \text{ rad/in.}$$

Ultimate Moment

$$f_{su} = f_s' \left(1 - 0.5 \frac{A_s}{b\ d} \frac{f_s'}{f_c'}\right) = 270 \left(1 - 0.5 \frac{0.153}{60} \frac{270}{6.5}\right) = 255.7 \text{ ksi}$$

$$k_u = \frac{A_s}{b\ d} \frac{f_{su}}{f_{cu}} = \frac{0.153}{60} \frac{255.7}{(0.85)(0.725)(6.5)} = 0.163$$

$$\epsilon_{su} = \epsilon_{ce} + \epsilon_{se} + \epsilon_{cu}\ (1 - k_u)/k_u$$

$$\epsilon_{su} = \frac{\frac{F_{se}}{A_c} + \frac{F_{se}\ e^2}{I_c}}{E_c} + \frac{(0.6)270}{28{,}500} + 0.003 \frac{1 - 0.163}{0.163} = 0.02125$$

$$M_{ult} = A_s\ f_{su}\ d \left(1 - 0.59 \frac{A_s}{b\ d} \frac{f_{su}}{f_c'}\right)$$

$$= 0.153(255.7)(10)\left(1 - 0.59 \frac{0.153}{60} \frac{255.7}{6.5}\right) = 368 \text{ in.-k}$$

$$P_{ult} = 2 \frac{\left[M_{ult} - (w\ \ell^2/8)\right]}{\ell/3} = \frac{(359)6}{108} = 19.9 \text{ k}$$

$$\varphi_{ult} = \frac{\epsilon_{cu}}{k_u\ d} = \frac{0.003}{1.63} = 1.84 \times 10^{-3} \text{ rad/in.}$$

$$\frac{M_{ult}}{M_{cr}} = \frac{368}{236} = 1.56 > 1.2$$

Deflection

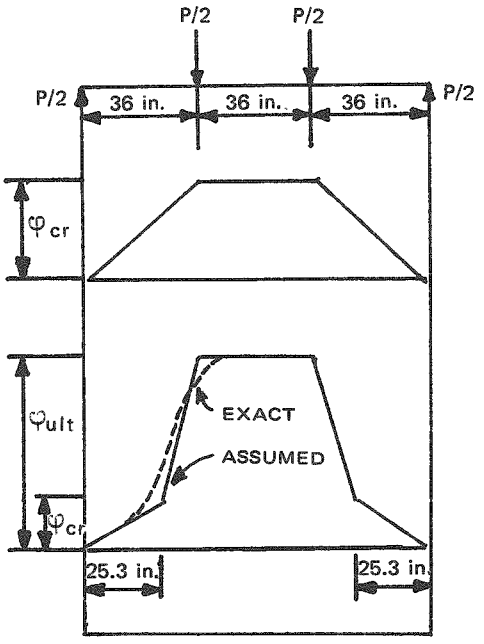

$$\Delta_{\ell cr} = \varphi_{cr} \left[18^2/2 + 36/2\ (18 + 12)\right] = 0.042 \text{ in.}$$

$$\Delta_{\ell ult} = \varphi_{cr} \left[25.3/2\ (36.1)\right] + \varphi_{ult}\ (18^2/2) + (\varphi_{ult} - \varphi_{cr})/2$$

$$\times \left[10.7\ (21.6)\right] + \varphi_{cr}\left[10.7\ (23.35)\right] = 0.55 \text{ in.}$$

Shear

Web Shear

$$v_{cw} = 3.5 \sqrt{f'_c} + 0.3\ f_{pc} + (V_p/b\ d) = 3.5 \sqrt{6500} + 0.3(344)$$

$$+ 0/b\ d = 385 \text{ psi}$$

$$V_{cw} = v_{cw}\ b\ d = 385(60) = 23.1 \text{ k}$$

Flexure Shear

$v_{ci} = 1.7\sqrt{f'_c} = 137$ psi → minimum

$V_{ci(min)} = 60(137) = 8.2$ kips $= V_{ci}$

$$v_{ci} = 0.6\sqrt{f'_c} + \frac{V_d + (V_\ell\, M_{cr}/M_{max})}{b\ d}$$

$M_{cr} = I/c\ (6\sqrt{f'_c} + f_{pe} - f_d) = 210$ in.-k

$V_\ell = P_{ult}/2 = 9.95$ k

X ft from support	V_d (k)	M_{max} (in.-k)	$\frac{V_d}{b\ d} + \frac{V_\ell\, M_{cr}}{b\ d\ M_{max}}$ (ksi)	v_{ci} (ksi)	V_{ci} (k)
2	0.188	239	0.149	0.197	11.8
2.33	0.163	278	0.128	0.176	10.6
2.66	0.139	318	0.112	0.160	9.6
3	0.113	358	0.099	0.147	8.8

Stirrups

Let S = 7.5 h = 9 in.,

$$A_v = \frac{(v_u - v_c)b\ S}{f_y} = 0.022 \text{ in.}$$

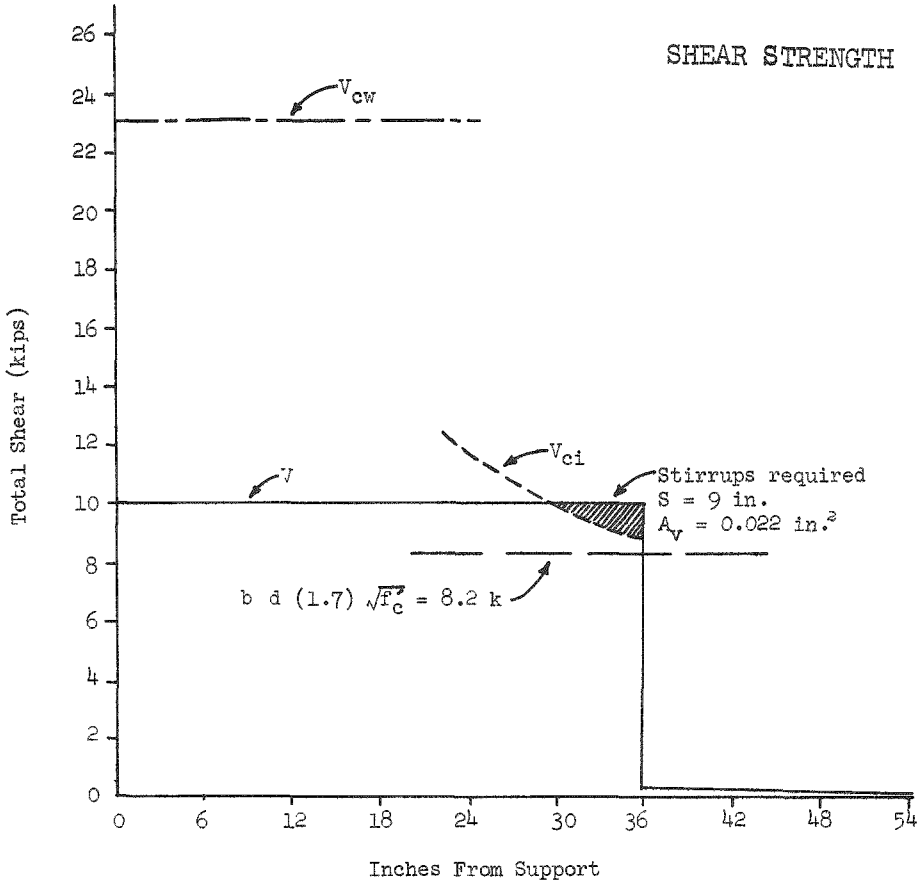

Anchorage Zone Reinforcement

Maximize T

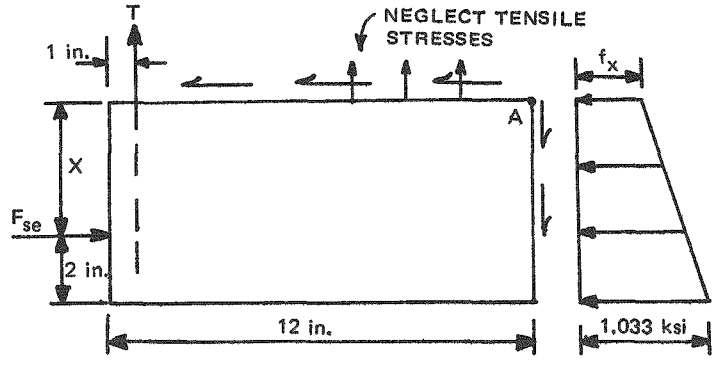

$\sum M_{@A}$

$$F_{se}\, x = 11\, T + f_x\, (6)\, \frac{(x+2)^2}{2} + \frac{(1.033 - f_x)}{2}\, (6)(x+2)\, \frac{2}{3}\, (x+2)$$

$$11\, T = -\, (x+2)^2\, (3f_x + 2.066 - 2f_x) + F_{se}\, x$$

$$T = -\, \frac{(x+2)^2}{2}\, (2.066 + f_x) + 2.254\, x$$

x (in.)	$\frac{(x+2)^2}{11}$ (in.^{2})	f_x (ksi)	$2.066 + f_x$ (ksi)	$2.254\, x$ (k)	T (k)
4	3.2727	0.344	2.410	9.016	1.13
3	2.2727	0.516	2.582	6.762	0.89
2	1.4545	0.688	2.754	4.508	0.51
3.5	2.75	0.430	2.496	7.889	1.03
4.5	3.841	0.258	2.324	10.143	1.22
5	4.4545	0.172	2.238	11.27	1.3
6	5.818	0.086	2.152	13.524	1

$T_{max} = 1.3$ k

$A_v = T/20$ ksi $= 1.3/20 = 0.065$ in.^{2}

Calculations for 12 in. by 12 in. by 10 ft Concrete Beam

$A_s = 3(0.153) = 0.459$ in.^{2} → Three 1/2 in. strands grade 270

$f_s' = 270$ ksi

$f_{se} = 0.6\, f_s' = 162$ ksi

$F_{se} = 0.6\, f_s' A_s = 74.36$ kips

$b = 12$ in.

$d = 10$ in.

$h = 12$ in.

$e = 4$ in.

$A_c = 144$ in.^{2}

$I_c = 1728$ in.^{4}

$w = 0.150$ k/ft

$\ell = 108$ in. $= 9$ ft

Initial Stresses After Prestressing Losses

$$\frac{f_{se}}{A_c} = \frac{74.36}{144} = -0.516 \text{ ksi} \rightarrow \text{Axial stress}$$

$$\frac{F_{se}\, e\, (h/2)}{I_c} = \frac{74.36(4)(6)}{1728} = \pm 1.033 \text{ ksi} \rightarrow \text{Eccentric stress}$$

$$\frac{w\, \ell^2}{8} \frac{(h/2)}{I_c} = \frac{0.15(9)^2(12)(6)}{8(1728)} = \pm 0.063 \text{ ksi} \rightarrow \text{Dead load stress}$$

Initial Stress Distribution

Cracking Moment

$$M_{cr} = \frac{I}{c}\left[f_r + \frac{F_{se}}{A_c} + \frac{F_{se}\ e\ (h/2)}{I_c}\right] = \frac{1728}{6}\ (0.605 + 1.549)$$

$$= 620 \text{ in.-k}$$

$$\sum M_{@\mathfrak{L}} = \frac{P_{cr}}{2}\left(\frac{\ell}{2} - \frac{\ell}{3}\right) + \frac{w\ \ell}{2}\left(\frac{\ell}{2} - \frac{\ell}{4}\right) - M_{cr} = 0$$

$$P_{cr} = 2\ \frac{\left[M_{cr} - (w\ \ell^2/8)\right]}{\ell/3} = \frac{6}{108}\ (620 - 18) = 33.4 \text{ k}$$

$$\varphi_{cr} = \frac{M_{cr}}{E_c\ I_c} = \frac{620}{4600(1728)} = 7.8 \times 10^{-5} \text{ rad/in.}$$

Ultimate Moment

$$f_{su} = f_s'\left(1 - 0.5\ \frac{A_s}{b\ d}\ \frac{f_s'}{f_c'}\right) = 270\left(1 - 0.5\ \frac{270}{6.5}\ \frac{0.459}{120}\right) = 248.6 \text{ ksi}$$

$$k_u = \frac{A_s}{b\ d}\ \frac{f_{su}}{f_{cu}} = \frac{0.459}{120}\ \frac{248.6}{4} = 0.238$$

$$\epsilon_{su} = \epsilon_{ce} + \epsilon_{se} + \epsilon_{cu}\,(1 - k_u)/k_u$$

$$\epsilon_{su} = 0.00026 + 0.00568 + 0.003\left(\frac{1 - 0.238}{0.238}\right) = 0.0155$$

$$M_{ult} = A_s\, f_{su}\, d\left(1 - 0.59\,\frac{A_s}{b\ d}\,\frac{f_{su}}{f'_c}\right)$$

$$= 0.459(248.6)(10)\left(1 - 0.59\,\frac{0.459}{120}\,\frac{248.6}{6.5}\right) = 1043 \text{ in.-k}$$

$$P_{ult} = 2\,\frac{\left[M_{ult} - (w\,\ell^2/8)\right]}{\ell/3} = \frac{6(1025)}{108} = 56.9 \text{ k}$$

$$\varphi_{ult} = \frac{0.003}{k_u\ d} = \frac{0.003}{2.38} = 1.26 \times 10^{-3} \text{ rad/in.}$$

$$\frac{M_{ult}}{M_{cr}} = \frac{1043}{620} = 1.68 > 1.2$$

Deflections

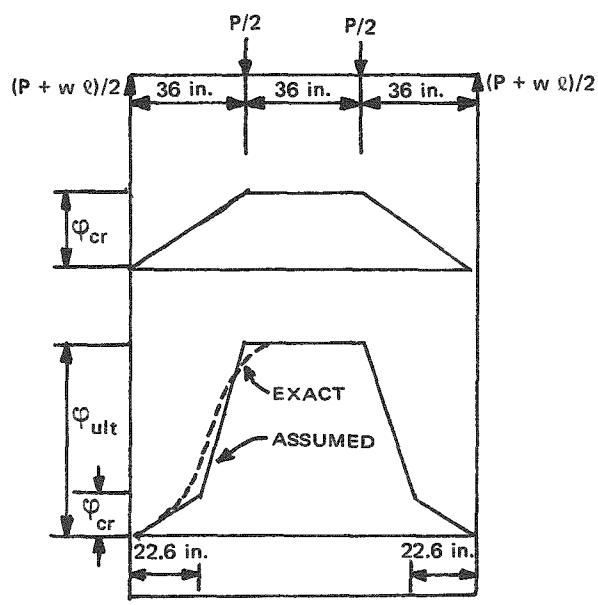

$$\Delta_{\text{cr}} = \varphi_{cr} \left[18^2/2 + 36/2\ (18 + 12)\right] = 0.05 \text{ in.}$$

$$\Delta_{\text{ult}} = \varphi_{cr} \left[22.6/2\ (18 + 13.4 + 22.6/3)\right] + \varphi_u\ (18^2/2)$$

$$+ (\varphi_u - \varphi_{cr})\left[13.4/2\ (18 + 13.4/3)\right] + \varphi_{cr}(13.4)(18 + 13.4/2)$$

$$= 0.44 \text{ in.}$$

Shear

Web Shear

$$v_{cw} = 3.5\sqrt{f'_c} + 0.3\ f_{pc} + V_p/b\ d = 3.5\sqrt{6500} + 0.3(516)$$

$$+ 0/b\ d = 437 \text{ psi}$$

$$V_{cw} = 0.437(120) = 52.4 \text{ k}$$

Flexure Shear

$$v_{ci} = 1.7\sqrt{f'_c} = 137 \text{ psi}$$

$$V_{ci(\min)} = 137(120) = 16.4 \text{ k}$$

$$v_{ci} = 0.6\sqrt{f'_c} + \frac{V_d + (V_\ell\ M_{cr}/M_{max})}{b\ d}$$

$$M_{cr} = I/c\ (6\sqrt{f'_c} + f_{pe} - f_d) = 567 \text{ in.-k}$$

$$V_\ell = P_{ult}/2 = 56.9/2 = 28.45 \text{ k}$$

X ft from support	V_d (k)	M_{max} (in.-k)	$\frac{V_d}{b\ d} + \frac{V_\ell\ M_{cr}}{b\ d\ M_{max}}$ (ksi)	v_{ci} (ksi)	V_{ci} (k)
2	0.375	683	0.200	0.248	29.7
2.33	0.325	797	0.171	0.219	26.3
2.66	0.275	910	0.150	0.198	23.8
3	0.225	1024	0.133	0.181	21.7

Stirrups

Let S = 7.5 h = 9 in.

$$A_v = \frac{(v_u - v_c)b\ S}{f_y} = 0.104 \text{ in.}^2$$

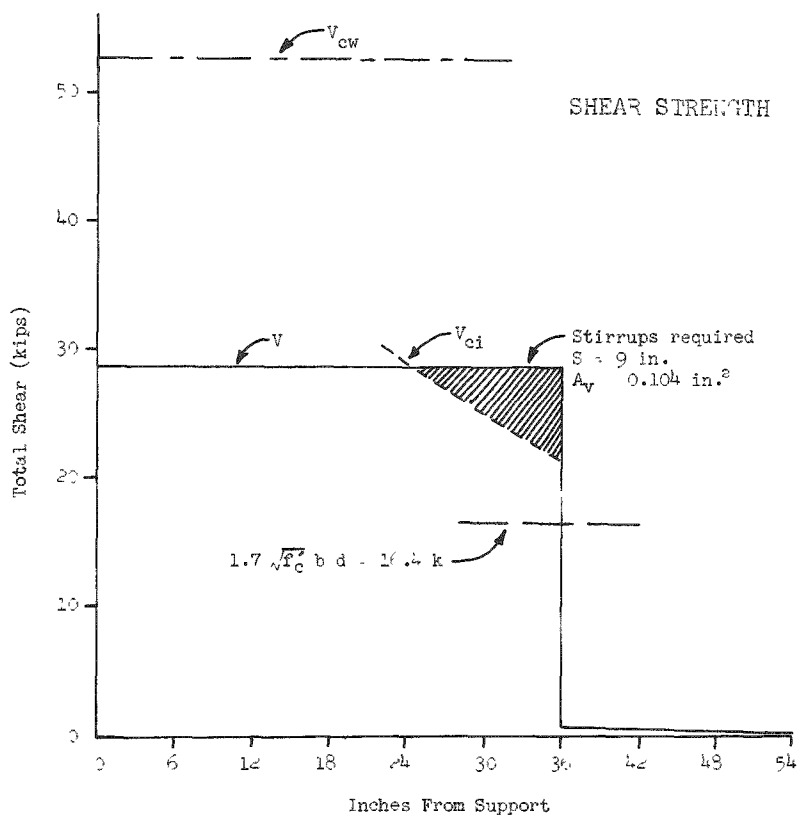

Anchorage Zone Reinforcement

Maximize T

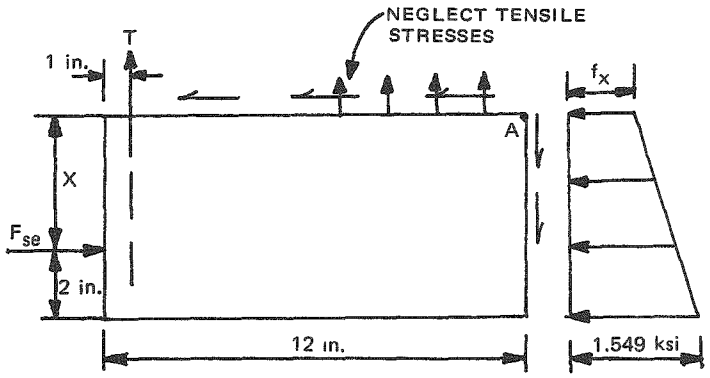

$\sum M_{@A}$

$$F_{se}\, x = 11\, T + f_x \frac{(x+2)^2}{2}(12) + (0.549 - f_x)\frac{(x+2)}{2}$$

$$\times \frac{2}{3}(x+2)(12) = 11\, T + f_x(x+2)^2(6) + (1.549 - f_x)$$

$$\times (x+2)^2(4)$$

$$T = -\frac{(x+2)^2}{11}(6.196 + 2f_x) + 6.76\, x$$

x (in.)	$\frac{(x+2)^2}{11}$ (in.^{2})	f_x (ksi)	$6.196 + 2f_x$ (ksi)	6.76 x (k)	T (k)
4	3.2727	0.516	7.228	27.04	3.4
3	2.2727	0.689	7.574	20.28	3.1
2	1.4545	0.860	7.916	13.52	2
5	4.4545	0.344	6.884	33.80	3.1

$T_{max} \cong 3.4$ k

$A_v = T/20$ ksi $= 3.4/20 = 0.17$ in.^{2}

Calculations for 14 in. by 32 in. by 40 ft Concrete Beam

$A_s = 38(0.049) = 1.862$ in.^{2} → Thirty-eight 1/4 in. wires grade 240

$f_s' = 240$ ksi

$f_{se} = 0.6(240) = 144$ ksi

$F_{se} = 1.862(144) = 268.13$ k

$b = 14$ in.

$d = 24$ in.

$h = 32$ in.

$e = 8$ in.

$A_c = 448$ in.^{2}

$I_c = 1/12\ (14)(32)^3 = 38229$ in.^{4}

$w = 0.466$ k/ft

$\ell = 36$ ft

Initial Stresses After Prestressing Losses

$$\frac{f_{se}}{A_c} = -\frac{268.13}{448} = -0.599 \text{ ksi} \rightarrow \text{Axial stress}$$

$$\frac{F_{se}\ e\ (h/2)}{I_c} = \pm\frac{268.13(8)(16)}{38229} = \pm 0.898 \text{ ksi} \rightarrow \text{Eccentric stress}$$

$$\frac{w\ \ell^2}{8}\frac{c}{I} = \frac{0.466(36)^2(12)(16)}{8(38229)} = \pm 0.379 \text{ ksi} \rightarrow \text{Dead load stress}$$

Initial Stress Distribution

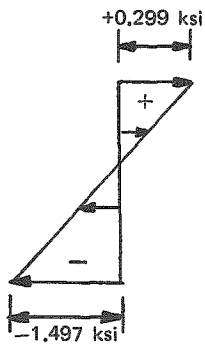

Top

Bottom

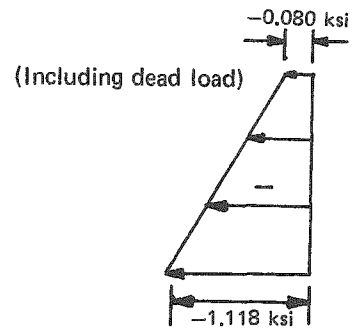

Cracking Moment

$$M_{cr} = \frac{I}{c}\left[f_r + \frac{F_{se}}{A_c} + \frac{F_{se}\ e\ (h/2)}{I_c}\right] = \frac{38229}{16}\ (2.102) = 5022\ \text{in.-k}$$

$$\sum M_{@\mathfrak{C}} = \frac{P_{cr}}{2}\left(\frac{\ell}{2} - \frac{\ell}{3}\right) + \frac{w\ \ell}{2}\left(\frac{\ell}{2} - \frac{\ell}{4}\right) - M_{cr} = 0$$

$$P_{cr} = 2\,\frac{\left[M_{cr} - (w\ \ell^2/8)\right]}{\ell/3} = \frac{6}{36(12)}\ (5022 - 906) = 57.2\ \text{k}$$

$$\varphi_{cr} = \frac{M_{cr}}{E_c\ I_c} = \frac{5022}{4600(38229)} = 2.86 \times 10^{-5}\ \text{rad/in.}$$

Ultimate Moment

$$f_{su} = f_s'\left(1 - 0.5\,\frac{A_s}{b\ d}\,\frac{f_s'}{f_c'}\right) = 240\left(1 - \frac{0.5(1.862)}{14(24)}\,\frac{240}{6.5}\right) = 215.4\ \text{ksi}$$

$$k_u = \frac{A_s}{b\ d}\,\frac{f_{su}}{f_{cu}} = \frac{1.862}{24(14)}\,\frac{215.4}{4} = 0.298$$

$$\epsilon_{su} = \epsilon_{ce} + \epsilon_{se} + \epsilon_{cu}\,(1 - k_u)/k_u$$

$$\epsilon_{su} = 0.000227 + 0.00505 + 0.003\,\frac{1 - 0.298}{0.298} = 0.0123$$

$$M_{ult} = A_s\, f_{su}\, d\left(1 - 0.59\,\frac{A_s}{b\ d}\,\frac{f_{su}}{f'_c}\right) = 8583 \text{ in.-k}$$

$$P_{ult} = 2\,\frac{M_{ult} - (w\,\ell^2/8)}{\ell/3} = \frac{6(8583 - 906)}{36(12)} = 106.6 \text{ k}$$

$$\varphi_{ult} = \frac{\epsilon_{cu}}{k_u\ d} = \frac{0.003}{0.298(24)} = 4.19 \times 10^{-4} \text{ rad/in.}$$

$$\frac{M_{ult}}{M_{cr}} = \frac{8583}{5022} = 1.71 > 1.2$$

Deflections

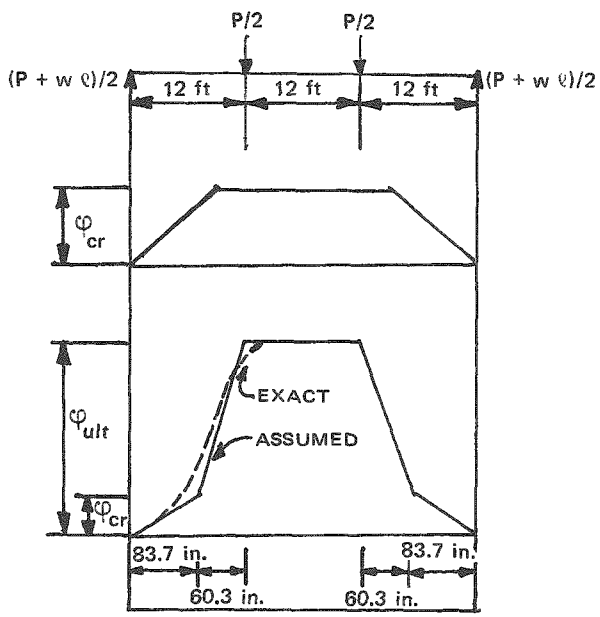

$$\Delta_{\phi cr} = \varphi_{cr} [72^2/2 + 144/2 (72 + 144/3)] = 0.32 \text{ in.}$$

$$\Delta_{\phi ult} = \varphi_u (72^2) + (\varphi_u - \varphi_{cr})[60.3(72 + 60.3/3)]/2$$

$$+ \varphi_{cr}[60.3(72 + 60.3/2)] + \varphi_{cr}[83.7/2 (72 + 60.3 + 83.7/3)]$$

$$= 1.086 + 1.084 + 0.176 + 0.192 = 2.54 \text{ in.}$$

Shear

Web Shear

$$v_{cw} = 3.5 \sqrt{f'_c} + 0.3 f_{pc} + V_p/b\ d = 3.5 \sqrt{6500} + 0.3(599)$$

$$+ 0/24(14) = 462 \text{ psi}$$

$$V_{cw} = v_{cw}\ b\ d = 24\ (14) = 155 \text{ k}$$

Flexure Shear

$$v_{ci} = 1.7 \sqrt{f'_c} = 137 \text{ psi}$$

$$V_{ci(min)} = 137(14)(24) = 46 \text{ k}$$

$$v_{ci} = 0.6 \sqrt{f'_c} + \frac{V_d + (V_\ell\ M_{cr}/M_{max})}{b\ d}$$

$$M_{cr} = I/c\ (6 \sqrt{f'_c} + f_{pe} - f_d) = 3785 \text{ in.-k}$$

$$V_\ell = P_{ult}/2 = 53.3 \text{ k}$$

X ft from support	V_d (k)	M_{max} (in.-k)	$\frac{V_d}{b\ d} + \frac{V_\ell\ M_{cr}}{b\ d\ M_{max}}$ (ksi)	v_{ci} (ksi)	V_{ci} (k)
12	2.80	7675	0.087	0.135	45.3
10	3.74	6396	0.105	0.153	51.4
8	4.68	5117	0.131	0.179	60.1
6	5.60	3836	0.173	0.221	74.2

Stirrups

Let S = 0.75 h = 24 in.

$$A_v = \frac{(v_u - v_c)b\ S}{f_y} = 0.168 \text{ in.}^2$$

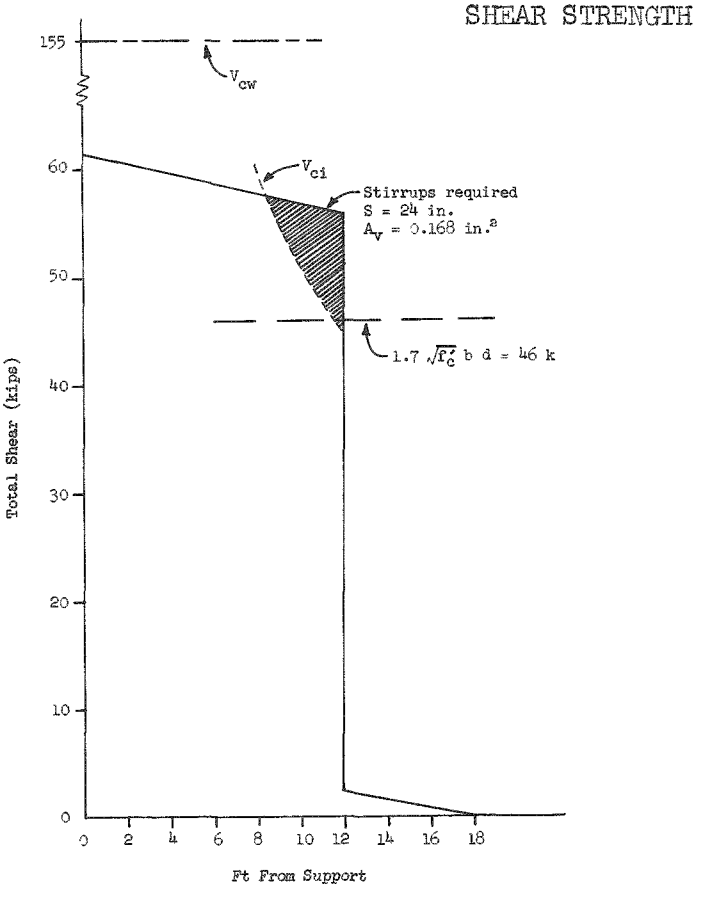

Anchorage Zone Reinforcement

Maximize T

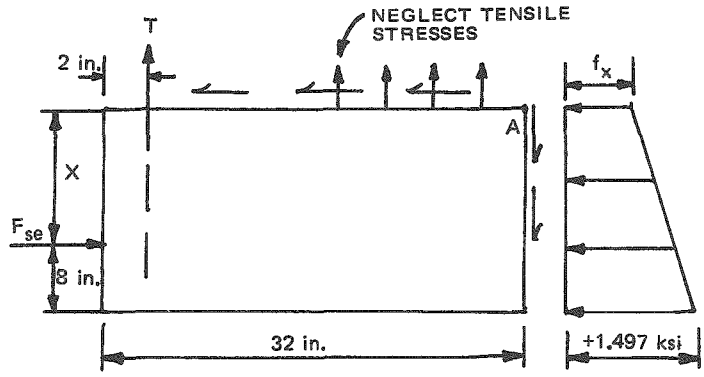

$$\sum M_{@A}$$

$$30\,T + f_x\,(14)\,\frac{(x+8)^2}{2} + \frac{(1.497 - f_x)}{2}\,(14)(x+8)^2\,\frac{2}{3} - F_{se}\,x = 0$$

$$30\,T = -14(x+8)^2\left(\frac{f_x}{2} + \frac{1.497}{3} - \frac{f_x}{3}\right) + 268.13\,x$$

$$T = -\frac{7}{90}\,(x+8)^2\,(f_x + 2.994) + 8.938\,x$$

x (in.)	$\frac{(x+2)^2}{11}$ ($in.^2$)	f_x (ksi)	$2.994 + f_x$ (ksi)	8.938 x (k)	T (k)
8	19.91	0.599	3.593	71.5	0
6	15.24	0.711	3.705	53.6	−2.86
4	11.20	0.824	3.818	35.8	−6.96
12	31.11	0.374	3.368	107.3	2.60
14	37.64	0.262	3.256	125.13	2.58

$T_{max} = 2.6$ k

$A_v = T/20 = 2.6/20 = 0.13\ in.^2$

APPENDIX B

A second formulation of the elevated-temperature polymer-silica cement material system was obtained for evaluation. Two mixes of twelve 51-mm cubes each were fabricated from the materials supplied. After curing for three days, five cubes from mix 1 were placed in an oven, where the temperature was to be maintained at 260°C, and an additional set of five-cube specimens was placed in a second oven, where the temperature was to be held at 816°C. Similarly, five-cube sets of mix 2 were placed in ovens to be maintained at 540 and 1093°C. The remaining two cubes of each set served as control specimens that were not exposed to elevated temperatures. Test procedures were the same as described in Section 3.2.3, except the longest period of exposure was changed from 94 to 56 days. Average compressive strengths and moduli of elasticity obtained for the room-temperature-cured specimens of mix 1 were 33 MPa and 16.5 GPa and for mix 2 these values were 21.3 MPa and 13.7 GPa, respectively. Table B.1 presents compressive strength and moduli of elasticity values as a percent of the room temperature values for the lengths of exposure and temperatures listed in the table.

Results listed in Table B.1 exhibit significant improvements over results obtained for the first elevated-temperature formulation of the polymer-silica cement tested (Table 9). Exposure of the specimens to temperatures of up to 538°C for periods of up to 56 days imparted substantial increases in both compressive strength and moduli of elasticity. Increases in these values were also imparted for exposures less than seven days at 816°C; however, for exposure periods longer than seven days, the compressive strengths and moduli of elasticity values obtained were less than those at room temperature. (Property retention was still >70% for this exposure.) However, the material was still not capable of exposure to 1093°C for periods of exposure as small as three days without flowing excessively. (Conversations with the supplier indicate that a material has been formulated that will not exhibit excessive distortion for exposure temperatures up to 1038°C.)

Table B.1. Polymer-silica elevated-temperature test results

Exposure temperature (°C)	Length of exposure at test temperature				
	3-day	7-day	14-day	28-day	56-day
	Relative compressive strength values[a] (%)				
260	157	148	170	147	182
538	223	254	253	172	173
816	163	113	82	82	74
1093	*b*	*b*	*b*	*b*	*b*
	Relative moduli of elasticity[a] (%)				
260	212	278	235	150	161
538	267		185	194	217
816	146	158	97	73	80
1093	*b*	*b*	*b*	*b*	*b*

[a]Relative to values obtained for specimens maintained at room temperature.

[b]Excessive material flow. Specimens not suitable for testing.

ORNL/TM-6478
Dist. Category UC-77

Internal Distribution

1. S. J. Ball
2. D. E. Bartine
3. M. E. Bender
4-9. J. P. Callahan
10. D. A. Canonico
11. J. A. Clinard
12. J. A. Conlin
13. J. H. Coobs
14. J. M. Corum
15. J. R. DiStefano
16. W. G. Dodge
17. J. R. Dougan
18. W. P. Eatherly
19. D. N. Fanning
20. Uri Gat
21. J. Griess
22. A. G. Grindell
23. W. L. Greenstreet
24. R. C. Gwaltney
25. J. F. Harvey
26. F. J. Homan
27. C. C. Hurtt
28-36. P. R. Kasten
37. M. Levenson
38. A. L. Lotts
39. R. E. MacPherson
40. A. P. Malinauskas
41. W. J. McAfee
42. J. G. Merkle
43. R. K. Nanstad
44-53. D. J. Naus
54. C. B. Oland
55. H. Postma
56. J. L. Rich
57. G. C. Robinson
58. J. P. Sanders
59. G. M. Slaughter
60. J. E. Smith
61. H. E. Trammell
62. M. Tobias
63. D. B. Trauger
64. J. R. Weir, Jr.
65. G. D. Whitman
66. R. P. Wichner
67. G. T. Yahr
68. ORNL Patent Office
69-70. Central Research Library
71. Document Reference Section
72-76. Laboratory Records Department
77. Laboratory Records, ORNL-RC

External Distribution

78-79. Director, Division of Nuclear Research and Applications, DOE, Washington, D.C. 20545
80. Director, Reactor Division, DOE, ORO
81-82. Assistant Manager, Energy Research and Development, DOE-ORO
83-258. For distribution as shown in TID-4500 under category UC-77, Gas-Cooled Reactor Technology

U S GOVERNMENT PRINTING OFFICE 1979-748 189/481